

Engineering Selective and Stable Methanol to Olefins Catalysts

Yarulina, Irina

DOI

[10.4233/uuid:27a5546b-f1c1-4ff7-b0b0-30172a75cc16](https://doi.org/10.4233/uuid:27a5546b-f1c1-4ff7-b0b0-30172a75cc16)

Publication date

2017

Document Version

Final published version

Citation (APA)

Yarulina, I. (2017). *Engineering Selective and Stable Methanol to Olefins Catalysts*. [Dissertation (TU Delft), Delft University of Technology]. <https://doi.org/10.4233/uuid:27a5546b-f1c1-4ff7-b0b0-30172a75cc16>

Important note

To cite this publication, please use the final published version (if applicable). Please check the document version above.

Copyright

Other than for strictly personal use, it is not permitted to download, forward or distribute the text or part of it, without the consent of the author(s) and/or copyright holder(s), unless the work is under an open content license such as Creative Commons.

Takedown policy

Please contact us and provide details if you believe this document breaches copyrights. We will remove access to the work immediately and investigate your claim.

Engineering Selective and Stable Methanol to Olefins Catalysts

Proefschrift

ter verkrijging van de graad van doctor
aan de Technische Universiteit Delft,
op gezag van de Rector Magnificus prof. ir. K.C.A.M. Luyben;
voorzitter van het College voor Promoties,
in het openbaar te verdedigen op
dinsdag 25 april 2017 om 10:00 uur

door

Irina YARULINA

scheikundig ingenieur

Lomonosov Moscow State University of Fine Chemical Technology, Russia
geboren te Comrat, Moldova, USSR

This dissertation has been approved by the
promotors: Prof. dr. F. Kapteijn and Prof. dr. J. Gascon

Composition of the doctoral committee:

Rector Magnificus	Chairman
Prof. dr. F. Kapteijn	Delft University of Technology, promotor
Prof. dr. J. Gascon	Delft University of Technology, promotor

Independent members:

Prof. dr. U. Olsbye	University of Oslo, Norway
Prof. dr. H. Schulz	Karlsruhe Institute of Technology, Germany
Prof. dr. J.A. Lercher	Technical University of Munich, Germany
Prof. dr. ir. E.J.M. Hensen	Eindhoven University of Technology
Prof. dr. E.J.R. Sudhölter	Delft University of Technology
Prof. dr. ir. T.J.H. Vlugt	Delft University of Technology, reserve member

The research described in this thesis has been conducted at the Catalysis Engineering section of the Chemical Engineering Department, Faculty of Applied Sciences (TNW), Delft University of Technology, with support of the Netherlands Organisation for Scientific Research (NWO) in the framework of the TASC Technology Area “Syngas, a Switch to Flexible New Feedstock for the Chemical Industry (TA-Syngas)”.

Cover design: <https://www.radioncicic.com>

Printed by: Ipskamp Printing, Enschede

ISBN: 978-94-028-0613-7

To my family

Contents:

Chapter 1	<i>Introduction: from MTH to MTO - Which Strings to Pull for the Desired Product Distribution</i>	1
Part I. 8-Ring Zeolites		
Chapter 2	<i>Methanol-to-Olefins Process over Zeolite Catalysts with DDR Topology: Effect of Composition and Structural Defects on Catalytic Performance</i>	17
Chapter 3	<i>Faster is not Always Better: Consequences of Secondary Zeolite Growth on Catalytic Performance in DMTO</i>	45
Part II. 10-Ring Zeolites		
Chapter 4	<i>The Importance of Heat Effects in the Methanol-to-Hydrocarbons Process over ZSM-5: on the Role of Mesoporosity on Catalyst Performance</i>	65
Chapter 5	<i>Suppression of the Aromatic Cycle in Methanol-to-Olefins Process over ZSM-5 By Post-synthetic Modification using Calcium</i>	79
Chapter 6	<i>On the Role of Lewis and Brønsted Acidity in Methanol-to-Olefins Process</i>	95
Appendices A-D		115
Summary and Outlook		137
Acknowledgements		150
List of Publications		152
About the Author		155

Chapter

1

***Introduction: from MTH to MTO -
Which Strings to Pull for the Desired
Product Distribution***

This chapter guides the reader through the history of the methanol-to-olefins process, presents the understanding of the mechanism and reveals the current challenges addressed in this thesis.

1.1. Setting up the Scene.

It happens often that many great discoveries or inventions are a matter of serendipity or twist of fate. The list of great accidents includes potato chips, saccharine, penicillin, and the methanol-to-hydrocarbons process (MTH). The latter was unintentionally discovered by the Mobil scientists in 1977.^[1] To make this discovery even more interesting, this happened in Mobil at the same time in two groups working independently from each other on the conversion of methanol to ethylene oxide and the methylation of isobutene, respectively. Both teams, however, used the same catalyst - ZSM-5. In absence of any co-feed, researchers observed complete conversion of methanol with the formation of a wide range of products, including olefins, paraffins, gasoline range of products and aromatics.^[2] Depending on the main fraction of the products, the name of the process varies from MTH to MTP (methanol-to-propylene), MTO (methanol-to-olefins), MTG (methanol-to-gasoline) or MTA (methanol-to-aromatics), the basics of the processes being rather similar. The possible reasons behind different product distribution will be elaborated further.

Urged by the oil crisis of 1973, further research on the newly born process advanced with giant strides. Already in 1979, the MTG developed by Mobil was chosen by the New Zealand government for the conversion of Maui off-shore natural gas reserves into gasoline.^[2] The plant began its operation in 1986. Currently, only in China there are approximately twenty MTO projects in operation, under construction, or in detailed design, while the amount of plants worldwide exceeds one hundred. Not all of them are based on Mobil technology. Alternative process designs were also developed by Dalian Institute of Chemistry and Physics, Lurgi, UOP/Hydro and Topsøe, yet targeting different product slates.^[3] The world demand for ethylene and propylene, however, forces industry to narrow product distribution to olefins only, which are traditionally produced by steam cracking. Furthermore, the US shale gas offers cheap ethylene through ethane dehydrogenation, which created a propylene supply gap, making it even a more preferable product.

Facing the current global situation of oil depletion and possible economic scenarios, the highly challenging objective of this work was to develop a catalyst where the product distribution in the MTO process would be limited to short chain olefins, with the preferential formation of propylene. Apart from being selective, an ideal catalyst also possesses additional properties, with stability against deactivation being the most critical one for the reaction at hand. All catalysts deactivate after a certain operation time and need to be regenerated. Stability determines strongly the process operation.

Since the MTH discovery, ZSM-5 catalyst remains one of the most studied and applied catalysts for methanol conversion, although, in principle, every single zeolite having Brønsted acidity with structure accessible for methanol should be able to catalyse the process.^[4] The Brønsted acid site is believed to be the active site of MTH (in combination with the organic species elaborated further in 1.2). It exists in the form of H^+ counterbalancing the negative charge of framework due to the presence of Al. Herein, the strength of acid sites, their location and distribution are of paramount importance determining catalyst

lifetime and product distribution. On the other hand, Brønsted acidity is not the only type of acidity existing in zeolites. Dealumination of framework can also lead to the formation of extra-framework Al acting as Lewis sites, their effect on MTO being still unclear and controversial. Another essential property of the zeolite actively utilized in the MTO process is shape selectivity – combination of catalysis with molecular sieving. Shape selectivity is one of the most important zeolite properties. It allows to control product distribution and will be further elaborated in this chapter.

To achieve control over product distribution, we obviously have to understand the reaction mechanism to further manipulate it in the desired direction; therefore the next paragraph will be dedicated to the up-to-date progress in mechanism understanding. As fairly mentioned by Olsbye *et al.*,^[5] the control over reaction mechanism “*is a huge challenge because it involves many elementary reactions occurring in both competing and consecutive ways throughout the whole process.*” Besides, one should know that since MTO employs zeolites as catalysts, the reaction will be affected by intracrystalline diffusion limitations associated with microporous materials. Finally, to highlight the complexity of the process, it is also important to mention that this is a highly exothermic process. The enthalpy of reaction depends on the product distribution and can vary strongly, being the highest when paraffins are produced.^[6]

1.2. Through Decades towards the Dual-Cycle Concept.

To highlight the importance and complexity of the MTH mechanism it suffices to mention that almost forty years of careful studies produced more than twenty distinct mechanisms summarized in several reviews.^[3-4, 7] It is important to start with the fact that MTO is an autocatalytic reaction.^[3b, 4]

The first step of the mechanism consists of methanol dehydration to give an equilibrated mixture of water, dimethyl ether (DME) and methanol. Next is the most mysterious stage involving formation of the first C-C bond, which still remains the chicken-and-egg problem of MTO.^[8] At first, it was believed that the first C-C bond is the result of the presence of traces of impurities that further autocatalyse the reaction. However, it was proven that even though feed impurities have an effect on the initial induction period, the amount of deactivating species and even on the coke location,^[9] due to the autocatalytic nature of MTH, the formation of the C-C bond can proceed in the absence of such impurities.^[3b, 5] Alternatively, the first C-C bond can be formed directly through coupling of two methanol or DME molecules. Several possible mechanisms were proposed including oxonium ylide,^[10] carbene^[11] and methane-formaldehyde routes.^[4-5, 12] As the proposed intermediates proved to be extremely unstable and calculated energy barriers are impossibly high,^[13] there is now a second wave of mechanism proposals for the direct C-C bond formation.^[14] For example, Lercher *et al.* proposed a carbonylation-based mechanism with an energy barrier of 80 kJ mol⁻¹ (in contrast to *ca.* 300 kJ mol⁻¹ in previous mechanisms) *via* formation of methyl acetates or acetic acid.^[15] Formation of these species was further evidenced by Weckhuysen *et al.*^[12] by employing a combination of UV/Vis diffuse reflectance spectroscopy and solid-state NMR spectroscopy. As the above-mentioned mechanism was proposed only months ago, one can

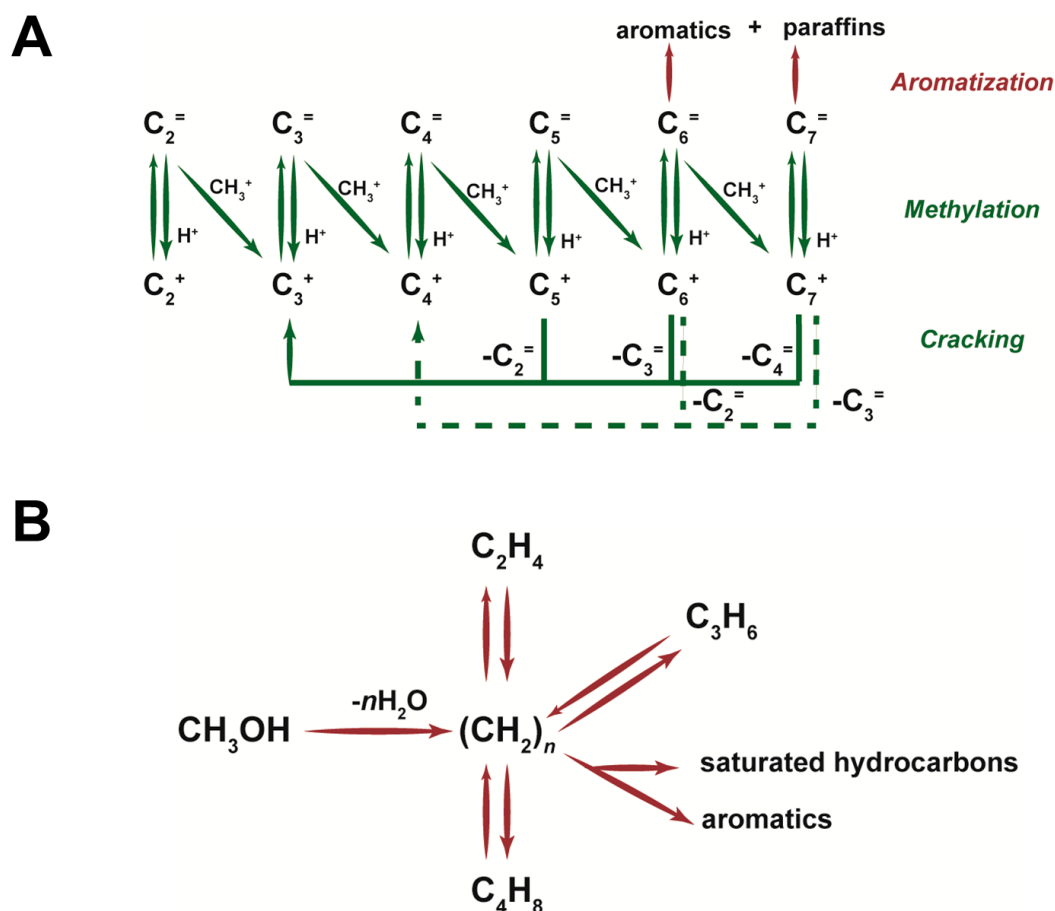


Figure 1. (A) Dessau's homologation/cracking mechanism for methanol conversion over ZSM-5.^[17] (B) Hydrocarbon pool proposed by Dahl and Kolboe.^[20]

expect dozens of new publications either witnessing or rejecting these proposed “new” intermediates in the near future. Since this thesis focuses on catalyst development rather than on unravelling the mechanism behind the formation of this first C-C bond, the next mechanistic step, the so called “dual-cycle”, is more relevant for this work.^[16] The mechanistic studies were performed using SAPO-34 and ZSM-5 as catalysts, though the findings for one catalyst should not be necessarily applied for another one.

In 1986, Dessau *et al.* proposed the formation of hydrocarbons over ZSM-5 as a result of consecutive methylation and cracking reactions, thus postulating the existence of an olefinic cycle (Figure 1A).^[17] The presence of paraffins and aromatics apart from olefins at the reactor outlet was explained by side-reactions involving hydrogen transfer and cyclization reactions.^[18] The role and participation of aromatics in the reaction mechanism was not yet understood or was simply ignored, though the experiments showing the effect of co-feeding aromatics were already performed and co-catalytic effect was

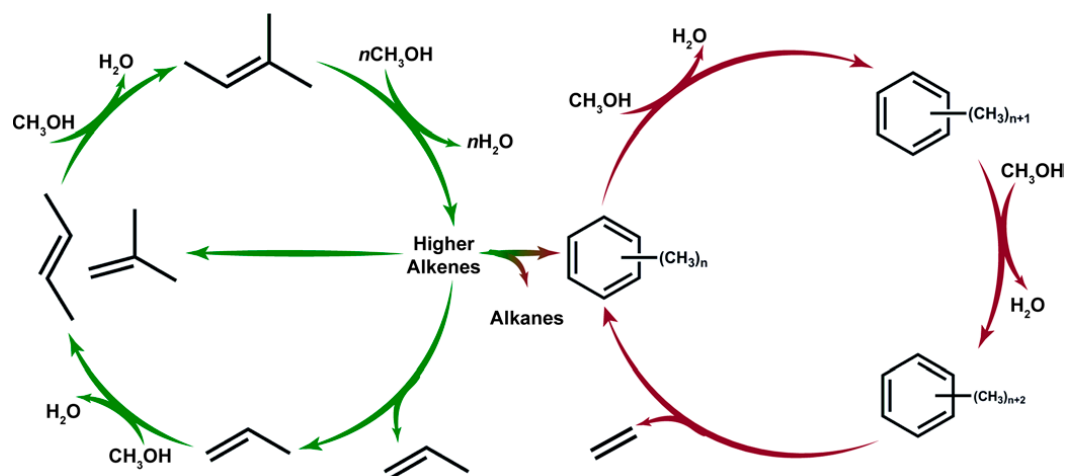


Figure 2. Dual-cycle concept for the conversion of methanol over ZSM-5.^[22]

admitted.^[19] A parallel type of mechanism, the so-called 'hydrocarbon-pool' was suggested by Dahl and Kolboe in the mid-90's when studying MTO over SAPO-34 (Figure 1B).^[20] It was initially proposed that the active site is an organic-inorganic hybrid consisting of a hydrocarbon pool $(CH_2)_n$ adsorbate on a Brønsted acid site. During the reaction course, methanol reacts with the hydrocarbon pool (HCP) *via* methylation forming ethylene and propylene. The nature of HCP however was not fully understood, apart from the fact that it could be close to ordinary coke. In following decades research activities were dedicated to answer the question: "What is exactly the hydrocarbon pool?" Haw *et al.* revealed a correlation between methylbenzenes in SAPO-34 cages and the formation of olefins, establishing them as the key components of HCP.^[21] It was also found that nature of active HCP species significantly differs depending on the zeolite topology especially for the large pore zeolites. For ZSM-5, however, by applying $^{12}C/^{13}C$ labelled methanol in transient switching experiments, it was found that methylbenzenes are the main source only for ethylene formation, while propylene and higher olefins are formed from interconversion and cracking reactions as was suggested by Dessau. These findings led to a proposal of the updated version of HCP mechanism stating the presence of two parallel cycles in the zeolite pores. The first cycle involves olefin conversion and produces mainly propylene, while the second one consists of dealkylation of methylbenzenes and its derivatives leading to ethylene formation. This is the state of the art mechanism, called the 'dual-cycle' mechanism (Figure 2). Considering the competing nature of the two cycles, one can speculate that a desired product range can be obtained by either selectively stimulating or suppressing one cycle (olefinic or aromatic) over the other.^[22] Three main strategies can in principle be identified to establish selectivity control based on mechanistic knowledge. They will be discussed in details in the next section.

It is important to mention that throughout the thesis the term “aromatic cycle” refers to the set of reactions involving formation of aromatic species and other reactions with the participation of aromatics.

1.3. Strategies to Control Selectivity.

1.3.1. Taking Advantage of Autocatalysis.

As was mentioned above, MTO has an autocatalytic character. Formation of the first products results in higher methanol conversions, as formed hydrocarbons enter methylation reactions thus increasing reaction rates.^[23] From this perspective, olefins and aromatics can be considered as competing catalysts. The excessive presence of a certain product promotes the cycle from which this product originates.^[18] So, the first strategy to enhance the yield to olefins is to increase their concentration by co-feeding.

Several works report on the effect of co-feeding olefins and/or aromatics with methanol on product distribution, however, with the main aim to shed light on mechanism details.^[19, 24] Recently, Ilias *et al.*^[25] and Sun *et al.*^[22] reported a thorough investigation on how to tune product selectivity by co-processing olefins and aromatics with methanol. Ilias *et al.*^[25] reported a 2.5-fold increase in selectivity for C₄-C₇ aliphatics when co-feeding propylene compared to results obtained by co-feeding toluene at 275°C. Sun *et al.* performed the same experiments but at 450°C, which are more industrially relevant conditions. In contrast, they reported unchanged selectivity to ethylene and higher selectivity to C₃₊ olefins. Within the C₃₊ product distribution, an enhanced selectivity to butenes at the expense of propene was observed. Co-feeding of aromatics caused higher yields to methane, ethylene and methylbenzenes, thus allowing tuning ethylene/propylene ratio on demand. Later, Sun *et al.*^[18] also showed that although the addition of higher olefins or alcohols did not change the product distribution, it still promoted the olefin based cycle. As a consequence, the rate of oxygenic coke formation was slowed down, leading to up to a 9-fold increase in catalyst lifetime. The same tendency was observed for ZSM-22: recycle of C₂-C₄ olefins led to improved stability and resistance to deactivation.^[26]

It should also be mentioned that the described strategy is already being applied at the industrial level in the Lurgi methanol-to-propylene (MTP) process.^[27] According to the patents, MTP is performed in a fixed bed reactor, the product mixture being separated into short chain olefins (C₂-C₄) and C₅₊ gasoline hydrocarbons, which are recycled to be converted to C₂-C₄ olefins.^[27c]

Nevertheless, the reports provided by Ilias *et al.* and Sun *et al.* showed that co-processing of olefins affects the C₄₊ fraction rather than the desired propylene, therefore other strategies should be considered.

1.3.2. Shape Selectivity.

1.3.2.1. Suppressing Aromatic Cycle through Topology Selection.

Methylbenzenes proved to be virtually inert for the production of propylene and butenes in ZSM-5 due to spatial restrictions caused by the topology.^[28] Moreover, formation of methylbenzenes is mostly

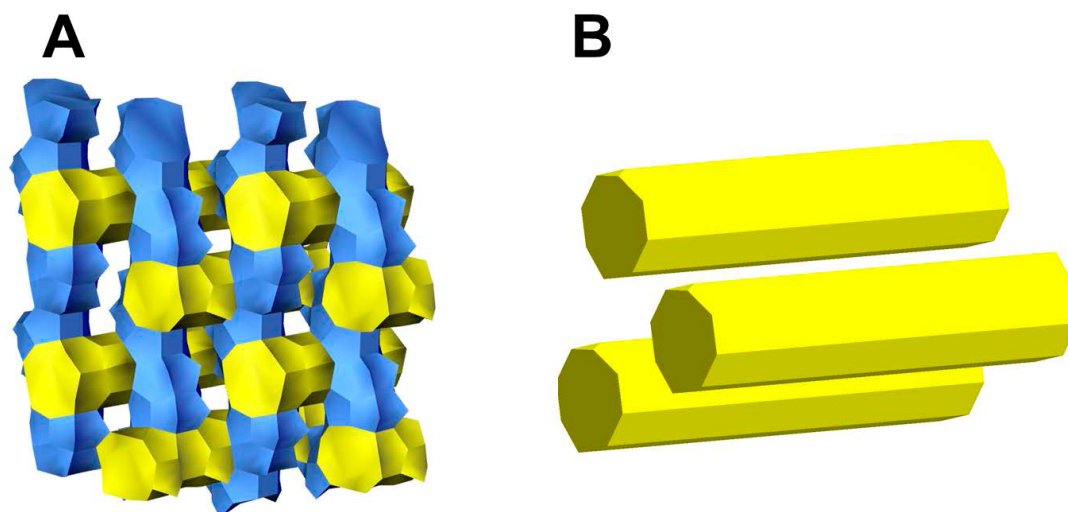


Figure 3. (A) ZSM-5 zeolite with MFI topology consisting of straight (yellow) and sinusoidal (blue) channels. (B) Unidirectional channels of 1D ZSM-22 with TON topology.

expected at the channel intersections as they cannot fit the channel confinement (Figure 3A). Their evolution can be, in principle, eliminated by controlling the Al location during the synthesis avoiding formation of an acid site at the channel intersection.^[28] On the other hand, choosing zeolite topologies with slightly smaller dimensions already ensures discarding the aromatic cycle. To the best of our knowledge, ZSM-22 with TON topology was the first catalyst for which the suppression of the aromatic cycle was postulated (Figure 3B).^[29] Analysis of the product distribution over 1D ZSM-22 (with channel dimensions 0.45×0.55 nm and absence of notorious intersections) revealed high selectivity for branched alkenes C_{5+} (>70% at 400°C) and a negligible amount of aromatics. Bleken *et al.*^[30] also showed that the more spacious the intersection dimension in a given zeolite is, the faster catalyst deactivates as it promotes higher concentration of polymethylated benzenes causing the deactivation by pore blocking and/or filling. Thus, the application of 1D zeolites (EU-1, ZSM-23, ZSM-48 or ZSM-22) with appropriate dimensions can be a route to narrow product distribution to olefins only.^[31] However, considering the amount of branched alkenes, the obtained product mixture rather meets the requirements for gasoline (after a hydrogenation step), propylene fraction being fairly low.^[31-32] On the other hand, in the absence of aromatic cycle, propylene selectivity can be further improved by optimizing reaction conditions and physicochemical properties of zeolites. Hunger *et al.*^[33] optimized the Brønsted acid site (BAS) density of ZSM-22 ($0.30 \text{ mmol}_{\text{BAS}}\text{g}^{-1}$), increasing propylene yield up to 38%. Yokoi *et al.*^[34] focused on crystal size optimization for ZSM-22, showing that nanosized ZSM-22 (100 nm) gives propylene yields up to 53% at 450°C. Unfortunately, the 1D pore structure of ZSM-22 also suffers from rather rapid deactivation in comparison with ZSM-5, and according to Hunger is not suitable for industrial application.^[33]

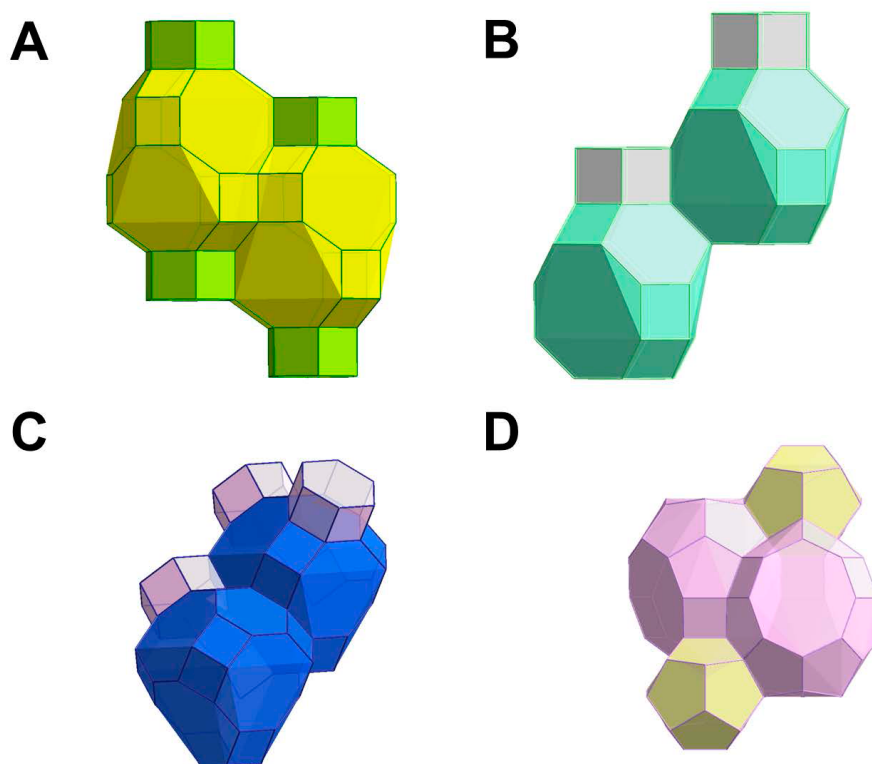


Figure 4. 8-ring zeolites with different topologies. (A) CHA; (B) LEV; (C) AEI; (D) DDR.

1.3.2.2. Stabilizing the Aromatic Cycle.

Unlike zeolites with small dimensions (like shown above for ZSM-22) that suppress the occurrence of the aromatic cycle, zeolites with cage-like voids (these are mostly 8-ring zeolites^[35]) are ideal to promote this cycle. The main features of 8-ring zeolites are not only the large cavity voids but specially the dimensions of the window openings. Limited by 8 T atoms, they are big enough to let short-chain olefins pass through, while any bigger molecule will be trapped inside the cage (Figure 4). Such a pore architecture guarantees high selectivity to the short-chain olefins (>90%),^[36] while slight differences in window or cage dimensions can affect product distribution and propylene/ethylene ratio.^[37] On the other hand, aromatics trapped inside the cages are not only responsible for the formation of olefins, but eventually lead to catalyst deactivation via formation of polycondensed aromatic species. The challenge is to achieve steady-state performance of the aromatic cycle by slowing down the coke formation. This can be also achieved by changing physico-chemical properties of 8-ring zeolites.^[38]

CHA topology (Figure 4A) is one of the most studied zeolites showing the longest lifetime among other 8-ring zeolites.^[3a, 39] This is believed to be due to the cylinder-like cavities with big dimensions,

which are able to host and stabilize polyalkylated methylbenzenes and condensed-ring aromatics, while the steric constraints imposed by smaller cages (for example, LEV) limit formation of bulkier species resulting in faster deactivation (compare 4A and 4B).^[40] The BAS strength plays a crucial role in the coke formation rate, mild acidity being more beneficial for longer lifetimes. Milder acidity, in turn, can be achieved by application of silicoaluminophosphates (SAPO).^[39]

Other 8-ring topologies are still being explored for the potential application in MTO process. For example, Davis *et al.*^[41] studied MTO over SSZ-39 catalyst with AEI topology. This zeolite belonging to AEI topology can be synthesized only with high Al content (Si/Al < 11), which leads to fast deactivation and high paraffins yields. By applying steaming,^[41-42] the authors tuned the Si/Al ratio decreasing it down to 50 – 100, thus achieving longer lifetimes and higher selectivity to short chain olefins with unusually high amount of propylene and butenes (propylene/ethylene/butene = 2.8/1/1.1), the basket-shape of AEI cage being responsible for the product distribution (Figure 4C). The same strategy was also applied to high Al SSZ-13^[42], RHO^[43] and KFI zeolites, leading to an increased olefins yield in all cases.

Some research was also performed in our group with zeolites with DDR topology (Figure 4D).^[44] This topology is characterized by window openings (0.44 × 0.36 nm) slightly different than those of CHA (0.38 × 0.38 nm). The particular dimensions of DDR allow uptake of short-chain unsaturated hydrocarbons, while saturated paraffins are excluded.^[45] As a result, the product distribution is characterized only by the presence of ethylene, propylene and butenes when testing catalyst in MTO at different temperatures (400–450°C), though the catalyst suffers from fast deactivation.

Controlling product distribution on desire by choosing the appropriate 8-ring topology with certain dimensions of cage and window opening represents a promising route to narrow products to short chain olefins only. The main challenge is to establish correlations between selectivities to products (including coke) and physicochemical properties of the zeolite, as their optimization may eventually stabilize the aromatic cycle and mitigate coking. This deserves some additional elaboration in addition to already performed work.

1.3.3. Suppressing Aromatic Cycle through Acid Site Modification.

Considering that the aromatic species are derived from long chain olefins due to hydride transfer reactions (Figure 2), another strategy to suppress formation of the aromatics is to tune the Brønsted acidity in such a way that it would be strong enough to perform methylation/cracking reactions but too weak to form aromatic species thus limiting mechanism to olefinic cycle only.^[4, 22] For example, Hunger *et al.*^[33] showed that optimization of the BAS density for ZSM-5 (0.13 mmol_{BAS} g⁻¹) can result in propylene selectivity as high as 51% at 450°C, which makes this zeolite the most promising for MTP application. MFI topology is one of the few topologies that can host both the aromatic and the olefinic cycle and the selective propagation of one over the other is a matter of optimizing amount and strength of acidity and/or reaction conditions. In case of Hunger *et al.*, improved selectivity to propylene can be rationalized on the basis of acid site isolation decreasing the probability of the olefins adsorbed on two neighbouring

acid sites to react giving long chain olefins which eventually can be either transformed to aromatics or cracked back to short chain olefins.^[46] On the other hand, application of ZSM-5 with a very low amount of acid sites results either in absence of MTO activity ($\text{Si/Al} > 1000$) or in a very short lifetime. The latter is due to the significantly lower amount of coke needed to fully deactivate the zeolite, since deactivation at high temperatures is due to acid site poisoning. Thus, decreasing the amount of Al in a zeolite is beneficial in terms of propylene yield but very disadvantageous due to faster deactivation, and an optimum must be sought.

Another option is to change the acid strength by modification of BAS.^[4, 47] There are numerous routes to achieve such modification, including incorporation of other non-metals into zeolite framework,^[48] ion-exchange with different cations, and impregnation with different salts.^[49] Among them, phosphorus incorporation into ZSM-5 is the most studied method of acidity modification, comprehensively discussed in an extensive review by Weckhuysen *et al.*^[47] There are several reasons leading to changes in amount and strength of acid sites due to phosphorus incorporation. First of all, the incorporation of phosphorus decreases the acid strength due to establishing intermolecular bonds between the zeolite framework and phosphoric acid.^[50] Besides, the overall amount of acid sites actually increases due to formation of different types of weak acid sites like P-OH, framework-belonging phosphates and even perturbed silanols.^[51] As a consequence of the modified acidity, generally higher selectivities to short chain olefins and longer lifetimes are observed.^[52] Hunger *et al.*^[52] and Haw *et al.*^[53] report that incorporation of phosphorus was conjugated with extensive dealumination and significant loss of surface area. This effect however was reversible after simple washing with water, leading to recovery of the strong acid sites.^[52, 54] By comparing catalytic performance of a phosphorus-modified sample and ZSM-5 with the same Si/Al ratio, Haw *et al.*^[53] concluded that the much lower selectivity to aromatics for P-modified sample is a result of additional spatial constraints introduced by presence of P-species inside the zeolite channels suppressing the formation of aromatics. However, on one hand, the authors did not demonstrate the creation of spatial constraints, on the other hand, the observed differences in catalytic behaviour are more logically explained on the basis of a significant decrease in the strength of acid sites. Besides the role of imposed Lewis acidity appearing due to extraframework Al species after P incorporation is generally overlooked.

A similar effect on catalytic performance is observed when zeolites are modified with alkaline-earth metals.^[55] Lots of work on the topic was performed in early 90-s and compiled in Stöcker's review.^[4] Recently, Zhang *et al.*^[56] refreshed the interest to the field by investigating the catalytic behaviour of Ca-modified ZSM-5. By increasing the Ca loading up to 12 wt.%, the authors observed that the amount of strong acid sites decreased by a factor of 22 (from 0.45 mmol g^{-1} down to 0.02 mmol g^{-1}) also admitting the appearance of Lewis acidity (not quantified) due to calcium incorporation. Remarkably, selectivity to short chain olefins increased from 42% up to 80% for pristine and modified ZSM-5 with 6 wt.% of Ca, respectively.

Remarkably, the above-mentioned modification can be applied to many other zeolites like mordenite,^[57] zeolite Y,^[58] ZSM-12 to improve selectivity in favour of propylene. For example, after dealumination with subsequent Ba²⁺ exchange, the normally rapidly deactivating mordenite showed lower coking rates, increased amount of short-chain olefins and decreased paraffins and aromatics formation, suggesting that the combination of these modifications led to a partial suppression of the aromatic cycle even in MOR, belonging to 12-ring zeolites normally favouring the aromatic cycle.

Obviously, the suppression of the aromatics formation can be achieved by modification with alkaline-earth metals. The described effect is normally attributed to the significantly weakened acid sites. However, the topic has to be revisited to answer multiple questions like “why are BAS disappearing?”, “is there any participation of Lewis acidity?”, “what is the exact effect of modification?” Answering these questions will give us further insight in this process and will open the door to important improvements in both catalyst lifetime and selectivity.

1.4. Outline of this Thesis.

The Methanol-to-Olefins process can be considered as alternative way to produce the base chemicals ethylene and propylene, their ratio being controlled on demand. The main challenge for catalyst engineers is to develop selective and stable catalysts, which can be done only by deep understanding of the reaction mechanism. As was shown in the previous three paragraphs, there is a number of strategies to control the reaction mechanism in order to narrow the product distribution down to olefins only, including (i) co-feeding olefins with methanol to propagate olefinic cycle, (ii) choosing a certain zeolite topology suppressing formation of the aromatic cycle or trapping aromatics inside the cages due to small window opening, and (iii) modification of the Brønsted acidity also to suppress formation of aromatic cycle through weakening of the acidity. Some of the above-mentioned strategies lead to the production of C₅+ olefins, which are out of the scope for this thesis.

Thus, this thesis focuses on two main approaches to achieve a high selectivity to short chain olefins: (i) *via* zeolite topology (See 1.3.2.2. *Stabilizing aromatic cycle*) and (ii) modification of Brønsted acidity (See 1.3.3. *Suppressing aromatic cycle through acid site modification*).

Part I (Chapters 2 and 3) focuses on the application of 8-ring zeolites for MTO. **Chapter 2** is dedicated to application of zeolites with DDR topology as catalysts for the MTO process. A thorough analysis of physico-chemical properties (acidity, crystal size, structural defects) is performed and linked to catalytic performance. Special attention is also paid to the analysis of trapped coke species by means of DRIFTS and dissolution-extraction experiments establishing relation to reaction conditions and zeolite acidity. As it was observed that the presence of structural defects in form of silanol nests leads to faster deactivation, **Chapter 3** mainly focuses on the origin and effect of structural defects in CHA and DDR zeolites. Comparison of zeolites synthesized by direct and seed-assisted methods revealed that faster growth kinetics leads to formation of internal defects and silanol nests in zeolites prepared by seed-

assisted method, independently on topology. These defects however can be healed by application of post-synthetic treatment with ammonium fluoride.

Part II is dedicated to the application of ZSM-5 with modified acidity. **Chapter 4** starts with an investigation of the reason behind different catalytic performance for zeolites with the same physico-chemical properties and tested under alike conditions. By mimicking conditions generally applied in literature, we show that due to exothermicity of the reaction, there is a temperature rise of 80°C inside the reactor bed. Monitoring the temperature in different positions of the reactor bed is shedding light on the peculiarity of reaction course. Analysis of the catalyst after three catalytic runs, shows significant dealumination due to steaming leading to loss of acidity. This Chapter highlights the importance of zeolite stability under relevant industrial conditions and provides a guide how to overcome temperature rise. **Chapter 5** is dedicated to modification of ZSM-5 by Ca. Different methods of calcium incorporation are investigated and calcium loading is optimized. Extensive analysis of acidic properties of the zeolites by means of NH₃ TPD, FTIR analysis with pyridine and CO as probe molecules, Solid State NMR with trimethylphosphine oxide (TMPO) as a probe molecule indicated transformation of Brønsted to Lewis acid sites. This modification led to suppression of the aromatic cycle. **Chapter 6** aims to identify the role of Brønsted and Lewis acidities in the MTO process. This is done by analysis of a number of catalysts generally applied in MTO (ZSM-5 with different Si/Al ratio, mesoporous ZSM-5 and modified with alkaline-earth metals) and establishing trends between selectivity, lifetime and amount of different acid sites.

Note that all chapters have been written as individual publications and can be read independently. As a result, some overlap may be present.

References.

- [1] F. J. Keil, *Microporous Mesoporous Mater.* **1999**, *29*, 49-66.
- [2] G. A. Olah, A. Goepfert, G. K. S. Prakash, *Beyond Oil and Gas: The Methanol Economy*, Weinheim, Germany, **2006**.
- [3] a) P. Tian, Y. Wei, M. Ye, Z. Liu, *ACS Catal.* **2015**, *5*, 1922-1938; b) U. Olsbye, S. Svelle, M. Bjorgen, P. Beato, T. V. W. Janssens, F. Joensen, S. Bordiga, K. P. Lillerud, *Angew. Chem. Int. Ed.* **2012**, *51*, 5810-5831.
- [4] M. Stöcker, *Microporous Mesoporous Mater.* **1999**, *29*, 3-48.
- [5] U. Olsbye, S. Svelle, K. P. Lillerud, Z. H. Wei, Y. Y. Chen, J. F. Li, J. G. Wang, W. B. Fan, *Chem. Soc. Rev.* **2015**, *44*, 7155-7176.
- [6] I. Yarulina, F. Kapteijn, J. Gascon, *Cat. Sci. Tech.* **2016**, *6*, 5320-5325.
- [7] D. Chen, K. Moljord, A. Holmen, *Microporous Mesoporous Mater.* **2012**, *164*, 239-250.
- [8] J. F. Haw, W. G. Song, D. M. Marcus, J. B. Nicholas, *Acc. Chem. Res.* **2003**, *36*, 317-326.
- [9] B. M. Weckhuysen, C. Vogt, J. Ruiz Martinez, *ChemCatChem* **2016**, 10.1002/cctc.201600860.
- [10] G. J. Hutchings, F. Gottschalk, M. V. M. Hall, R. Hunter, *J. Chem. Soc., Faraday Trans.* **1987**, *83*, 571-583.
- [11] C. D. Chang, A. J. Silvestri, *J. Catal.* **1977**, *47*, 249-259.
- [12] A. D. Chowdhury, K. Houben, G. T. Whiting, M. Mokhtar, A. M. Asiri, S. A. Al-Thabaiti, S. N. Basahel, M. Baldus, B. M. Weckhuysen, *Angew. Chem.* **2016**, 10.1002/ange.201608643.
- [13] D. Lesthaeghe, V. Van Speybroeck, G. B. Marin, M. Waroquier, *Angew. Chem. Int. Ed.* **2006**, *45*, 1714-1719.
- [14] A. Comas-Vives, M. Valla, C. Copéret, P. Sautet, *ACS Centr. Sci.* **2015**, *1*, 313-319.
- [15] Y. Liu, S. Müller, D. Berger, J. Jelic, K. Reuter, M. Tonigold, M. Sanchez-Sanchez, J. A. Lercher, *Angew. Chem. Int. Ed.* **2016**, *55*, 5723-5726.
- [16] S. Svelle, F. Joensen, J. Nerlov, U. Olsbye, K. P. Lillerud, S. Kolboe, M. Bjorgen, *J. Am. Chem. Soc.* **2006**, *128*, 14770-14771.
- [17] R. M. Dessau, R. B. Lapierre, *J. Catal.* **1982**, *78*, 136-141.
- [18] X. Sun, S. Mueller, Y. Liu, H. Shi, G. L. Haller, M. Sanchez-Sanchez, A. C. van Veen, J. A. Lercher, *J. Catal.* **2014**, *317*, 185-197.
- [19] T. Mole, J. A. Whiteside, D. Seddon, *J. Catal.* **1983**, *82*, 261-266.
- [20] a) I. M. Dahl, S. Kolboe, *Catal. Lett.* **1993**, *20*, 329-336; b) I. M. Dahl, S. Kolboe, *J. Catal.* **1994**, *149*, 458-464.
- [21] a) W. G. Song, J. F. Haw, J. B. Nicholas, C. S. Heneghan, *J. Am. Chem. Soc.* **2000**, *122*, 10726-10727; b) J. F. Haw, D. M. Marcus, *Top. Catal.* **2005**, *34*, 41-48.
- [22] X. Sun, S. Mueller, H. Shi, G. L. Haller, M. Sanchez-Sanchez, A. C. van Veen, J. A. Lercher, *J. Catal.* **2014**, *314*, 21-31.
- [23] S. N. Khadzhiev, M. V. Magomedova, E. G. Peresyphkina, *Pet. Chem.* **2015**, *55*, 503-521.
- [24] W. Z. Wu, W. Y. Guo, W. D. Xiao, M. Luo, *Chem. Eng. Sci.* **2011**, *66*, 4722-4732.
- [25] S. Ilias, A. Bhan, *J. Catal.* **2012**, *290*, 186-192.
- [26] S. Teketel, U. Olsbye, K. P. Lillerud, P. Beato, S. Svelle, *Appl. Catal., A* **2015**, *494*, 68-76.
- [27] a) H. Bach, L. Brehm, S. Jensen, P. Trabold, H. Koppel, WO 2004018089 A1, **2004**; b) M. Rothaemel, W. Boll, G. Birke, H. Koempel, W. Liebner, H. Bach, US 8785708 B2, **2006**; c) M. Rothaemel, U. Finck, T. Renner, H. Buchold, WO2006136433A1, **2006**; d) G. Birke, H. Bach, US 20140018593 A1, **2014**.
- [28] T. Liang, J. Chen, Z. Qin, J. Li, P. Wang, S. Wang, G. Wang, M. Dong, W. Fan, J. Wang, *ACS Catal.* **2016**, *6*, 7311-7325.
- [29] a) S. Teketel, S. Svelle, K.-P. Lillerud, U. Olsbye, *ChemCatChem* **2009**, *1*, 78-81; b) S. Teketel, U. Olsbye, K. P. Lillerud, P. Beato, S. Svelle, *Microporous Mesoporous Mater.* **2010**, *136*, 33-41.
- [30] F. Bleken, W. Skistad, K. Barbera, M. Kustova, S. Bordiga, P. Beato, K. P. Lillerud, S. Svelle, U. Olsbye, *Phys. Chem. Chem. Phys.* **2011**, *13*, 2539-2549.
- [31] S. Teketel, W. Skistad, S. Benard, U. Olsbye, K. P. Lillerud, P. Beato, S. Svelle, *ACS Catal.* **2012**, *2*, 26-37.
- [32] S. Teketel, L. F. Lundegaard, W. Skistad, S. M. Chavan, U. Olsbye, K. P. Lillerud, P. Beato, S. Svelle, *J. Catal.* **2015**, *327*, 22-32.
- [33] M. Dybala, P. Becker, D. Trefz, E. Klemm, A. Fischer, H. Jakob, M. Hunger, *Appl. Catal., A* **2016**, *510*, 233-243.
- [34] A. K. Jamil, O. Muraza, M. Yoshioka, A. M. Al-Amer, Z. H. Yamani, T. Yokoi, *Ind. Eng. Chem. Res.* **2014**, *53*, 19498-19505.
- [35] M. Moliner, C. Martinez, A. Corma, *Chem. Mater.* **2014**, *26*, 246-258.
- [36] a) D. Chen, K. Moljord, T. Fuglerud, A. Holmen, *Microporous Mesoporous Mater.* **1999**, *29*, 191-203; b) J. R. Chen, J. Z. Li, Y. X. Wei, C. Y. Yuan, B. Li, S. T. Xu, Y. Zhou, J. B. Wang, M. Z. Zhang, Z. M. Liu, *Catal. Commun.* **2014**, *46*, 36-40.

- [37] Y. Bhawe, M. Moliner-Marin, J. D. Lunn, Y. Liu, A. Malek, M. Davis, *ACS Catal.* **2012**, *2*, 2490-2495.
- [38] a) R. Martinez-Franco, Z. B. Li, J. Martinez-Triguero, M. Moliner, A. Corma, *Cat. Sci. Tech.* **2016**, *6*, 2796-2806; b) Z. B. Li, J. Martinez-Triguero, P. Concepcion, J. H. Yu, A. Corma, *Phys. Chem. Chem. Phys.* **2013**, *15*, 14670-14680.
- [39] F. Bleken, M. Bjorgen, L. Palumbo, S. Bordiga, S. Svelle, K.-P. Lillerud, U. Olsbye, *Top. Catal.* **2009**, *52*, 218-228.
- [40] J. Z. Li, Y. X. Wei, J. R. Chen, S. T. Xu, P. Tian, X. F. Yang, B. Li, J. B. Wang, Z. M. Liu, *ACS Catal.* **2015**, *5*, 661-665.
- [41] M. Dusselier, M. A. Deimund, J. E. Schmidt, M. E. Davis, *ACS Catal.* **2015**, *5*, 6078-6085.
- [42] Y. W. Ji, M. A. Deimund, Y. Bhawe, M. E. Davis, *ACS Catal.* **2015**, *5*, 4456-4465.
- [43] Y. W. Ji, J. Birmingham, M. A. Deimund, S. K. Brand, M. E. Davis, *Microporous Mesoporous Mater.* **2016**, *232*, 126-137.
- [44] Y. Kumita, J. Gascon, E. Stavitski, J. A. Moulijn, F. Kapteijn, *Appl. Catal., A* **2011**, *391*, 234-243.
- [45] a) W. Zhu, F. Kapteijn, J. A. Moulijn, J. C. Jansen, *Phys. Chem. Chem. Phys.* **2000**, *2*, 1773-1779; b) W. Zhu, F. Kapteijn, J. A. Moulijn, M. C. den Exter, J. C. Jansen, *Langmuir* **2000**, *16*, 3322-3329.
- [46] S. M. T. Almutairi, B. Mezari, E. A. Pidko, P. C. M. M. Magusin, E. J. M. Hensen, *J. Catal.* **2013**, *307*, 194-203.
- [47] H. E. van der Bij, B. M. Weckhuysen, *Chem. Soc. Rev.* **2015**, *44*, 7406-7428.
- [48] F. Yaripour, Z. Shariatnia, S. Sahebdehfar, A. Irandoukht, *Microporous Mesoporous Mater.* **2015**, *203*, 41-53.
- [49] A. Galadima, O. Muraza, *Ind. Eng. Chem. Res.* **2015**, *54*, 4891-4905.
- [50] Y. Huang, X. Dong, M. Li, M. Zhang, Y. Yu, *RSC Adv.* **2014**, *4*, 14573-14581.
- [51] a) P. Tynjala, T. T. Pakkanen, *Microporous Mesoporous Mater.* **1998**, *20*, 363-369; b) H. E. van der Bij, F. Meirer, S. Kalirai, J. Wang, B. M. Weckhuysen, *Chem. Eur. J.* **2014**, *20*, 16922-16932; c) H. Vinek, G. Rimplmayr, J. A. Lercher, *J. Catal.* **1989**, *115*, 291-300.
- [52] M. Dyballa, E. Klemm, J. Weitkamp, M. Hunger, *Chem. Ing. Tech.* **2013**, *85*, 1719-1725.
- [53] S. M. Abubakar, D. M. Marcus, J. C. Lee, J. O. Ehresmann, C.-Y. Chen, P. W. Kletnieks, D. R. Guenther, M. J. Hayman, M. Pavlova, J. B. Nicholas, J. F. Haw, *Langmuir* **2006**, *22*, 4846-4852.
- [54] M. Derewinski, P. Sarv, X. Y. Sun, S. Muller, A. C. van Veen, J. A. Lercher, *J. Phys. Chem. C* **2014**, *118*, 6122-6131.
- [55] I. A. Bakare, O. Muraza, M. Yoshioka, Z. H. Yamani, T. Yokoi, *Cat. Sci. Tech.* **2016**.
- [56] a) S. Zhang, B. Zhang, Z. Gao, Y. Han, *React. Kinet. Mech. Cat.* **2010**, *99*, 447-453; b) S. Zhang, B. Zhang, Z. Gao, Y. Han, *Ind. Eng. Chem. Res.* **2010**, *49*, 2103-2106.
- [57] a) M. Sawa, M. Niwa, Y. Murakami, *Appl. Catal., A* **1989**, *53*, 169-181; b) M. Sawa, K. Kato, K. Hirota, M. Niwa, Y. Murakami, *Appl. Catal., A* **1990**, *64*, 297-308.
- [58] N. Davidova, D. Shopov, N. Jaeger, G. Schulzেকloff, *React. Kinet. Catal. Lett.* **1979**, *12*, 229-234.

Part I. 8-Ring Zeolites



Chapter

2

Methanol-to-Olefins Process over Zeolite Catalysts with DDR Topology: Effect of Composition and Structural Defects on Catalytic Performance

A systematic study of the effect of physicochemical properties affecting catalyst deactivation, overall olefin selectivity and ethylene/propylene ratio during the methanol-to-olefins (MTO) process is presented for two zeolites with the DDR topology, namely Sigma-1 and ZSM-58. Both catalysts show high selectivity towards light olefins and completely suppress the formation of hydrocarbons larger than C₄, with selectivity to ethane not exceeding 1% and some traces of propane. By applying seeded growth approach, a series of Sigma-1 zeolites with tunable crystal size and acidity was synthesized. For this series the highest methanol throughput at 450 °C before deactivation was found for crystals 0.5 μm in size with an acidity corresponding to 0.5 Al atoms per zeolite cage, and a selectivity to ethylene and propylene reaching 90%. Comparison between ZSM-58 and Sigma-1 catalysts with similar morphologies and acidity under the same process conditions revealed a three times higher throughput of methanol in case of ZSM-58. The analysis of functional surface groups, assessed through FT-IR, revealed the presence of internal silanols and silanol nests due to the multiple defects in Sigma-1 responsible for faster catalyst deactivation. These silanol defects can be selectively removed (confirmed by FT-IR) from the zeolite framework by applying a mild treatment in presence of NaOH/CTAB, leading to an improved catalyst lifetime. Co-feeding experiments with short olefins and water show low reactivity of primary MTO products, which only react at the surface of the catalyst particles. These results demonstrate that migration of the reaction zone in case of DDR catalysts hardly affects catalyst stability, product composition and nature of deactivating species. The nature of these species depends mostly on reaction temperature: at low temperatures deactivation occurs mainly due to the formation of inert adamantane species, while at high temperatures poly-condensed aromatic hydrocarbons play a major role in deactivation.

This Chapter is based on the following publication:

I. Yarulina, J. Goetze, C. Gücüyener, L. van Thiel, A. Dikhtiarenko, J. Ruiz-Martinez, B. M. Weckhuysen, J. Gascon, F. Kapteijn, *Cat. Sci. Tech.* **2016**, *6*, 2663-2678

2.1. Introduction.

Due to the growing demand for propylene and ethylene, the search for efficient alternative routes to the synthesis of light olefins is now at the forefront of industrial and academic research.^[1] Among these routes, the methanol-to-hydrocarbons (MTH) conversion^[2] has gained a lot of attention during the last few decades.

The reaction pathway includes conversion of methanol over acidic zeolites, with SAPO-34 (CHA) and ZSM-5 (MFI) being successfully implemented in industry.^[3] Several alternative processes are commercially available, and most of these rely on zeolite ZSM-5 as catalyst. These include the Mobil Oil MTG process, the Topsøe integrated gasoline synthesis (TIGAS) process, and the Lurgi methanol-to-propylene (MTP) process.^[3] In the latter case, the selectivity is optimized towards propylene rather than C5+ by tuning the reaction conditions (*i.e.*, high temperature and low pressure) and by recycling long chain hydrocarbons.^[4] In the Norsk Hydro/UOP methanol-to-olefins (MTO) process, mostly ethylene and propylene are produced using SAPO-34 as the catalyst material.^[5]

However, there are still several drawbacks associated with the relatively low stability of SAPO-34 towards multiple regenerations due to the presence of phosphorus in its framework, and to the broad product distribution when using ZSM-5. Furthermore, for both catalytic materials, the energy intensive separation of the olefin/paraffin product mixtures is a major disadvantage.

Facing the abovementioned issues, there is still a great interest in finding appropriate zeolite topologies that would deliver a narrower product distribution, while displaying an excellent stability. Preferably only ethylene and propylene should be produced, while control towards the formation of one of these products would be ideal. From this perspective, the search should continue taking small pore zeolites with large cavities into account. Such small pore zeolites are able to host inside their cavities the so-called "hydrocarbon pool" - the key intermediate, also containing stable inactive compounds causing deactivation,^[6] while allowing only small hydrocarbons to leave their cavities through smaller windows.

Recently, DDR was identified as a promising 8-ring zeolite structure for the MTO process.^[7] There are three zeolites belonging to the DDR family, namely DD3R,^[8] its pure silica version, and two Al-containing variants reported in literature, Sigma-1,^[9] and ZSM-58.^[10] Both DD3R and Sigma-1 are synthesized using adamantylamine as Structure Directing Agent (SDA), while methyltropylium iodide is employed for ZSM-58 synthesis.

The key properties of DDR were discovered while testing it in separation of olefin/paraffin mixtures.^[11] This material takes up only certain unsaturated molecules (ethylene, propylene, *trans* but-2-ene and butadiene),^{[12],[13]} while saturated C3 and C4 molecules are excluded. This molecular sieving exclusion principle based on zeolite topology should be responsible for the high selectivity to ethylene and propylene during the MTO process. In turn, the ethylene-to-propylene ratio could be tuned by varying operating conditions and/or physicochemical properties of the zeolite.^[14] A great deal of work has been devoted to the investigation of the effect of crystal size and acid strength on the MTO performance of

different zeolite frameworks focusing mainly on SAPO-34.^[15] However, in most cases the synthesis routes towards different morphologies and acidic composition involved a variation in SDAs, zeolite precursor composition or Si sources. Variation of these parameters might also lead to Al zoning,^[16] formation of structural defects in the zeolite framework,^[17] and other effects that would eventually affect reaction performance. Having said that, it is worth mentioning the recent findings for ZSM-5^[18] on the effect of coke formation governed by the presence of non-acidic silanol groups and internal defects. Though the correlation between amount of coke and internal defects has been established for ZSM-5, there are no studies confirming the same interdependence for other systems. As a consequence, there are no data available on healing/removing of these defects for other zeolites, especially for structures with 8-membered ring (8MR) pore openings.

In this work we systematically study the effect of physicochemical properties on catalyst deactivation, overall olefin selectivity and ethylene-to-propylene ratio using Sigma-1 and ZSM-58 zeolites with DDR topology as two case studies. All parameters were investigated independently, using always the same gel precursor composition, tuning zeolite morphology and acidity only by changing the amount of Al and by using as-synthesized material as seeds. By applying this approach, we could identify the effects of catalyst composition on reaction performance and the nature of species that lead to catalyst deactivation, with special emphasis on the effect of catalyst structural defects,^[17, 19] something often overlooked in the open literature for 8MR zeolites.

2.2. Experimental.

2.2.1. Synthesis of DDR Zeolites.

1-Adamantylamine (ADA, 97 %), colloidal silica (Ludox HS-40, 40 %), sodium aluminate (Al_2O_3 (50-56 %), Na_2O (40-45%)), ammonium nitrate (98%), hexadecyltrimethylammonium bromide (CTAB, $\geq 99\%$), sodium hydroxide ($\geq 98\%$), methyl iodide (99.5 %), tropine ($\geq 97\%$), methanol ($\geq 99.9\%$) were purchased from Sigma-Aldrich and used as received without any further purification.

Firstly, Sigma-1 crystals used for the preparation of seeds were synthesized at 180 °C for 6 days using a molar composition of ADA: Na_2O : SiO_2 : Al_2O_3 : H_2O = 20:3:60:1:2400 as described elsewhere, ADA being used as a template molecule.^[20] The obtained crystals were subjected to the wet ball-milling by using the procedure reported by Charkhi *et al.*^[21] as basis.

A Retsch mixer mill MM2 equipped with zirconia grinding jar of 10 mL and zirconium oxide grinding balls of 2 mm diameter in size were used for the wet-ball milling. In each step, 2 g zeolite was wet ball milled using 9 g zirconium oxide balls in 2 mL deionized water medium for 4 h with a vibrational frequency of 50 Hz. After each wet-ball milling, zirconium oxide balls were washed with approximately 30 mL (± 5 mL) of deionized water and separated from the solution. This solution was then centrifuged for 12 min to obtain a mother liquor with particles smaller than 200 nm. After removal of the mother liquor, precipitated powder was dried overnight at 80°C and used in the next wet-ball milling step. Due to low

yield in the first two wet-ball milling steps, the mother liquor obtained at these stages was added to the deionized water used in the next stages during cleaning of the zirconia balls to avoid unnecessary dilution. From the 3rd step on, approximately 8 mL mother liquor was obtained from each step of the wet-ball milling. After 12 subsequent wet-ball milling steps, 80 mL of 0.5 wt% seeding solution with a 6-6.5 pH was obtained.

Subsequent syntheses were performed by addition of either ball-milled or as-synthesized crystals (0.1 wt.%) with molar composition of ADA:Na₂O:SiO₂:Al₂O₃:H₂O = 20:3:60:x:2400, reducing synthesis time from 6 days to 8 - 20 h depending on the Al content.

The as-synthesized materials were calcined at 650°C for 10 h in a static oven. The calcined samples were ion-exchanged three times in aqueous NH₄NO₃ solution (1 M, 80°C, 2 h, 100 mL per gram of zeolite) followed by calcination at 550°C.

A modified sample was obtained by treating calcined at 650°C Sigma-1 with 20 ml solution per gram of zeolite of 0.075 M NaOH and 0.5 M CTAB solution.^[22] This modified sample was further subjected to calcination at 550°C to remove CTAB followed by ion-exchange as outlined above.

ZSM-58 crystals were synthesized as reported elsewhere using methyltropylium iodide (MTI) as template,^[7] keeping the SiO₂/Al₂O₃ ratio 110, and subjected to calcination and ion-exchange as described above.

MTI was prepared by adding drop-wise 25.1 g methyl iodide to a solution 25.0 g tropine in 100 g ethanol at 0°C. The resulted suspension was left for 3 days for stirring. After washing with 100 g ethanol and filtering, the resulted powder was dried at 80 °C for 12 h.

2.2.2. Catalyst Characterization.

The XRD patterns of the powders are recorded in Bragg–Brentano geometry with a Bruker D8 Advance X-ray diffractometer equipped with a LynxEye position-sensitive detector. Measurements were performed at RT by using monochromatic CoK α ($\lambda=1.788970$ Å) radiation between $2\theta=5^\circ$ and 50° .

The Pawley fitting of the experimental data was performed using Reflex Plus module of the Accelrys Material Studio software package. The refinement of unit cell parameters giving values of $a = b = 13.8068(1)$ Å, $c = 40.8500(1)$ Å, $\beta = \alpha = 90^\circ$, $\gamma = 120^\circ$ suggested a close agreement with the one expected for DDR zeolite as reported in the Atlas of Zeolite Framework Types.^[23] Zero offset, the scale factor, six background terms and profile parameters were refined during Pawley fitting. The profiles have been modeled as a pseudo-Voigt function. Corresponding refinement results are summarized in Table A1 and plotted in Figure A1 in Appendix A.

Images were recorded using a JEOL JSM-6010LA with a standard beam potential of 10 kV and an Everhart-Thornley detector. X-ray microanalysis (SEM/EDX) confirmed the elemental composition in the sample by scanning microscopy (SEM) coupled with a dispersive X-ray microanalysis system (EDX) with a Silicon-drift detector.

Elemental analysis was performed with PerkinElmer Optima 4300 DV instrument. The samples were first digested in an aqueous mixture of 1% HF and 1.25% H₂SO₄. After dilution, analysis was done by inductively coupled plasma optical emission spectrometry (ICP-OES).

N₂ adsorption was carried out using Tristar II 3020 Micromeritics at -196°C. Prior to the experiment, samples were outgassed at 350°C for 16 h.

Temperature-programmed NH₃ desorption (NH₃-TPD) was measured by AutoChem II chemisorption analyzer (Micromeritics). Approximately 0.2 g material was first degassed under He flow at 400°C and then saturated with NH₃ at 200°C during 1 h using a flow of 1.65 % NH₃ in He. The gas mixture was then switched back to He and the sample was purged at 200°C for about 1 h to remove weakly adsorbed NH₃ molecules. TPD was subsequently recorded under He flow, from 200°C to 800°C. All flow rates were adjusted to 25 mL min⁻¹, and the heating rates were 10°C min⁻¹ during different stages of experiment.

Transmission FT-IR spectroscopy was performed using a Nicolet Nexus spectrometer at 4 cm⁻¹ resolution equipped with an extended KBr beam splitting and a mercury cadmium telluride (MCT) cryo-detector. The pellets were placed in an IR quartz cell equipped with CaF₂ windows. A movable sample holder allows the sample to be placed in the infrared beam for the measurements or into the furnace for thermal treatments. The cell is connected to a vacuum line for pretreatment. The specimen is activated in vacuum at 400°C for 16 h to remove adsorbed species. After this step, the samples were cooled down to -130°C and CO was dosed up to 30 mbar.

Thermogravimetric analysis (TGA) was performed by means of a Mettler Toledo TGA/SDTA851e on 20 mg samples under flowing 100 mL/min air at a heating rate of 5°C min⁻¹ up to 1000°C. The amount of coke formed during the reaction was calculated from the weight loss between 150°C and 800°C for completely deactivated catalysts (after feeding at least 10 g methanol/g zeolite).

DRIFTS analysis was carried out in a Thermo Scientific Nicolet 8700 spectrometer, equipped with a high-temperature cell with CaF₂ windows (HVC Praying Mantis Harrick) and a DGTS detector. The spectra were collected after 128 scans and a resolution of 4 cm⁻¹, under 20 mL min⁻¹ He flow. KBr spectra (at given temperatures) are used as background. Before collecting the spectra, samples deactivated after 5 h MTO process were preheated in a He flow at 120°C for 60 min to remove water.

Hydrocarbons that were retained in the catalyst after testing were investigated by dissolution experiments. Typically, 15 mg spent catalyst was dissolved in 1 mL 50% HF in a Teflon container. The organic compounds were extracted from the water phase by the addition of three times 1 mL CH₂Cl₂. Analysis of the extracted phase was performed on a GCMS-QP2010Ultra GC/MS system, equipped with a Zoex ZX1 thermal modulator and an Agilent VF-5ms and VF-17ms column in series. Hereinafter, the term 'retained hydrocarbons' or 'coke' is used to describe all compounds that are detectable by this method.

2.2.3. Catalyst Testing.

Catalytic experiments were carried out in a Microactivity Reference unit (PID Eng&Tech) at 380°C - 475°C and ambient pressure. The catalyst (1.75 g, 250-420 µm sieve fraction) was placed in a fixed-bed with internal diameter 9 mm. An HPLC pump (307 5-SC-type piston pump, Gilson) was used to feed methanol to the reactor system. The temperature was recorded by a thermocouple placed in the middle of the catalytic bed. A weight-hourly space velocity (WHSV) of 2 g_{MeOH} g_{cat}⁻¹ h⁻¹, a 1:1 molar feed composition of N₂ and MeOH and atmospheric pressure are applied and referred to as standard operating conditions at the different temperatures. Quasi isothermal conditions were achieved without any diluent (Figure A2 in Appendix A) unlike the case of the more active ZSM-5 requiring dilution with SiC elaborated further in Chapter 4.^[24]

The product mixture was analyzed online with an Interscience CompactGC equipped with a 15 m capillary RTX-1 (1% diphenyl-, 99% dimethylpolysiloxane) column.

Conversion, selectivities and yields were calculated on a molar carbon basis. Thus, conversion was defined as the fraction of light oxygenates (methanol and dimethyl ether) consumed during the process:

$$X = \frac{n_{C,MeOH_{in}} - n_{C,oxy_{out}}}{n_{C,MeOH_{in}}} \cdot 100\% \quad (1)$$

the selectivity towards ethylene (2) and propylene (3) was calculated based on the carbon number as follows:

$$S_{ethylene} = \frac{2 \cdot n_{C_2H_4}}{n_{C,MeOH_{in}} - n_{C,oxy_{out}}} \cdot 100\% \quad (2)$$

$$S_{propylene} = \frac{3 \cdot n_{C_3H_6}}{n_{C,MeOH_{in}} - n_{C,oxy_{out}}} \cdot 100\% \quad (3)$$

and the yield of a component *i* was defined from its selectivity and methanol conversion:

$$Y_i = \frac{S_i \cdot X}{100} \quad (4)$$

Total molar flow rate at the outlet ϕ_{out} was calculated based on the N₂ flow as an internal standard and its molar fraction y_{N_2} in the outlet flow (Equation 5). Since N₂ is an inert gas, its flow rate is equal to the inlet one.

$$y_{N_2} = \frac{\phi_{N_2}}{\phi_{N_2} + \phi_{out}} \quad (5)$$

Prior to each experiment, mixture containing N₂ and MeOH was bypassed through the reactor to GC to calculate response factors. In turn, response factors for individual products were obtained by calibration with a gas mixture containing all hydrocarbons up to C5.

Hence, the molar flowrate of a component *i* (ϕ_i) could be calculated from the Equation 6:

$$\phi_i = y_i \cdot (\phi_{N_2} + \phi_{out}) \quad (6)$$

Table 1. Catalytic properties of the zeolites with the DDR topology under study.

Sample	SiO ₂ /Al ₂ O ₃ ^a (mol mol ⁻¹)	SiO ₂ /Al ₂ O ₃ ^b (mol mol ⁻¹)	NH ₃ capacity ^c (mmol NH ₃ g ⁻¹)	Throughput (g _{MeOH} g _{cat} ⁻¹)	C2 ⁷ /C3 ^{3d} (mol mol ⁻¹)	C2 ⁷ /C2 ^d (mol mol ⁻¹)	C3 ⁷ /C3 ^d (mol mol ⁻¹)	Coke ^e (wt.%)
Sigma1-120-M	120	117	0.281	1.3	0.7	21	>>10 ³	8.1
Sigma1-210-M	200	207	0.160	2.0	-	-	-	-
Sigma1-315-M	399	314	0.105	2.5	1.0	39	>>10 ³	10.5
Sigma1-415-M	724	417	0.080	2.5	-	-	-	-
Sigma1-315-L	406	317	0.105	1.6	0.8	34	>>10 ³	9.6
Sigma1-315-S	420	317	0.105	3.6	1.1	52	>>10 ³	11.7
Sigma1-315-S-m	404	317	0.104	6.5	1.0	62	>>10 ³	12.1
ZSM-58	110	111	0.296	4.5	-	-	-	11.8

^a determined from ICP. ^{b,c} determined from NH₃-TPD. ^d calculated from Table A2 based on integral selectivities. ^e from TGA measurements of spent catalysts used at 450°C

Table 2. Catalytic properties of the zeolites with the DDR topology under the study.

Sample	Particle size ^a (μm)	S _{meso} ^b (m ² g ⁻¹)	S _{BET} ^c (m ² g ⁻¹)
Sigma1-120-M	2.7	20	313
Sigma1-210-M	2.7	14	349
Sigma1-315-M	2.4	7	364
Sigma1-415-M	2.5	5	371
Sigma1-315-L	4.6	12	340
Sigma1-315-S	0.5	15	357
Sigma1-315-S-m	0.5	51	403
ZSM-58	0.6-1.8	22	372

^a determined from SEM. ^b t-Plot method. ^c BET plot applied to the N₂ isotherm.

where y_i is the molar fraction of component i in the N₂ diluted gas phase and is directly obtained from GC analysis.^[25]

The performance results are presented in graphs as a function of the methanol throughput per amount of catalyst used (g_{MeOH} g_{cat}⁻¹). The methanol conversion is an apparent one as it reflects the disappearance of this component, which can be due to chemical conversion or to retention on the catalyst. Parameters related to catalyst performance are summarized in Table 1.

Methanol throughput before deactivation is defined as overall MeOH throughput fed through the catalytic bed before the breakthrough of oxygenates ($X \approx 98\%$), indicating deactivation. Turnover numbers (TON) are defined as the total amount of MeOH converted per Brønsted Acid Site (BAS) before the conversion decreases below 98%. The amount of BAS was calculated from NH₃-TPD. Ethylene / propylene (C2/C3) ratios (Table 1) are calculated for the experiments carried out at 450°C taking into account integral selectivities.

Co-feeding experiments were performed keeping N₂ flowrates equal to the ones used in MTO experiments and adding ethylene, propylene and/or water flows to obtain the desired mixtures.

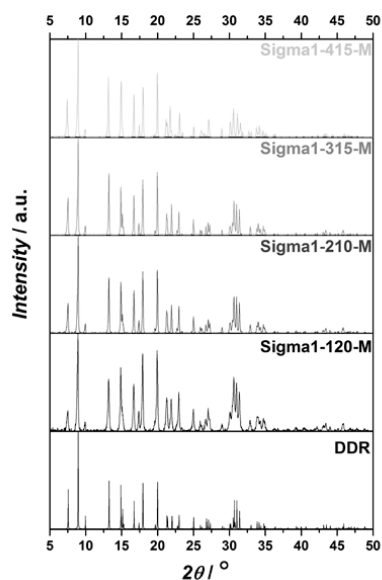


Figure 1. XRD patterns of calcined Sigma-1 zeolites compared with the DDR powder patterns.

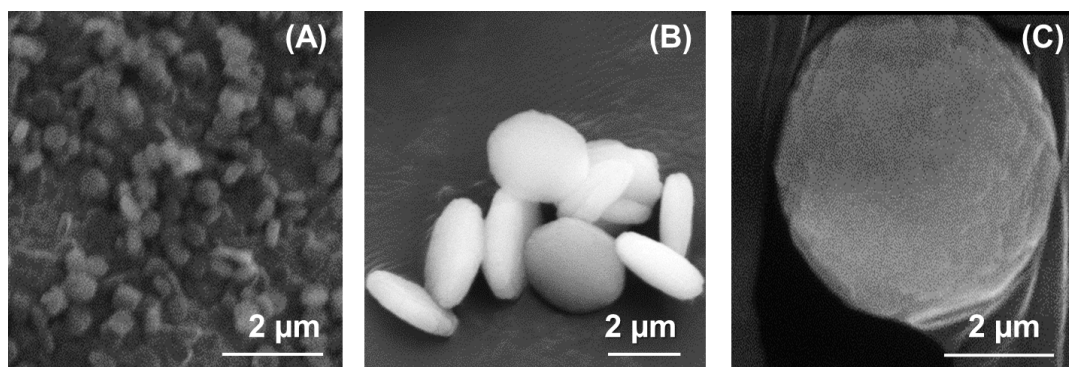


Figure 2. SEM micrographs of (A) Sigma1-315-S (B) Sigma1-315-M (C) Sigma1-315-L with $\text{SiO}_2/\text{Al}_2\text{O}_3 = 315$.

Typically, after testing a catalyst for 5 h to ensure almost complete deactivation, the MeOH flow was stopped and the catalyst was cooled down under N_2 flow. Later, the spent catalyst was transferred into a vial for further analysis of the trapped species.

2.3. Results.

In this section the main properties and catalytic performance of the synthesized zeolites are described: (i) a series of Sigma-1 catalysts with different composition and particle size, (ii) a post-synthetically treated Sigma-1 catalyst and (iii) a series of ZSM-58 catalysts, produced with a different template.

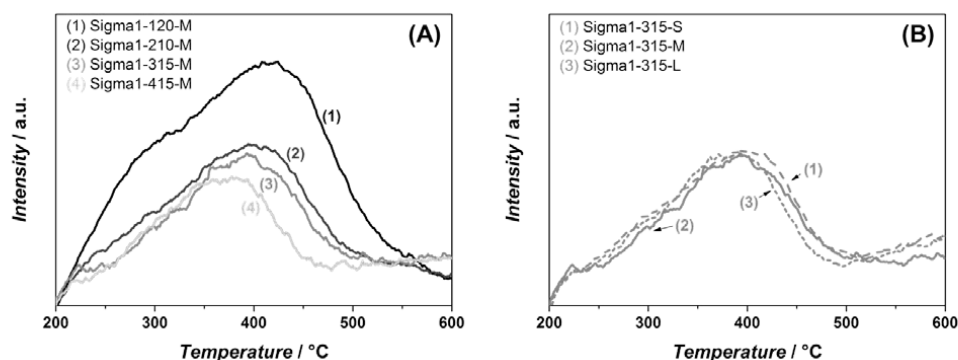


Figure 3. NH_3 TPD profiles of Sigma-1 zeolites with different $\text{SiO}_2/\text{Al}_2\text{O}_3$ ratio and medium crystal size (A), and of different crystal sizes with $\text{SiO}_2/\text{Al}_2\text{O}_3$ ratio = 315 (B).

2.3.1. Synthesis and Characterization of Sigma-1 zeolite.

Powder XRD patterns shown in Figure 1 together with reference peaks for DDR topology confirm that the synthesized catalysts consist only of pure DDR phase. SEM micrographs of zeolites synthesized with the same composition, but using different size of seeds are shown in Figure 2. By using seeds with crystal sizes of 0.08, 0.5 and 2.5 μm , zeolites of 0.5, 2.5 and 4.6 μm with very narrow size distributions can be synthesized, respectively. The formed crystallites have a similar aspect ratio, with round slab shape. On the basis of their crystal size and NH_3 TPD results (Table 1, 2), the zeolites are denoted as Sigma1-X-Y, where X refers to the actual $\text{SiO}_2/\text{Al}_2\text{O}_3$ ratio (120, 210, 315, 415), while Y is related to crystal size (S – 0.5 μm ; M – 2.5 μm ; L – 4.6 μm). On the basis of the same nomenclature, the modified sample is denoted as Sigma1-315-S-m. When analyzing image of Sigma1-315-L (Figure 2C), the observed intergrowth and aggregation infers an adhesive mechanism of growth, characteristic of the secondary growth mechanism taking place in the presence of seeds.^[26]

The acidic properties of the synthesized materials were assessed by NH_3 TPD (Figure 3). For all samples, the desorption peak at high temperatures is assigned to the desorption of ammonia from Brønsted acid sites.^[7] Both the amount and the strength of acidity correlate well with the amount of Al in the zeolite. The more Al in the zeolite the more acid sites, while the maximum of the desorption peak shifts from 420°C (Sigma1-120-M) to 375°C (Sigma1-415-M), indicating the weakening of acid sites with decreasing of Al content. Similar desorption temperatures for Sigma1-415-M, Sigma1-315-M and Sigma1-210-M indicate that their acid sites are isolated and possess a similar acid strength. The desorption peak of Sigma1-120-M is also characterized by a shoulder at 300°C, indicating the presence of weaker Lewis acidity. Comparison of acidic properties of zeolites with similar composition, but different crystal size does not reveal any changes either in the amount of acid sites or in their acid strength.

Additionally, FT-IR spectroscopy of adsorbed CO (Figure 4) was studied on Sigma1-120-M (A₁, A₂), ZSM-58 (B₁, B₂), Sigma1-315-S (C₁, C₂) and Sigma1-315-S-m (D₁, D₂) in order to assess surface groups

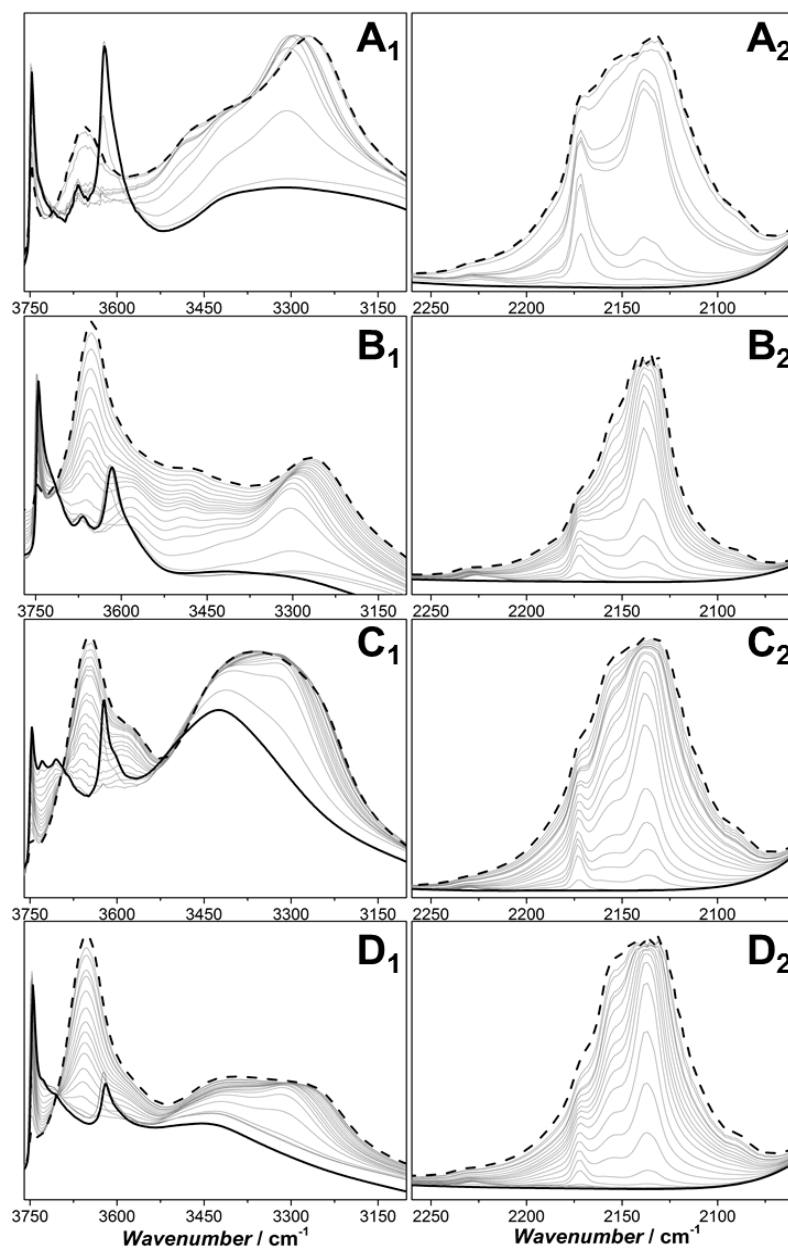


Figure 4. FT-IR spectra measured at $-130\text{ }^{\circ}\text{C}$ after increasing dosages of CO on (A) Sigma1-120-M; (B) ZSM-58; (C) Sigma1-315-S; (D) Sigma1-315-S-m. Panels A₁, B₁, C₁ and D₁ report the spectra in the hydroxyl group range ($3760\text{-}3100\text{ cm}^{-1}$), while panels A₂, B₂, C₂ and D₂ report the CO vibrational mode region ($2260\text{-}2060\text{ cm}^{-1}$). The bold solid line corresponds to the pre-treated catalysts in vacuum, while the dashed black curves represent spectra collected at 30 mbar CO equilibrium.

and acid strength. The FT-IR spectra of pretreated samples show a complex absorption with a maximum

at 3747-3745 cm^{-1} attributed to terminal Si-OH hydroxyl groups, located at the internal and external surface of the zeolite.^[27] Sigma1-315-S is also characterized by the presence of a triplet with maxima at 3747 cm^{-1} (HF), 3729 cm^{-1} (LF) and 3706 cm^{-1} (LF). The latter two represent vicinal silanol groups where only oxygen participates in H-bonding and the proton is relatively mobile.^[28] Further analysis reveals absorption bands around 3668 cm^{-1} for Sigma1-120-M and ZSM-58, pointing to the presence of extra-framework Al. An absorption band with a maximum at 3616 cm^{-1} is observed for all samples and represents Brønsted acidic OH groups. The broad band at about 3450 cm^{-1} , which is especially prominent for Sigma1-120-M (Figure 4A₁) and Sigma1-315-S (Figure 4C₁), suggests the presence of silanol nests originating from structural defects.^[29] Upon interaction with CO, the bands associated with Brønsted acidity decrease at the same time as a band at $\sim 3300 \text{ cm}^{-1}$ develops. The exact position of this band and shift in σ_{OH} is different for each sample: $\Delta\sigma_{\text{OH}} = 355 \text{ cm}^{-1}$ (Sigma1-120-M), $\Delta\sigma_{\text{OH}} = 351 \text{ cm}^{-1}$ (ZSM-58), $\Delta\sigma_{\text{OH}} = 313 \text{ cm}^{-1}$ (Sigma1-315-S), $\Delta\sigma_{\text{OH}} = 317 \text{ cm}^{-1}$ (Sigma1-315-S-m). The higher the $\text{SiO}_2/\text{Al}_2\text{O}_3$ ratio, the lower is the $\Delta\sigma_{\text{OH}}$, indicating lower acid strength, in agreement with NH_3 TPD results.

In the CO stretching region (Figure 4, panels A₂, B₂, C₂, D₂), a band located at 2171 cm^{-1} appears at low CO coverage.^[14a] This component arises from the interaction with strong Brønsted acid sites. At high CO coverage, the bands at about 2156 and 2138 cm^{-1} become more prominent, corresponding to CO interacting with silanol groups and liquid-like CO condensed in the zeolite pores, respectively. It should be also mentioned that the CO region is additionally characterized by the presence of components at 2227 cm^{-1} , protuberant for Sigma1-120-M and ZSM-58 (Figure 4, panels A₂, B₂). They are tentatively assigned to CO adsorbed on extraframework Al^{3+} .^[30]

2.3.2. Catalytic Results.

As previously reported by Kumita *et al.*^[7] for DDR catalysts, no olefins bigger than C5 are observed when Sigma-1 is used as catalyst, independently of the applied process conditions. In addition, the formation of paraffins is very low, with ethane yields lower than 1% and some traces of propane (Table 1). Formation of DME is only observed once MeOH conversion drops below 100% becoming the main product at the catalyst deactivation stage. The overall product distribution of catalysts is reported in Appendix A (Table A2).

In the next paragraphs, the effect of process conditions on catalyst life-time and selectivity is extensively described.

2.3.2.1. Effect of Temperature.

Figure 5 summarizes results obtained for Sigma1-315-M catalysts over the range of temperatures between 380 and 475°C. The MeOH throughput before deactivation (Figure 5A) increases with increasing reaction temperature, however without significant changes between 450 and 475°C. As reported elsewhere,^[31] higher temperatures favor ethylene formation (maximum yield 44 %), while

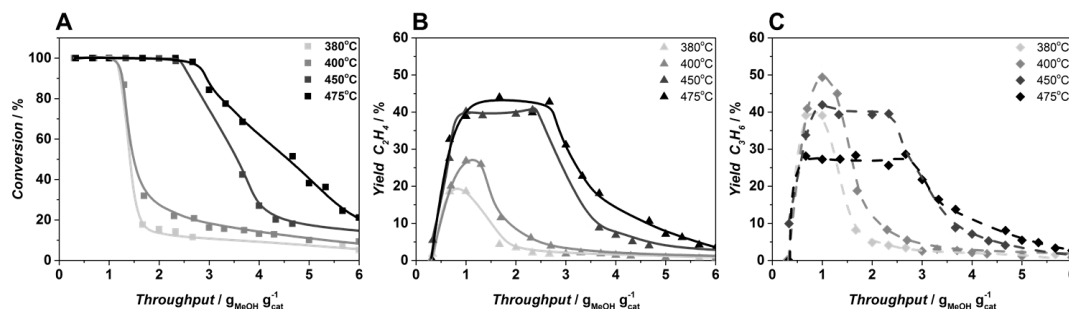


Figure 5. Methanol conversion (A), yield of ethylene (B) and propylene (C) at 380°C (□, ▲, ◆), 400°C (■, ▲, ◆), 450°C (■, ▲, ◆) and 475°C (■, ▲, ◆) obtained in MTO process over Sigma1-315-M zeolite with SiO₂/Al₂O₃ = 315 and crystal size of 2.5 μm at standard operation conditions.

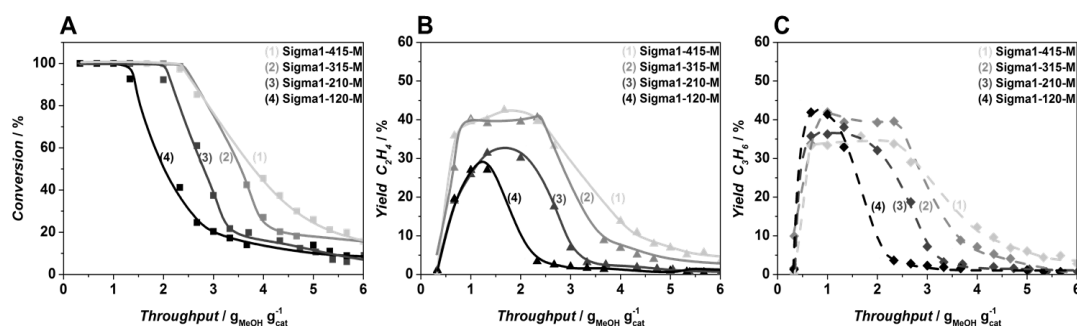


Figure 6. Methanol conversion (A), yield of ethylene (B) and propylene (C) at 450 °C, obtained in MTO process over Sigma1-415-M (■, ▲, ◆), Sigma1-315-M (■, ▲, ◆), Sigma1-210-M (■, ▲, ◆), and Sigma1-120-M (■, ▲, ◆) zeolite at standard operation conditions.

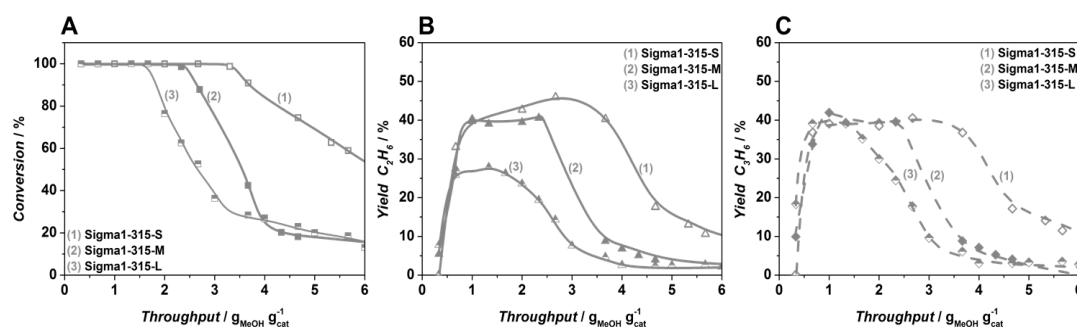


Figure 7. Methanol conversion (A), yield of ethylene (B) and propylene (C) at 450 °C, obtained in MTO process over Sigma1-315-S (□, △, ◇), Sigma1-315-M (■, ▲, ◆), Sigma1-315-L (◇, △, □) zeolite at standard operation conditions.

propylene is the main product at lower temperatures, with yields as high as 50 %. The ethylene-to-propylene ratio varies from 0.5 to 1.6 when comparing results for 380°C and 475°C, while the maximum overall yield of ethylene and propylene together reaches 83 % at 450°C. The yield of butenes follows the

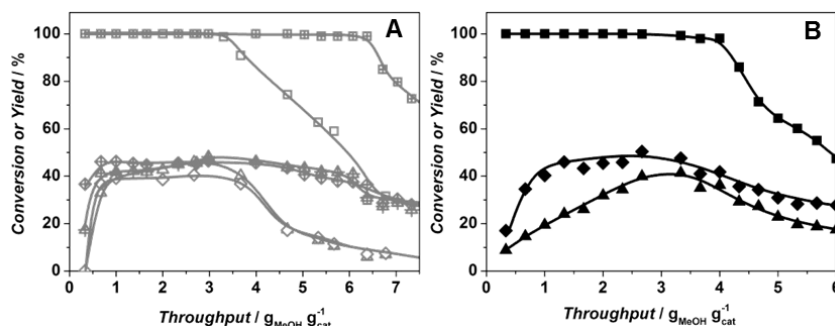


Figure 8. Methanol conversion (■), ethylene (▲) and propylene (◆) yields of (A) Sigma1-315-S (□, △, ◇) and Sigma1-315-S-m (▣, ▤, ▥); (B) ZSM-58 (■, ▲, ◆) ($\text{SiO}_2/\text{Al}_2\text{O}_3 = 110$, 0.6-1.8 μm) at 450 °C and standard operation conditions.

same trend as propylene, reaching a maximum of 14 % at 380°C and not exceeding 5 % at 475°C. Based on these results and on additional experiments performed at varying the Si/Al ratio, 450°C was chosen as the optimal reaction temperature and will be used as reference condition to compare the different Sigma-1 catalysts.

2.3.2.2. Effect of $\text{SiO}_2/\text{Al}_2\text{O}_3$ Ratio.

In order to investigate the effect of the amount of acid sites and their strength on catalytic activity and selectivity, catalysts with different $\text{SiO}_2/\text{Al}_2\text{O}_3$ ratios were synthesized while maintaining the mean crystallite size. Figure 6A compares catalytic performance at 450°C for four Sigma-1 zeolites with different acidity, but the same crystal size. The methanol throughput is inversely related to the amount of Al in the system, the difference in catalytic activity becoming less pronounced at high $\text{SiO}_2/\text{Al}_2\text{O}_3$ ratio. Thus, in both cases, for Sigma1-415-M and Sigma1-315-M, deactivation occurs after feeding 2.5 g of methanol per gram of catalyst. Based on the comparable catalytic activity of the abovementioned catalysts, a similar product distribution was expected, which is observed only for the yield towards ethylene. The maximum ethylene yield (Figure 6B) increases from 28 % (Sigma1-120-M) up to 43 % (Sigma1-415-M), being the highest for the least acidic zeolite. The opposite trend is observed for the propylene yield (Figure 6C): the highest yield (43 %) is monitored for Sigma1-120-M. To sum up, the C2/C3 ratio increases from 0.7 (Sigma1-120-M) to 1.3 (Sigma1-415) and the maximum overall yield (ethylene plus propylene) of 83 % is observed for Sigma1-315-M. Therefore the effect of crystal size was further investigated using the $\text{SiO}_2/\text{Al}_2\text{O}_3$ ratio of 315.

2.3.2.3. Effect of Crystal Size.

Methanol conversion and yield to ethylene and propylene as a function of time on stream for zeolite Sigma1-315-M with crystal size 0.5, 2.5, and 4.6 μm are shown in Figure 7. In line with previous reports,^[32] a strong interdependence of MeOH throughput before deactivation with crystal size is observed, namely the methanol throughput increases from 1.6 g/g to 3.6 g/g when comparing Sigma1-

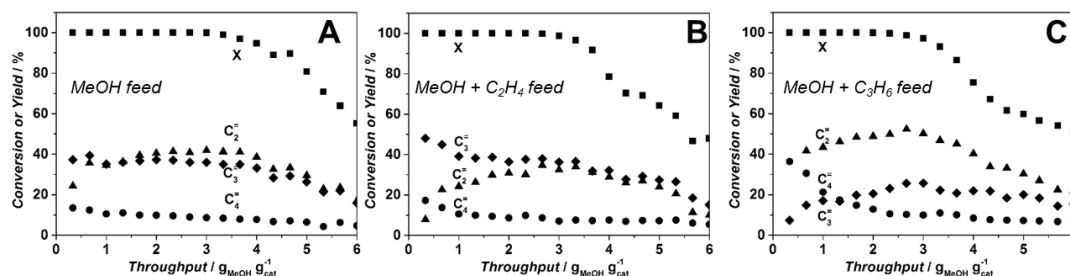


Figure 9. Methanol conversion (■), ethylene (▲), propylene (◆) and butenes (●) yields obtained over Sigma1-315-S tested at 450°C and standard operating conditions (A) 50%MeOH + 50% N₂; (B) 45%MeOH + 10%C₂H₄ + 45%N₂; (C) 45%MeOH + 10%C₃H₆ + 45%N₂.

315-L and Sigma1-315-S. In turn, ethylene yield increases from 28 % to 46 % with decreasing crystal size, while the propylene yield remains around 40 % for all samples. Crystal size does not affect the yield for butenes either, in both cases it is about 10 %, therefore the observed difference is attributed to the increased selectivity towards coke in the zeolite cages.

The catalytic performance of Sigma1-315-S-m, resulting from mild post-synthetic modification of Sigma1-315-S, shows a significantly increased overall MeOH throughput before deactivation from 3.6 to 6.6 g/g with a slight increase of propylene yield up to 45 % (Figure 8A).

2.3.2.4. ZSM-58 with a SiO₂/Al₂O₃ Ratio of 110.

Figure 8B shows results of catalytic performance of another DDR-type zeolite, ZSM-58, with SiO₂/Al₂O₃ = 110 synthesized for the sake of comparison with Sigma-1. The MeOH throughput reaches 4.6 g/g, being around three times higher in comparison with Sigma1-120-M (Figure 6A), the zeolite with the closest physicochemical characteristics. Ethylene and propylene yield steadily increase up to 40 and 50 %, respectively, after which deactivation starts and MeOH conversion to hydrocarbons rapidly drops.

2.3.2.5. Co-feeding experiments.

To estimate the reactivity of the main products, ethylene and propylene, and the effect of their presence on product distribution, co-feeding experiments were performed by addition of 10 % of olefin to the initial reaction mixture used in the above-described experiments. Figure 9 shows that the presence of olefins does not affect catalyst lifetime, as the MeOH throughput before deactivation reaches 3.6 g MeOH per gram of catalyst in all cases. In contrast, some differences can be found upon investigation of product yields. Co-feeding of ethylene leads, during the first reaction minutes, to an increased propylene yield of 50% instead of the initial 39% observed in the experiment without co-feeding.

This increase in propylene yield seems to be at the expense of ethylene formation. However, after having fed 2 g MeOH per gram of catalyst, the product distribution changes with decreasing propylene yield and increasing ethylene yield, becoming similar to the yields when only MeOH was fed (Figure 9A and 9B). Co-feeding of propylene, however, affects mainly formation of butenes, especially during the

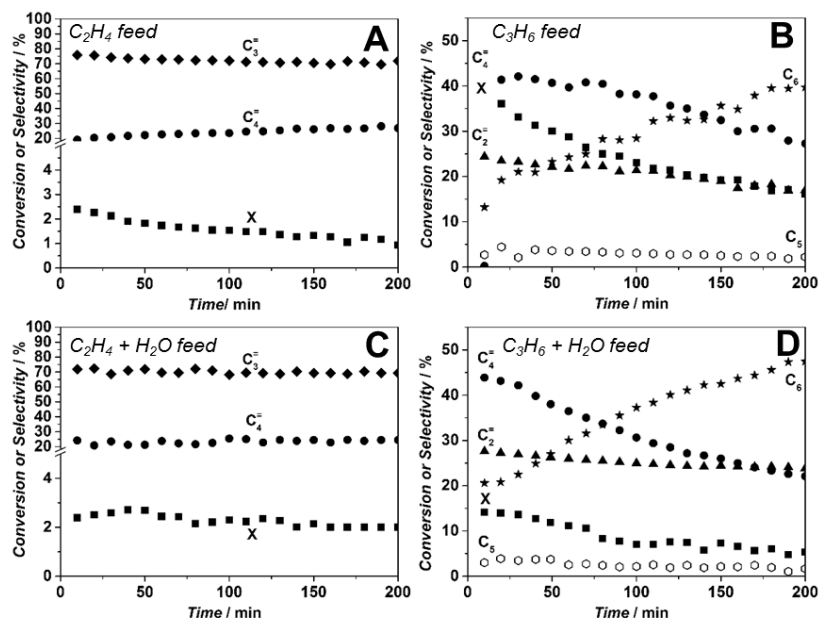


Figure 10. Product distribution in co-feeding experiments performed over Sigma1-315-S at 450 °C (a) 10% C_2H_4 + 90% N_2 ; (b) 10% C_3H_6 + 90% N_2 ; (c) 45% H_2O + 10% C_2H_4 + 45% N_2 ; (d) 45% H_2O + 10% C_3H_6 + 45% N_2 .

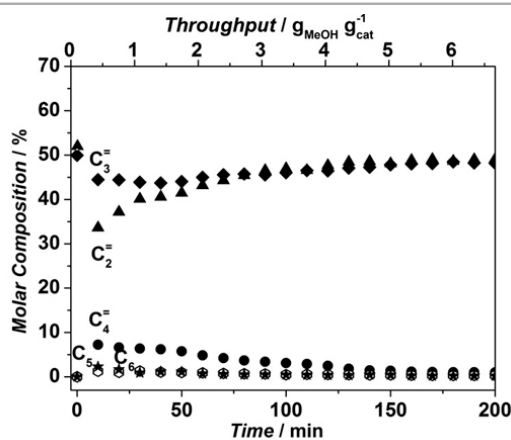


Figure 11. Product distribution in co-feeding C_2H_4 and C_3H_6 in the presence of water over Sigma1-315-S at 450°C.

first minutes of the reaction (40% vs. 20% without co-feeding). Nevertheless, the butenes yield rapidly drops to a constant level of 10%, while the ethylene yield reaches 53% at the expense of a lower formation of propylene (26%) suggesting, a higher probability of propylene to participate in consecutive reactions.

Furthermore, as was shown by Schulz,^[33] the reaction zone in a catalytic bed tends to migrate through the bed, *i.e.* first MeOH reacts in the first (upper) part of the catalytic bed, once the hydrocarbon pool is formed, the reaction front moves slowly downstream. Therefore it is essential to find out whether the formed olefins can undergo subsequent conversion in the absence of MeOH. For that reason, experiments were performed mimicking the bottom part.

Figure 10 (A and C) shows that feeding either ethylene or ethylene/water mixtures lead to a negligible conversion of around 2%, with the formation of propylene and butenes (80 and 20%, respectively). Addition of water only seems to maintain this ethylene conversion for longer periods (Figure 10C). When propylene is fed in the absence of water, an initial conversion of 40% is observed, quickly dropping to 20% (Figure 10B). The product stream in this case contains ethylene, butenes and C6 hydrocarbons. However, when water is co-fed together with propylene, simulating a situation much closer to that of the bottom bed during MTO operation, much lower initial conversions are observed (Figure 10D). In this case, the initial conversion of 15% rapidly dropped to around 6% and stayed at the same level, with a product distribution being close to the one where only propylene was fed. Interestingly, apart from butenes and ethylene, the product composition also included some C5 and up to 45% C6 hydrocarbons, something not observed for the MTO experiments using catalysts with the DDR topology.

After feeding propylene, the catalyst was subjected to the MTO reaction at standard operating conditions to see whether the C5 and C6 hydrocarbon formation was indicative for catalyst deactivation. However, the observed catalyst lifetime and selectivities were identical to the ones shown on the Figure 9A in an ordinary MTO experiment, indicating that these C5 and C6 species are formed on the external surface of the zeolite and do not affect coke formation related to MTO inside the zeolite cage.

Finally, as the product mixture obtained from Sigma1-315-S tested at 450 °C consisted mainly of ethylene and propylene, also an experiment co-feeding ethylene, propylene and water was performed to mimic a situation where olefins can react with each other in absence of MeOH. Figure 11 shows that although initially the product mixture contained equal molar amounts of ethylene and propylene, both decreased upon formation of butenes and some very small amounts of C5 and C6 products. Initially, ethylene was consumed more than propylene in this experiment, and their conversion gradually declined until the composition returned to that of the feed mixture. The amount of butenes formed followed the ethylene and propylene conversion. Considering the above results, we conclude that the participation of ethylene and propylene in interconversions reactions is very minor.

2.3.2.6. Coke Formation.

To characterize the coke species and to elucidate their relation with catalyst selectivity, a DRIFT spectroscopic analysis was performed of the most stable catalytic system, Sigma1-315-S, after deactivation at four different temperatures and of the spent deactivated zeolites with different acidity and crystal size used at 450°C. Figure 12 summarizes the obtained results in the region of 2700-3100 cm⁻¹,

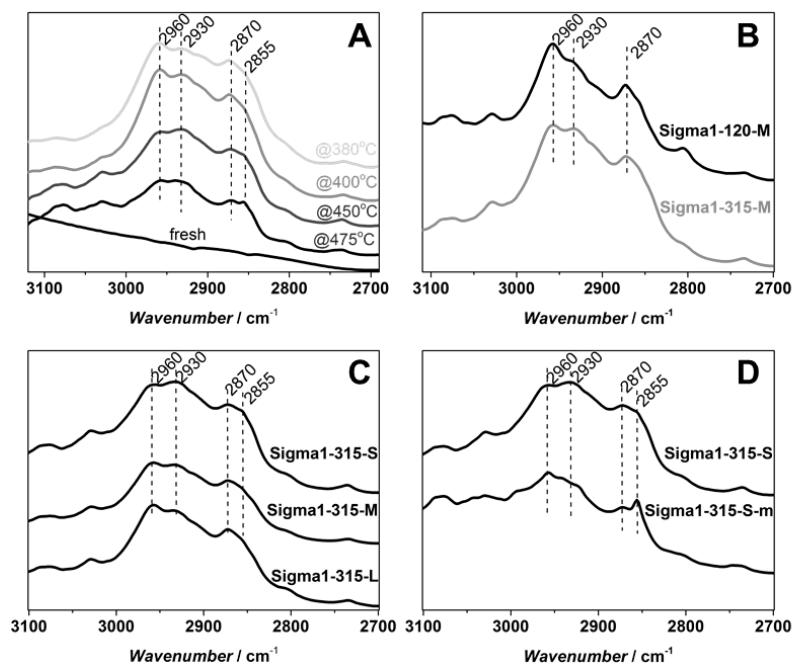


Figure 12. DRIFT spectra of spent Sigma1-315-S catalyst used at different temperatures (A); Sigma1-120-M and Sigma1-315-M at 450 °C (B); Sigma1-315-S, Sigma1-315-M and Sigma1-315-L at 450 °C (C); Sigma1-315-S and desilicated Sigma1-315-S-m at 450 °C (D).

characteristic of C-H bond vibrations. The spectra over the entire spectral range can be found in Appendix A (Figure A3).

Bands at around 2960 cm⁻¹, 2930 cm⁻¹ and 2870 cm⁻¹ are present in all deactivated samples. For spent catalyst used at 380°C and 400°C (Figure 12A) the band at 2960 cm⁻¹ is more intense than the one at 2930 cm⁻¹. However, it steadily decreases with increasing reaction temperature and already at 450°C the band at 2930 cm⁻¹ is dominant. Figures 9B and 9C show that the ratio between the intensities of bands at 2930 cm⁻¹ and 2960 cm⁻¹ depends on acidity and crystal size. The latter band is more pronounced in samples with higher acidity (Sigma1-120-M) and large crystal size (Sigma1-315-L). The spectra obtained for the spent desilicated Sigma1-315-S-m are different from the non-modified samples: an additional band appears at 2856 cm⁻¹ and the band at 2960 cm⁻¹ shifts to 2958 cm⁻¹. Both bands at 2960 cm⁻¹ and 2930 cm⁻¹ are ascribed to the C-H stretching from methyl group in methylated benzenes and/or naphthalenes in the pores of the deactivated zeolites.^[34] The presence of bands in the region of 2960-2930 cm⁻¹ shows the presence of aromatics with different substituents indicating different formed species depending on the acidity and morphology of the catalyst as well as the testing conditions. The broad band at 2930-2925 cm⁻¹ is characteristic for highly alkylated benzenes, naphthalenes and phenanthrenes.^[34] The band at 2870 cm⁻¹ represents asymmetric stretching of the C-H bond from methyl group CH(CH₃),^[35] while at 2855 cm⁻¹ C-H from methanol or DME.^[36]

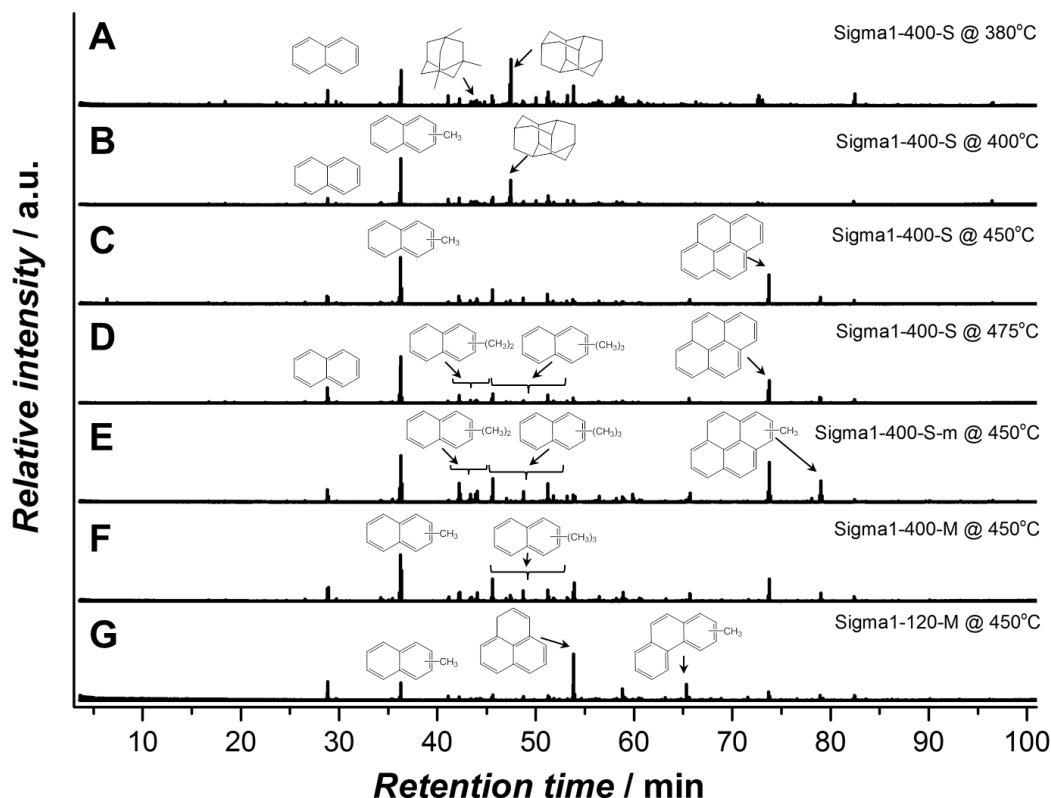


Figure 13. GC-MS chromatograms of the hydrocarbon compounds retained in the various spent (deactivated) Sigma-1 zeolites used at different temperatures.

Additionally, a band at $\sim 3030\text{ cm}^{-1}$ could be identified in all catalysts, becoming more prominent in samples deactivated at temperatures higher than 400°C . Bands in this region are attributed to aromatic C-H stretching vibrations, implying the presence of partially substituted aromatics.^[37]

The region at $1250 - 1700\text{ cm}^{-1}$ (Figure A2 in Appendix A) is characterized by bands (1600 and 1567 cm^{-1}) already described for deactivated DDR samples.^[7] In line with Kumita *et al.* observations, also a broad band at around 1600 cm^{-1} was observed, which is a combination of carbonaceous hydrogen deficient deposits^[38] and aromatic $\nu(\text{C}=\text{C})$ modes.^[39] The intensity of the band at 1567 cm^{-1} varies from sample to sample, being the highest for the one with the highest acidity (Sigma1-120-M) indicating a higher concentration of alkylnaphthalenes and phenanthrene and pyrene structures^[40] trapped in the cages.

The spent catalysts chosen for DRIFTS were further analysed by dissolving the samples in HF, followed by extraction with CH_2Cl_2 and analysis of the extract with GC-MS. Figure 13 shows that the nature of retained species is dependent on both reaction conditions and physicochemical properties of the zeolites with naphthalenic species being dominant. The fraction of methylbenzenes was found to be

negligibly small or even completely absent in some cases. Panels A - D show that the organic residue in the spent catalysts is characterized by mono-alkylated naphthalenes, being the main fraction for all samples except for Sigma1-315-S used at 380 °C, the lowest operation temperature. Interestingly, the main fraction of trapped species in this sample is represented by diadamantane, product of adamantane condensation. These species could also be found in all other deactivated samples, but their fraction significantly decreases with increasing reaction temperature. The formation of diamondoid hydrocarbons in cages of 8MR zeolites at lower temperatures was recently reported by Wei *et al.*^[41] Chen *et al.*^[42] also attributed the formation of adamantane hydrocarbons to spatial constraints imposed by the cage structure and attributed prompt deactivation at low temperatures to preferential formation of adamantanes over methylbenzenes. Further analysis of the organic residue in spent Sigma1-315-S reveals the formation of pyrene species, with an increased contribution at higher reaction temperatures.

In contrast with Sigma1-315-M, species trapped in Sigma1-120-M deactivated at 450°C are mostly represented by phenalene and phenanthrenic species and almost no alkylated naphthalene derivatives. Comparison of zeolites with the same acidity but different crystal size (Sigma1-315-S vs. Sigma1-315-M) does not reveal any difference in the species found in the spent catalysts.

The total amount of retained organic material analyzed by TGA is observed to be dependent on the amount of acid sites and crystal size. The amount of coke retained in zeolite cages increases from 8.1 to 10.5 wt.% for samples with $\text{SiO}_2/\text{Al}_2\text{O}_3 = 120$ and 400, respectively. Moreover, for samples with $\text{SiO}_2/\text{Al}_2\text{O}_3 = 400$ the coke content measured after use at 450 °C varies from 9.6 to 11.7 wt.% for samples with crystal size 4.6 and 0.5 μm , respectively. However, the amount of coke linearly increases for catalysts having a MeOH throughput before deactivation of less than 4 g/g, reaching 12 wt.% for materials that converted more than 4 g MeOH per gram catalyst, indicating that the catalytic improvement is due to the slowing down coke formation kinetics or due to the changing chemistry of the species itself (Figure A4).

2.4. Discussion.

The MTO process is among the most challenging catalytic processes from a fundamental perspective. In spite of the large number of investigations, still many questions regarding mechanism and reactivity are to be answered. One of the most striking observations is the difference in catalytic behavior among different zeolite topologies. In case of 8MR zeolites, the carbon pool mechanism seems to dominate the formation of products.^[6a] The nature of this mechanism, which proceeds *via* the formation of aromatics that obviously do not fit through small pore zeolites, makes catalyst testing rather challenging. Indeed, classical kinetic testing at low conversion levels, in contrast to recent examples with ZSM-5,^[31, 43] is not possible when 8MR zeolites are used. Inspired by these recent examples, we have performed experiments at varying space velocities. In every case, 100 % conversion and similar throughputs before deactivation were reached, in clear contrast to what was observed in case of ZSM-5. These experiments point at a much higher reactivity of 8MR zeolites and to the fact that kinetic control

cannot be achieved during catalyst testing. As a consequence, comparison between different catalysts has traditionally been done at 100 % conversion, see for example the review article of Stöcker^[2] about the comparison of different zeolites.

A logical consequence of catalyst testing at 100 % conversion is the appearance of the so-called migrating reaction zone, first proposed by Schulz.^[33] Along this line, one can envisage the existence of at least two different zones in the catalytic bed, namely: the part of the bed where methanol is still present and the part of the bed where primary MTO products (short-chain olefins and water) participate in secondary reactions in the absence of methanol. This phenomenon might imply the dependence of the catalyst lifetime on the ratios of these zones in the catalytic bed and makes mechanistic discussions based on such testing conditions rather doubtful, as demonstrated for ZSM-5 over the last few years.^[31, 43]

With this background, the assumption of a similar situation in case of 8MR zeolites is not straightforward. The migrating reaction zone considers that reaction products will diffuse into zeolite pores in the bottom part of the reactor and react further. This is indeed something feasible in case of 10MR or 12MR zeolites, where diffusivities of coefficients at reaction temperature for i.e. propylene have been estimated to be in the range of $10^{-8} \text{ m}^2 \text{ s}^{-1}$. In contrast, for 8MR zeolites, such as CHA or DDR, diffusivities of at least two orders of magnitude smaller ($10^{-10} \text{ m}^2 \text{ s}^{-1}$) have been reported for propylene.^[44] When considering these numbers, one can anticipate that reaction of primary products in the bottom part of the reactor will be diffusion limited (*i.e.* to achieve half saturation capacity for propene of a $1 \mu\text{m}$ DDR crystal would take circa 20 minutes under reaction conditions, considering that there is no co-adsorption of other products like water). The co-feeding experiments confirm this hypothesis. On one hand, the presence of additional ethylene or propylene together with methanol does not alter the catalyst lifetime, pointing to a negligible interaction of formed olefins with coke precursors, which are of the same nature based on the results obtained from DRIFTS. Considering further the stage in the catalytic bed where the main products, ethylene, propylene and mixtures thereof, can undergo consecutive reactions in the presence of water, Figure 10 indicates a negligible conversion of ethylene and a conversion of propylene with the production of butenes and C6 hydrocarbons. The appearance of longer hydrocarbons, which are not able to diffuse out of the DDR structure due to their big kinetic diameter,^[45] indicates that they are formed on the outer surface of the crystals and that propylene reacts mostly at the surface of the particles as it does not have enough time to diffuse into the pores of Sigma-1, while the less reactive ethylene passes through the reactor basically without being converted. Thus, on the outer surface of the crystals, propylene dimerization to C6 and cracking of C6 to C4 and C2 is taking place, both reactions being catalyzed by external acid sites.^[46]

These results demonstrate, that a mechanistic analysis, especially when referring to coke formation in small pore systems (8MR), can, with a large degree of confidence, be made based on results obtained at 100% conversion. Clearly, in order to fully assess selectivity to different products, co-feeding experiments should be performed.

Coming back to the catalyst itself, the Sigma-1 zeolite with DDR topology is a noteworthy nominee among 8MR zeolites displaying outstanding selectivities to light olefins (*i.e.*, propene) and hardly any formation of paraffins (Table 1), something highly relevant from the application perspective. Indeed, the selective formation of olefins means large savings as the separation of short olefin/paraffin mixtures is among the most energy intensive processes in chemical industry.^[47]

Despite the fact that the synthesis of Sigma-1 zeolite was patented in 1987 by Stewart,^[9] the number of publications dealing with this material is rather low. This is probably due to the long synthesis and difficult reproducibility of materials with DDR topology, as extensively discussed by Gücüyener *et al.*^[11b] However, the application of as-synthesized material as seeds does not only accelerate the synthesis^[11a] but also leads to the pure phase with narrow crystal size distribution. The seed inductive effect described by Yu *et al.* for ZSM-5^[48] explains the role of seeds as a recognition effect, promoting nucleation of alike building units and acting as nuclei for the growth of zeolite crystals.

As already observed for ZSM-5,^[7] Sigma-1 displays up to 90 % selectivity to ethylene and propylene almost without any propane being formed. The observed behavior lies in the unique structure of DDR cage and pore opening with dimensions of 4.4×3.6 Å, excluding molecules with kinetic diameter bigger than the window.^[12, 45]

The ethylene-to-propylene ratio of the product mixture could be tuned by both varying reaction conditions and catalyst composition and morphology. As a general observation, the parameters leading to the highest selectivity to ethylene also lead to the lowest selectivity to propylene, already pointing at competing reaction pathways to form these molecules.

At lower temperatures, the formation of propylene is favored over ethylene, while the MeOH throughput before deactivation is two times smaller. According to the generally accepted dual-cycle mechanism for the MTO process,^[49] the observed behavior is tentatively attributed to kinetic competition between the two cycles. On the other hand, the ethylene/propylene ratio strongly depends on temperature as a consequence of extent of higher olefins cracking. First principle chemical kinetics calculations for the methylation of ethylene and propene show much higher activation energies for ethylene methylation pathway and hence methylation rates are one order magnitude higher when comparing ethylene and propylene.^[50] Quick catalyst deactivation observed at lower temperatures could be ascribed to the formation of diamondoid species. On the basis of literature evaluation^[41-42] and our own observations, one can suggest that at lower reaction temperatures 8MR zeolites with a cage-like structure promote formation of adamantane derivatives which are inert and lead to cage blocking. Their formation is probably favored due to the chemical and structural similarity to the SDAs (interaction of SDA with a cage is stable *a priori*) which points to the relatively low entropy contribution to the free energy barriers leading to high reaction rates.^[51] Higher reaction temperatures promote the cracking cycle together with elimination of ethylene from alkylated aromatics, but at this stage pyrene species (Figure 13) start contributing to catalyst deactivation as these larger aromatic structures do not leave space for functionalization. The prevalence of dealkylation and/or cracking reactions at high

temperatures was demonstrated by Qian *et al.*,^[52] who showed kinetic and mechanistic differences occurring in hydrocarbon pool at high and low temperatures by applying the combination of UV/Vis, confocal fluorescence, and synchrotron-based IR micro-spectroscopic techniques. It has to be mentioned as well that the presence of phenanthrene and pyrene species (Figure 13) is surprising, as at most naphthalene derivatives fit in a DDR cage. This may indicate that polycyclic species should have been formed on the outer surfaces of the zeolite and/or in defects.^[14a]

The Si/Al ratio is another parameter that affects both MeOH throughput before deactivation of the catalyst and selectivity to light olefins. Application of zeolites with $\text{SiO}_2/\text{Al}_2\text{O}_3=120$, which corresponds to one Al per cage of zeolite, leads to a fast deactivation, while the $\text{SiO}_2/\text{Al}_2\text{O}_3=315$ with 0.5 Al atoms per cage gives the best results, in terms of MeOH throughput and ethylene and propylene yields. NH_3 TPD results demonstrate that the Al content defines not only the amount but also the strength of acid sites. Application of zeolites with moderate acidity, characterized by an NH_3 desorption peak in the range of 375-385°C significantly increases MeOH throughput before deactivation. Interestingly, FT-IR spectroscopy and dissolution experiments demonstrate that, depending on the strength of acidity, the formed 'coke' species are different, the presence of methylbenzenes/methylnaphthalenes being more prominent present in spent Sigma-415-S, the zeolite with the lowest acidity. Moreover, the maximum concentration of methylbenzenes and methylnaphthalenes coincides with the maximum yield of ethylene, confirming the hypothesis that ethylene originates from the aromatic cycle. Furthermore, analysis of coke species formed over more acidic Sigma1-120-M shows the lowest amount of methyl-substituted aromatics corresponds to the lowest yield of ethylene than comparing Sigma1-120-M with other samples.

The observed findings regarding the effect of Si/Al ratio are in contradiction with the ZSM-58 results, where the best catalytic performance was found for zeolites with $\text{SiO}_2/\text{Al}_2\text{O}_3=110$ and a further decrease in acidity (higher ratios) led to an abrupt loss of activity.^[7] However, in case of ZSM-58 the decreasing acidity was accompanied by an increased particle size, distorting the effect of acidity by additional diffusional limitations. In general, literature evaluation confirms that the MTO reaction requires application of zeolites with moderate to low acidity,^[40, 53] but the catalytic activity at such high Si/Al ratios was, to the best of our knowledge, never reported before. According to Guisnet,^[54] a faster catalyst deactivation with higher Al content is related to a high density of acid sites, which provokes a higher interaction probability between intermediates, leading to faster formation of coke. TGA analysis of spent catalysts with different acidity shows that the most acidic zeolites contain the lowest amount of coke (8.1 wt.% vs. 10.5 wt.%), suggesting either a different nature of the coke species or a faster pore blockage in case of more acidic zeolites. Considering that the nature of occluded species for samples deactivated at the same temperature seems to be similar, *vide supra*, we speculate that more acidic Sigma-1 catalysts deactivate faster due to the preferential location of carbonaceous species in close proximity to the 8MR windows rather than inside the zeolite cavities, leading to a faster blockage of the 2D porosity.^[55]

To confirm that differences observed for ZSM-58 are mainly due to a crystal size effect rather than to differences in the $\text{SiO}_2/\text{Al}_2\text{O}_3$ ratio, the catalytic performance of zeolites with 3 different crystal sizes with the $\text{SiO}_2/\text{Al}_2\text{O}_3 = 315$ ratio was investigated, while maintaining the same synthesis precursor gel composition. The comparison of these results with contradictory literature is not trivial. The absence of crystal size effect on overall selectivity to light olefins,^[56] an increased olefins selectivity with crystal size reduction,^[32b, 57] and an increasing propylene selectivity and decreasing ethylene selectivity when applying particles with a smaller crystal size^[32a] have been reported by different authors in case of SAPO-34. In all cases the observed effects were attributed to an increasing catalyst effectiveness with decreasing particle size, *i.e.* the extent of particle utilization and/or shortening of diffusion pathway of products preventing their further conversion to undesired compounds in consecutive reactions.^[58]

In contrast, Khare *et al.*^[43a] have shown that for zeolites with MFI topology the increase of the light olefins selectivity was associated with an increase of the particle size due to propagation of aromatic-based catalytic cycle, *i.e.* an increased amount of methylbenzenes responsible for ethylene formation. In case of the DDR catalysts, based on the performed co-feeding experiments, we can conclude that the increase in ethylene selectivity with decreasing particle size is due to the higher external surface to volume ratio of the smaller particles. The co-feeding experiments undoubtedly demonstrate that propylene is prone to react in the external surface region of these particles, while the less reactive ethylene would pass the bottom part of the catalyst bed almost unaltered. In view of these results, we tentatively explain differences observed in the literature for SAPO-34 and ZSM-5 by different reactivity of surface sites and diffusion properties of these zeolites, the latter is due to size and shape of the cages/cavities.

An increased MeOH throughput for smaller particles is attributed to the shortening of the diffusion pathway of reactants and products and related to the accessibility of the crystals during MTO. Qian *et al.*^[52, 59] mapped the distribution of Brønsted acid sites and retained organic species in SAPO-34 and SSZ-13 50 μm in size crystals by applying synchrotron-based IR micro-spectroscopy. The 2D map shows that the concentration of alkylated aromatics is non-homogenous with the lowest concentration profile in the central part of the crystal, *i.e.* it is not utilized in the MTO reaction. The observed findings go in line with the proposed mechanism, namely firstly formed methoxy species are homogeneously distributed in the crystals, while secondly formed aromatics alter the accessibility of the crystal, being mainly formed at the outer rim of the particle, blocking the core. The smaller the crystal the bigger its accessible volume, which is confirmed by a quantitative coke analysis: smaller crystals hold around 11.7 wt.% of coke, in contrast to bigger crystals, with a coke content of 9.6 wt.%. Higher concentration of aromatics, in turn, leads to the higher amount of produced ethylene, which goes in line with our observations. This is further confirmed by the fact that, according to the GC-MS results (Figure 13 C and F), the nature of organic species found in the deactivated catalysts is independent of crystal size.

Optimization of crystal size and acidity in Sigma-1 zeolites led to a significant improvement of MeOH throughput before catalyst deactivation. However the maximum MeOH throughput obtained for Sigma1-

315-S still did not outperform the performance of ZSM-58 with an acidity comparable to Sigma-1-120-M, confirmed by CO FTIR (Figures 4 A₁ and B₁) and NH₃ TPD (Figure A5 in Appendix A). FT-IR spectra of pretreated samples show that Sigma-1 catalysts (Figures 4 A₁ and C₁) are characterized by the presence of a broad band assigned to silanol nests. In contrast, ZSM-58 samples do not contain these species (Figure 4B₁). According to Bordiga and co-workers,^[27] these nests could be eliminated by treating the sample at higher temperatures, but the fact that all as-synthesized zeolites were calcined at the same temperature, while during the CO FT-IR experiment they were pretreated under the same conditions points to their stability in case of Sigma-1. As the presence of silanol nests is the only difference observed for Sigma-1 and ZSM-58, we tentatively suggest that they are responsible for the increased coke formation rate and faster catalyst deactivation in case of Sigma-1. Moreover, FT-IR spectra of the desilicated Sigma-1-315-S-m is characterized by significantly decreased intensity of the band at 3450 cm⁻¹ in comparison with the parent Sigma-1-315-S, implying that mild treatment in NaOH/CTAB solution led to the selective removal of Si from nests of hydrogen bonded silanol groups, leading to the improved catalytic performance. This modification only led to a slight increase in mesoporous surface area (15 m²/g vs. 52 m²/g, Figure A6), suggesting that internal defects were healed via Si rearrangement inside the zeolite.

Results reported by Barbera *et al.*, confirm our observations.^[18b] Recently, these authors showed that the deactivation of a series of ZSM-5 catalysts correlated with the relative intensities of silanols rather than with the amount of acid sites, suggesting possible “retention effects” of silanols on coke precursor that lead to a faster activity loss.

The presence of a larger number of defects in the Sigma-1 catalysts can be related to the fact that secondary growth was used for the synthesis of these solids, since faster crystal growth might lead to the formation of more defects either at the interphase seed-crystal or on the whole crystal lattice. Independently of the reason, the current results demonstrate the importance of lattice defects on the deactivation of zeolites during the MTO process. This fact, hardly considered in literature,^[60] has a much bigger importance than many other parameters normally studied and will certainly be key for the large scale implementation of MTO processes, since both industrial catalyst production and continuous regeneration may lead to the formation of additional lattice defects that will eventually affect the rate of coke formation.

In general, two-dimensional ZSM-58 and Sigma-1 zeolites with DDR topology exhibit catalyst lifetimes typical for the 8MR family,^[42, 61] which are much shorter than for ZSM-5 belonging to 10MR.^[31, 43b] Catalyst lifetime expressed in grams of MeOH converted per gram of catalyst for these zeolites does not exceed 10 g/g, CHA being an exception. It should be also mentioned, that other 2D 8MR like UFI^[61a] or LEV^[42] show even shorter lifetimes in comparison with 2D DDR. A faster deactivation of 2D 8MR is related to the higher probability of blocking the pores in one direction in comparison with 3D 8MR zeolites. As was already stated above, the unique properties of 8 MR zeolites originate from the cage and window dimensions, determining their catalytic/separation properties. Bhawe *et al.*^[61b] have shown

that ethylene selectivity increases with decreasing cage size, the highest ethylene yield being obtained for LEV having the smallest cage dimensions. In general, ethylene and propylene are the dominant products for 8MR zeolites, but formation of products up to C6 is also possible.^[42] From this perspective, DDR zeolites with very small pore openings have an advantage in comparison with other 8MR zeolites due to the negligible formation of paraffins and no products higher than C4.

2.5. Conclusions.

The results here presented confirm the high selectivity of zeolites with the DDR topology for the formation of ethylene and propylene (up to a 90%) when used as catalysts in the MTO process. Such high selectivities are the result of an ideal combination between cage geometry and window size that allows only C2 and C3 olefins to leave the cages of this zeolite. From an application perspective, this size restriction is very important. Since pure C3 olefin is formed, the separation of products becomes much less energy intensive.

One of the crucial parameters for catalyst stability is the overall zeolite acidity and strength. It was found that decreasing acidity of the zeolite from $\text{SiO}_2/\text{Al}_2\text{O}_3 = 120$ to $\text{SiO}_2/\text{Al}_2\text{O}_3 = 315$ leads to a two-fold increase in methanol throughput before full deactivation occurs. Furthermore, a decrease in the crystal size of Sigma-1 zeolite with optimized acidity led to almost two times improved throughput, ascribed to an improved utilization of the 2D porosity of this material.

The influence of internal framework defects on MTO performance has been shown to be of the utmost importance. The presence of a larger number of silanol nests in Sigma-1 resulted in a faster deactivation than in case of ZSM-58, where such defects were hardly observed. According to our results, the presence of structural defects leads to a faster coke formation kinetics and therefore to a rapid deactivation. Upon removal of silanol nests from Sigma-1, the catalytic performance becomes comparable to the one of ZSM-58. Indeed, the presence of structural defects has a much bigger importance than many other parameters usually studied and will certainly be key for the large scale implementation of MTO processes based on these materials, since both industrial catalyst production and continuous regeneration may lead to the formation of additional crystal defects that will eventually influence coke formation rate.

References.

- [1] J. S. Plotkin, *Catal. Today* **2005**, *106*, 10-14.
- [2] M. Stöcker, *Microporous Mesoporous Mater.* **1999**, *29*, 3-48.
- [3] F. J. Keil, *Microporous Mesoporous Mater.* **1999**, *29*, 49-66.
- [4] H. Ito, K. Honda, K. Oyama, N. Chikamatsu, K. Hiraoka, A. Okita, Jgc Corporation, **2013**.
- [5] J. Q. Chen, A. Bozzano, B. Glover, T. Fuglerud, S. Kvisle, *Catal. Today* **2005**, *106*, 103-107.
- [6] a) I. M. Dahl, S. Kolboe, *Catal. Lett.* **1993**, *20*, 329-336; b) I. M. Dahl, S. Kolboe, *J. Catal.* **1994**, *149*, 458-464; c) C.-M. Wang, Y.-D. Wang, Y.-J. Du, G. Yang, Z.-K. Xie, *Catal. Sci. Technol.* **2016**.
- [7] Y. Kumita, J. Gascon, E. Stavitski, J. A. Moulijn, F. Kapteijn, *Appl. Catal., A* **2011**, *391*, 234-243.
- [8] H. Gies, B. Marler, *Zeolites* **1992**, *12*, 42-49.
- [9] A. Stewart, in *GB2193202-A; GB2193202-B*, Imperial Chem Ind Plc, **1988**.
- [10] E. W. Valyocsik, D. H. Olson, P. G. Rodewald, Mobil Oil Corp, **1987**.
- [11] a) J. Gascon, W. Blom, A. van Miltenburg, A. Ferreira, R. Berger, F. Kapteijn, *Microporous Mesoporous Mater.* **2008**, *115*, 585-593; b) C. Gücüyener, J. van den Bergh, A. M. Joaristi, P. Magusin, E. J. M. Hensen, J. Gascon, F. Kapteijn, *J. Mater. Chem.* **2011**, *21*, 18386-18397.
- [12] W. Zhu, F. Kapteijn, J. A. Moulijn, M. C. den Exter, J. C. Jansen, *Langmuir* **2000**, *16*, 3322-3329.
- [13] W. Zhu, F. Kapteijn, J. A. Moulijn, J. C. Jansen, *Phys. Chem. Chem. Phys.* **2000**, *2*, 1773-1779.
- [14] a) F. Bleken, M. Bjorgen, L. Palumbo, S. Bordiga, S. Svelle, K.-P. Lillerud, U. Olsbye, *Top. Catal.* **2009**, *52*, 218-228; b) Q. Qian, J. Ruiz-Martinez, M. Mokhtar, A. M. Asiri, S. A. Al-Thabaiti, S. N. Basahel, B. M. Weckhuysen, *Catal. Today* **2014**, *226*, 14-24; c) T. Armadori, L. J. Simon, M. Digne, T. Montanari, M. Bevilacqua, V. Valtchev, J. Patarin, G. Busca, *Appl. Catal., A* **2006**, *306*, 78-84.
- [15] a) G. J. Yang, Y. X. Wei, S. T. Xu, J. R. Chen, J. Z. Li, Z. M. Li, J. H. Yu, R. R. Xu, *J. Phys. Chem. C* **2013**, *117*, 8214-8222; b) K. Y. Lee, H. J. Chae, S. Y. Jeong, G. Seo, *Appl. Catal., A* **2009**, *369*, 60-66.
- [16] a) R. von Ballmoos, W. M. Meier, *Nature* **1981**, *289*, 782-783; b) V. Gabova, J. Dedecek, J. Cejka, *Chem. Commun.* **2003**, 1196-1197.
- [17] S. Svelle, L. Sommer, K. Barbera, P. N. R. Vennestrom, U. Olsbye, K. P. Lillerud, S. Bordiga, Y. H. Pan, P. Beato, *Catal. Today* **2011**, *168*, 38-47.
- [18] a) P. Sazama, B. Wichterlova, J. Dedecek, Z. Tvaruzkova, Z. Musilova, L. Palumbo, S. Sklenak, O. Gonsiorova, *Microporous Mesoporous Mater.* **2011**, *143*, 87-96; b) K. Barbera, F. Bonino, S. Bordiga, T. V. W. Janssens, P. Beato, *J. Catal.* **2011**, *280*, 196-205.
- [19] Z. Ristanovic, J. P. Hofmann, U. Deka, T. U. Schuelli, M. Rohnke, A. M. Beale, B. M. Weckhuysen, *Angew. Chem., Int. Ed.* **2013**, *52*, 13382-13386.
- [20] M. F. De Lange, T. J. H. Vlught, J. Gascon, F. Kapteijn, *Microporous Mesoporous Mater.* **2014**, *200*, 199-215.
- [21] A. Charkhi, H. Kazemian, M. Kazemeini, *Powder Technol.* **2010**, *203*, 389-396.
- [22] T. Biemelt, C. Selzer, F. Schmidt, G. Mondin, A. Seifert, K. Pinkert, S. Spange, T. Gemming, S. Kaskel, *Microporous Mesoporous Mater.* **2014**, *187*, 114-124.
- [23] C. Baerlocher, L. B. McCusker, D. H. Olson, *Atlas of Zeolite Framework Types*, Elsevier Science, **2007**.
- [24] I. Yarulina, F. Kapteijn, J. Gascon, *Catal. Sci. Technol.* **2016**, *6*, 5320-5325.
- [25] S. Sartipi, H. Jansma, D. Bosma, B. Boshuizen, M. Makkee, J. Gascon, F. Kapteijn, *Rev. Sci. Instrum.* **2013**, *84*.
- [26] C. S. Cundy, P. A. Cox, *Microporous Mesoporous Mater.* **2005**, *82*, 1-78.
- [27] S. Bordiga, L. Regli, D. Cocina, C. Lamberti, M. Bjorgen, K. P. Lillerud, *J. Phys. Chem. B* **2005**, *109*, 2779-2784.
- [28] S. Bordiga, P. Ugliengo, A. Damin, C. Lamberti, G. Spoto, A. Zecchina, G. Spano, R. Buzzoni, L. Dalloro, F. Rivetti, *Top. Catal.* **2001**, *15*, 43-52.
- [29] S. Bordiga, I. Roggero, P. Ugliengo, A. Zecchina, V. Bolis, G. Artioli, R. Buzzoni, G. Marra, F. Rivetti, G. Spano, C. Lamberti, *J. Chem. Soc., Dalton Trans* **2000**, 3921-3929.
- [30] A. Zecchina, G. Spoto, S. Bordiga, *Phys. Chem. Chem. Phys.* **2005**, *7*, 1627-1642.
- [31] X. Sun, S. Mueller, Y. Liu, H. Shi, G. L. Haller, M. Sanchez-Sanchez, A. C. van Veen, J. A. Lercher, *J. Catal.* **2014**, *317*, 185-197.
- [32] a) B. P. C. Hereijgers, F. Bleken, M. H. Nilsen, S. Svelle, K.-P. Lillerud, M. Bjorgen, B. M. Weckhuysen, U. Olsbye, *J. Catal.* **2009**, *264*, 77-87; b) D. Chen, K. Moljord, T. Fuglerud, A. Holmen, *Microporous Mesoporous Mater.* **1999**, *29*, 191-203.
- [33] H. Schulz, M. Wei, *Top. Catal.* **2014**, *57*, 683-692.
- [34] J. W. Park, G. Seo, *Appl. Catal., A* **2009**, *356*, 180-188.
- [35] J. Pater, F. Cardona, C. Canaff, N. S. Gnep, G. Szabo, M. Guisnet, *Ind. Eng. Chem. Res.* **1999**, *38*, 3822-3829.
- [36] T. R. Forester, R. F. Howe, *J. Am. Chem. Soc.* **1987**, *109*, 5076-5082.

- [37] S. Chiaberge, G. Guglielmetti, L. Montanari, M. Salvalaggio, L. Santolini, S. Spera, P. Cesti, *Energy and Fuels* **2009**, *23*, 4486-4495.
- [38] M. Rozwadowski, M. Lezanska, J. Wloch, K. Erdmann, R. Golembiewski, J. Kornatowski, *Chem. Mater.* **2001**, *13*, 1609-1616.
- [39] H. S. Cerqueira, P. Ayrault, J. Datka, P. Magnoux, M. Guisnet, *J. Catal.* **2000**, *196*, 149-157.
- [40] J. W. Park, S. J. Kim, M. Seo, S. Y. Kim, Y. Sugi, G. Seo, *Appl. Catal., A* **2008**, *349*, 76-85.
- [41] Y. X. Wei, J. Z. Li, C. Y. Yuan, S. T. Xu, Y. Zhou, J. R. Chen, Q. Y. Wang, Q. Zhang, Z. M. Liu, *Chem. Commun.* **2012**, *48*, 3082-3084.
- [42] J. R. Chen, J. Z. Li, Y. X. Wei, C. Y. Yuan, B. Li, S. T. Xu, Y. Zhou, J. B. Wang, M. Z. Zhang, Z. M. Liu, *Catal. Commun.* **2014**, *46*, 36-40.
- [43] a) R. Khare, D. Millar, A. Bhan, *J. Catal.* **2015**, *321*, 23-31; b) X. Sun, S. Mueller, H. Shi, G. L. Haller, M. Sanchez-Sanchez, A. C. van Veen, J. A. Lercher, *J. Catal.* **2014**, *314*, 21-31.
- [44] a) A. F. Combariza, G. Sastre, A. Corma, *J. Phys. Chem. C* **2009**, *113*, 11246-11253; b) D. H. Olson, M. A. Cambor, L. A. Villaescusa, G. H. Kuehl, *Microporous Mesoporous Mater.* **2004**, *67*, 27-33.
- [45] W. Zhu, F. Kapteijn, J. A. Moulijn, *Chem. Commun.* **1999**, 2453-2454.
- [46] S. Sartipi, M. Makkee, F. Kapteijn, J. Gascon, *Catal. Sci. Technol.* **2014**, *4*, 893-907.
- [47] J. van den Bergh, C. Gucuyener, E. A. Pidko, E. J. M. Hensen, J. Gascon, F. Kapteijn, *Chem.-Eur. J.* **2011**, *17*, 8832-8840.
- [48] Q. Yu, Q. Zhang, J. Liu, C. Li, Q. Cui, *CrystEngComm* **2013**, *15*, 7680-7687.
- [49] S. Svelle, F. Joensen, J. Nerlov, U. Olsbye, K. P. Lillerud, S. Kolboe, M. Bjorgen, *J. Am. Chem. Soc.* **2006**, *128*, 14770-14771.
- [50] J. Van der Mynsbrugge, J. De Ridder, K. Hemelsoet, M. Waroquier, V. Van Speybroeck, *Chem.-Eur. J.* **2013**, *19*, 11568-11576.
- [51] V. Van Speybroeck, K. De Wispelaere, J. Van der Mynsbrugge, M. Vandichel, K. Hemelsoet, M. Waroquier, *Chem. Soc. Rev.* **2014**, *43*, 7326-7357.
- [52] Q. Qian, J. Ruiz-Martinez, M. Mokhtar, A. M. Asiri, S. A. Al-Thabaiti, S. N. Basahel, H. E. van der Bij, J. Kornatowski, B. M. Weckhuysen, *Chem.-Eur. J.* **2013**, *19*, 11204-11215.
- [53] Q. Zhu, J. N. Kondo, R. Ohnuma, Y. Kubota, M. Yamaguchi, T. Tatsumi, *Microporous Mesoporous Mater.* **2008**, *112*, 153-161.
- [54] M. Guisnet, L. Costa, F. R. Ribeiro, *J. Mol. Catal. A: Chem.* **2009**, *305*, 69-83.
- [55] M. Opanasenko, W. Roth, J. Cejka, *Catal. Sci. Technol.* **2015**.
- [56] W. Dai, G. Wu, L. Li, N. Guan, M. Hunger, *ACS Catal.* **2013**, *3*, 588-596.
- [57] S. Wilson, P. Barger, *Microporous Mesoporous Mater.* **1999**, *29*, 117-126.
- [58] J. Gascon, J. R. van Ommen, J. A. Moulijn, F. Kapteijn, *Catal. Sci. Technol.* **2015**, *5*, 807-817.
- [59] Q. Qian, J. Ruiz-Martinez, M. Mokhtar, A. M. Asiri, S. A. Al-Thabaiti, S. N. Basahel, B. M. Weckhuysen, *ChemCatChem* **2014**, *6*, 772-783.
- [60] U. Olsbye, S. Svelle, M. Bjorgen, P. Beato, T. V. W. Janssens, F. Joensen, S. Bordiga, K. P. Lillerud, *Angew. Chem., Int. Ed.* **2012**, *51*, 5810-5831.
- [61] a) J. W. Park, J. Y. Lee, K. S. Kim, S. B. Hong, G. Seo, *Appl. Catal., A* **2008**, *339*, 36-44; b) Y. Bhawe, M. Moliner-Marín, J. D. Lunn, Y. Liu, A. Malek, M. Davis, *ACS Catal.* **2012**, *2*, 2490-2495.

Chapter

3

***Faster is not Always Better: Consequences
of Secondary Zeolite Growth on Catalytic
Performance in DMTO***

Zeolites with DDR (Sigma-1 and ZSM-58) and CHA (SSZ-13) topology were synthesized by seed assisted and direct hydrothermal synthesis in order to investigate the effects of fast crystal growth on catalytic performance. Application of a small amount of seeds (0.1% wt.) significantly reduced synthesis time of all the studied zeolites. XRD and NH₃-TPD analyses did not reveal any difference in crystallinity and acidity. On the other hand, IR spectroscopy clearly demonstrates the presence of multiple defects, internal silanols (3729 cm⁻¹) and silanol nests (3400 cm⁻¹), as a result of accelerated crystal growth kinetics. Comparison of catalytic properties in the dimethyl ether to olefins (DMTO) process at 400°C and 450°C revealed that, despite smaller crystal sizes, zeolites prepared by secondary growth display shorter lifetimes due to faster coking, the latter being a result of silanols promoting hydrogen transfer reactions. Fluoride treatment of CHA removed silanols and prolonged its lifetime. This work highlights the importance of zeolite quality for catalytic application and the necessity to optimize current synthetic protocols based on secondary growth.

This Chapter is based on the following publication:

I. Yarulina, A. Dikhtiarenko, F. Kapteijn, J. Gascon, *Cat. Sci. Tech.* **2017**, 7, 300-309.

3.1. Introduction.

Zeolites are microporous aluminosilicates widely employed in chemical industry as molecular sieves and catalysts.^[1] Due to their unique properties such as ability to ion-exchange, thermal and chemical stability and shape selectivity; they are the working horses in many processes ranging from waste water treatment^[2] to gas separation^[3] and catalysis.^[4] Fluid catalytic cracking (FCC), hydrocracking and methanol to hydrocarbons (MTH) are among the most important industrial processes utilizing zeolites as catalysts. In all of them, the active site is a proton - Brønsted acid - counterbalancing negative charge of zeolite framework due to the insertion of Al. However, catalysis by zeolites is not limited to Brønsted acidity. For instance, similar isomorphous substitutions with tetravalent elements such as Sn- or Zr- may act as Lewis acid sites to catalyse Baeyer-Villiger reaction,^[5] aldol condensation^[6] and many other reactions^[7] of interest.^[8] Besides, zeolites can host different metals in the form of nanoparticles or as counter ions, such as in case of Cu-CHA for the selective catalytic reduction (SCR) of NOx.^[9]

Given the relatively large number of known zeolite frameworks and their outstanding properties, one could easily argue that zeolites should be even more extensively used in large-scale processes. However, issues associated with the high price of certain structure directing agents, large synthesis times and, in some cases, reproducibility issues, still hamper zeolite scale up.^[5, 10]

In order to address most of these issues, the application of secondary (or seeded) growth has been proposed.^[11] The idea behind this method is rather simple: a certain amount of crystals of the desired topology is added to the mixture prior to hydrothermal synthesis. If the amount of crystals is big enough (10 – 25 wt.% relative to silica source) crystallization proceeds without structure-directing agent (SDA).^[12] On the other hand, even negligible amount of crystals ($\approx 0.1\%$) significantly decrease the crystallization time in the presence of an SDA. For example, Yu *et al.*^[13] reported ultrafast synthesis of SAPO-34 in the presence of seeds in 10 min. The faster formation of products is attributed to the fact that addition of seeds suppresses the necessity of a nucleation step either by partial dissolution of seeds to provide growth surface for new crystals^[14] or *via* a core-shell growth mechanism.^[15]

Naturally, fast crystal growth might lead to the formation of some framework imperfections, which in turn can affect physical and chemical (read as catalytic) properties. Thus, the aim of this work is to compare structural and catalytic properties of zeolites obtained *via* seeded growth approach with the ones synthesized *via* direct hydrothermal synthesis. In this spirit, we synthesized a series of 8MR zeolites with two different topologies (DDR and CHA) using both methods and targeting the same morphology and acidity and assessed their catalytic properties in the Dimethyl Ether-to-Olefins process. DMTO (and the methanol to olefins process, MTO) is very sensitive to parameters related to quality of crystals, such as Si and Al distribution,^[16] presence of defects,^[17] and thus serves as an excellent probe reaction to assess even small differences in zeolite quality.

Table 1. Experimental details on zeolite synthesis procedure.

Sample	Zeolite	Type of growth	Seeds	Gel composition	Time, h
				SDA:Na ₂ O:SiO ₂ :Al ₂ O ₃ :H ₂ O	
D-DDR ₁	Sigma-1	Direct	-	20 : 3 : 60 : 1 : 2400	144
S ₁ -DDR ₁	Sigma-1	Seeded	BM [†] D-DDR ₁	20 : 3 : 60 : 1 : 2400	16
S ₂ -DDR ₁	Sigma-1	Seeded	S ₁ -DDR ₁	20 : 3 : 60 : 1 : 2400	16
D-DDR ₂	ZSM-58	Direct	-	15 : 10 : 60 : 1 : 2400	120
S-DDR ₂	ZSM-58	Seeded	BM [†] D-DDR ₂	15 : 10 : 60 : 1 : 2400	16
D ₁ -CHA	SSZ-13	Direct	-	20 : 10 : 100 : 1 : 4400	120
D ₂ -CHA	SSZ-13	Direct	-	20 : 10 : 100 : 1 : 4400	24
S ₁ -CHA	SSZ-13	Seeded	BM [†] D ₁ -CHA	20 : 10 : 100 : 1 : 4400	16

[†]Ball-milled

3.2. Experimental.

3.2.1. Synthesis of Zeolites.

N,N,N-trimethyl-1-adamantammonium hydroxide (TMAdaOH) was provided by SACHEM, Cab-O-Sil M5 was provided by Cabot. The rest of the chemicals were purchased from Sigma-Aldrich. All chemicals were used as received.

The detailed synthetic procedures for the preparation of zeolites with DDR topology (ZSM-58 and Sigma-1) was reported previously by our group.^[18]

SSZ-13 (CHA) was synthesized following the work by Zhu *et al.*^[19] with some modifications. In a typical procedure, a 25% wt. solution of TMAdaOH was mixed with a solution of 0.077 g sodium aluminate and 0.32 g sodium hydroxide in 8.51 g deionized water. When the solution became clear, 2.78 g fumed silica Cab-O-Sil M5 and 21.43 g deionized water were added and kept for aging for 4 h under the stirring. The obtained mixture was transferred to autoclaves and subjected to hydrothermal synthesis at 160°C for 24 or 120 h.

After crystallization, zeolites were thoroughly washed with deionized water and dried overnight. These solids were used as starting material for the preparation of seeds *via* ball-milling. The exact procedure can be found elsewhere.^[18a]

Subsequent syntheses of zeolites with DDR and CHA topology were performed by seed assisted growth using the ball-milled crystals (0.1 wt.% relative to silica source).

The following nomenclature based on synthesis type and framework type code (FTC) was used in the course of the current work: **X – FTC**, where X stands for type of synthesis (D – direct hydrothermal, S – seeded), while FTC is either DDR₁ (Sigma-1), DDR₂ (ZSM-58) or CHA (SSZ-13). Details on gel composition, synthesis time and nomenclature can be found in Table 1. The as-synthesized crystals were calcined for 10 h at 650°C and converted to their protonic forms by triple ion-exchange in an aqueous NH₄NO₃ solution (1 M, 80°C, 2 h, 100 mL per gram zeolite) followed by calcination at 550°C.

Fluoride modified S₁-CHA-F was obtained from S₁-CHA following the method described by Xu *et al.*^[20] For a typical procedure, 1.2 g S₁-CHA was dispersed in 20 ml 0.013M NH₄F solution and left stirring at room temperature until complete evaporation of water (approximately 48 h). The obtained solid was further dried at 80°C for 16 h followed by calcination at 600°C for 6 h.

3.2.2. Characterization of Zeolites.

The XRD patterns of the powders were recorded in Bragg–Brentano geometry with a Bruker D8 Advance X-ray diffractometer equipped with a LynxEye position-sensitive detector. Measurements were performed at RT by using monochromatic CoK α ($\lambda=1.788970$ Å) radiation between $2\theta = 5^\circ$ and 50° .

Images were recorded using a JEOL JSM-6010LA with a standard beam potential of 10 kV and an Everhart-Thornley detector. X-ray microanalysis (SEM/EDX) confirmed the elemental composition in the sample by scanning electron microscopy (SEM) coupled with a dispersive X-ray microanalysis system (EDX) with a Silicon-drift detector.

A Malvern Nano ZS zetasizer was used for the analysis of particle size of the wet ball-milled crystals with dynamic light scattering (DLS).

N₂ adsorption was carried out using Tristar II 3020 Micromeritics sorptometer at -196°C. Prior to the experiment samples were outgassed at 350°C for 16 h.

Temperature-programmed NH₃ desorption (NH₃-TPD) was measured by AutoChem II chemisorption analyzer (Micromeritics). Approximately 0.2 g material was first degassed under He flow at 400°C and then saturated with NH₃ at 200°C during 1 h using a flow of 1.65 % NH₃ in He. The gas mixture was then switched back to He and the sample was purged at 200°C for about 1 h to remove weakly adsorbed NH₃ molecules. TPD was subsequently recorded under He flow, from 200°C to 800°C. All flow rates were adjusted to 25 mL min⁻¹, and the heating rates were 10°C min⁻¹ during different stages of experiment.

Transmission FT-IR spectroscopy was performed using a Nicolet Nexus spectrometer at 4 cm⁻¹ resolution equipped with an extended KBr beam splitting and a mercury cadmium telluride (MCT) cryo-detector. The pellets were placed in an IR quartz cell equipped with CaF₂ windows. A movable sample holder allows the sample to be placed in the infrared beam for the measurements or into the furnace for thermal treatments. The cell is connected to a vacuum line for pretreatment. The specimen is activated in vacuum at 400°C for 16 h to remove adsorbed species.

3.2.3. Catalyst Testing.

Dimethyl ether to olefins (DMTO) experiments were performed in a Microactivity Reference unit (PID Eng&Tech) at 400°C and 450°C and ambient pressure. For each experiment, 0.5 g catalyst (pressed, crushed and sieved to particle sizes 250-420 μm) was placed in a fixed-bed with internal diameter of 9 mm. Conversion, selectivities and yields were calculated on a molar carbon basis. Detailed description of the set-up and calculations can be found below:^[18a, 21]

Table 2. Catalytic properties of the zeolites with the DDR topology under the study.

Sample	Particle size ^a (μm)	S_{meso}^b ($\text{m}^2 \text{g}^{-1}$)	S_{BET}^c ($\text{m}^2 \text{g}^{-1}$)	V_{micro}^b ($\text{cm}^3 \text{g}^{-1}$)	$\text{SiO}_2/\text{Al}_2\text{O}_3^e$ (mol mol^{-1})	NH_3 capacity ^e ($\mu\text{mol NH}_3 \text{g}^{-1}$)
D-DDR ₁	12-15	20	250	0.10	111	295
S ₁ -DDR ₁	0.4	30	320	0.13	107	306
S ₂ -DDR ₁	5	9	300	0.13	103	318
D-DDR ₂	0.5-1.6	22	370	0.14	111	296
S-DDR ₂	0.5	17	310	0.13	113	290
D ₁ -CHA	5-8	7	780	0.30	159	207
D ₂ -CHA	0.3-1.4	20	770	0.30	168	196
S ₁ -CHA	0.6-0.7	8	750	0.29	158	208
S ₁ -CHA-F	0.6-0.7	18	540	0.23	-	-

^a From SEM images. ^b *t*-plot method applied to the N₂ isotherm. ^c BET method applied to the N₂ isotherm. ^e From NH₃-TPD measurements.

$$X = \frac{n_{C,DME_{in}} - n_{C,DME_{out}}}{n_{C,DME_{in}}} \cdot 100\% \quad (1)$$

the selectivity towards ethylene (2) and propylene (3) was calculated based on the carbon number as follows:

$$S_{\text{ethylene}} = \frac{2 \cdot n_{C_2H_4}}{2 \cdot n_{C,DME_{in}} - 2 \cdot n_{C,DME_{out}}} \cdot 100\% \quad (2)$$

$$S_{\text{propylene}} = \frac{3 \cdot n_{C_3H_6}}{2 \cdot n_{C,DME_{in}} - 2 \cdot n_{C,DME_{out}}} \cdot 100\% \quad (3)$$

and the yield of a component *i* was defined from its selectivity and methanol conversion:

$$Y_i = \frac{S_i \cdot X}{100} \quad (4)$$

Dimethyl ether (DME) was chosen instead of methanol due to several reasons. Application of DME allowed to achieve very high dilution with nitrogen (DME : N₂ = 1 : 19) at the same time avoiding exothermic dehydration of methanol to DME, thus getting rid of heat effects intervention.^[21] For a typical experiment, a mixture of 5 mol% of dimethyl ether (DME) in nitrogen was used at a weight-hourly space velocity (*WHSV*) of 1.23 g_{DME} g_{cat}⁻¹ h⁻¹. The product mixture was analyzed online with an Interscience CompactGC equipped with a 15 m capillary RTX-1 (1% diphenyl-, 99% dimethylpolysiloxane) column and a flame ionization detector.

Catalytic results are presented as a function of the DME throughput per amount of catalyst used (g_{DME} g_{cat}⁻¹) and defined as the total amount of DME fed to the catalytic bed before the conversion of DME dropped below 80%. Selectivities reported in Table 4 are integral values calculated during the active period of the catalyst. The typical evolution of ethylene and propylene selectivities as a function of time is shown in the Appendix B (Figures B7-B9).

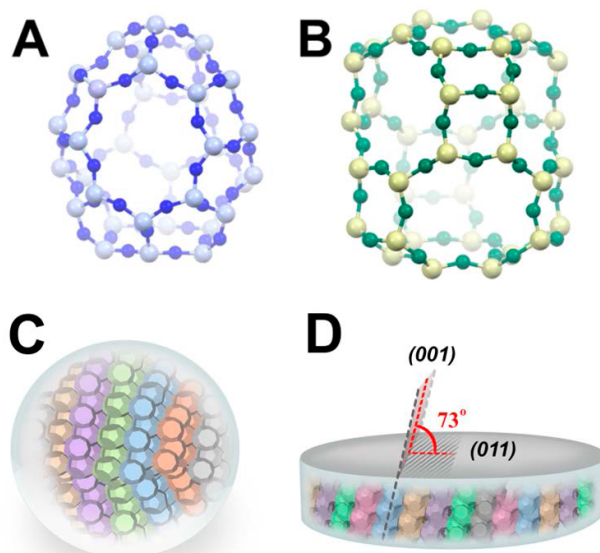


Figure 1. Accessible cage structures of DDR (A) and CHA (B) frameworks. Arrangement of 8MR-jointed 2D pore substructure layers of DDR in (C) spherical and (D) disk-like crystals.

3.3. Results and Discussion.

3.3.1. Results.

3.3.1.1. Characterization of DDR and CHA Zeolites.

The accessible cage structures of DDR ($7.1 \times 9.4 \text{ \AA}$) and CHA ($6.7 \times 10.9 \text{ \AA}$) are shown in Figure 1. Both topologies belong to the 8-membered ring family (8MR) characterized by large cavities with small window openings. DDR has a 2D porosity, while CHA possesses a 3D pore structure.

Comparison of powder XRD patterns of the synthesized materials with their reference patterns^[22] reveals that in all cases the desired topology was obtained and no crystalline impurities could be observed (Figure B1).

Notably, the experimental diffraction pattern of the sample D-DDR₁ shows around 13.3° higher diffraction intensity than expected from the theoretical XRD pattern revealing a preferred orientation of the particles. Consequently, the XRD pattern was subjected to a whole pattern refinement in order to figure out the habit of the crystallites and the direction of their preferred orientation (Figure B2). The refinement results reveal that the D-DDR₁ particles tend to orient preferably along the (011) plane. Moreover, the G_1 -factor of 0.023 suggests a platy habit of the crystals, which has been confirmed by scanning electron microscopy. The D-DDR₁ crystals have a disk-like shape and grow preferentially along directions perpendicular to the (0*kl*) crystallographic planes developing a (011) crystal surface. Therefore, the top and bottom surfaces of the D-DDR₁ crystals preferably expose (011) lattice planes

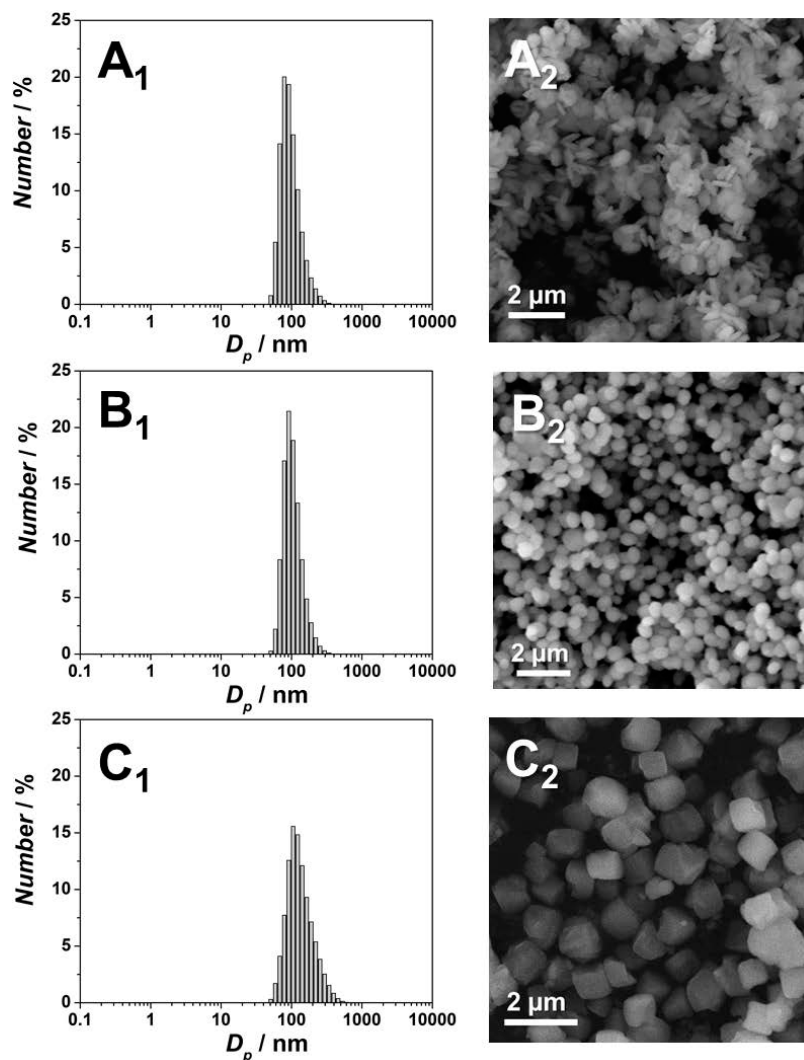


Figure 2. Particle size distribution of seeds (A_1 , B_1 , C_1) obtained by DLS, and SEM images of zeolites (A_2 , B_2 , C_2) obtained from these seeds. A_2 – S_1 -DDR₁, B_2 – S-DDR₂, C_2 – S_1 -CHA.

along with equivalent ($0kl$) ones, as represented in Figure 1D. These 2D substructures lay in the (001) plane and intersect the top and bottom surfaces of the D-DDR₁ round slabs with inclination angle of 73° , as shown in Figure 1D. Considering this structural arrangement within the crystallite, the diffusion through 8MR channel system is expected to be faster in the disk-like crystals than in spherical particles (Figures 1C and 1D).

Analysis of SEM pictures shows that direct hydrothermal synthesis led to the formation of crystals with disk (Sigma-1), spherical (ZSM-58) and cubic (SSZ-13) shape with relatively broad size distribution (Figure B3, Table 2). On the other hand, seeded growth resulted in the formation of crystals with a

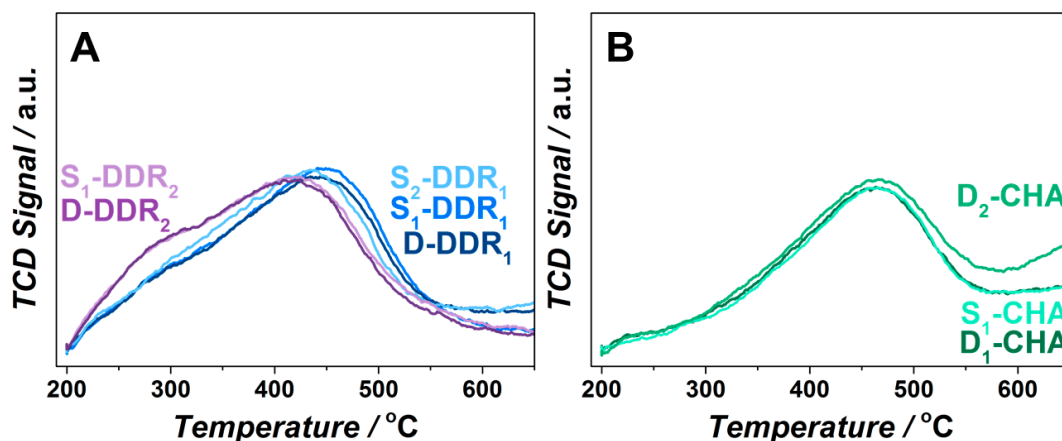


Figure 3. NH_3 -TPD profiles of zeolites with DDR (A) and CHA (B) topology.

narrow size distribution, all particles having similar crystal size (400-600 nm), independently of the topology (Figure 2). DLS analyses of seeding solutions employed for the seeded growth synthesis show that in all cases they contained nanoparticles with an average size of 100 nm. These results suggest that the final crystal size obtained *via* seeded synthesis is more a function of the initial size of seeds than of the zeolite topology. Such interdependence is an indisputable advantage of the seeded growth technique as it allows tuning the particle size.

NH_3 -TPD shows that all catalysts possess a similar amount of acid sites independently of the topology and synthesis protocol. For all zeolites, TPD curves are characterized by the presence of one desorption maximum at 410°C (ZSM-58), 450°C (Sigma-1) or 460°C (SSZ-13). The desorption curves of ZSM-58 (D-DDR₂ and S₁-DDR₂) are also characterized by the presence of a shoulder at 280°C that can be indicative for the presence of weaker acid sites (Figure 3).

Structural differences in the hydroxyl region were investigated by means of IR (Figure 4). The full spectra can be found in the Appendix B (Figure B4). For all samples, the two expected absorbances are always present at 3747 cm^{-1} , characteristic from the $\nu(\text{OH})$ of terminal silanols from external surfaces and at 3616 cm^{-1} , associated to the $\nu(\text{OH})$ of bridging silanols (Brønsted acid sites).^[23]

For D-DDR₁, the band at 3747 cm^{-1} is less prominent, in a good agreement with the relatively larger particle size of this sample. Zeolites Sigma-1 synthesized by seeded growth (S₁-DDR₁ and S₂-DDR₁) display an additional very broad band at 3400 cm^{-1} attributed to silanol nests, progressively increasing from S₁-DDR₁ to S₂-DDR₁.

These silanol nests, arising from defects in the zeolite framework, represent clusters of silanols interacting *via* medium strength hydrogen bonding. These defects in turn can originate from removal of framework atoms or from incomplete condensation. Interestingly, the spectrum of S₂-DDR₁ is characterized by a complex triplet, where, together with the band at 3747 cm^{-1} , two additional vibrations at 3729 and 3706 cm^{-1} are observed. These have been attributed to silanols in different environments

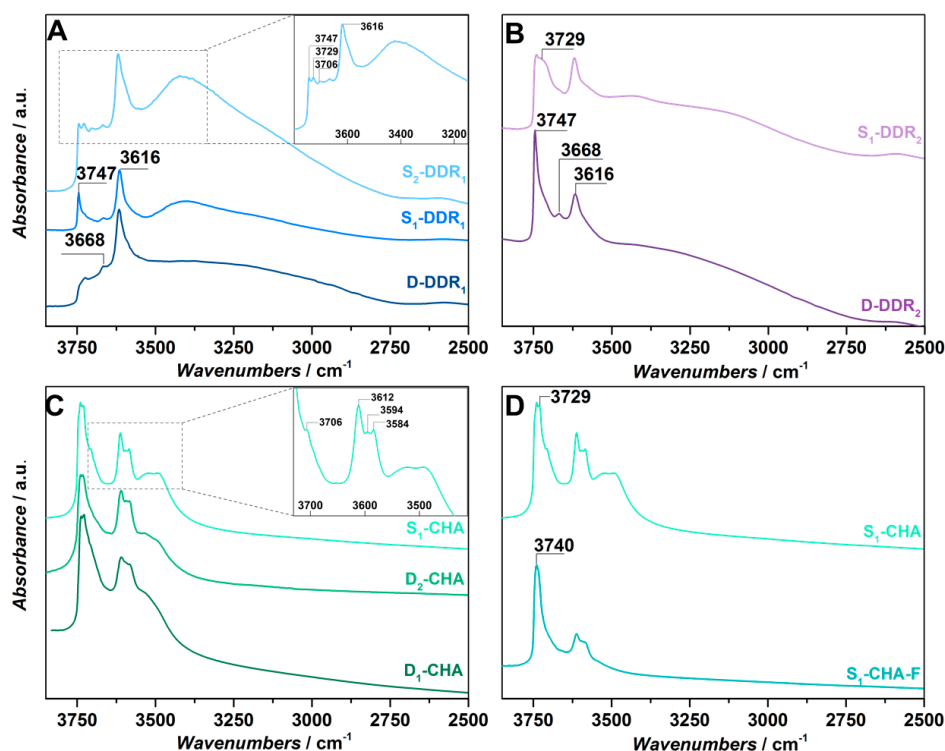


Figure 4. FTIR spectra in the OH-stretching region of activated Sigma-1 (A), ZSM-58 (B), SSZ-13(C) and modified SSZ-13 (D) zeolites.

but inside the micropores and terminating inner defects.^[17, 24] These OHs are slightly more acidic than the band associated with external silanols and are notorious for faster deactivation due to coke retention.^[17]

ZSM-58 zeolites display very similar features. For S₁-DDR₂ through secondary growth, a broad band is observed with two maxima at 3747 cm⁻¹, 3729 cm⁻¹ and additional overlapping bands pointing to multiple inner defects. The band at 3400 cm⁻¹ is also more prominent in comparison with D-DDR₂.

Some of the spectra are also characterized by the presence of the band at 3668 cm⁻¹ due to the presence of extraframework Al.

The IR spectra obtained from the SSZ-13 samples are rather complex. The Brønsted acidity region is characterized by a triplet with maxima at 3612 cm⁻¹, 3594 cm⁻¹ and 3584 cm⁻¹.

Bordiga *et al.*^[25] identified two bands in SSZ-13 with Si/Al=11.6 at 3616 cm⁻¹ and 3584 cm⁻¹ and ascribed them to protons of the same strength. The band arising at 3616 cm⁻¹ was attributed to the proton located at the 8MR windows while at 3584 cm⁻¹ to the proton isolated from the neighbouring cages. The presence of the third peak in our case implies the presence of additional protons in a different geometric position, most likely within the cages. For all samples, silanols are recognised by a doublet at 3740 (isolated silanols) and 3729 cm⁻¹ and an additionally appearing band centred at

Table 3. Comparison of catalyst lifetime at different temperatures.

Sample	t_{50} (h)		Throughput ($\text{g}_{\text{DME}} \text{g}_{\text{cat}}^{-1}$)		Coke ^a (wt.%)	Coking rate ($\text{mg g}_{\text{cat}}^{-1} \text{h}^{-1}$)
	400°C	450°C	400°C	450°C		
D-DDR ₁	0.3	0.7	0.4	0.9	3.2	45.7
S ₁ -DDR ₁	1.1	1.6	1.4	2.0	8.8	55.0
S ₂ -DDR ₁	0.2	0.4	0.2	0.5	4.3	107.5
D-DDR ₂	1.3	1.7	1.6	2.1	8.4	49.4
S-DDR ₂	1.0	1.5	1.2	1.8	9.2	61.3
D ₁ -CHA	2.6	2.6	3.2	3.2	11.8	45.4
D ₂ -CHA	4.5	3.6	5.5	4.4	12	33.3
S ₁ -CHA	3.1	2.0	3.8	2.5	10.5	52.5
S ₁ -CHA-F	3.5	2.9	4.3	3.6	10.2	35.2

^a From TGA measurements of deactivated at 450°C catalyst.

3706 cm^{-1} for S₁-CHA. Silanol nests are present in all samples as a broad component at around 3520 cm^{-1} , but S₁-CHA is also characterized by a second broad band at around 3490 cm^{-1} . In contrast to parent S₁-CHA, fluoride-modified S₁-CHA-F (Figure 4D) is characterized by a singlet at 3740 cm^{-1} representing isolated silanols, while broad components (3490 and 3520 cm^{-1}) related to silanol nests completely disappear. The ratio of the bands in triplet (3612 cm^{-1} , 3594 cm^{-1} and 3584 cm^{-1}) representing Brønsted acidity seems to remain unchanged, though band absorbance is lower.

3.3.1.2. Catalytic Activity in DMTO.

The different zeolites under study were tested in the DMTO process. We have recently shown that zeolites with DDR topology have the highest lifetime in MTO process at relatively high temperatures (>450°C).^[18a] In case of SSZ-13, many studies show that, for this topology, milder temperatures ($\approx 400^\circ\text{C}$) are favourable for longer lifetime.^[26] For this reason, two different temperatures (400°C and 450°C) were selected to allow for a meaningful comparison. Figure 5 and Table 3 show the obtained lifetimes and related throughput, while conversion as a function of time is presented in the Appendix B (Figure B6). In line with previous papers dedicated to Sigma-1 and ZSM-58,^[18] zeolites with DDR topology display an up to twice higher throughput at 450°C in comparison with 400°C. The fast deactivation of DDR zeolites at 400°C was attributed to the formation of diamondoid species remaining in the zeolite cages and in contrast to methylbenzenes not reacting further with methanol.^[18a]

Interestingly, there is no direct correlation between catalyst lifetime and particle size. Large crystals (10-15 μm) of directly synthesized D-DDR₁ show longer lifetimes than much smaller S₂-DDR₁ at 450°C (Table 3, 0.9 vs 0.5 $\text{g}_{\text{DME}} \text{g}_{\text{cat}}^{-1}$). Accordingly, the nanosized S-DDR₂ with multiple internal defects displays slightly worse performance than its micrometer hydrothermally synthesized counterpart D-DDR₂.

To demonstrate that the observed relation is not topology dependent, the catalytic behaviour of SSZ-13 was also investigated. First of all, in contrast to Sigma-1 and ZSM-58, SSZ-13, except D₁-CHA, show longer lifetimes at 400°C. However, even at 450°C there is a noticeable difference in lifetimes for DDR and CHA in favour of CHA. Such a prolonged lifetime of these catalysts is explained on the basis of the

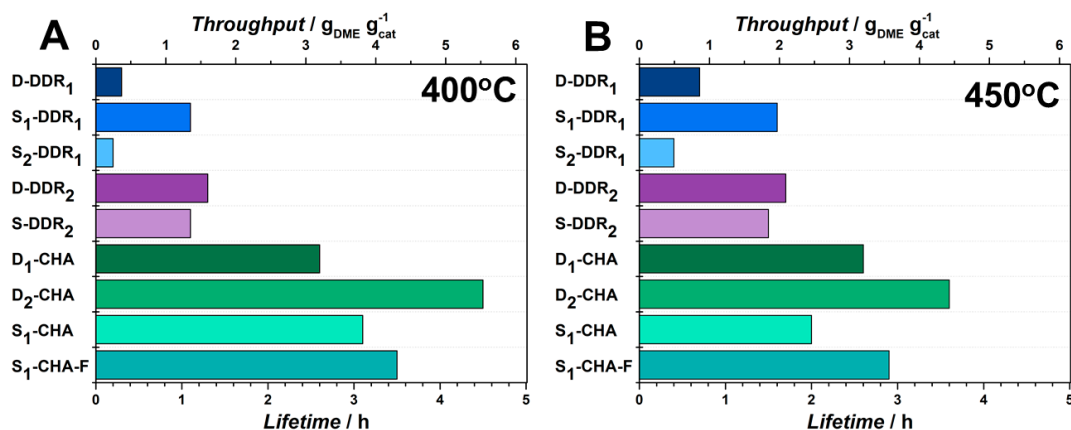


Figure 5. Lifetime of zeolite catalysts under study at 400°C (A) and 450°C (B) in DMTO process.

bigger dimensions and particular shape of the main CHA cage, which is able to accumulate more aromatics and is believed to stabilize “hydrocarbon pool” species.^[27] Furthermore, there is a higher probability of blocking the 2D pore network of ZSM-58 and Sigma-1 than the 3D porosity of SSZ-13, leading to a faster deactivation of DDR. According to the literature,^[28] the diamondoid species can be also formed in CHA cage, however, below 300°C leading to the prompt deactivation as in case of DDR. Thus the different optimum temperatures for DDR (450°C) and CHA (400°C) can be related to the nature of active species formed at these temperatures and their participation either in aromatic cycle or coke formation. In turn, the formation of different aromatic species is defined by cage architecture, location and strength of the acid site.

The highest DME throughput (5.5 g_{DME} g_{cat}⁻¹) is observed for D₂-CHA at 400°C followed by S₁-CHA (3.8 g_{DME} g_{cat}⁻¹). It is obvious that, despite minor differences in size and acidity, noticeable differences are found in DME throughputs. Moreover, D₁-CHA, whose lifetime seems to be temperature independent, outperforms S₁-CHA at 450°C, clearly showing that the quality of the crystal is more important than its size. Fluoride modification seems to have positive effect on catalyst lifetime as it results in higher DME throughput for S₁-CHA-F in comparison with S₁-CHA, which is especially noticeable at 450°C (3.6 vs 2.5 g_{DME} g_{cat}⁻¹).

To summarize, an important tendency is found: zeolites prepared by seeded growth deactivate faster than directly synthesized zeolites. As the only substantial difference between these zeolites is the presence of internal silanols and silanol nests, faster deactivation is attributed to the presence of these features.^[17]

3.3.1.3. Product Selectivities.

Product selectivities observed at 400°C and 450°C in DMTO are shown in Table 4. Ethylene, propylene and butenes are the main products for both DDR and CHA topologies with some presence of

Table 4. Product selectivities obtained in DMTO process over zeolites under study at 400°C and 450°C.

Sample	Selectivity ^a , %									
	C1-C4		C2 [≠]		C3 [≠]		C4 [≠]		C5-6	
	400°C	450°C	400°C	450°C	400°C	450°C	400°C	450°C	400°C	450°C
D-DDR ₁	3	2	37	42	39	32	7	7	1	1
S ₁ -DDR ₁	5	2	25	38	47	43	15	13	2	2
S ₂ -DDR ₁	1	2	22	32	45	42	10	10	1	1
D-DDR ₂	4	3	23	39	48	41	15	11	2	2
S-DDR ₂	2	2	21	32	45	44	13	12	5	5
D ₁ -CHA	7	4	42	50	35	31	12	10	5	5
D ₂ -CHA	4	3	47	55	33	28	11	9	6	5
S ₁ -CHA	6	3	40	51	37	32	13	10	4	4
S ₁ -CHA-F	4	3	41	51	37	31	12	9	6	6

^a Integral values calculated during the active period of the catalyst.

higher hydrocarbons and paraffins. The amount of paraffins and higher hydrocarbons is especially noticeable for CHA catalyst (up to 10%), which has larger dimensions of cage and pore openings. For

DDR zeolites, higher hydrocarbons are mostly formed on the external surface as they cannot pass the window opening. Independently on topology, higher temperatures lead to higher selectivities to ethylene and lower selectivities to propylene and butenes as a result of kinetic competition between the aromatic and olefinic cycle.^[18a] The maximum selectivity of ethylene for all catalysts under study (Figures B7 – B9) coincides with the breakthrough of DME as a result of accumulation of methylbenzenes and polycondensed methylated species, responsible not only for ethylene formation but also for deactivation.^[29] Moreover, under the same conditions, the amount of produced ethylene on CHA catalysts is at least 10% higher than for Sigma-1 and ZSM-58. It is also important to mention that for DDR catalysts, due to very short lifetime and high rate of coking, the carbon balance is not always completely closed. Especially, D-DDR₁, S₂-DDR₁ at 400°C exhibit high selectivities towards coke formation (>10%).

Though the method of zeolite preparation (direct vs seeded) has a noticeable effect on catalyst lifetime, there is no pronounced relation between product distribution and method of preparation.

3.3.2. Discussion.

Seeding was shown to be an appropriate way to significantly reduce synthesis time and a tool to control particle size, which makes it very attractive from a large-scale application perspective. Recently Mintova *et al.*^[30] examined some common issues of zeolite crystal growth, including nucleation *via* seeding. Among the advantages of seeded growth authors also listed reduced formation of undesired phase and fast nuclei formation. Obviously, the weak point is that seeded growth approach can often lead to aggregation and intergrown crystals.^[31] This aggregation seems to be correlated with the amount of seeds used. As zeolites in this work were synthesized with very low amount of seeds (0.1% wt.), neither aggregation nor intergrowth was observed.

Valtchev *et al.* fairly mentioned that, although the seeded method is already widely used, the mechanism is barely known.^[31b] It is generally accepted that the main role of seeds is to provide both surface for secondary nucleation and primary building units.^[32] However, the way this can be achieved is still a matter of discussion. Xiao *et al.* demonstrated that zeolites crystallize on the surface of seeds *i.e.* forming core-shell structures.^[15, 33] The crystal growth proceeds on partially dissolved seeds in alkaline media, but without dissolution to primary building blocks. An attempt to crystallize zeolite BEA only in the presence of primary building blocks resulted in an amorphous phase.^[15] On the other hand, Okubo *et al.* suggest that seeds are disaggregated into much smaller subunits that, in turn, provide surface for crystal growth, *i.e.* again through partial dissolution, however, herein building units play the key factor.^[34] Authors showed further that it is possible to synthesize zeolites using seeds of other topology, which have common building units. The mechanisms proposed by Xiao *et al.*^[15, 33] and Okubo *et al.*^[14] for the SDA-free synthesis of zeolites, in principle, hold well for this work. However, considering the very small amount of seeds used for zeolite synthesis in this work, we tentatively suggest that dissolution of seeds proceeds to much smaller aggregates in comparison to previously mentioned works, giving rise to nuclei which act as a core to build new zeolite crystals. With this little amount of seeds, application of SDA is necessary. The size of the formed nuclei would then depend on the initial size of the seeds and determine the final crystal size. Thus, the 100 nm seeds led to formation of crystals with particle size < 500 nm. If the latter are used as seeds these crystals result in the formation of 2.5 μm particle, 2.5 μm seeds will form 5 μm and so on.

Considering that build-up of the crystal starts not from the elementary building unit but already from the pre-formed core, the formation of a framework with T-site vacancies can be anticipated. From this perspective, the secondary growth of building units can be compared - to a certain degree - with random Tetris® blocks which are not always matching the surface and thus leaving some "gaps" in crystal structure. These "gaps" or T-vacancies are saturated with protons from the nearest oxygens giving rise to the hydroxyl nests and/or other silanol defects.^[35] The term *hydroxyl nest* represents the defect where a SiO_4 or AlO_4 tetrahedron is replaced with four hydroxyls. The structural defect can also exist in the form of *geminal* silanols $=\text{Si}(\text{OH})_2$ or bridged *vicinal* silanols. It is important to mention that the defects seen *via* spectroscopic tools (NMR and FTIR mainly) are only the tip of the iceberg, as the majority of them cannot be observed directly. This is the consequence of continuous transformation of structural defects due to dehydroxylation, dehydration or deprotonation happening already at room temperature. The dynamic behaviour of these defects causes drastic changes in characteristic signals obtained by NMR and FTIR.^[35]

In general, there are many possible reasons leading to the formation of defects, dealumination being the most common but not the only one.^[7] Fernandez *et al.*^[36] have shown that formation and location of silanol defects can be governed by the SDA during zeolite crystallization. In this case, defects are located in close proximity to the template. In this work, we highlight another origin of defects coming from a mismatching crystal growth.^[35]

The catalytic testing of synthesized zeolites in DMTO process revealed that zeolites prepared by seeded growth deactivate much faster than directly hydrothermally synthesized materials. In our previous work, we have already extensively discussed influence of defects on prominently deactivating Sigma-1 in the MTO process.^[18a] In addition, due to the preferential orientation of lattice planes with an inclination angle of 73° to the disk (Figure 1D), the diffusion pathway for Sigma-1 is defined by the thickness of the crystal (≈ 100 nm for S₁-DDR₁). This dimension is at least 5 times smaller than for defect-free spherical D-DDR₂. Despite such five-fold shorter diffusion pathway in case of S₁-DDR₁, these catalysts show slightly shorter lifetime in DMTO process (Figure 5), again highlighting the importance of crystal quality. This observation highlights that effect coming from structural defects outweighs crystal size effect. The increased amount of defects facilitates formation of internal coke, significantly affecting the rate of deactivation. This relationship between defects and catalyst deactivation is already a well-established feature explained by the so called “retention effect” of coke species.^[17, 37] Sazama *et al.* showed that defective sites in ZSM-5 facilitate hydrogen transfer reactions thus producing higher amount of paraffins and aromatics and leading to twice faster deactivation.^[38] On the other hand, faster crystal growth kinetics in the presence of seeds, might also lead to different distribution of Al in the zeolite framework in comparison to zeolites synthesized by direct hydrothermal growth, thus affecting catalytic performance.^[39] There are many parameters affecting Al distribution like pH, SDA, precursors and synthesis conditions.^[40] According to Dedecek, “*the greater heterogeneity of mixtures results finally in higher population of Al pairs and vice versa rather homogeneous up to clear up solutions lead to higher population of single Al atoms.*”^[40] Adapted to our case, there is a higher probability of Al-zoning for catalysts prepared by seeding as a consequence of starting from heterogeneous seed-containing synthesis solution. Formation of Al-rich regions in turn can lead to higher coking rates due to higher probability of olefins from the two nearest sites to form aromatics.^[37, 41] This effect should be further explored.

The comparison of selectivities obtained for defective and non-defective zeolites in this work does not reveal significant difference in product distribution. Logically, for 8MR zeolites, selectivities are rather governed by the cage and window dimensions.^[27] On the other hand, enhanced hydrogen transfer reactions would speed up coke formation rate. Indeed, the analysis of coking rate (Table 3) expressed as the mass of coke formed during the active period shows that rate of coke formation is almost twice higher for seeded zeolites than for hydrothermally synthesized ones (compare D-DDR₁ vs S₂-DDR₁ and D₂-CHA vs S₁-CHA).

The results obtained in this work highlight the importance of crystal quality, which turns out to be more important than particle size. Though seeded growth approach allows tuning crystal size on demand and significantly reduces synthesis time, its negative impact on DMTO (MTO, MTH, MTG) catalysis outweighs all listed advantages. Further optimization of zeolite synthetic procedures based on secondary growth approach is required. From this perspective, synthesis of zeolites in fluoride media is rather promising. It has been shown that with the assistance of fluoride, synthesized crystals possess less

defects,^[42] while post-synthetic treatment with $\text{FeF}_3/\text{NH}_4\text{HF}_2$ selectively removes internal silanols from synthesized zeolites improving catalyst lifetime by a factor of ten.^[43] Valtchev *et al.* compared synthesis of nano-ZSM-5 by seed assisted method in OH^- and F^- media, the latter possessing significantly less structural defects.^[44] In this work, the post-synthetic fluoride treatment with NH_4F was chosen as a tool to heal defects in zeolite crystals. IR results clearly demonstrated that such treatment led to selective removal of silanol nests and internal silanols from zeolite crystal. Unlike for ZSM-5, fluoride treatment did not lead to the generation of mesopores in SSZ-13, however led to a noticeable surface area loss. Despite this loss in surface area ($\approx 30\%$) and micropore volume ($\approx 20\%$), S₁-CHA-F showed longer lifetimes in DMTO process and lower coking rates. One has to be aware that concentration of NH_4F had to be thoroughly optimized as further increase in F^- concentration led to removal of Brønsted acid sites from the zeolite framework (Figure B5).

Herein, we have further confirmed the negative impact of defects arising from seeded growth on DMTO performance. It is also important to mention that there are a number of reactions that are catalysed solely by defects. Abate *et al.* dedicated a paragraph in the recent perspective about the role of defects in such reactions like Beckmann rearrangement, etherification of 5-hydroxymethylfurfural (HMF) to produce, for instance, biodiesel components.^[7] Thus, the seeding method to produce defective zeolites can be beneficial for future applications in reactions catalysed by hydroxyl nests.

3.4. Conclusions.

Zeolites with DDR (Sigma-1 and ZSM-58) and CHA (SSZ-13) topology were synthesized by direct hydrothermal synthesis and seed assisted method. Synthesized zeolites appeared to have similar amount of Brønsted acid sites. However, zeolites prepared by seeded growth contain a significant amount of internal silanols and hydroxyl nests due to the fast crystal growth kinetics. These multiple defects have a negative impact on catalytic performance in the DMTO process in terms of lifetime, but did not affect product distribution. Such deactivation behaviour is a consequence of the silanols participating in hydrogen transfer reactions and thus speeding up coke formation rate. These silanols can be selectively removed from by treatment with NH_4F . All zeolites under study exhibited high selectivities to ethylene, propylene and butenes ($>90\%$), selectivities being dependent on reaction temperature ($\uparrow T \rightarrow \uparrow S_{2=}, \downarrow S_{3=-C_{4=}}$) and size of cage ($\uparrow \text{size} \rightarrow \uparrow S_{2=}, \downarrow S_{3=-C_{4=}}$).

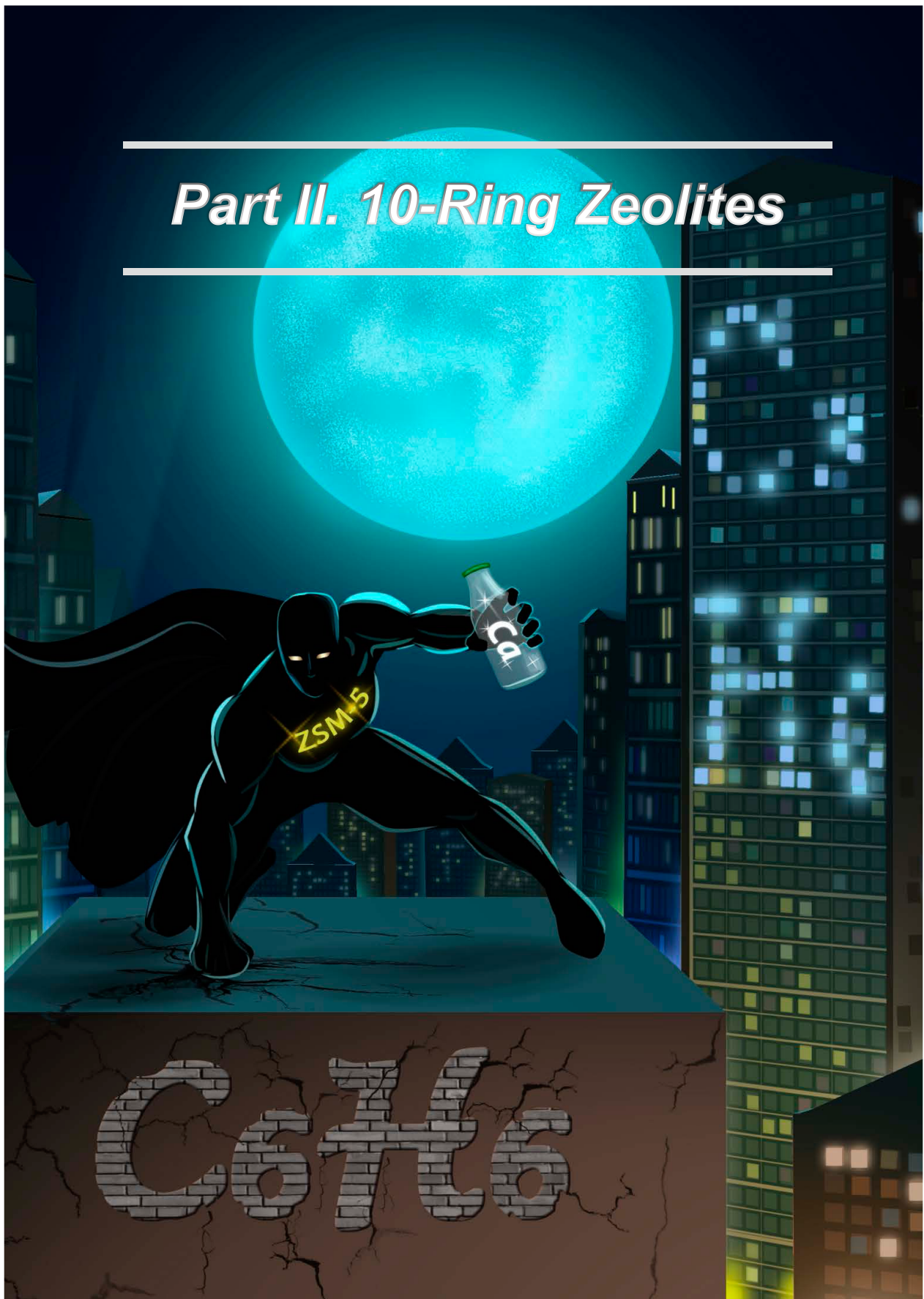
References.

- [1] J. Weitkamp, *Solid State Ionics* **2000**, *131*, 175-188.
- [2] S. B. Wang, Y. L. Peng, *Chem. Eng. J.* **2010**, *156*, 11-24.
- [3] a) N. Kosinov, J. Gascon, F. Kapteijn, E. J. M. Hensen, *J. Membr. Sci.* **2016**, *499*, 65-79; b) E. E. McLeary, J. C. Jansen, F. Kapteijn, *Microporous Mesoporous Mater.* **2006**, *90*, 198-220; c) J. Gascon, F. Kapteijn, B. Zornoza, V. Sebastian, C. Casado, J. Coronas, *Chem. Mater.* **2012**, *24*, 2829-2844.
- [4] a) A. Corma, *J. Catal.* **2003**, *216*, 298-312; b) K. Tanabe, W. F. Holderich, *Appl. Catal., A* **1999**, *181*, 399-434.
- [5] A. Corma, L. T. Nemeth, M. Renz, S. Valencia, *Nature* **2001**, *412*, 423-425.
- [6] J. D. Lewis, S. Van de Vyver, Y. Roman-Leshkov, *Angew. Chem. Int. Ed.* **2015**, *54*, 9835-9838.
- [7] S. Abate, K. Barbera, G. Centi, P. Lanzafame, S. Perathoner, *Cat. Sci. Tech.* **2016**, *6*, 2485-2501.
- [8] H. Bekkum, H. W. Kouwenhoven, *Zeolite Manual for the Organic Chemist*, mijnbestseller.nl, **2012**.
- [9] A. M. Beale, F. Gao, I. Lezcano-Gonzalez, C. H. F. Peden, J. Szanyi, *Chem. Soc. Rev.* **2015**, *44*, 7371-7405.
- [10] a) J. Gascon, J. R. van Ommen, J. A. Moulijn, F. Kapteijn, *Cat. Sci. Tech.* **2015**, *5*, 807-817; b) C. Gücüyener, J. van den Bergh, A. M. Joaristi, P. Magusin, E. J. M. Hensen, J. Gascon, F. Kapteijn, *J. Mater. Chem.* **2011**, *21*, 18386-18397; c) J. Gascon, W. Blom, A. van Miltenburg, A. Ferreira, R. Berger, F. Kapteijn, *Microporous Mesoporous Mater.* **2008**, *115*, 585-593; d) C. Liu, L. Bai, J. M. Zhang, D. Hu, M. Li, G. F. Zeng, Y. F. Zhang, W. Wei, Y. H. Sun, *Microporous Mesoporous Mater.* **2016**, *225*, 312-322.
- [11] M. Moliner, C. Martinez, A. Corma, *Chem. Mater.* **2014**, *26*, 246-258.
- [12] Q. M. Wu, X. Wang, G. D. Qi, Q. Guo, S. X. Pan, X. J. Meng, J. Xu, F. Deng, F. T. Fan, Z. C. Feng, C. Li, S. Maurer, U. Muller, F. S. Xiao, *J. Am. Chem. Soc.* **2014**, *136*, 4019-4025.
- [13] Q. Sun, N. Wang, G. Guo, J. Yu, *Chem. Commun.* **2015**, *51*, 16397-16400.
- [14] Y. Kamimura, S. Tanahashi, K. Itabashi, A. Sugawara, T. Wakihara, A. Shimojima, T. Okubo, *J. Phys. Chem. C* **2011**, *115*, 744-750.
- [15] B. Xie, H. Y. Zhang, C. G. Yang, S. Y. Liu, L. M. Ren, L. Zhang, X. J. Meng, B. Yilmaz, U. Muller, F. S. Xiao, *Chem. Commun.* **2011**, *47*, 3945-3947.
- [16] R. Martinez-Franco, Z. Li, J. Martinez-Triguero, M. Moliner, A. Corma, *Cat. Sci. Tech.* **2016**, *6*, 2796-2806.
- [17] K. Barbera, F. Bonino, S. Bordiga, T. V. W. Janssens, P. Beato, *J. Catal.* **2011**, *280*, 196-205.
- [18] a) I. Yarulina, S. Bailleul, A. Pustovarenko, J. R. Martinez, K. D. Wispelaere, J. Hajek, B. M. Weckhuysen, K. Houben, M. Baldus, V. Van Speybroeck, F. Kapteijn, J. Gascon, *ChemCatChem* **2016**, *8*, 3057-3063; b) Y. Kumita, J. Gascon, E. Stavitski, J. A. Moulijn, F. Kapteijn, *Appl. Catal., A* **2011**, *391*, 234-243.
- [19] Q. J. Zhu, J. N. Kondo, R. Ohnuma, Y. Kubota, M. Yamaguchi, T. Tatsumi, *Microporous Mesoporous Mater.* **2008**, *112*, 153-161.
- [20] T. Xu, Q. Zhang, H. Song, Y. Wang, *J. Catal.* **2012**, *295*, 232-241.
- [21] I. Yarulina, F. Kapteijn, J. Gascon, *Cat. Sci. Tech.* **2016**, *6*, 5320-5325.
- [22] C. Baerlocher, L. B. McCusker, D. H. Olson, *Atlas of Zeolite Framework Types*, Elsevier Science, **2007**.
- [23] S. Bordiga, P. Ugliengo, A. Damin, C. Lamberti, G. Spoto, A. Zecchina, G. Spano, R. Buzzoni, L. Dalloro, F. Rivetti, *Top. Catal.* **2001**, *15*, 43-52.
- [24] F. Thibault-Starzyk, A. Vimont, J. P. Gilson, *Catal. Today* **2001**, *70*, 227-241.
- [25] S. Bordiga, L. Regli, D. Cocina, C. Lamberti, M. Bjorgen, K. P. Lillerud, *J. Phys. Chem. B* **2005**, *109*, 2779-2784.
- [26] F. Bleken, M. Bjorgen, L. Palumbo, S. Bordiga, S. Svelle, K. P. Lillerud, U. Olsbye, *Top. Catal.* **2009**, *52*, 218-228.
- [27] a) Y. Bhawe, M. Moliner-Marin, J. D. Lunn, Y. Liu, A. Malek, M. Davis, *ACS Catal.* **2012**, *2*, 2490-2495; b) J. W. Park, J. Y. Lee, K. S. Kim, S. B. Hong, G. Seo, *Appl. Catal., A* **2008**, *339*, 36-44; c) J. Z. Li, Y. X. Wei, J. R. Chen, S. T. Xu, P. Tian, X. F. Yang, B. Li, J. B. Wang, Z. M. Liu, *ACS Catal.* **2015**, *5*, 661-665.
- [28] J. R. Chen, J. Z. Li, Y. X. Wei, C. Y. Yuan, B. Li, S. T. Xu, Y. Zhou, J. B. Wang, M. Z. Zhang, Z. M. Liu, *Catal. Commun.* **2014**, *46*, 36-40.
- [29] E. Borodina, F. Meirer, I. Lezcano-Gonzalez, M. Mokhtar, A. M. Asiri, S. A. Al-Thabaiti, S. N. Basahel, J. Ruiz-Martinez, B. M. Weckhuysen, *ACS Catal.* **2015**, *5*, 992-1003.
- [30] J. Grand, H. Awala, S. Mintova, *CrystEngComm* **2016**, *18*, 650-664.
- [31] a) N. Ren, J. Bronic, B. Subotic, X. C. Lv, Z. J. Yang, Y. Tang, *Microporous Mesoporous Mater.* **2011**, *139*, 197-206; b) G. Majano, A. Darwiche, S. Mintova, V. Valtchev, *Ind. Eng. Chem. Res.* **2009**, *48*, 7084-7091.
- [32] Q. Yu, Q. Zhang, J. Liu, C. Li, Q. Cui, *CrystEngComm* **2013**, *15*, 7680-7687.
- [33] B. Xie, J. Song, L. Ren, Y. Ji, J. Li, F.-S. Xiao, *Chem. Mater.* **2008**, *20*, 4533-4535.
- [34] K. Itabashi, Y. Kamimura, K. Iyoki, A. Shimojima, T. Okubo, *J. Am. Chem. Soc.* **2012**, *134*, 11542-11549.
- [35] A. A. Sokol, C. R. A. Catlow, J. M. Garces, A. Kuperman, *J. Phys. Chem. B* **2002**, *106*, 6163-6177.
- [36] E. Dib, J. Grand, S. Mintova, C. Fernandez, *Chem. Mat.* **2015**, *27*, 7577-7579.

CHAPTER THREE

- [37] U. Olsbye, S. Svelle, M. Bjorgen, P. Beato, T. V. W. Janssens, F. Joensen, S. Bordiga, K. P. Lillerud, *Angew. Chem. Int. Ed.* **2012**, *51*, 5810-5831.
- [38] P. Sazama, B. Wichterlova, J. Dedecek, Z. Tvaruzkova, Z. Musilova, L. Palumbo, S. Sklenak, O. Gonsiorova, *Microporous Mesoporous Mater.* **2011**, *143*, 87-96.
- [39] N. Danilina, F. Krumeich, S. A. Castelanelli, J. A. van Bokhoven, *J. Phys. Chem. C* **2010**, *114*, 6640-6645.
- [40] J. Dedecek, Z. Sobalik, B. Wichterlova, *Catal. Rev. Sci. Eng.* **2012**, *54*, 135-223.
- [41] T. Liang, J. Chen, Z. Qin, J. Li, P. Wang, S. Wang, G. Wang, M. Dong, W. Fan, J. Wang, *ACS Catalysis* **2016**, *6*, 7311-7325.
- [42] P. Tian, Y. X. Wei, M. Ye, Z. M. Liu, *ACS Catal.* **2015**, *5*, 1922-1938.
- [43] M. R. Li, Y. P. Zhou, C. Ju, Y. M. Fang, *Appl. Catal., A* **2016**, *512*, 1-8.
- [44] Z. X. Qin, L. Lakiss, L. Tosheva, J. P. Gilson, A. Vicente, C. Fernandez, V. Valtchev, *Adv. Funct. Mater.* **2014**, *24*, 257-264.

Part II. 10-Ring Zeolites



Chapter

4

The Importance of Heat Effects in the Methanol-to-Hydrocarbons Process over ZSM-5: on the Role of Mesoporosity on Catalyst Performance

Interpretation of catalytic performance during the MTH process is hampered by heat transport phenomena. We demonstrate that important hot spots can occur during lab scale catalyst testing of ZSM-5, even when a large catalyst bed dilution is applied. Formation of mesopores in ZSM-5 leads to partial mitigation of these effects because of a lower generation of heat per unit catalyst volume due to a combination of a lower active site concentration, a lower zeolite density and a slight weakening of the zeolite acidity.

This Chapter is based on the following publication:

I. Yarulina, F. Kapteijn, J. Gascon, *Catal. Sci. Technol.* **2016**, *6*, 5320-5325.

4.1. Introduction.

The methanol-to-hydrocarbons (MTH) process comprises the conversion of methanol over acidic zeolites. Although this process was patented already in 1977^[1] and widely applied since 2010 at the industrial level,^[2] there is currently a great interest in improving selectivity towards propylene and in enhancing catalyst lifetime. In order to achieve this objective, many scientific publications focus on the application of mesoporous zeolites to prolong catalyst lifetime *via* improving diffusion properties.^[3] Despite the initial success of mesoporous zeolites in MTH catalysis,^[4] some recent studies have shown that not every mesoporous zeolite is equally effective.^[5] In this line, Michels *et. al.* ^[6] have shown that, under industrially relevant conditions, blends of microporous zeolites and binders can easily outperform purely mesoporous catalysts.

In contrast to the huge efforts devoted to materials development, very little effort has been devoted to studies at the reactor level, something surprising considering the high exothermicity of the reaction (the reaction enthalpy of methanol dehydration is -24 kJ mol^{-1} , while reaction enthalpies for the formation of olefins vary from -11 kJ mol^{-1} for ethylene to -53 kJ mol^{-1} for butene).^[7] Guo *et. al.*^[8] calculated for a single-bed adiabatic reactor an adiabatic temperature rise of more than 200°C , which will obviously result in accelerated coke deposition, possible catalyst degradation and a different product scope under these highly nonisothermal conditions. In turn, analysis of literature reveals controversial results^[4b, 6] reported for the same catalytic system (ZSM-5, Zeolyst, Si/Al=40) and/or catalysts with similar physicochemical properties^[9] tested under alike conditions. These results suggest that reactor configuration together with heat and mass transport are of high importance when it comes to catalyst lifetime and process selectivity. Here, we highlight the large impact of catalyst testing conditions on data reproducibility and catalyst deactivation.^[10] Taking mesoporous zeolites as case study, we demonstrate that active site isolation and its consequences for catalyst acidity and heat generation are the main reasons behind improved lifetime and selectivity, rather than the usually claimed improvement of diffusion properties.

4.2. Experimental.

4.2.1. Catalyst Preparation.

ZSM-5 zeolite (Si/Al = 40) was purchased from Zeolyst. Mesoporous ZSM-5 was prepared by desilication with 1 M NaOH at 70°C for 1 h followed by acid leaching in 1 M HNO₃ aqueous solution to remove extraframework Al. The post synthetic method for the production of mesoporous ZSM-5 was adapted from Sartipi *et. al.*^[11] ZSM-5 in the ammonium form was calcined at 550°C for 5 h to get the protonic H-ZSM-5. Desilication of H-ZSM-5 powder was carried out in a 1 M NaOH aqueous solution under stirring at 70°C for 1 h in a capped container ($\text{volume}_{\text{base solution}}/\text{mass}_{\text{parent H-ZSM-5}} = 8.0 \text{ cm}^3 \text{ g}^{-1}$). This treatment was followed by immediate quenching in a water-ice bath and centrifugation to separate the zeolite powder from the solution.

Table 1. Detailed characteristics of the catalyst bed in dilution experiments performed at $WHSV = 8 \text{ h}^{-1}$, $m_{\text{catalyst}} = 0.5 \text{ g}$, $\text{MeOH:N}_2 = 1:1$ and reactor ID 9 mm.

ZSM-5 :SiC (wt/wt)	ZSM-5 : SiC (vol / vol)	L_{bed} (cm)	$F(\text{MeOH})$ (mmol min ⁻¹)
1:0	1:0	1.4	2.1
1:3	1:0.9	2.7	2.1
1:6	1:1.8	3.9	2.1

Table 2. Detailed characteristics of the catalyst bed and conditions in 3 TC experiments ($WHSV = 4 \text{ h}^{-1}$, $\text{MeOH:N}_2 = 1:1$, reactor ID 9 mm).

Catalyst	L_{bed} (cm)	m_{cat} (g)	m_{SiC} (g)	$F(\text{MeOH})$ (mmol min ⁻¹)
ZSM-5	5	1.75	0	3.6
ZSM-5 + SiC	5	0.63	3.78	1.3
Meso-ZSM-5	5	1.44	0	3.0

Desilication was followed by intensive washing with water until neutral pH was reached. Desilicated ZSM-5 was dried overnight at 120 °C for 12 h and calcined at 550 °C for 5 h. Yield of the desilication procedure was 25% (averaged from four experiments starting from ca. 20 g of H-ZSM-5).

Subsequently, desilicated ZSM-5 was acid treated in 1 M HNO_3 aqueous solution ($\text{volume}_{\text{acid solution}}/\text{mass}_{\text{zeolite}} = 28.6 \text{ cm}^3 \text{ g}^{-1}$) at 70 °C 2 h under stirring in an oil bath. After quenching, the sample was thoroughly washed with deionized water, dried and calcined in the same manner as after the above mentioned desilication procedure.

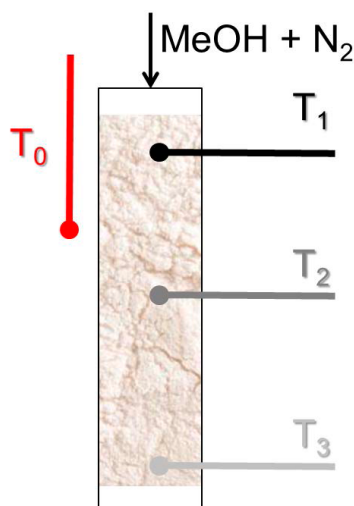
4.2.2. Catalyst Characterization.

N_2 adsorption at -196°C was carried out using a Tristar II 3020 analyzer (Micromeritics). Prior to the experiment, samples were outgassed under vacuum at 350 °C for 16 h.

Scanning electron microscopy (SEM) images were recorded using a JEOL JSM-6010LA with a standard beam potential of 10 kV and an Everhart-Thornley detector. X-ray microanalysis (SEM/EDX) confirmed the elemental composition in the sample by (SEM) coupled to a dispersive X-ray microanalysis system (EDX) with a Silicon-drift detector.

The XRD patterns of the powders were recorded in Bragg–Brentano geometry with a Bruker D8 Advance X-ray diffractometer equipped with a LynxEye position-sensitive detector. Measurements were performed at RT by using monochromatic $\text{CoK}\alpha$ ($\lambda = 1.788970 \text{ \AA}$) radiation between $2\theta = 5^\circ$ and 50° .

Temperature-programmed NH_3 desorption (NH_3 -TPD) was measured by an AutoChem II chemisorption analyzer (Micromeritics). Approximately 0.2 g of the material was first degassed under He flow at 400 °C and then saturated with NH_3 at 200 °C during 1 h using a flow of 1.65 % NH_3 in He. The gas mixture was then switched back to He and the sample was purged at 200 °C for about 1 h to remove weakly adsorbed NH_3 molecules. TPD was subsequently recorded under He flow, from 200 °C to 800 °C. All flow rates were adjusted to 25 mL min^{-1} , and the heating rates were $10 \text{ }^\circ\text{C min}^{-1}$ during different stages of experiment.



Scheme 1. Three thermocouples (T_1 , T_2 , T_3) monitoring the temperatures at different heights inside the catalytic bed. Thermocouple outside (T_0) is used to control temperature.

Transmission FT-IR spectroscopy using pyridine as a probe molecule was performed using a Nicolet 6700 spectrometer equipped with a MCT/B detector. The zeolite samples were activated in vacuum at 400 °C for 16 h to remove adsorbed species. After activation, pellets were saturated with pyridine vapor and further evacuated at 160 °C for 2 h. Spectra were recorded in the 1000-4000 cm^{-1} range at 4 cm^{-1} resolution and are an average of 128 scans. The amount of Brønsted (BAS) and Lewis (LAS) acid sites was derived from the bands at 1545 and 1456 cm^{-1} as described elsewhere.^[12]

4.2.3. Catalyst Testing.

Catalytic experiments were carried out in a Microactivity Reference unit (PID Eng&Tech) at 400°C - 500°C and ambient pressure as described elsewhere.^[13] The catalyst (pressed, crushed and sieved to particle sizes 250-420 μm) was placed in a fixed-bed with internal diameter 9 mm I.D. reactor equipped with three thermocouples (3 TC) monitoring the temperatures at different heights inside the catalytic bed during MTH experiments and catalyst regeneration (Scheme 1, T_1 , T_2 , T_3). Another thermocouple outside in contact with the reactor wall (Scheme 1, T_0) was used to control temperature. Reaction lifetime was investigated as a function of temperature, degree of catalyst dilution with SiC ($m_{\text{cat}} : m_{\text{SiC}} = 1 : 0-6$) and reactor diameter (4, 7, 9 mm). Detailed characteristic of the catalyst beds can be found in Table 1 and 2.

Catalyst regeneration was achieved by continuous flowing of a mixture of N_2 (30 mL min^{-1}) and air (30 mL min^{-1}) for 8 h at 550°C followed by cooling down the catalytic bed to reaction temperature under N_2 flow (30 mL min^{-1}).

An HPLC pump (307 5-SC-type piston pump, Gilson) was used to feed methanol to the reactor system. Weight-hourly space velocities (WHSV) of 8 and 4 $\text{g}_{\text{MeOH}} \text{g}_{\text{cat}}^{-1} \text{h}^{-1}$, a 1:1 molar feed composition of N_2 and MeOH and atmospheric pressure were utilized.

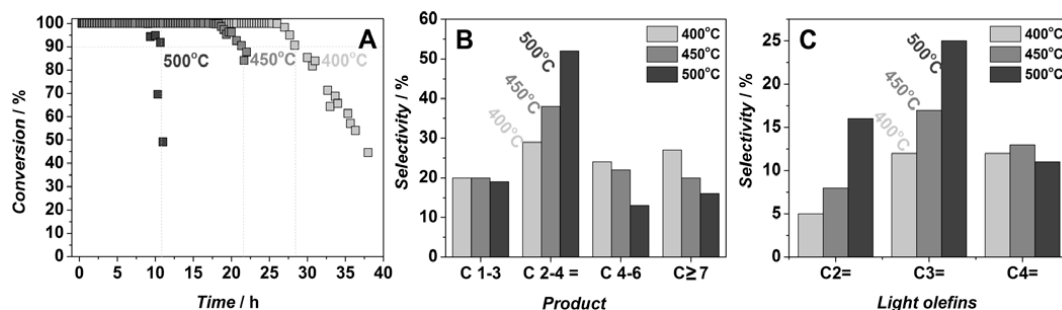


Figure 1. Conversion versus time-on-stream (A), corresponding integral product selectivities (B) and integral light olefins product selectivities (C) for different temperatures over ZSM-5. $WHSV = 8 \text{ h}^{-1}$, $\text{MeOH:N}_2=1:1$, reactor ID 9 mm.

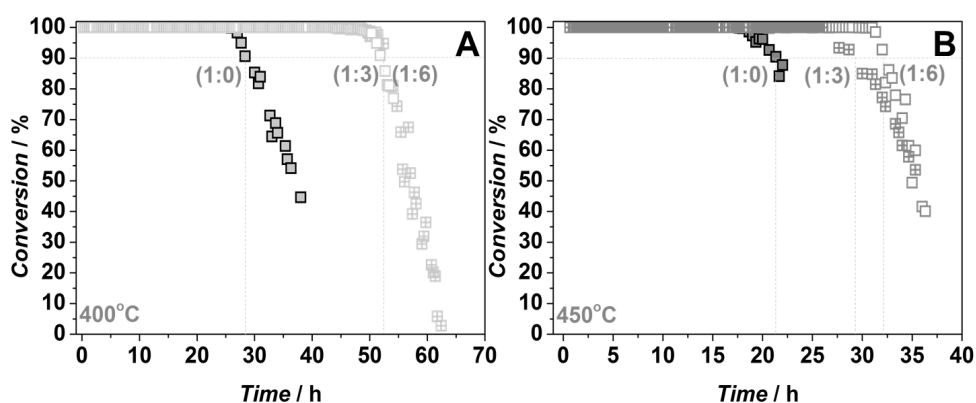


Figure 2. Conversion as a function of time-on-stream over ZSM-5 diluted with different amounts of SiC at 400 °C (A) and at 450 °C (B). ZSM-5 : SiC = 1:0 ; 1:3; 1:6 wt/wt. $WHSV = 8 \text{ h}^{-1}$, $\text{MeOH:N}_2=1:1$, reactor ID 9 mm.

Conversion, selectivities and yields were calculated on a molar carbon basis. Thus, conversion was defined as the carbon-based fraction of light oxygenates (methanol and dimethyl ether) consumed during the reaction:

$$X = \frac{n_{C,MeOH_{in}} - n_{C,MeOH_{out}} - 2 \cdot n_{C,DME_{out}}}{n_{C,MeOH_{in}}} \cdot 100\% \quad (1)$$

the selectivity towards produced hydrocarbons was calculated according to the carbon number of the product. i.e. for ethylene (2) and propylene (3):

$$S_{ethylene} = \frac{2 \cdot n_{C_2H_4}}{n_{C,MeOH_{in}} - n_{C,oxy_{out}}} \cdot 100\% \quad (2)$$

$$S_{propylene} = \frac{3 \cdot n_{C_3H_6}}{n_{C,MeOH_{in}} - n_{C,oxy_{out}}} \cdot 100\% \quad (3)$$

and the yield of a component i was defined from its selectivity and methanol conversion:

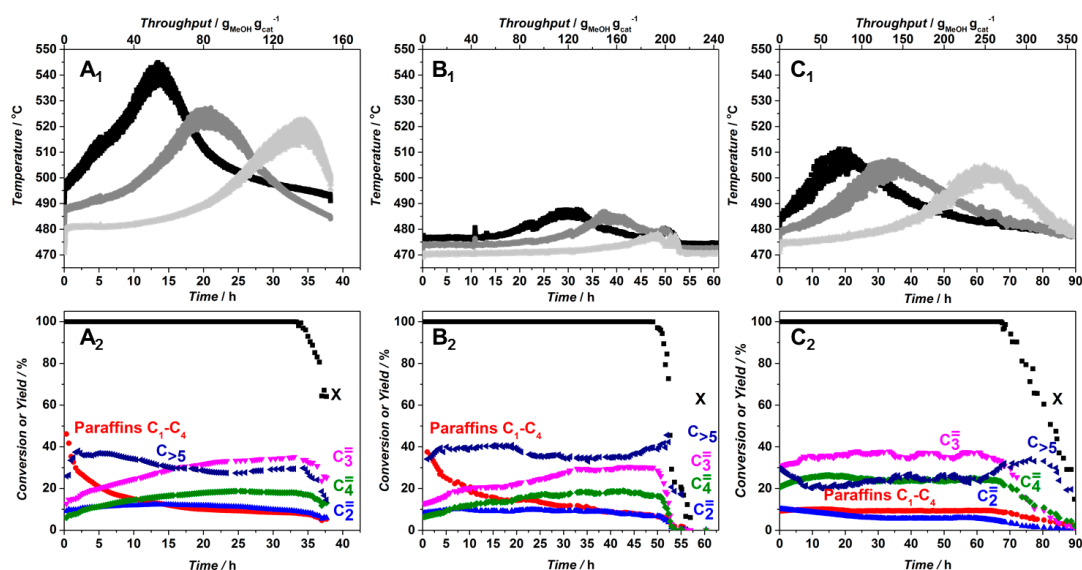


Figure 3. Temperature profiles (A_1 ; B_1 ; C_1) and corresponding product distribution (A_2 , B_2 , C_2) as a function of time-on-stream for ZSM-5 (A_1 , A_2), ZSM-5 : SiC= 1:6 wt/wt (B_1 , B_2) and mesoporous ZSM-5 (C_1 , C_2). Set-point temperature 470 °C, $L_{bed} = 5$ cm, $WHSV = 4$ h $^{-1}$, MeOH:N $_2$ =1:1. C $_{>5}$ indicates hydrocarbons with 5 or more C atoms.

$$Y_i = \frac{S_i \cdot X}{100} \quad (4)$$

The performance results are presented in graphs as a function of the methanol throughput per amount of catalyst used ($g_{MeOH} g_{cat}^{-1}$) and defined as overall MeOH throughput fed through the catalytic bed before the conversion of oxygenates drops below 90 %. Note that the selectivities and yields presented in the time-on-stream graphs are the instantaneous values. The bar graphs represent the integral values over the whole experiment.

4.3. Results and Discussion.

First of all, catalyst deactivation was studied as a function of reaction temperature, always using undiluted, fresh ZSM-5. In line with the literature available,^[6, 14] the catalyst lifetime depends on reaction temperature: it decreases from 27 to 10 h when temperature rises from 400 °C to 500 °C (Figure 1A). Moreover, selectivity to C $_2$ -C $_4$ olefins increases from 28 to 52 %, indicating a much higher selectivity to propylene at higher temperatures (Figure 1B and C).

Considering the relatively high partial pressure of methanol in the feed (0.5 bar) and operation at full conversion, conditions commonly used in the MTH process, utilization of a catalyst bed diluent such as silicon carbide (SiC) is of high importance, mainly due to the improved heat conduction in the bed, to the lower heat production per unit volume, to the larger wall heat exchange area, and to a decreased effect of axial dispersion.^[15] Indeed, dilution of catalyst with an inert is frequently, but not always, applied in MTH catalytic tests at the laboratory scale.^[6, 16]

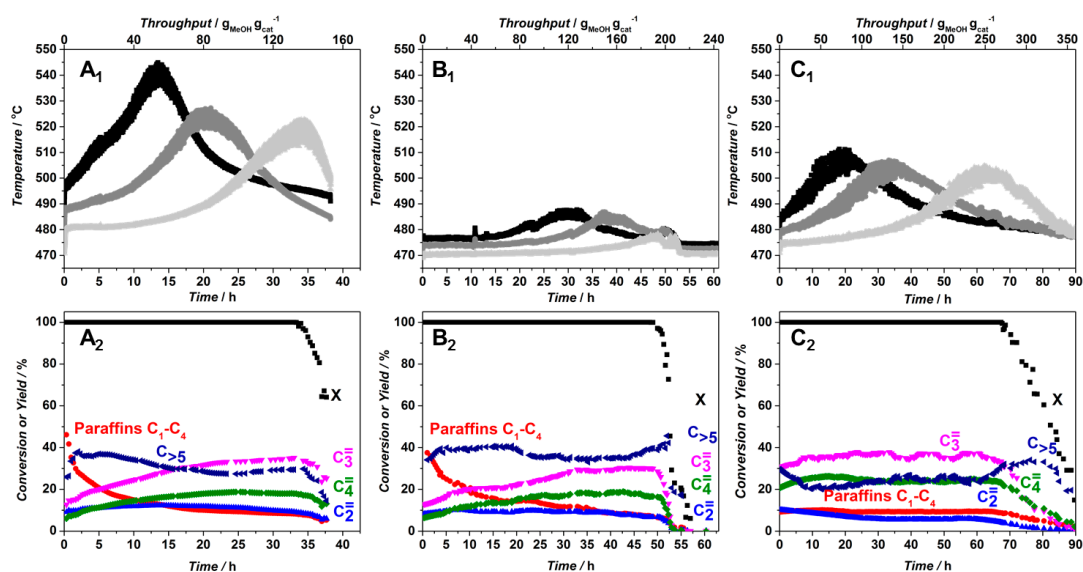


Figure 3. Temperature profiles (A_1 ; B_1 ; C_1) and corresponding product distribution (A_2 , B_2 , C_2) as a function of time-on-stream for ZSM-5 (A_1 , A_2), ZSM-5 : SiC = 1:6 wt/wt (B_1 , B_2) and mesoporous ZSM-5 (C_1 , C_2). Set-point temperature 470 °C, $L_{bed} = 5$ cm, $WHSV = 4$ h⁻¹, MeOH:N₂=1:1. C_{>5} indicates hydrocarbons with 5 or more C atoms.

Therefore, in addition to the above mentioned experiments, the same parent ZSM-5 catalyst was tested in the presence of different amounts of SiC (ZSM-5:SiC = 1:3 and 1:6 wt/wt, equivalent to 1:0.9 and 1:1.8 vol/vol, see Table 1). These experiments clearly demonstrate the strong effects of heat generation on catalyst deactivation (Figure 2). At 400°C, catalyst lifetime increased from 27 to 52 h, independent of the chosen ZSM-5 to SiC ratio (Figure 2A). At 450°C, there is a slight lifetime difference of 3 h depending on the chosen ratio (Figure 2B). Thus, by choosing the appropriate amount of diluent (Catalyst:SiC=1:6 wt/wt or 1:1.8 vol/vol) the catalyst lifetime could be extended by a factor of two at all studied temperatures. These data already indicate the strong non-isothermal behaviour of the process and the necessity to take measures to ensure isothermal operation, such as using large amounts of diluent. On the other hand, a too large degree of dilution may lead to an inhomogeneous catalyst distribution and feed bypassing, meaning that an optimum has to be found in every case.^[15b]

To follow heat dispersion in the axial direction, the same experiments were performed while monitoring the temperature at different positions inside the catalytic bed as a function of time. The data obtained for pure ZSM-5 (no dilution) under conditions generally applied in literature demonstrate a temperature rise inside of the reactor of 80°C (Figure 3A₁). Moreover the three temperature maxima confirm moving active zone behaviour during MTH process.^[17] Once the first region of the bed has deactivated, which corresponds to the first temperature maximum of 547°C, observed after 12 h TOS, the reaction zone slowly moves downwards. The third maximum coincides with MeOH breakthrough, indicating full catalyst deactivation. The observed difference in maximum temperature rise between the

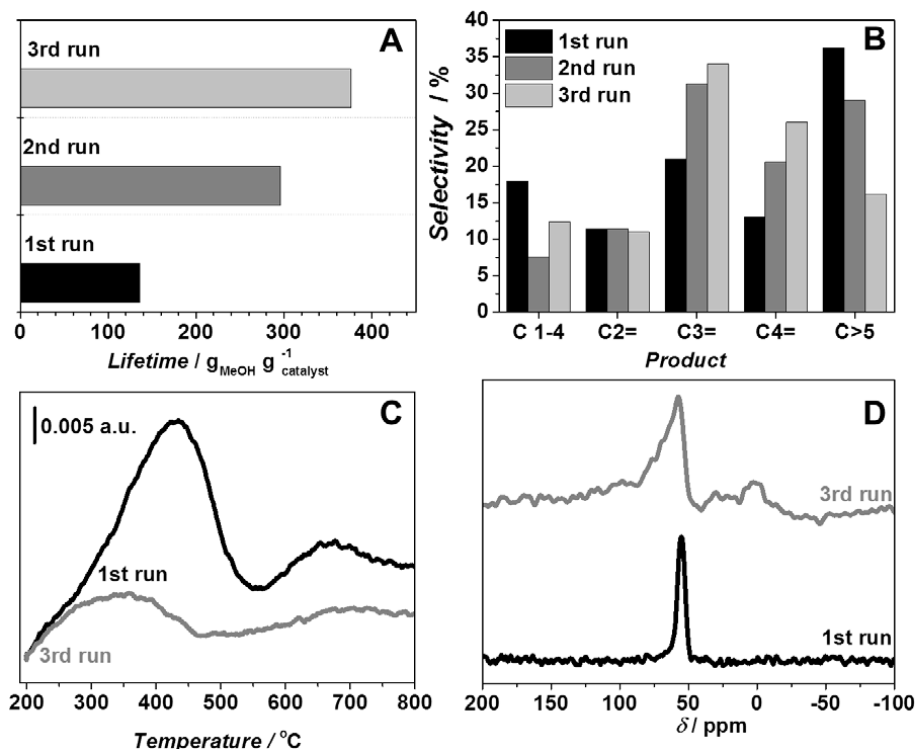


Figure 5. MTH lifetime over undiluted ZSM-5 in three consecutive runs with regeneration in between tested at 470 °C, $L_{bed} = 5$ cm, $WHSV = 4$ h⁻¹, MeOH:N₂=1:1 (A) and corresponding integral selectivities (B). NH₃ TPD profiles of fresh ZSM-5 and regenerated after three catalytic runs (C) and corresponding ²⁷Al MAS NMR (D).

first and second thermocouple (around 20°C) and the fact that product composition at the exit of the reactor is not constant (Figure 3B₁) are also in line with the moving reaction zone behaviour during MTH. In such a scenario, primary products of MTH at the top of the bed would further interact with the fresh zeolite downstream, partly deactivating the catalyst and resulting in less heat released in the lower part of the reactor. Differences in product distribution versus time-on-stream could also be explained on the same grounds. On the other hand, considering the large temperature increase and the fact that water is the main product of MTH, stability of the zeolite framework under the applied conditions may be another point of concern that would also explain the above highlighted literature inconsistencies.^[18]

To verify the latter hypothesis, the deactivated catalyst was subjected to two additional runs under the same reaction conditions with oxidative regeneration steps in between. Figures 4 and 5 show an increased, by a factor of three, catalyst lifetime in the third run, while product distribution changed towards short chain olefins. Especially C3 and C4 formed at the expenses of paraffins and higher products (Figure 5B). On the other hand, Figure 4 demonstrates that, after the first run, similar temperature maxima are reached in all three thermocouples, suggesting that, already during the first run, the zeolite at the bottom of the bed suffers from steaming. After the third run the catalyst was

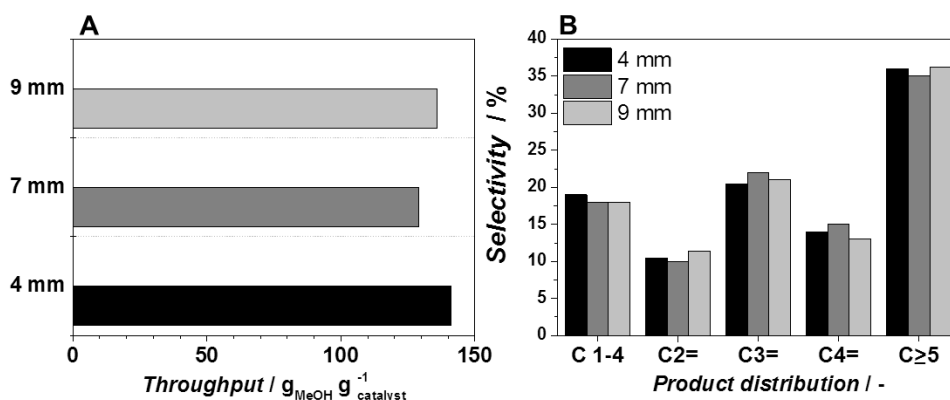


Figure 6. Catalyst lifetime (throughput) (A) obtained over undiluted ZSM-5 tested in reactors with different ID (4, 7, 9 mm) at 470 °C. $L_{\text{bed}} = 5 \text{ cm}$, $WHSV = 4 \text{ h}^{-1}$, $\text{MeOH}:\text{N}_2=1:1$. Corresponding integral product selectivities (B).

regenerated and subjected to characterization to explain the observed differences in catalytic behaviour. NH_3 TPD results (Figure 5C) show a significantly decreased amount of acid sites, while solid-state ^{27}Al NMR indicates formation of extra-framework Al species^[19] which are not observed in the parent ZSM-5 (Figure 5D). These results indicate extensive catalyst dealumination by steaming during the course of reaction, leading to an important loss of acidity. Weaker acid sites favour olefin formation^[20] (most likely by partially suppressing the formation of aromatics) and lead to longer catalyst lifetimes, as already demonstrated in literature.^[21] In turn, higher temperatures result in a bigger extent of dealumination and hence weaker acid sites, thus partially explaining higher olefins (especially propylene) production at higher temperatures (Figure 1).

Temperature profiles measured when using SiC as diluent (Figure 3B₁) show much smaller, but not negligible, temperature rises inside the reactor. The product distribution is similar to the one observed for the non-diluted catalyst with slightly lower selectivities to C3-C4 olefins along with longer catalyst lifetimes, in line with the results presented in Figure 1 and as consequence of the lower overall temperature inside of the reactor. To verify whether radial heat transfer also affects catalyst lifetime, we performed MTH experiments in reactors with different diameter (4, 7, 9 mm) keeping the same bed length and WHSV by adjusting flowrates. No significant differences were found in products selectivity and lifetime when utilizing these reactors (Figure 6). These similarities in catalytic performance indicative identical heat distribution in the radial direction, though one would expect a lower temperature rise in a reactor with smaller diameter.^[22] On the other hand, the observed effect can be explained as a result of interference of heat effect with acid site effect. In principle, a lower temperature rise in a 4 mm reactor would result in lower extent of dealumination, preserving the stronger acid sites which in turn would lead to a higher coking rate and therefore faster deactivation.

Finally, in view of these findings, we formulated the hypothesis that longer lifetimes generally observed in case of mesoporous ZSM-5 could be -partially- due to the fact that creation of extra pores has to lead to site isolation and to a lower generation of heat per unit volume of zeolite. In such a case,

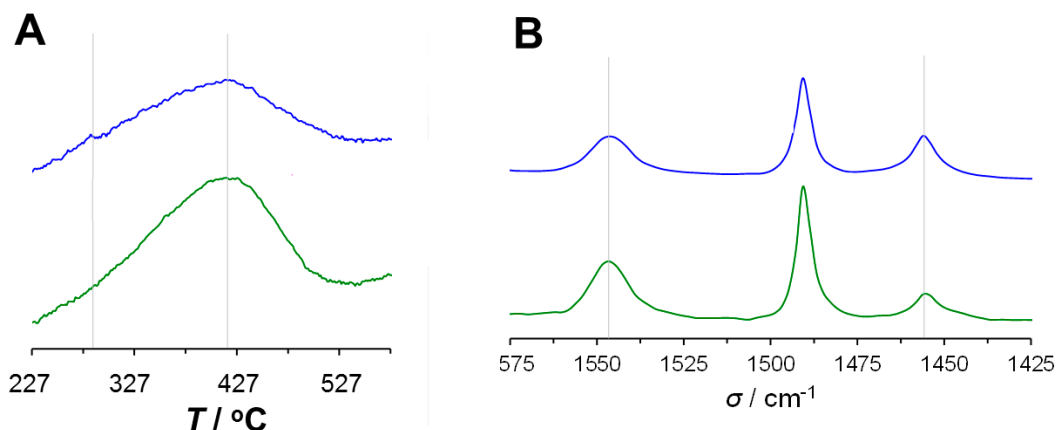


Figure 7. (A) NH_3 TPD profiles of parent ZSM-5 (green) and desilicated and acid washed ZSM-5 (blue). (B) IR spectra of parent ZSM-5 (green) and desilicated, acid washed, ZSM-5 (blue) upon pyridine adsorption.

formation of hot spots should be reduced. Mesoporous ZSM-5 prepared according to the procedure described elsewhere^[23] was tested in MTH under the same conditions as pristine ZSM-5. Catalytic results (Figure 3C₁) show a doubled lifetime for the undiluted mesoporous *versus* the pristine ZSM-5, in good agreement with literature.^[4a, 24] The temperature profiles are characterized by three equivalent maxima around 510°C, thus a $\Delta T = 40^\circ\text{C}$, half of that observed for the parent material. Moreover, significant changes are observed in product distribution. Considerably less paraffins and ethylene and more propylene and butylene are formed (Figure 3C₂). These results are in clear contrast with the trends observed with the pristine zeolite, where an increase in propylene selectivity was observed upon increasing temperature inside of the reactor (cf. Figure 1 and 3). These, *a priori*, controversial results can be explained as a consequence of the desilication process. In spite of the similar Si/Al ratio of the desilicated sample, a lower concentration of acid sites along with a slight decrease in their strength is clear from NH_3 -TPD and Pyridine adsorption (Figures 7A and 7B). Furthermore, additional pores (empty space) are created, which leads to a decrease in density by 22% for the mesoporous zeolite (Table 2) and to a further reduction in acid site concentration (per zeolite volume). The combination of these two factors leads to the formation of less aromatics^[20] and to a lower generation of heat per unit catalyst volume, resulting in a higher selectivity to propylene and in prolonged catalyst lifetimes, as experimentally observed. This indicates that not only on the catalyst bed level heat production should be considered, but also on the catalyst particle level. As a consequence, both active site concentration ('site isolation') and their strength should be kept under control.

4.4. Conclusions.

In conclusion, our results demonstrate a strong effect of heat generation inside the catalytic bed that has clear consequences on catalyst lifetime during MTH over ZSM-5. The high reaction enthalpy leads

to serious difficulties to reach isothermal behaviour during catalyst testing at lab scale, even in the presence of significant amounts of bed diluent. These results partially explain differences found in literature for exactly the same catalytic systems. Moreover, under conditions relevant for industrial application, this specific zeolite (one of the most widely reported in literature) can easily undergo extensive *in-situ* dealumination. This fact is often ignored and deserves special attention. Finally, by monitoring temperature inside the catalytic bed for different catalytic systems, we conclude that the prolonged catalyst lifetime of mesoporous ZSM-5 is due to a lower generation of heat per zeolite unit volume and to changes in the acidity of the catalyst upon post-synthetic desilication. Although improvements in diffusion properties after similar procedures have been clearly demonstrated, ^[25] our results indicate that heat dissipation and catalyst acidity play a more important role in MTH chemistry.

References.

- [1] C. D. Chang, A. J. Silvestri, *J. Catal.* **1977**, *47*, 249-259.
- [2] P. Tian, Y. Wei, M. Ye, Z. Liu, *ACS Catal.* **2015**, *5*, 1922-1938.
- [3] a) U. Olsbye, S. Svelle, M. Bjorgen, P. Beato, T. V. W. Janssens, F. Joensen, S. Bordiga, K. P. Lillerud, *Angew. Chem. Int. Ed.* **2012**, *51*, 5810-5831; b) J. Gascon, J. R. van Ommen, J. A. Moulijn, F. Kapteijn, *Catal. Sci. Technol.* **2015**, *5*, 807-817; c) J. Perez-Ramirez, C. H. Christensen, K. Egeblad, C. H. Christensen, J. C. Groen, *Chem. Soc. Rev.* **2008**, *37*, 2530-2542; d) S. Lopez-Orozco, A. Inayat, A. Schwab, T. Selvam, W. Schwieger, *Adv. Mater.* **2011**, *23*, 2602-2615.
- [4] a) M. Bjorgen, F. Joensen, M. S. Holm, U. Olsbye, K.-P. Lillerud, S. Svelle, *Appl. Catal., A* **2008**, *345*, 43-50; b) M. Choi, K. Na, J. Kim, Y. Sakamoto, O. Terasaki, R. Ryoo, *Nature* **2009**, *461*, 246-U120.
- [5] a) M. Milina, S. Mitchell, P. Crivelli, D. Cooke, J. Perez-Ramirez, *Nat. Commun.* **2014**, *5*, 10; b) M. Milina, S. Mitchell, D. Cooke, P. Crivelli, J. Perez-Ramirez, *Angew. Chem. Int. Ed.* **2015**, *54*, 1591-1594.
- [6] N.-L. Michels, S. Mitchell, J. Perez-Ramirez, *ACS Catal.* **2014**, *4*, 2409-2417.
- [7] P. Kumar, J. W. Thybaut, S. Svelle, U. Olsbye, G. B. Marin, *Ind. Eng. Chem. Res.* **2013**, *52*, 1491-1507.
- [8] W. Y. Guo, W. Z. Wu, M. Luo, W. D. Xiao, *Fuel Process. Technol.* **2013**, *108*, 133-138.
- [9] S. Zhang, B. Zhang, Z. Gao, Y. Han, *Ind. Eng. Chem. Res.* **2010**, *49*, 2103-2106.
- [10] D. E. Mears, *J. Catal.* **1971**, *20*, 127-131.
- [11] S. Sartipi, K. Parashar, M. Jose Valero-Romero, V. P. Santos, B. van der Linden, M. Makkee, F. Kapteijn, J. Gascon, *J. Catal.* **2013**, *305*, 179-190.
- [12] C. A. Emeis, *J. Catal.* **1993**, *141*, 347-354.
- [13] I. Yarulina, J. Goetze, C. Gücüyener, L. van Thiel, A. Dikhtiarenko, J. Ruiz-Martinez, B. M. Weckhuysen, J. Gascon, F. Kapteijn, *Catal. Sci. Technol.* **2016**.
- [14] a) W. Wu, W. Guo, W. Xiao, M. Luo, *Fuel Process. Technol.* **2013**, *108*, 19-24; b) W. J. H. Dehertog, G. F. Froment, *Appl. Catal., A* **1991**, *71*, 153-165.
- [15] a) R. J. Berger, J. Perez-Ramirez, F. Kapteijn, J. A. Moulijn, *Appl. Catal., A* **2002**, *227*, 321-333; b) J. Perez-Ramirez, R. J. Berger, G. Mul, F. Kapteijn, J. A. Moulijn, *Catal. Today* **2000**, *60*, 93-109.
- [16] a) M. M. Mertens, S. N. Vaughn, ExxonMobil Chemical Patents Inc., 2013; b) D. Mier, A. G. Gayubo, A. T. Aguayo, M. Olazar, J. Bilbao, *AIChE J.* **2011**, *57*, 2841-2853.
- [17] a) H. Schulz, M. Wei, *Top. Catal.* **2014**, *57*, 683-692; b) H. Schulz, *Catal. Today* **2010**, *154*, 183-194; c) S. Muller, Y. Liu, M. Vishnuvarthan, X. Y. Sun, A. C. van Veen, G. L. Haller, M. Sanchez-Sanchez, J. A. Lercher, *J. Catal.* **2015**, *325*, 48-59; d) S. Ilias, A. Bhan, *J. Catal.* **2012**, *290*, 186-192.
- [18] a) M. Ibanez, M. Gamero, J. Ruiz-Martinez, B. M. Weckhuysen, A. T. Aguayo, J. Bilbao, P. Castano, *Catal. Sci. Technol.* **2016**, *6*, 296-306; b) D. W. Gardner, J. J. Huo, T. C. Hoff, R. L. Johnson, B. H. Shanks, J. P. Tessonnier, *ACS Catal.* **2015**, *5*, 4418-4422; c) M. Nielsen, R. Y. Brogaard, H. Falsig, P. Beato, O. Swang, S. Svelle, *ACS Catal.* **2015**, *5*, 7131-7139.
- [19] a) E. Brunner, H. Ernst, D. Freude, T. Frohlich, M. Hunger, H. Pfeifer, *J. Catal.* **1991**, *127*, 34-41; b) C. Ding, X. Wang, X. Guo, S. Zhang, *Catal. Commun.* **2008**, *9*, 487-493.
- [20] M. Westgård Erichsen, K. De Wispelaere, K. Hemelsoet, S. L. C. Moors, T. Deconinck, M. Waroquier, S. Svelle, V. Van Speybroeck, U. Olsbye, *J. Catal.* **2015**, *328*, 186-196.
- [21] M. Stöcker, *Microporous Mesoporous Mater.* **1999**, *29*, 3-48.
- [22] A. Grah, U. Nowak, M. Schreier, R. Adler, *Heat Mass Transfer.* **2009**, *45*, 417-425.
- [23] S. Sartipi, M. Alberts, V. P. Santos, M. Nasalevich, J. Gascon, F. Kapteijn, *ChemCatChem* **2014**, *6*, 142-151.
- [24] a) Y. Wei, P. E. de Jongh, M. L. M. Bonati, D. J. Law, G. J. Sunley, K. P. de Jong, *Appl. Catal., A* **2015**, *504*, 211-219; b) S. L. Zhang, Y. J. Gong, L. L. Zhang, Y. S. Liu, T. Dou, J. Xu, F. Deng, *Fuel Process. Technol.* **2015**, *129*, 130-138; c) J. Kim, M. Choi, R. Ryoo, *J. Catal.* **2010**, *269*, 219-228.
- [25] a) J. C. Groen, W. Zhu, S. Brouwer, S. J. Huynink, F. Kapteijn, J. A. Moulijn, J. Perez-Ramirez, *J. Am. Chem. Soc.* **2007**, *129*, 355-360; b) J. Perez-Ramirez, C. H. Christensen, K. Egeblad, C. H. Christensen, J. C. Groen, *Chem. Soc. Rev.* **2008**, *37*, 2530-2542; c) J. Karger, R. Valiullin, *Chem. Soc. Rev.* **2013**, *42*, 4172-4197; d) L. Guedre, M. Milina, S. Mitchell, J. Perez-Ramirez, *Adv. Funct. Mater.* **2014**, *24*, 209-219.

Chapter

5

***Suppression of the Aromatic Cycle in
Methanol-to-Olefins Process over ZSM-5
By Post-synthetic Modification using
Calcium***

Incorporation of Ca in ZSM-5 results in a twofold increase of propylene selectivity (53%), a total light olefin selectivity of 90%, and a nine times longer catalyst lifetime (throughput 792 g MeOH/g catalyst) in the methanol-to-olefins (MTO) process. Analysis of the product distribution and theoretical calculations reveal that post-synthetic modification with Ca^{2+} leads to the formation of CaOCaOH^+ that strongly weakens the acid strength of the zeolite. As a result, the rate of hydride transfer and oligomerization reactions on these sites is greatly reduced, resulting in the suppression of aromatic species formation. Our results further highlight the importance of acid strength on product selectivity and zeolite lifetime in MTO chemistry.

This Chapter is based on the following publication:

I. Yarulina, S. Bailleul, A. Pustovarenko, J. R. Martinez, K. D. Wispelaere, J. Hajek, B. M. Weckhuysen, K. Houben, M. Baldus, V. Van Speybroeck, F. Kapteijn, J. Gascon, *ChemCatChem* **2016**, *8*, 3057-3063.

5.1. Introduction.

The discovery of the methanol-to-gasoline (MTG) process over ZSM-5 catalysts by Mobil Corporation in 1977^[1] opened an oil-free route for the synthesis of hydrocarbons. Since then, a great deal of effort has been devoted to mechanistic studies that led to a better understanding of this catalytic process.

The evolution in mechanism comprehension started from understanding the first C-C bond formation (which is still under the debate)^[2] and slowly developed to the currently accepted dual-cycle concept.^[3] An important milestone in MTO history was the introduction of the “hydrocarbon pool” concept by Dahl and Kolboe,^[4] who proposed the existence of intermediates, of similar nature to coke, responsible for olefin formation. These intermediates were later clarified to be methylbenzenes and/or their protonated versions.^[5] Transient ¹²C/¹³C experiments performed over ZSM-5 however showed that while ethylene is predominantly formed through the abovementioned aromatic species, propylene and higher alkenes are formed through olefin methylation and cracking reactions.^[3b, 5] These observations led to the acceptance of the so called dual-cycle mechanism, involving the presence of two cycles, namely, a methylation/cracking cycle, where mostly propylene is produced, and an aromatic cycle, responsible for ethylene and aromatics formation and catalyst deactivation.

Sun *et al.*^[3c, 6] have shown that one cycle can be promoted over the other by co-feeding species participating in these cycles, *i.e.* co-feeding of propylene led to an increased selectivity of olefinic species, while co-feeding of aromatics promoted the formation of methane, ethylene and aromatic species.

An approach to suppress the aromatic cycle is currently of utmost interest as it is the key to prolong catalyst lifetime and to increase the selectivity to propylene. Teketel *et al.*^[7] have shown, using ZSM-22, that by choosing the appropriate zeolite topology^[8] the methylation/cracking cycle can be promoted over the aromatic one.

Considering that aromatic species are formed from higher alkenes, another approach to suppress their formation would involve tuning the acidity of the catalyst, since less acidic catalysts are known to promote the alkene cycle.^[9] In this way, it would be possible to produce olefins *via* the methylation/cracking cycle but their further conversion to aromatics would be restricted.

Some studies, mainly performed in the early 1990s, showed that modification of ZSM-5 with some elements like Ca,^[10] B^[11] or P^[12] leads to the increased formation of olefins. Many of these results were very promising but did not receive the worthwhile attention as “*the most valuable ethylene was formed very little*”.^[13] Nowadays, the industrial focus has shifted towards propylene. In this work we demonstrate that, in case of Ca containing ZSM-5, the observed high selectivities to propylene and butenes and low selectivities to ethylene are due to the promotion of the olefinic cycle over the aromatic cycle.

5.2. Experimental.

5.2.1. Synthesis of Catalysts.

Ca-modified ZSM-5 catalysts were prepared from commercial ZSM-5 (Zeolyst, CBV 8014). Ca-ZSM5-IE was prepared by ion-exchange with 1 M $\text{Ca}(\text{NO}_3)_2 \cdot 4\text{H}_2\text{O}$ solution at 80 °C for 2 h repeated three times with filtration step in between and followed by calcination at 550 °C. 6Ca-ZSM5-SSIE was prepared by solid-state ion-exchange with $\text{Ca}(\text{CH}_3\text{COO})_2$. SSIE was achieved by grinding required amount of calcium acetate with commercial ZSM-5 for 30 minutes in a mortar followed by calcination at 550 °C. 6Ca-ZSM5-EW was prepared by wet impregnation. In a typical procedure the required amount of $\text{Ca}(\text{NO}_3)_2 \cdot 4\text{H}_2\text{O}$ was dissolved in 5 mL of water. 4 g Zeolite was added to this solution and left overnight under the stirring at room temperature. Subsequently, the catalyst was dried for 12 h at 80 °C and calcined at 550 °C. 6Ca-ZSM5-IWI, 4Ca-ZSM5-IWI, 2Ca-ZSM5-IWI, 1Ca-ZSM5-IWI were prepared by incipient wetness impregnation. 4g Parent zeolite was impregnated with 1.06 g of $\text{Ca}(\text{NO}_3)_2 \cdot 4\text{H}_2\text{O}$ solution corresponding to the total pore volume of the zeolite. After impregnation, catalysts were kept overnight in a desiccator followed by drying for 12 h at 80 °C and calcination at 550 °C. A heating rate of 2 °C min^{-1} and static air conditions were applied in all cases for calcination.

5.2.2. Characterization of Catalysts.

N_2 adsorption at -196 °C K was carried out using a Tristar II 3020 analyzer (Micromeritics). Prior to the experiment, samples were outgassed under vacuum at 350 °C for 16 h.

Toluene adsorption measurements were carried out at 25 °C using Micromeritics 3Flex equipped with a 15 mL stainless steel vapor vessel.

Images were recorded using a JEOL JSM-6010LA with a standard beam potential of 10 kV and an Everhart-Thornley detector. X-ray microanalysis (SEM/EDX) confirmed the elemental composition in the sample by scanning electron microscopy (SEM) coupled with a dispersive X-ray microanalysis system (EDX) with a Silicon-drift detector.

The XRD patterns of the powders were recorded in Bragg–Brentano geometry with a Bruker D8 Advance X-ray diffractometer equipped with a LynxEye position-sensitive detector. Measurements were performed at RT by using monochromatic $\text{CoK}\alpha$ ($\lambda = 1.788970 \text{ \AA}$) radiation between $2\theta = 5^\circ$ and 50° .

Elemental analysis was performed with a PerkinElmer Optima 4300 DV instrument. The samples were first digested in an aqueous mixture of 1% HF and 1.25% H_2SO_4 . After dilution, analysis was done by inductively coupled plasma optical emission spectrometry (ICP-OES).

Temperature-programmed NH_3 desorption (NH_3 -TPD) was measured by an AutoChem II chemisorption analyzer (Micromeritics). Approximately 0.2 g of the material was first degassed under He flow at 400 °C and then saturated with NH_3 at 200 °C during 1 h using a flow of 1.65 % NH_3 in He. The gas mixture was then switched back to He and the sample was purged at 200 °C for about 1 h to remove

weakly adsorbed NH₃ molecules. TPD was subsequently recorded under He flow, from 200 °C to 800 °C. Flow rates and heating rates were 25 mL min⁻¹ and 10 °C min⁻¹ respectively for all TPD experiments.

Transmission FT-IR spectroscopy using CO as a probe molecule was performed using a Nicolet Nexus spectrometer at 4 cm⁻¹ resolution equipped with an extended KBr beam splitting and a mercury cadmium telluride (MCT) cryo-detector. The pellets were placed in an IR quartz cell equipped with CaF₂ windows. A movable sample holder allows the sample to be placed in the infrared beam for the measurements or into the furnace for thermal treatments. The cell is connected to a vacuum line for pretreatment. The specimen is activated in vacuum at 400 °C for 16 h to remove adsorbed species. After this step, the samples were cooled down to -130 °C and CO was dosed up to 30 mbar.

Transmission FT-IR spectroscopy using pyridine as a probe molecule was performed using a Nicolet 6700 spectrometer equipped with MCT/B detector. The specimen was activated in vacuum at 400 °C for 16 h to remove adsorbed species. After activation, pellets were saturated with pyridine vapor and further evacuated at 160 °C for 2 h. Spectra were recorded in 1000-4000 cm⁻¹ range at 4 cm⁻¹ resolution and co-addition of 128 scans. The amount of Brønsted (BAS) and Lewis (LAS) acid sites was derived from the bands at 1545 and 1456 cm⁻¹ as described elsewhere using extinction coefficients of 1.67 and 2.22 respectively.^[14] Assuming that one molecule of pyridine is adsorbed on one acid site, the following expressions were used to calculate C_{BAS} and C_{LAS}^[14b]:

$$C_{BAS} = 1.88 \cdot IA(B) \cdot R^2/W \quad (1)$$

$$C_{LAS} = 1.42 \cdot IA(L) \cdot R^2/W \quad (2)$$

where *IA* (BAS, LAS) is integrated absorbance of BAS or LAS band (cm⁻¹), *R* – radius of catalyst disk (cm), while *W* – weight of catalyst sample (mg).

For solid-state NMR measurements using TMPO as a probe molecule, the preparation procedure was adapted from Wiper *et al.*^[15] 50 mg of TMPO was dissolved in 15 mL of anhydrous CH₂Cl₂ in an Ar glove box. 15 mL of this solution was added to the dehydrated at 400 °C for 16 h zeolite and left under the stirring for 1 h. Subsequently, materials were heated at 150 °C for 1 h under vacuum to allow homogeneous distribution of TMPO. Finally, cooled down samples were transferred into a zirconia MAS rotor (3.2 mm). Solid-state NMR ³¹P spectra were recorded on a Bruker spectrometer operating at a ¹H Larmor frequency of 500 MHz equipped with a triple resonance 3.2mm Magic Angle Spinning (MAS) probe, using an MAS frequency of 19 kHz. After a ¹H 90 pulse, ¹H-³¹P cross-polarization (CP) was achieved by applying simultaneously a 46 kHz ³¹P and a 94 kHz ¹H RF field (ramp 70-100%) with a contact time of 4.2 ms. During acquisition 83kHz SPINAL64 proton decoupling^[16] was applied. For each experiment, 256 scans were used with a recycle delay of 4 s.

5.2.3. Catalyst Testing.

Catalytic experiments were carried out in a Microactivity Reference unit (PID Eng&Tech) at 500 °C and ambient pressure. The catalyst (pressed, crushed and sieved to particle sizes 250-420 μm) was

placed in a fixed-bed with internal diameter 9 mm for standard experiments. An HPLC pump (307 5-SC-type piston pump, Gilson) was used to feed methanol to the reactor system. A weight-hourly space velocity (*WHSV*) of $8 \text{ g}_{\text{MeOH}} \text{ g}_{\text{cat}}^{-1} \text{ h}^{-1}$, a $\text{N}_2 : \text{MeOH} = 1:1$ molar feed composition and atmospheric pressure were utilized. The product mixture was analyzed online with an Interscience CompactGC equipped with a 15 m capillary RTX-1 (1% diphenyl-, 99% dimethylpolysiloxane) column and a flame ionization detector. Conversion, selectivities and yields were calculated on a molar carbon basis. Conversion, selectivities and yields were calculated on a molar carbon basis. Thus, conversion was defined as the carbon-based fraction of light oxygenates (methanol and dimethyl ether) consumed during the reaction:

$$X = \frac{n_{\text{C,MeOH}_{\text{in}}} - n_{\text{C,MeOH}_{\text{out}}} - 2 \cdot n_{\text{C,DME}_{\text{out}}}}{n_{\text{C,MeOH}_{\text{in}}}} \cdot 100\% \quad (3)$$

the selectivity towards ethylene (4) and propylene (5) was calculated based on the carbon number as follows:

$$S_{\text{ethylene}} = \frac{2 \cdot n_{\text{C}_2\text{H}_4}}{n_{\text{C,MeOH}_{\text{in}}} - n_{\text{C,oxy}_{\text{out}}}} \cdot 100\% \quad (4)$$

$$S_{\text{propylene}} = \frac{3 \cdot n_{\text{C}_3\text{H}_6}}{n_{\text{C,MeOH}_{\text{in}}} - n_{\text{C,oxy}_{\text{out}}}} \cdot 100\% \quad (5)$$

and the yield of a component *i* was defined from its selectivity and methanol conversion:

$$Y_i = \frac{S_i \cdot X}{100} \quad (6)$$

The performance results are presented in graphs as a function of the methanol mass throughput per amount of catalyst used ($\text{g}_{\text{MeOH}} \text{ g}_{\text{cat}}^{-1}$) and defined as overall MeOH throughput fed through the catalytic bed before the conversion of oxygenates drops to 80 %. Selectivities were taken after testing catalysts for 1.5 hour. It should be also mentioned that for Ca-modified samples steady state was achieved after approximately 40 minutes on stream and product distribution did not change significantly (Figure D1) after that time. In case of ZSM-5, no steady was achieved, early stages being characterized by the high selectivity towards paraffins decreasing with time on stream in favor of olefins.

5.3. Results and Discussion.

In this work, we modified the acidity of commercial ZSM-5 *via* Ca incorporation and investigated, using a combined experimental and theoretical approach, how this modification changes the nature of the acid sites, which in turn leads to the suppression of the aromatic species favouring the olefinic cycle, leading to enhanced propylene formation.

The parent ZSM-5 zeolite used for the preparation of the Ca containing catalysts was purchased from Zeolyst (Si/Al=40, CBV8014). Depending on the method of preparation, the obtained catalysts are

Table 1. Textural and catalytic properties of the ZSM-5 catalyst materials under study.

Entry	Catalyst	$V_{\text{total}}^{\text{a}}$ ($\text{cm}^3 \text{g}^{-1}$)	$V_{\text{micro}}^{\text{a}}$ ($\text{cm}^3 \text{g}^{-1}$)	$S_{\text{BET}}^{\text{a}}$ ($\text{m}^2 \text{g}^{-1}$)	$S_{\text{micro}}^{\text{a}}$ ($\text{m}^2 \text{g}^{-1}$)	C_{AS}^{b} ($\mu\text{mol g}^{-1}$)	$C_{\text{BAS}}^{\text{c}}$ ($\mu\text{mol g}^{-1}$)	$C_{\text{LAS}}^{\text{c}}$ ($\mu\text{mol g}^{-1}$)	Throughput ^d ($\text{g}_{\text{MeOH}} \text{g}_{\text{cat}}^{-1}$)	$S(\text{C}_{3=})$ ($\text{C mol}\%$)
1	ZSM-5	0.256	0.152	448	363	387	232	35	88	25
2	Ca-ZSM5-IE	0.273	0.145	429	344	402	138	108	264	39
3	6Ca-ZSM5-	0.212	0.111	323	267	171	128	0	136	39
4	6Ca-ZSM5-	0.199	0.110	336	276	374	38	208	304	43
5	6Ca-ZSM5-IWI	0.226	0.124	385	310	384	29	240	504	53
6	4Ca-ZSM5-IWI	0.223	0.126	387	313	381	27	240	480	45
7	2Ca-ZSM5-IWI	0.238	0.128	392	315	332	40	228	792	39
8	1Ca-ZSM5-IWI	0.246	0.138	418	334	347	66	198	272	46

^aFrom N_2 adsorption. ^bConcentration of acid sites (AS) derived from NH_3 TPD. ^cConcentration of Brønsted (BAS) and Lewis (LAS) acid sites derived from Pyridine IR. ^dAmount of methanol (g) converted per g of zeolite before conversion decreases below 80%.

denoted as Ca-ZSM5-IE, 6Ca-ZSM5-SSIE, 6Ca-ZSM5-IWI, 6Ca-ZSM5-EW, where IE, SSIE, IWI and EW stand for ion-exchange, solid state ion-exchange, incipient wetness impregnation and wet impregnation, respectively. All catalysts were prepared aiming at a 6 wt. % Ca loading. Another set of catalysts was prepared by incipient wetness impregnation by varying Ca loading from 1 to 6 wt. % respectively. Details about catalyst preparation can be found in Experimental Section. XRD results show (Figure D2) that the original MFI topology is preserved in all samples.^[12a]

Textural properties displayed in Table 1 demonstrate that Ca incorporation produces a small decrease in micropore volume, while no additional mesopores are created. NH_3 TPD results (Table 1 and Figure 1A-B) show that the concentration of acid sites for all catalysts except for 6Ca-ZSM5-SSIE is similar to the parent ZSM-5, while the desorption maximum shifts from 435 °C to 290 °C for 6Ca-ZSM5-EW and 6Ca-ZSM5-IWI, already indicating a qualitative weakening in the strength of these acid sites upon Ca incorporation. Direct observation of the zeolite IR spectrum in Figure 1C shows the disappearance of the 3600 cm^{-1} band characteristic for the Brønsted hydroxyl stretching, implying the transformation or titration of most Brønsted acid sites upon Ca incorporation. Since NH_3 TPD is not an adequate tool to quantify the nature and strength of acid sites,^[17] the catalysts under study were additionally characterized by FT-IR spectroscopy using pyridine as a probe molecule (Figure 1D-E). Parent ZSM-5 shows two IR bands at 1546 cm^{-1} and 1455 cm^{-1} representing adsorption of pyridine on Brønsted and Lewis acid sites, respectively. The Lewis acidity in the parent zeolite is ascribed to extra-framework Al species^[14a] but can be a result of both extra-framework and perturbed framework Al.^[18] Incorporation of Ca into the zeolite caused a significant decrease of Brønsted acidity for all samples, especially for 6Ca-ZSM5-EW and 6Ca-ZSM5-IWI, for which the vibration at 1545 cm^{-1} almost completely disappeared, in line with IR spectra of OH region (Figure 1C). Along with the disappearance of Brønsted acidity, a new pyridine band at 1446 cm^{-1} , assigned to acid sites of Lewis nature, arises for Ca-containing catalysts, indicating transformation of strong Brønsted acid sites to Lewis acid ones. Interestingly, Ca-ZSM5-IE displays both IR bands at 1455 and 1446 cm^{-1} and can be considered as an intermediate between ZSM-5 and 6Ca-ZSM5-IWI, having medium acidic properties. Figure 1E and Table

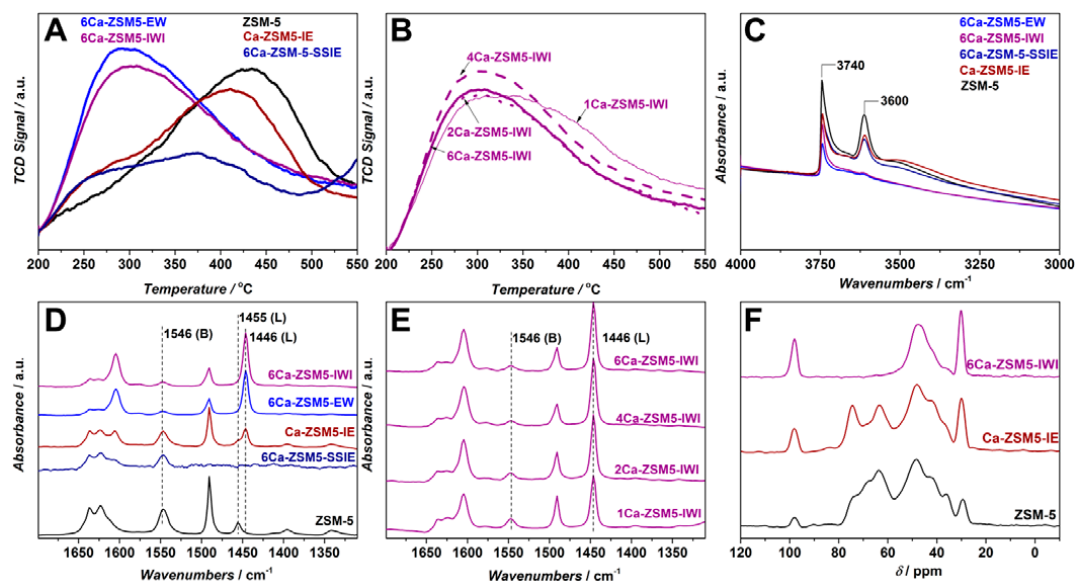


Figure 1. Acidity characterization of Ca-containing ZSM-5 catalysts and parent ZSM-5. (A – B) NH_3 -TPD profiles, (C) FT-IR spectra in the OH-stretching region (D-E) FT-IR spectra of adsorbed pyridine, (F) ^1H - ^{31}P CP MAS NMR spectra for TMPO adsorbed on 6Ca-ZSM5-IWI, Ca-ZSM5-IE and ZSM-5.

1 show that the amount of Brønsted acid sites gradually decreases by increasing Ca loading from 1 to 6 wt.%.

In order to obtain a full picture of the acidic properties of these catalysts, we performed additional characterization by solid-state NMR using trimethylphosphine oxide (TMPO) as a probe molecule (Figure 1F). Several ^{31}P resonance peaks at 99, 75, 67, 63, 47, 43, 36 and 30 ppm are observed. The resonance peak at 30 ppm is ascribed to “mobile” TMPO, while peaks at 47, 43 and 36 ppm are characteristic for physisorbed TMPO.^[19] Peaks in the range between 60 and 90 ppm are arising from TMPOH^+ complexes on Brønsted acid sites.^[20] Peak at 99 ppm can be attributed to very strong Lewis acid sites.^[21] Adsorption of TMPO on Ca-ZSM5-IE resulted in the appearance of similar peaks; however, a significant decrease of the resonance at 67 ppm suggests that, during ion-exchange, Ca preferentially occupies certain Brønsted acid sites. In contrast, in the spectra of 6Ca-ZSM5-IWI the peaks in the 60-90 ppm range are absent. In summary, the extensive acidity characterization performed demonstrates the transformation of Brønsted into Lewis acidity.

FT-IR spectroscopy using CO as a probe molecule (Figure 2) shows the appearance of a band at around 2200 cm^{-1} gradually shifting to 2179 cm^{-1} (Figure 2B₂) for 6Ca-ZSM5-IWI in comparison to ZSM-5 (Figure 2A₁) characterized by the band at 2174 cm^{-1} typical for CO adsorbed on the bridging hydroxyls. The band at 2200 cm^{-1} (Figure 2B₂) originates from the electrostatic interaction between CO and Ca^{2+} species. Moreover, the fact that this band is broad and asymmetric indicates the presence of Ca^{2+} species of different nature and at different positions within the zeolite framework. At higher CO coverage,

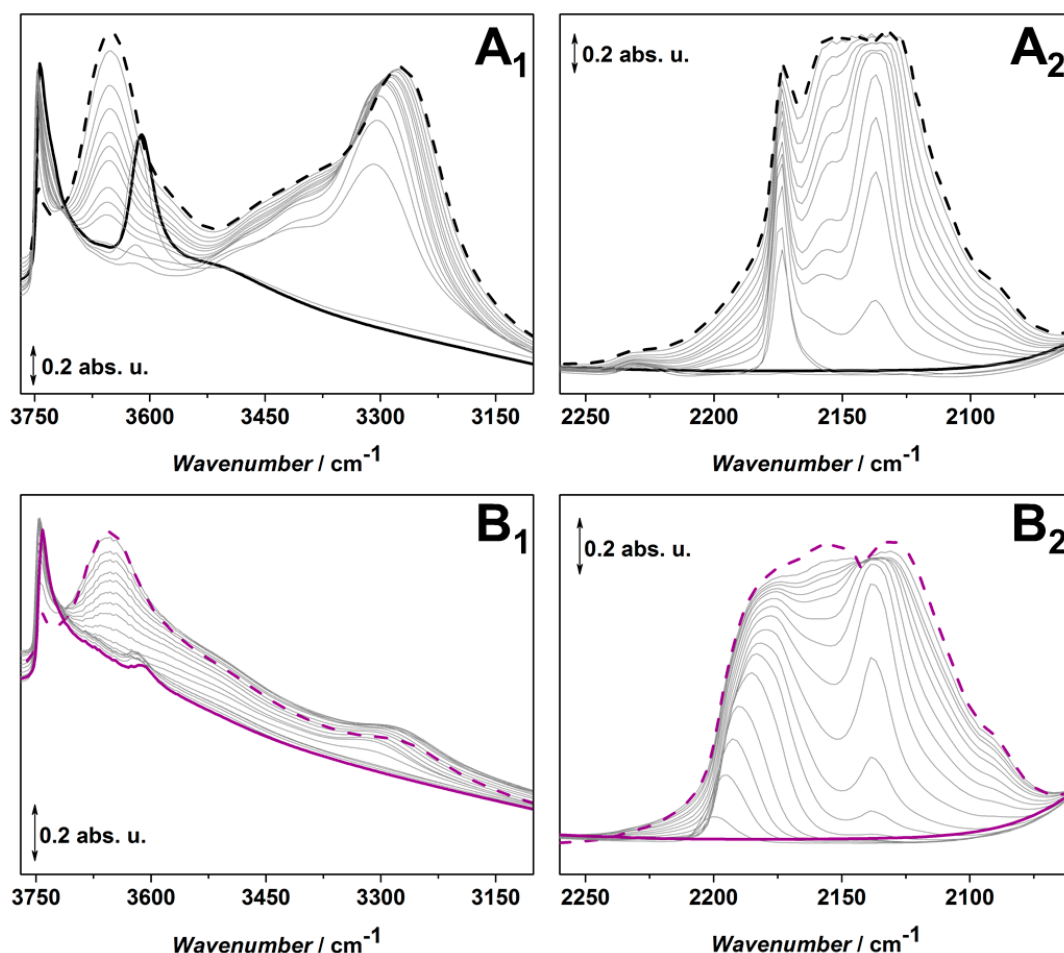


Figure 2. FT-IR spectra measured at $-130\text{ }^{\circ}\text{C}$ after adding increasing dosages of CO on (A) ZSM-5 and (B) 6-CaZSM5-IWI. Panels A₁ and B₁ report the spectra in the hydroxyl group range ($3760\text{--}3100\text{ cm}^{-1}$), while panels A₂ and B₂ report the CO vibrational mode region ($2260\text{--}2060\text{ cm}^{-1}$). The bold solid line represents pretreated catalysts in vacuum, while the dashed black curves represent spectra collected at 30 mbar CO equilibrium.

the development of a band at 2174 cm^{-1} is also observed, suggesting residual presence of Brønsted acidity.

The as-prepared catalysts were tested at $500\text{ }^{\circ}\text{C}$ in the MTO process. Such a relatively high reaction temperature was chosen due to the fact that higher temperatures favour the formation of short chain olefins.^[22] Furthermore, because of their lower acidity, some of the catalysts were not catalytically active below $475\text{ }^{\circ}\text{C}$. Figure 3A₁ shows that incorporation of Ca into ZSM-5 prolonged catalyst lifetime. Herein, the method of catalyst preparation is crucial to obtain the longest lifetime and selectivity to propylene, the best results being obtained using catalyst prepared by IWI (504 vs 88 g MeOH converted per gram of catalyst). As shown above, other preparation methods are less effective in weakening zeolite acidity and led to shorter catalyst lifetimes. Remarkably, Ca incorporation caused significant changes in product

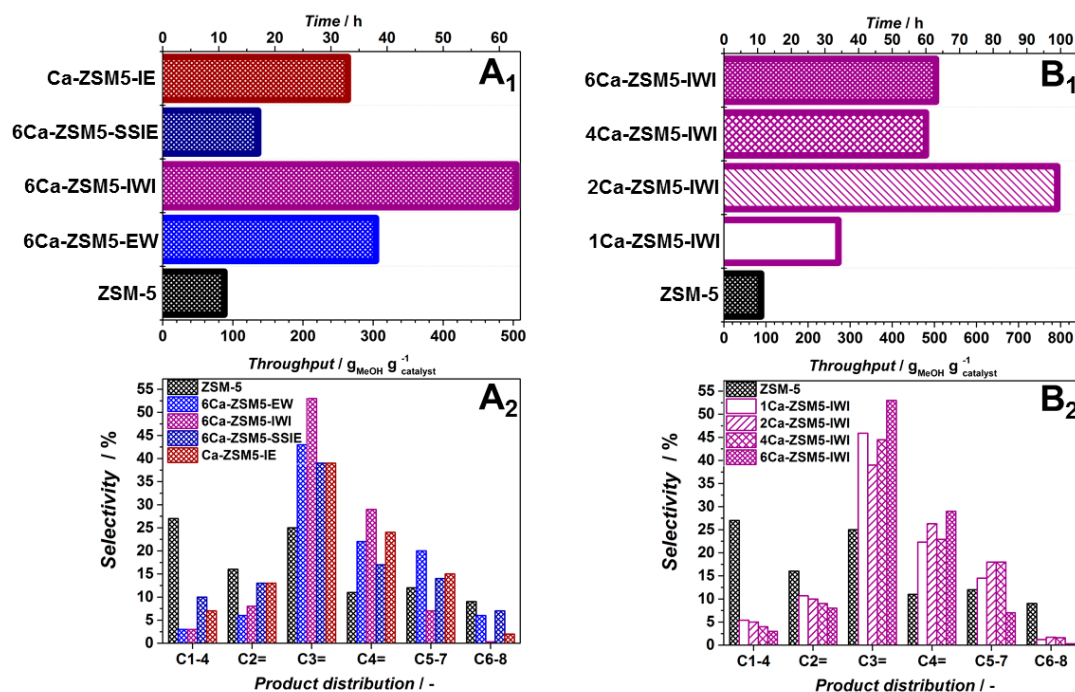


Figure 3. Methanol conversion over Ca-modified ZSM-5 (A) prepared by different methods and (B) over Ca-modified ZSM-5 prepared by the IWI method with different Ca loading. Panels (A₁, B₁) report catalyst lifetime, while panels (A₂, B₂) report product distribution. All catalysts were tested at 500°C. $M_{cat} = 0.5$ g, $WHSV = 8$ g_{MeOH} g_{cat}⁻¹ h⁻¹, MeOH:N₂ = 1:1.

distribution (Figure 3A₂), the most important being a decrease in the formation of paraffins and ethylene. For 6Ca-ZSM5-IWI and 6Ca-ZSM5-EW, selectivity to paraffins and to ethylene drop from 27 down to 3 % and from 16 % to 8 and 6 %, respectively, when compared with the parent ZSM-5. Moreover, 6Ca-ZSM5-IWI showed only negligible formation of aromatics in comparison to parent ZSM-5 (compare $S_{C6-8} = 0.5\%$ and 9% respectively, Figure 3A₂). Both the much lower selectivity to aromatics and remarkably lower ethylene productivity indicate - to a large extent - the suppression of the aromatic cycle. Indeed, ethylene is considered to be the main product of this cycle^[3b, 5, 23]. On the other hand, the lower paraffin selectivity indicates the partial suppression of intermolecular hydride transfer reactions responsible for the conversion of olefins to paraffins and aromatics.^[23a] The latter is considered to be the bridging step between the olefinic and aromatic cycles. We thus conclude that the observed suppression of the aromatic cycle is achieved by reducing the rate of hydride transfer and oligomerization reactions on significantly weaker acid sites.^[24]

As catalyst 6Ca-ZSM5-IWI prepared by IWI showed the highest selectivity to propylene (53%) and butenes (29%) and the longest lifetime, this method was used to further to optimize the Ca content. NH₃ TPD and pyridine FT-IR (Figures 1B and 1E) show that all samples possess a similar concentration of

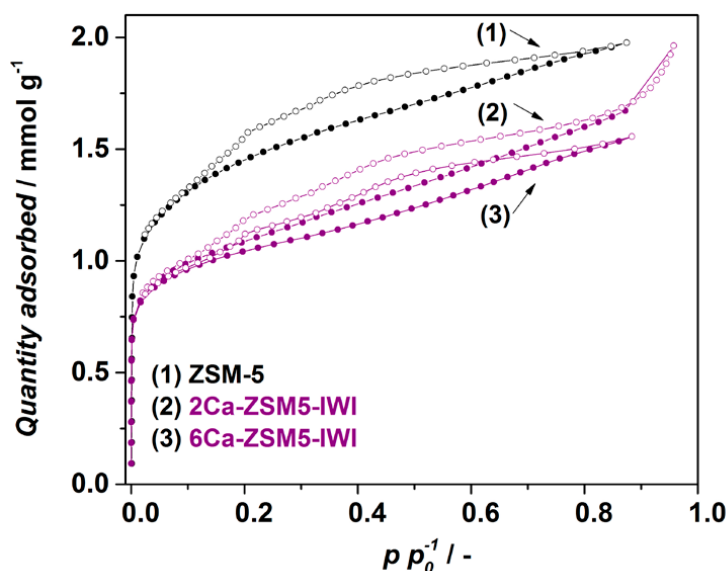


Figure 4. Toluene adsorption-desorption isotherms at 25°C of ZSM-5 (1), 2Ca-ZSM5-IWI (2) and 6Ca-ZSM5-IWI (3).

acid sites and modification with Ca caused almost complete disappearance of Brønsted acidity as was observed for 6Ca-ZSM5-IWI.

Catalytic experiments (Figure 3B₁) showed that by employing a Ca loading of 2 wt.% with a molar ratio of Ca to Al 2:1 (Table D1), catalyst lifetime was further prolonged up to 99 h, corresponding to 792 g of MeOH converted per gram of catalyst before deactivation, which is 9 times longer than the commercial ZSM-5. The selectivities to propylene (39%) and butenes (26%) were slightly lower than for 6Ca-ZSM5-IWI (Figure 3B₂). Observed differences in selectivities caused by different Ca loadings are tentatively attributed to additional spatial restrictions caused by Ca deposition inside the micropores, i.e. reducing micropore volume (see Table 1), resulting in less aromatics formation, thus enhancing formation of propylene and decreasing formation of ethylene (Figure 3B₂). However, based on toluene adsorption isotherms (Figure 4), shape selective effects can be ruled out. Whether bulkier aromatic molecules^[12b, 23a], as suggested by Abubakar *et al.*^[25] on P-modified ZSM-5, can be formed inside of the pores of the Ca modified ZSM-5 catalyst is still not clear.

As mentioned in the introduction, a great deal of effort has been dedicated in the open literature to the modification of acid sites and its consequences in MTO performance,^[26] including Ca modification.^[10a, 10b, 27] For example, Zhang *et al.*^[10b] by modifying ZSM-5 with Ca(NO₃)₂ achieved propylene selectivity up to 50 % with catalyst lifetime increasing from 13 to 75 h at *WHSV*=4.2 h⁻¹. Observed differences were attributed to the acid site weakening through the formation of acid-base centers but without spectroscopic evidence to support this hypothesis. Further, the observed large decrease in paraffin and ethylene selectivities was not discussed either by these authors. High selectivity

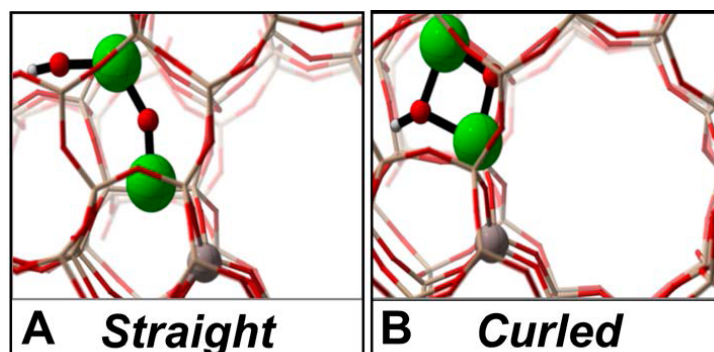


Figure 5. Representation of suggested active sites in Ca-ZSM-5 with straight (A) and curled (B) configuration. In this figure, the following color code is used: H is white, O is red, Al is grey, Si is cream and Ca is green.

towards propylene is generally demonstrated for mesoporous ZSM-5.^[28] It is claimed that this is a result of both improved diffusion properties and acid site strength modification. However, according to Olsbye *et al.*^[29] the observed differences are not yet satisfactorily described and explained. By creating mesopores in ZSM-5, Mei *et al.*^[28a] reached selectivity to propylene of around 42% together with a considerable drop in the production of paraffins (from 20.5 down to 5.7%) and ethylene (from 15.3 down to 4.2%). These results were rationalized on the basis of a different contribution of the aromatic and olefinic route, i.e. by partial suppression of the aromatic cycle. On the other hand, the modification of the acidity might simply lead to a lower amount of working acid sites, i.e. – partial - poisoning. Indeed, application of ZSM-5 with a high SiO₂/Al₂O₃ ratio, and therefore a much lower density of acid sites, has been widely reported^[30] with light olefin selectivity increasing upon decreasing Al content. Although very effective in terms of selectivity, these zeolites with low Al content usually deactivate faster^[12a] due to selective coke deposition on the few active sites. We tentatively suggest that the promotional effect of acid site modification is mainly related to the decreasing the strength of acid sites rather than their amount. Thus, the biggest difference between decreasing Al content and ‘poisoning’ (or ‘modifying’) acid sites with Ca is that in the former case the amount of acid sites has been lowered while in the latter their strength has been weakened through changing their nature but preserving their amount.

To obtain molecular level insight into the nature of the active site of the pristine and Ca-modified catalysts, a set of periodic Density Functional Theory (DFT) calculations were performed using the Vienna Ab Initio Simulation Package (VASP).^[31] Simulation details are provided in Appendix D.^[32] Inspired by earlier literature reports^[10a, 33] and the experimentally determined optimal Ca:Al ratio of 2, we calculated the electronic energies for a systematic set of CaO-CaOH⁺ structures coordinated to framework oxygens near the Al substitution and with different orientations in the channel intersections (Figures D7 and D8). An overview of all considered structures is given in the Appendix D. We assumed isolated Brønsted acid sites in the pristine H-ZSM-5 material, which is a realistic representation since the experimentally used Si/Al ratio amounts to 40. We observed two stable configurations of Ca species as displayed in Figure 5: the CaO-CaOH⁺ tail may adopt either a straight (Figure 5A) or curled (Figure 5B)

configuration. The latter is electronically more stable. A detailed comparison of the vibrational frequencies of the modified Ca-ZSM-5 and pristine ZSM-5 yields some distinct differences for the Ca-modified ZSM-5 catalyst. The calculated OH stretch frequency of the H-ZSM-5 catalyst at 3684 cm^{-1} shifts upwards to 3848 cm^{-1} and 3796 cm^{-1} for the straight and curled Ca chains in the Ca-ZSM-5 catalyst, respectively, located in the range of less acidic silanol groups (3740 cm^{-1}), which corresponds with the spectra shown in Figure 1C.^[34] These calculations suggest that the active site in Ca-ZSM-5 catalysts is a combination of multiple $\text{CaO}(\text{CaOH})^+$ structures and the shift of the OH stretch frequencies indeed points towards a lower Brønsted acidity of the Calcium modified catalyst.

5.4. Conclusions.

In conclusion, the post-synthetic incorporation of Ca into ZSM-5 leads to the formation of $\text{CaO}(\text{CaOH})^+$ species that strongly weaken the acid strength of the parent zeolite. As a result, the rate of hydride transfer and oligomerization reactions on these sites is greatly reduced, resulting in the increased total light olefin selectivity in the range of a 90%. These results further demonstrate the importance of acid strength on product selectivity and zeolite lifetime in MTO chemistry.

References.

- [1] C. D. Chang, C. T. W. Chu, Mobil Oil Corp, **1977**.
- [2] a) A. Comas-Vives, M. Valla, C. Copéret, P. Sautet, *ACS Cent Sci.* **2015**, *1*, 313-319; b) D. Lesthaeghe, V. Van Speybroeck, G. B. Marin, M. Waroquier, *Angew. Chem. Int. Ed.* **2006**, *45*, 1714-1719.
- [3] a) K. Hemelsoet, J. Van der Mynsbrugge, K. De Wispelaere, M. Waroquier, V. Van Speybroeck, *ChemPhysChem* **2013**, *14*, 1526-1545; b) U. Olsbye, S. Svelle, M. Bjorgen, P. Beato, T. V. W. Janssens, F. Joensen, S. Bordiga, K. P. Lillerud, *Angew. Chem. Int. Ed.* **2012**, *51*, 5810-5831; c) X. Sun, S. Mueller, Y. Liu, H. Shi, G. L. Haller, M. Sanchez-Sanchez, A. C. van Veen, J. A. Lercher, *J. Catal.* **2014**, *317*, 185-197.
- [4] I. M. Dahl, S. Kolboe, *Catal. Lett.* **1993**, *20*, 329-336.
- [5] M. Bjorgen, S. Svelle, F. Joensen, J. Nerlov, S. Kolboe, F. Bonino, L. Palumbo, S. Bordiga, U. Olsbye, *J. Catal.* **2007**, *249*, 195-207.
- [6] X. Sun, S. Mueller, H. Shi, G. L. Haller, M. Sanchez-Sanchez, A. C. van Veen, J. A. Lercher, *J. Catal.* **2014**, *314*, 21-31.
- [7] S. Teketel, W. Skistad, S. Benard, U. Olsbye, K. P. Lillerud, P. Beato, S. Svelle, *ACS Catal.* **2012**, *2*, 26-37.
- [8] S. Teketel, L. F. Lundegaard, W. Skistad, S. M. Chavan, U. Olsbye, K. P. Lillerud, P. Beato, S. Svelle, *J. Catal.* **2015**, *327*, 22-32.
- [9] M. Westgård Erichsen, K. De Wispelaere, K. Hemelsoet, S. L. C. Moors, T. Deconinck, M. Waroquier, S. Svelle, V. Van Speybroeck, U. Olsbye, *J. Catal.* **2015**, *328*, 186-196.
- [10] a) S. Zhang, B. Zhang, Z. Gao, Y. Han, *Ind. Eng. Chem. Res.* **2010**, *49*, 2103-2106; b) S. Zhang, B. Zhang, Z. Gao, Y. Han, *React. Kinet. Mech. Catal.* **2010**, *99*, 447-453; c) A. M. AlJarallah, U. A. ElNafaty, M. M. Abdillahi, *Appl. Catal., A* **1997**, *154*, 117-127.
- [11] N. V. Klyueva, N. D. Tien, K. G. Ione, *React. Kinet. Catal. Lett.* **1985**, *29*, 427-432.
- [12] a) J. Liu, C. Zhang, Z. Shen, W. Hua, Y. Tang, W. Shen, Y. Yue, H. Xu, *Catal. Commun.* **2009**, *10*, 1506-1509; b) H. E. van der Bij, B. M. Weckhuysen, *Chem. Soc. Rev.* **2015**, *44*, 7406-7428; c) J. C. Vadrine, A. Auroux, P. Dejaifve, V. Ducarme, H. Hoser, S. Zhou, *J. Catal.* **1982**, *73*, 147-160.
- [13] M. Stöcker, *Microporous Mesoporous Mater.* **1999**, *29*, 3-48.
- [14] a) S. Sartipi, K. Parashar, M. Jose Valero-Romero, V. P. Santos, B. van der Linden, M. Makkee, F. Kapteijn, J. Gascon, *J. Catal.* **2013**, *305*, 179-190; b) C. A. Emeis, *J. Catal.* **1993**, *141*, 347-354.
- [15] P. V. Wiper, J. Amelse, L. Mafra, *J. Catal.* **2014**, *316*, 240-250.
- [16] L. R. Fung, A. K. Khitrin, K. Ermolaev, *J. Magn. Reson.* **2000**, *142*, 97-101.
- [17] L. Rodriguez-Gonzalez, U. Simon, *Meas. Sci. Technol.* **2010**, *21*.
- [18] J. Brus, L. Kobera, W. Schoefberger, M. Urbanova, P. Klein, P. Sazama, E. Tabor, S. Sklenak, A. V. Fishchuk, J. Dedeczek, *Angew. Chem. Int. Ed.* **2015**, *54*, 541-545.
- [19] a) Q. Zhao, W. H. Chen, S. J. Huang, Y. C. Wu, H. K. Lee, S. B. Liu, *J. Phys. Chem. B* **2002**, *106*, 4462-4469; b) A. Zheng, S.-J. Huang, W.-H. Chen, P.-H. Wu, H. Zhang, H.-K. Lee, L.-C. de Menorval, F. Deng, S.-B. Liu, *J. Phys. Chem. A* **2008**, *112*, 7349-7356.
- [20] S. Hayashi, K. Jimura, N. Kojima, *Microporous Mesoporous Mater.* **2014**, *186*, 101-105.
- [21] W.-H. Chen, H.-H. Ko, A. Sakthivel, S.-J. Huang, S.-H. Liu, A.-Y. Lo, T.-C. Tsai, S.-B. Liu, *Catal. Today* **2006**, *116*, 111-120.
- [22] N.-L. Michels, S. Mitchell, J. Perez-Ramirez, *ACS Catal.* **2014**, *4*, 2409-2417.
- [23] a) J. F. Haw, W. G. Song, D. M. Marcus, J. B. Nicholas, *Acc. Chem. Res.* **2003**, *36*, 317-326; b) R. Khare, D. Millar, A. Bhan, *J. Catal.* **2015**, *321*, 23-31.
- [24] L. R. Aramburo, E. de Smit, B. Arstad, M. M. van Schooneveld, L. Sommer, A. Juhin, T. Yokosawa, H. W. Zandbergen, U. Olsbye, F. M. F. de Groot, B. M. Weckhuysen, *Angew. Chem. Int. Ed.* **2012**, *51*, 3616-3619.
- [25] S. M. Abubakar, D. M. Marcus, J. C. Lee, J. O. Ehresmann, C. Y. Chen, P. W. Kletnieks, D. R. Guenther, M. J. Hayman, M. Pavlova, J. B. Nicholas, J. F. Haw, *Langmuir* **2006**, *22*, 4846-4852.
- [26] a) M. Khanmohammadi, S. Amani, A. B. Garmarudi, A. Niaei, *Chin. J. Catal.* **2016**, *37*, 325-339; b) F. L. Bleken, S. Chavan, U. Olsbye, M. Boltz, F. Ocampo, B. Louis, *Appl. Catal., A* **2012**, *447*, 178-185.
- [27] a) K. Omata, Y. Yamazaki, Y. Watanabe, K. Kodama, M. Yamada, *Ind. Eng. Chem. Res.* **2009**, *48*, 6256-6261; b) J. Li, S. Liu, H. Zhang, E. Lu, P. Ren, J. Ren, *Chin. J. Catal.* **2016**, *37*, 308-315.
- [28] a) C. Mei, P. Wen, Z. Liu, H. Liu, Y. Wang, W. Yang, Z. Xie, W. Hua, Z. Gao, *J. Catal.* **2008**, *258*, 243-249; b) F. L. Bleken, K. Barbera, F. Bonino, U. Olsbye, K. P. Lillerud, S. Bordiga, P. Beato, T. V. W. Janssens, S. Svelle, *J. Catal.* **2013**, *307*, 62-73; c) J. Ahmadvour, M. Taghizadeh, *J. Nat. Gas Sci. Eng.* **2015**, *23*, 184-194.
- [29] U. Olsbye, S. Svelle, K. P. Lillerud, Z. H. Wei, Y. Y. Chen, J. F. Li, J. G. Wang, W. B. Fan, *Chem. Soc. Rev.* **2015**, *44*, 7155-7176.

- [30] a) C. D. Chang, C. T. W. Chu, R. F. Socha, *J. Catal.* **1984**, *86*, 289-296; b) C. T. W. Chu, C. D. Chang, *J. Catal.* **1984**, *86*, 297-300.
- [31] J. Hafner, *J. Comput. Chem.* **2008**, *29*, 2044-2078.
- [32] a) V. Van Speybroeck, K. De Wispelaere, J. Van der Mynsbrugge, M. Vandichel, K. Hemelsoet, M. Waroquier, *Chem. Soc. Rev.* **2014**, *43*, 7326-7357; b) V. Van Speybroeck, K. Hemelsoet, L. Joos, M. Waroquier, R. G. Bell, C. R. A. Catlow, *Chem. Soc. Rev.* **2015**, *44*, 7044-7111.
- [33] a) A. V. Larin, G. M. Zhidomirov, D. N. Trubnikov, D. P. Vercauteren, *J. Comput. Chem.* **2010**, *31*, 421-430; b) G. Li, E. A. Pidko, R. A. van Santen, Z. Feng, C. Li, E. J. M. Hensen, *J. Catal.* **2011**, *284*, 194-206; c) G. Li, E. A. Pidko, R. A. van Santen, C. Li, E. J. M. Hensen, *J. Phys. Chem. C* **2013**, *117*, 413-426; d) G. Yang, Y. Wang, D. H. Zhou, X. C. Liu, X. W. Han, X. H. Bao, *J. Mol. Catal. A: Chem.* **2005**, *237*, 36-44; e) G. M. Zhidomirov, A. V. Larin, D. N. Trubnikov, D. P. Vercauteren, *J. Phys. Chem. C* **2009**, *113*, 8258-8265.
- [34] a) T. Armaroli, L. J. Simon, M. Digne, T. Montanari, M. Bevilacqua, V. Valtchev, J. Patarin, G. Busca, *Appl. Catal., A* **2006**, *306*, 78-84; b) C. Carteret, *J. Phys. Chem. C* **2009**, *113*, 13300-13308.

CHAPTER FIVE

Chapter

6

***On the Role of Lewis and Brønsted Acidity
in the Methanol-to-Olefins Process***

Brønsted and Lewis acidity are the two main performance descriptors in MTO for a wide range of as-synthesized and post-synthetically modified ZSM-5 based catalysts. Independently on the amount of Lewis acid sites, selectivity to propylene correlates negatively with the concentration of Brønsted acid sites: the highest propylene selectivity ($\approx 50\%$) is achieved with the lowest density of Brønsted acid sites ($0.07\ \mu\text{mol}\cdot\text{m}^{-2}$), while the opposite trend is observed for ethylene selectivity, indicating the competing nature of the formation of these olefins. Further, Lewis acidity has an impact on catalyst stability and coking rate. Methanol throughput – a measure of the catalyst lifetime – is a function of the Lewis/Brønsted acid sites ratio. A prolonged lifetime for zeolites having Lewis acidity is tentatively explained on the basis of their affinity to coke precursors. By withdrawing coke precursors from Brønsted acid sites, the latter are set free from deactivation and can further participate in methylation reactions, essential in the MTO mechanism.

6.1. Introduction.

The methanol-to-olefins (MTO) process belongs to the branch of acid-catalysed reactions.^[1] It is of high interest as it can alleviate the progressively growing demand for olefins. Moreover, the possibility to control the propylene/ethylene ratio makes it even more appealing as the product distribution can be easily adjusted according to the market demands.^[2]

In MTO zeolites are utilized as catalysts. Among those, ZSM-5 with MFI topology is probably the most promising one, able to work under industrially relevant conditions for thousands of hours.^[3] This relatively long lifetime is guaranteed by the 3D micropore system consisting of two sets of intersecting 10-ring channels hampering formation of polycondensed aromatic species notorious for fast deactivation. Topology is an important^[4] yet not the only parameter in defining the performance of the catalyst in this reaction.^[5] Obviously, for acid catalysed reactions, accessibility,^[6] strength,^[7] distribution^[8], amount^[9] and nature^[10] of acid sites are of paramount importance.

Acid strength examination is quite often limited to only Brønsted acidity – a proton counterbalancing a negative charge of the zeolite framework due to Al insertion.^[11] This is rather understandable, as the Brønsted acid site (BAS) is believed to be the active site for MTO process, mechanistically described by the dual-cycle concept.^[5, 12] According to this mechanism, two cycles exist in the zeolite cages – an alkene- and an aromatic-based cycle. The alkene cycle involves methylation of lower olefins and subsequent cracking reactions of higher olefins yielding predominantly propylene and other olefins. Higher olefins, on the other hand, can be converted to aromatics *via* hydrogen-transfer and cyclization reactions giving rise to the aromatic-based cycle, where mainly aromatics and ethylene *via* side-chain and paring mechanistic pathways are formed. Thus, the active site is not solely a BAS but rather a combination of BAS with adsorbed intermediate species.^[13]

Undoubtedly, the BAS is the leading actor of the reaction mechanism, but the MTO process should not be considered as the play of one performer. There are other parameters influencing catalytic performance, collaterally affecting the course of the reaction. For example, the excessive presence of silanols in defective zeolites might affect deactivation rate as a result of aromatics interaction with slightly acidic silanols.^[14] On the other hand, modification of zeolites with different non-metals like phosphorus,^[15] boron^[16] or alkaline-earth metals^[17] does not only prolongs catalyst lifetime but also improves selectivity to short-chain olefins. Multiple explanations generally tend to rationalize the observed improvement by a decreased density of BAS due to poisoning, which in turn leads to lower coking rates as a result of decreased cyclization and hydride transfer reactions. Another possible explanation was reported, which argues that imposed spatial constraints narrow the pore openings and thus affect shape selectivity.^[18] Little attention was however given to the Lewis acidity arising due to this type of modification. It is generally accepted that the above-mentioned modifications do not only lead to a decrease of BAS but also to acid sites weakening as a result of the appearance of Lewis acid sites (LAS).

This chapter intends to shed light on the role of BAS and LAS in the MTO process. To clarify whether the improved lifetime and selectivity to olefins for modified zeolites is the result of decreased BAS or to the presence of LAS, we prepared a series of zeolites *via* different methods having different amounts of BAS and LAS. By establishing correlations between the type and concentration of acid sites with lifetime and selectivity to ethylene and propylene – main descriptors of MTO performance – we will elucidate the role of each type of site.

6.2. Experimental.

6.2.1. Synthesis of Catalysts.

Catalysts denoted as Z (**Z1**, **Z2**, **Z3**) are microporous ZSM-5. **Z1** was obtained by calcination at 550 °C of commercially available ZSM-5 (CBV 8014) to obtain its protonic form. **Z2** and **Z3** were hydrothermally synthesized following the procedure described by Fan *et al.*^[19] In a typical synthesis, NaAlO₂ (0.025 and 0.010 g for **Z2** and **Z3** respectively), 16.8 mL 1M tetrapropylammonium hydroxide, and 8.4 mL tetraethyl orthosilicate were mixed in 15.6 mL water, aged at 100 °C for 2 h and subsequently left for stirring for 16 h. The synthesis solutions were subjected to hydrothermal synthesis at 180 °C for 24 h. The as-synthesized material was calcined at 550 °C for 10 h in a static oven to remove the template. The calcined material was converted to the protonic form by triple ion-exchange with NH₄NO₃ (1 M, 80 °C, 2 h, 100 mL per gram of zeolite) followed by calcination at 550 °C.

M1 is a mesoporous zeolite obtained from **Z1** by desilication and acid leaching as described elsewhere.^[20] Desilication of **Z1** was carried out in a 1 M NaOH aqueous solution in a capped vessel ($\text{volume}_{\text{base solution}}/\text{mass}_{\text{Z1}} = 8.0 \text{ mL g}^{-1}$) and under stirring at 70 °C for 1 h in an oil bath. This treatment was followed by immediate quenching in a water-ice bath and centrifugation to separate the zeolite powder from the solution. The residue of the desilicating agent was removed from the zeolite crystallites by subsequent redispersion in deionized water and centrifugation cycles until neutral pH was reached. Desilicated ZSM-5 was dried overnight at 120 °C for 12 h and calcined at 550 °C for 5 h. The yield of the desilication procedure was 25% (average of four experiments starting from ca. 20 g H-ZSM-5).

Catalysts denoted as AE were obtained by modification of **Z1** with alkaline-earth metals as described elsewhere.^[21] **AE1** was prepared by solid-state ion-exchange with Ca(CH₃COO)₂. The required amount of calcium acetate (to achieve 6 wt.% of Ca) was ground with **Z1** for 30 min followed by calcination at 550 °C. **AE2** was prepared by triple ion-exchange with 1 M Ca(NO₃)₂·4H₂O at 80 °C for 2 h followed by calcination at 550 °C. **AE3**, **AE4**, **AE5** were prepared by incipient wetness impregnation with an aqueous solution of Ca(NO₃)₂·4H₂O (2.4 M, 4.0 M and 6.0 M, respectively). The samples were subsequently dried in a desiccator followed by drying for 12 h at 80 °C and calcination at 550 °C. **AE6** and **AE7** were prepared by incipient wetness impregnation with 2.4 M Sr(NO₃)₂ and 2.4 M Mg(NO₃)₂·6H₂O respectively and post-treated following a similar procedure as that for sample **AE3**.

6.2.2. Characterization of Catalysts.

N₂ adsorption at -196°C was carried out using a Tristar II 3020 analyzer (Micromeritics). Prior to the experiment, samples were outgassed under vacuum at 350 °C for 16 h.

Microscopy images were recorded using a JEOL JSM-6010LA with a standard beam potential of 10 kV and an Everhart-Thornley detector. X-ray microanalysis (SEM/EDX) confirmed the elemental composition in the sample by scanning electron microscopy (SEM) coupled with a dispersive X-ray microanalysis system (EDX) with a Silicon-drift detector.

The XRD patterns of the powders were recorded in Bragg–Brentano geometry with a Bruker D8 Advance X-ray diffractometer equipped with a LynxEye position-sensitive detector. Measurements were performed at RT by using monochromatic CoK α ($\lambda = 1.788970 \text{ \AA}$) radiation between $2\theta = 5^\circ$ and 50° .

Temperature-programmed NH₃ desorption (NH₃-TPD) was measured by an AutoChem II chemisorption analyzer (Micromeritics). Approximately 0.2 g of the material was first outgassed under He flow at 400 °C and then saturated with NH₃ at 200 °C during 1 h using a flow of 1.65 % NH₃ in He. The gas mixture was then switched back to He and the sample was purged at 200 °C for about 1 h to remove weakly adsorbed NH₃ molecules. TPD was subsequently recorded under He flow, from 200 °C to 800 °C. Flow rates and heating rates were 25 mL min⁻¹ and 10 °C min⁻¹ respectively for all TPD experiments.

Transmission FT-IR spectroscopy using CO as a probe molecule was performed using a Nicolet Nexus spectrometer at 4 cm⁻¹ resolution and co-addition of 128 scans equipped with an extended KBr beam splitting and a mercury cadmium telluride (MCT) cryo-detector. The pellets were placed in an IR quartz cell equipped with CaF₂ windows. A movable sample holder allows the sample to be placed in the infrared beam for the measurements or into the furnace for thermal treatments. The cell is connected to a vacuum line for pretreatment. The specimen is activated in vacuum at 400 °C for 16 h to remove adsorbed species. After this step, the samples were cooled down to -130 °C and CO was dosed in steps up to 30 mbar and recording the spectra at each step.

Transmission FT-IR spectroscopy using pyridine as a probe molecule was performed using a Nicolet 6700 spectrometer equipped with a MCT/B detector. For the wafer preparation, 50 mg of catalyst was used without any dilution. The specimen was activated in vacuum at 400 °C for 16 h to remove adsorbed species. After activation, wafers were saturated with pyridine vapor and further evacuated at 160 °C for 2 h. Spectra were recorded in 1000-4000 cm⁻¹ range at 4 cm⁻¹ resolution and co-addition of 128 scans. The amount of Brønsted (BAS) and Lewis (LAS) acid sites was derived from the bands at 1545 and 1456 cm⁻¹ as described elsewhere using extinction coefficients of 1.67 and 2.22, respectively.^[22] Assuming that one molecule of pyridine is adsorbed on one acid site; the following expressions were used to calculate C_{BAS} and C_{LAS} :

$$C_{BAS} = 1.88 \cdot IA(B) \cdot R^2/W \quad (1)$$

$$C_{LAS} = 1.42 \cdot IA(L) \cdot R^2/W \quad (2)$$

where IA (BAS, LAS) is the integrated absorbance of the BAS or LAS band (cm^{-1}), R – radius of catalyst disk (cm), while W – mass of catalyst sample (mg).

^1H MAS NMR (Magic Angle Spinning Nuclear Magnetic Resonance) measurements were performed on a 11.7 Tesla Bruker DMX500 NMR spectrometer operating at a ^1H Larmor frequency of 500 MHz. A Bruker triple resonance 4 mm MAS probe head with a sample rotation rate of 10 kHz was used. ^1H NMR spectra were recorded with a 90° pulse of 5 μs duration and 3 s interscan delay. Double Quantum (DQ) experiments were performed using the back-to-back (BABA) recoupling sequence for excitation and reconversion of the DQ coherences with a 100 μs duration. The 2D RFDR (Radio Frequency-Driven Recoupling) experiments were implemented *via* the application of rotor-synchronised 180-degree pulses (one inversion pulse per rotor period) for homonuclear dipolar recoupling. A total mixing time duration of 1.6 ms was used. The dehydration of the samples was performed under high vacuum (10^{-5} mbar) at two temperatures. Moderated dehydration was done at 200 $^\circ\text{C}$ for 1 h and the complete dehydration was done at 450 $^\circ\text{C}$ for 17 h. The dehydrated zeolites were placed into the 4 mm MAS NMR zirconia rotor under inert conditions and transferred to the NMR probe head. ^1H chemical shift was calibrated using tetramethylsilane (TMS).

6.2.3. Catalyst Testing.

Catalytic experiments were carried out in a Microactivity Reference unit (PID Eng&Tech) at 500 $^\circ\text{C}$ and ambient pressure. The catalyst (pressed, crushed and sieved to particle sizes 250-420 μm) was mixed with SiC (6:1 wt.%) and placed in a fixed-bed with an internal diameter of 9 mm for standard experiments. An ISCO pump was used to feed methanol to the reactor system. A weight-hourly space velocity ($WHSV$) of 8 $\text{g}_{\text{MeOH}} \text{g}_{\text{cat}}^{-1} \text{h}^{-1}$, a $\text{N}_2 : \text{MeOH} = 1:1$ molar feed composition and atmospheric pressure were utilized. The product mixture was analyzed online with an Interscience CompactGC equipped with a 15 m capillary RTX-1 (1% diphenyl-, 99% dimethylpolysiloxane) column and a flame ionization detector. Conversion, selectivities and yields were calculated on a molar carbon basis. Thus, conversion was defined as the carbon-based fraction of light oxygenates (methanol and dimethyl ether) consumed during the reaction:

$$X = \frac{n_{C,\text{MeOH}_{in}} - n_{C,\text{MeOH}_{out}} - 2 \cdot n_{C,\text{DME}_{out}}}{n_{C,\text{MeOH}_{in}}} \cdot 100\% \quad (3)$$

The selectivity towards ethylene (4) and propylene (5) was calculated based on the carbon number as follows:

$$S_{\text{ethylene}} = \frac{2 \cdot n_{C_2H_4}}{n_{C,\text{MeOH}_{in}} - n_{C,\text{oxy}_{out}}} \cdot 100\% \quad (4)$$

Table 1. Textural and acidic properties of the ZSM-5 materials under study

Entry	Catalyst	V_{total}^a ($cm^3 g^{-1}$)	V_{micro}^a ($cm^3 g^{-1}$)	S_{BET}^a ($m^2 g^{-1}$)	S_{micro}^a ($m^2 g^{-1}$)	n_{AS}^b ($\mu mol g^{-1}$)	n_{BAS}^c ($\mu mol g^{-1}$)	n_{LAS}^c ($\mu mol g^{-1}$)	C_{BAS}^d ($\mu mol m^{-2}$)	C_{LAS}^d ($\mu mol m^{-2}$)	LAS/BAS ^e
1	Z1	0.26	0.15	448	363	387	232	35	0.52	0.08	0.15
2	Z2	0.22	0.15	425	340	60	50	12	0.12	0.03	0.24
3	Z3	0.21	0.17	429	355	25	28	11	0.07	0.03	0.39
4	M1	1.20	0.12	575	261	132	99	77	0.17	0.13	0.78
5	AE1	0.21	0.11	323	267	171	128	1	0.40	0.003	0.01
6	AE2	0.27	0.15	429	344	402	138	108	0.32	0.25	0.78
7	AE3	0.24	0.13	392	315	332	40	228	0.10	0.56	5.70
8	AE4	0.22	0.13	387	313	381	27	240	0.07	0.62	8.89
9	AE5	0.23	0.12	385	310	384	29	240	0.08	0.62	8.28
10	AE6	0.20	0.13	379	273	251	85	108	0.22	0.29	1.27
11	AE7	0.22	0.14	417	322	340	76	217	0.18	0.52	2.86

^a From N₂ adsorption.^b Concentration of acid sites (AS) derived from NH₃ TPD.^c Concentration of Brønsted (BAS) and Lewis (LAS) acid sites derived from Pyridine IR.^d Site density of Brønsted (BAS) and Lewis (LAS) sites obtained by n_{BAS}/S_{BET} and n_{LAS}/S_{BET} respectively.^e Obtained by n_{LAS}/n_{BAS}

$$S_{propylene} = \frac{3 \cdot n_{C_3H_6}}{n_{C,MeOH_{in}} - n_{C,ox}y_{out}} \cdot 100\% \quad (5)$$

and the yield of a component i was defined from its selectivity and methanol conversion:

$$Y_i = \frac{S_i \cdot X}{100} \% \quad (6)$$

The performance results are presented in graphs as a function of the methanol mass throughput per amount of catalyst used ($g_{MeOH} g_{cat}^{-1}$), and defined as the overall amount MeOH fed through the catalytic bed before the conversion of oxygenates drops below 80 %. Presented selectivities are integral values.

6.3. Results and Discussion.

6.3.1. Assessing Type and Amount of Acid Sites.

To establish acidity-performance correlations, it is important to identify the amount and type of acid sites in the zeolite. Herein, we have chosen two main approaches to control the amount of acid sites: pre-synthetic and post-synthetic modification, respectively. Thus, it is critical to determine not only the concentration of acid sites but also their nature and strength, as all these parameters can result in different catalytic behaviour. Pre-synthetically modified zeolites (Z2, Z3) were obtained by varying the amount of Al in the synthesis solution, aiming for a lower Al content than in the commercial Z1 (Si/Al=40). As a result, zeolites with Si/Al=300 (Z2) and Si/Al=650 (Z3) were synthesized. XRD results (Figure 1A) show that catalysts have the expected MFI topology, while the crystal size (0.2 – 0.4 μm) is

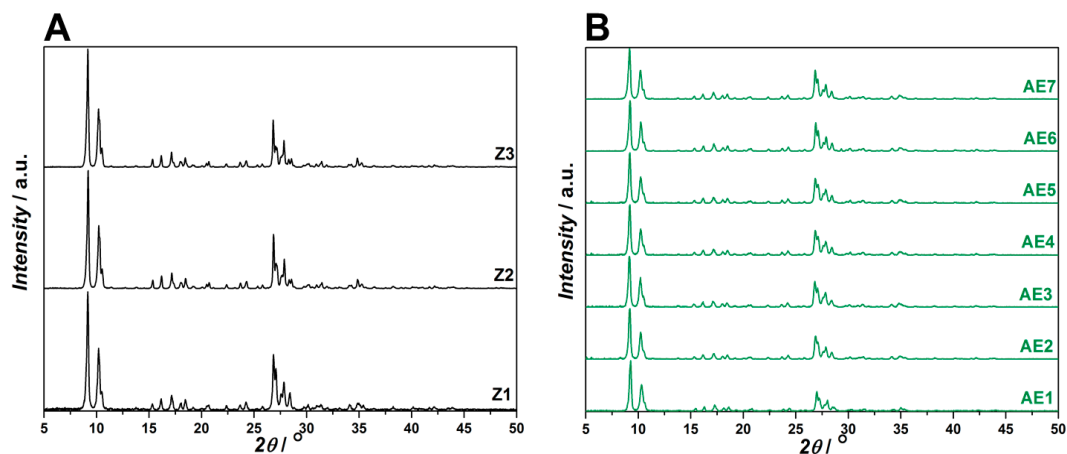


Figure 1. XRD patterns of zeolites ZSM-5 with MFI topology (A) with different Si/Al ratio and (B) modified with alkaline-earth metals.

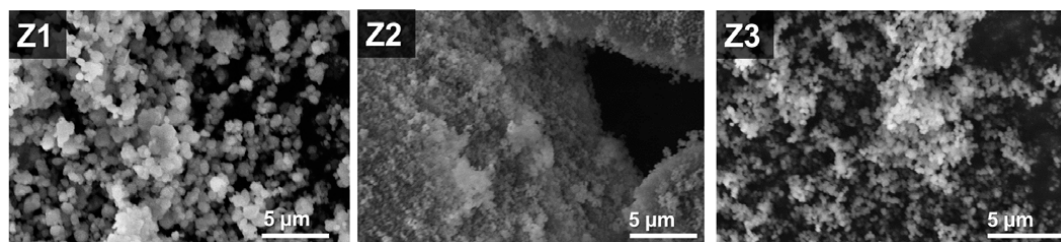


Figure 2. Representative SEM pictures of zeolites Z1, Z2 and Z3 with different Si/Al ratio.

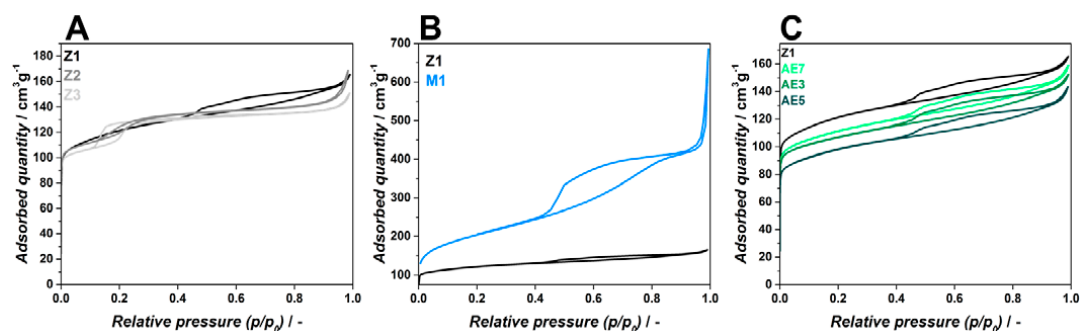


Figure 3. N₂ adsorption isotherms at -196 °C of (A) zeolites with different Si/Al ratio; (B) desiccated M1 and (C) zeolites modified with different alkaline-earth metals, namely AE7 modified with Mg, AE3 modified with Ca and AE5 modified with Sr.

slightly smaller than for Z1 (0.4-1.0 μm) (Figure 2). Interestingly, Z2 and Z3 are also characterized by the existence of a hysteresis loop in the pre-capillary condensation region in the N₂ isotherm (Figure 3A).^[23]

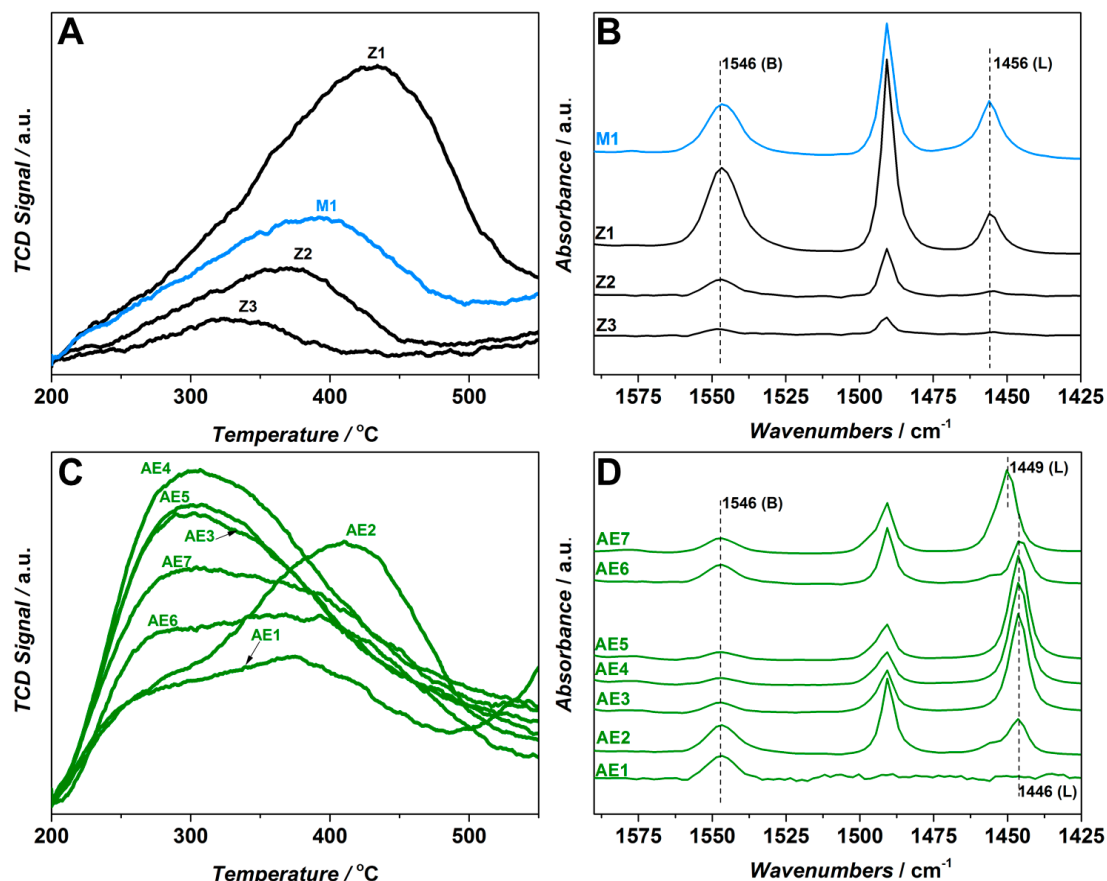


Figure 4. Acidity characterization of zeolites under study. (A) and (C) NH₃-TPD profiles, (B) and (D) FT-IR spectra of adsorbed pyridine.

This hysteresis loop appears due to the phase transition from a disordered phase to a lattice-like fluid phase and depends on the Si/Al ratio.^[24] It becomes less evident with the increasing Al content and completely disappears for Z1 sample with Si/Al=40.

On the other hand, post-synthetic modification by demetalation involves the treatment of zeolites with various desilicating and dealuminating agents and represents a simple and scalable method to vary the amount of Al and/or Si in the zeolite framework.^[25] This post-synthetic method of acidity modification leads, however, to the generation of mesopores, which are generally credited for improved lifetimes in MTO.^[26] We also adopted this procedure to change the acid sites concentration in the parent Z1 thus producing sample M1. As expected, this post-synthetic modification caused a significant increase in the mesoporous surface area changing the shape of the N₂ isotherm from type I to type IV (Figure 3B). NH₃ TPD profiles for Z1, Z2, Z3 and M1 are described by the presence of the single maximum shifting from 330°C to 430°C for Z3 and Z1 respectively, the area decreasing in the following sequence Z1>M1>Z2>Z3 (Figure 4A). In line with NH₃ TPD results, FT-IR spectra of adsorbed pyridine show the

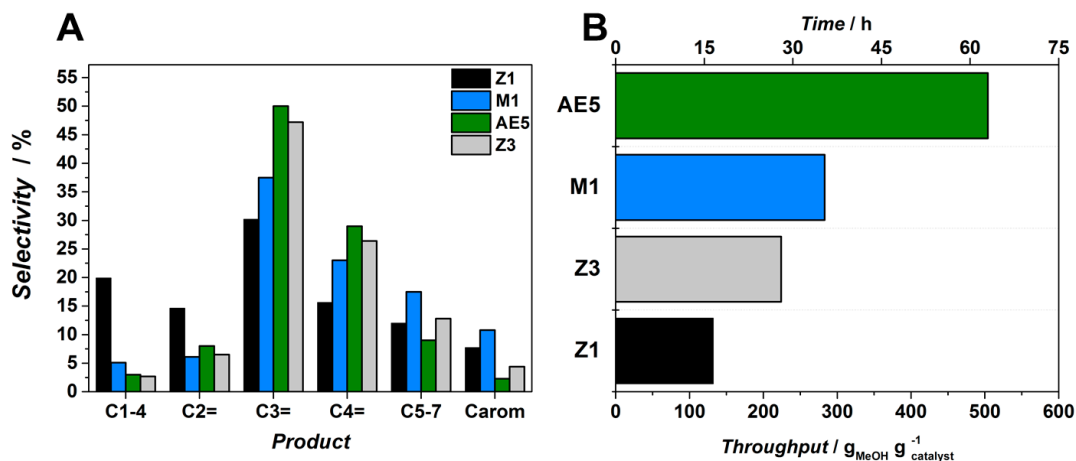


Figure 5. Methanol conversion over pre-synthetically (Z1, Z3) and post-synthetically (M1, AE5) modified ZSM-5 tested at 500°C in MTO. (A) Product distribution; (B) Catalyst lifetime. $M_{\text{cat}} = 0.5 \text{ g}$, $WHSV = 8 \text{ g}_{\text{MeOH}} \text{g}_{\text{cat}}^{-1} \text{h}^{-1}$.

same trend: the area of a band at 1546 cm^{-1} , corresponding to Brønsted acidity gradually decreases, being the lowest for Z3 (Figure 4B). IR spectra of Z1 and M1 samples are also characterized by the presence of the band at 1456 cm^{-1} attributed to the interaction of pyridine with Lewis acid sites. Lewis acidity in these samples results from the presence of extraframework Al or perturbed Al species.^[27]

Alternatively, the acidity of as-synthesized zeolites can be tuned by post-synthetic incorporation of different cations and non-metals.^[17b] In the previous chapter, we have shown that incorporation of Ca leads to a significantly improved selectivity to propylene and to longer lifetimes.^[21] Inspired by these results, we have prepared a series of samples from Z1 modified by alkaline-earth metals (Mg, Ca, Sr). Another series of samples was prepared by Ca incorporation with different loadings and prepared by different methods, as described above. In total, seven different samples were prepared and denoted as AE. Full characterization details for these samples (XRD, SEM, N_2 adsorption) can be found in Figures 1-3. As a result of alkaline-earth metal incorporation, both surface area (S_{BET}) and pore-volume (V_p) gradually decreased with an increase of alkaline-earth loading as a result of partial blocking of the micropore surface (Figure 3C). The incorporation of alkaline-earth metals causes considerable changes in acidity. The BAS concentration decreases from $232 \mu\text{mol g}^{-1}$ to $27 \mu\text{mol g}^{-1}$ (compare Z1 and AE4 in Table 1). Another clear difference between Z1 sample and AE series is the appearance of a significantly higher concentration of Lewis acid sites (Figure 4D) characterized by the band at 1446 cm^{-1} . For Mg-modified AE7, this band is shifted to 1449 cm^{-1} .

Interestingly, a comparison of the acidic properties of the zeolites under study reveals that Z3 possesses the same concentration of Brønsted acid sites as AE4 and AE5. The only difference between these samples is the presence of a notable amount of Lewis sites resulting from Ca incorporation.

6.3.2. Effect of Pre-synthetic and Post-synthetic Modification on MTO process.

Table 2. Catalytic properties of the ZSM-5 catalyst under study.

Entry	Catalyst	LAS/BAS ^a	C ₂ ^{ab} (%)	C ₃ ^{ab} (%)	Throughput ^c (g _{MEOH} g _{cat} ⁻¹)	Coke ^d (%)	Coking rate ^e (mg _{coke} g _{MEOH} ⁻¹)	BSCR ^f (mg _{coke} m ² μmol ⁻¹ g _{MEOH} ⁻¹)
1	Z1	0.15	14.6	30.2	132	19.2	1.5	2.8
2	Z2	0.24	11.3	41.6	156	16.7	1.1	9.1
3	Z3	0.39	6.5	47.2	224	9.6	0.4	6.6
4	M1	0.78	6.2	37.5	283	32.6	1.2	6.7
5	AE1	0.01	12.2	36.8	136	25.7	1.9	4.8
6	AE2	0.78	10.5	33.9	264	21.5	0.8	2.5
7	AE3	5.70	9.0	38.4	792	22.1	0.3	2.7
8	AE4	8.89	7.3	43.4	480	8.4	0.2	2.5
9	AE5	8.28	7.5	51.0	504	3.2	0.1	0.8
10	AE6	1.27	13.0	41.8	205	22.1	1.1	4.8
11	AE7	2.86	11.5	39.6	824	31.9	0.4	2.1

^a Obtained by n_{LAS}/n_{BAS} ^b Integral values taken during the active period of catalyst.^c Total amount of MEOH converted per gram of catalyst before conversion drops down to 80%.^d From TGA of spent catalyst.^e Coke (mg_{coke} g_{catalyst}⁻¹) divided by Throughput (g_{MEOH} g_{catalyst}⁻¹)^f Coking rate normalized per C_{BAS}

The impact of the acidic properties arising from pre-synthetic and post-synthetic modification was evaluated in the methanol-to-olefins process. This reaction - which is believed to utilize Brønsted proton as the active site - would be obviously very sensitive to any changes in concentration and type of acid sites. For the sake of clarity, we will focus our discussion in this section on three representative samples from each type of modification, namely: Z3, M1, AE5.

On the other hand, to understand the consequences of post-synthetic modification, we also compared modified samples (M1 and AE5) with the parent material (Z1). Results of catalytic testing for these samples are shown in Figure 5, while the conversion of methanol and selectivities to the main products as a function of time are shown on Figures 6 -7 and summarized in Table 2. First of all, Z1 with Si/Al=40 exhibits the shortest lifetime in comparison to the other samples, it deactivates after 16.5 h on stream, which corresponds to 132 g_{MEOH} g_{catalyst}⁻¹ (Figures 5B and 6A). The integral selectivities are shown in Figure 5A. When it comes to product selectivity (Figure 6), during the first reaction hours, a large amount of paraffins is formed, while with time-on-stream there is a decrease in ethylene selectivity, while production of propylene remains fairly stable. As expected, the lower concentration of Brønsted acidity in Z3 prolongs the catalyst lifetime up to 28 h (Figure 6B), in good agreement with literature.^[28] According to Mores *et al.*^[28] the higher the Si/Al ratio the higher the formation rate of methylated aromatic species, in turn leading to faster coking rates. The nature of coking species, however, remains the same. Z3 is characterized by steady formation of products, propylene being the dominant one (up to 48 %). Another

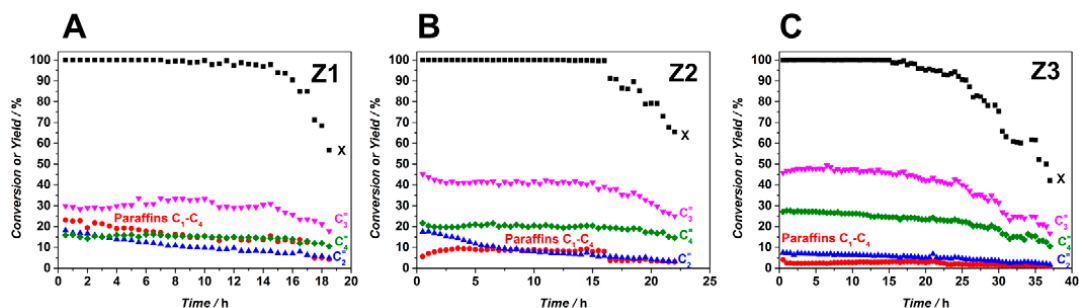


Figure 6. Methanol conversion (*black*) and yield of C₁-C₄ paraffins (*red*), ethylene (*blue*), propylene (*pink*) and butenes (*green*) as a function of time-on-stream for (A) Z1; (B) Z2 and (C) Z3.

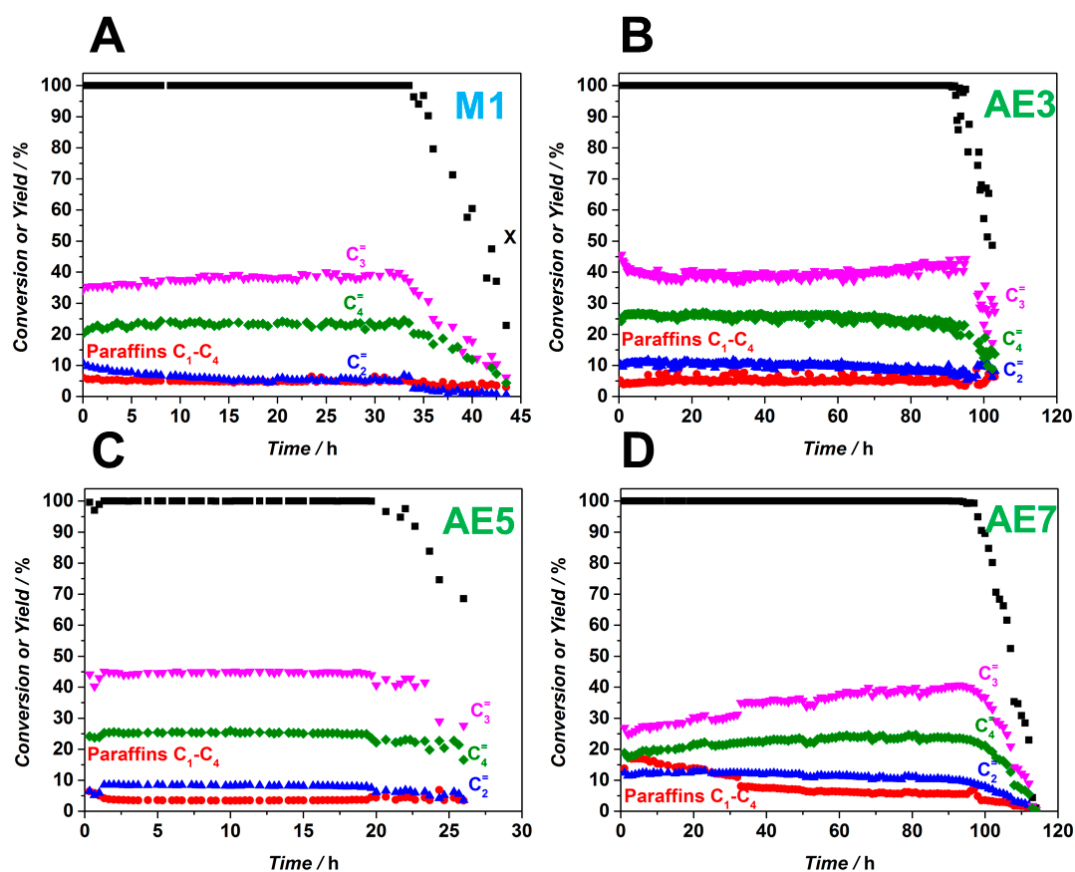


Figure 7. Methanol conversion (*black*) and yield of C₁-C₄ paraffins (*red*), ethylene (*blue*), propylene (*pink*) and butenes (*green*) as a function of time-on-stream for (A) M1; (B) AE3; (C) AE5 and (D) AE7.

striking difference in the product distribution is the decreased amount of paraffins, ethylene and

aromatics in comparison with Z1, having eight times higher amount of acid sites. As ethylene and aromatics are the main products of the aromatic cycle,^[3, 26a] and considering that the formation of paraffins is due to the hydrogen transfer reactions,^[29] sharp decrease in the formation of all these products suggests a reduced participation of the aromatic cycle for Z3. The main explanation for this observation, as hypothesized by Guisnet,^[30] lies in the higher probability of condensation reactions for zeolites with higher acid site densities accompanied by stronger interaction of coke precursors with stronger acid sites.

On the other hand, isolation of Brønsted acid sites by simply decreasing the amount of Al leads to higher propylene yields as observed for Z3 (Figures 5A and 6C).^[2] Further comparison of Z3 with AE5 confirms that concentration of Brønsted acid sites seems to be the main descriptor for the observed selectivities. These two catalysts, having a very similar concentration of acid sites exhibit almost identical selectivities to paraffins, ethylene and propylene. On the other hand, AE5 prepared by post-synthetic modification with Ca displays a two times longer lifetime (Figure 5A and 7C), suggesting that although Brønsted acidity indeed plays an important role in catalyst lifetime by decreasing coke formation rate, there are other more critical parameters that influence catalyst lifetime. The only obvious difference between these two catalysts is the presence of Lewis acidity in AE5 arising due to Ca incorporation.

Demetalated M1 shows a longer lifetime and higher selectivity to propylene in comparison to the parent Z1. Analysis of porous and acidic properties reveals a decrease in the concentration of Brønsted acid sites and a higher surface area – two main factors explaining the observed changes. The improved stability towards the deactivation of mesoporous zeolites is generally explained by a facilitated molecular transport,^[31] along with a higher external (= mesopore) surface area that provides more space for coke deposition.^[32] On the other hand an increased selectivity to propylene can be explained by the decreased concentration of acid sites,^[26a] while a higher selectivity to aromatic products in comparison to parent Z1 is a consequence of the presence of mesopores, alleviating the spatial constraint.^[32b]

6.3.3. Establishing Acidity-Performance Relationship.

The previous paragraph touched on the appreciable tendency of zeolites with a lower BAS concentration to yield higher quantities of propylene. This tendency seemed to be independent on the method of zeolite modification. To elaborate further on this relationship, the integral propylene selectivity was related to changes in BAS concentration. It should be kept in mind that different methods of post-synthetic modification do not only affect acidic but also the textural properties of the catalyst. If demetalation of M1 is beneficial for the increase in surface area, modification with alkaline-earth metals leads to the loss of both micropore volume and surface area in case of AE samples. Obviously, the changes in surface area are expected to have an impact on catalytic properties and have to be taken into consideration. To account for changes in textural properties, we normalized the concentration of BAS (n_{BAS}) by the BET area (S_{BET}), thus converting this quantity to an acid site surface density (c_{BAS}). Figures 8A and 8B show the integral propylene and ethylene selectivity as a function of Brønsted acid

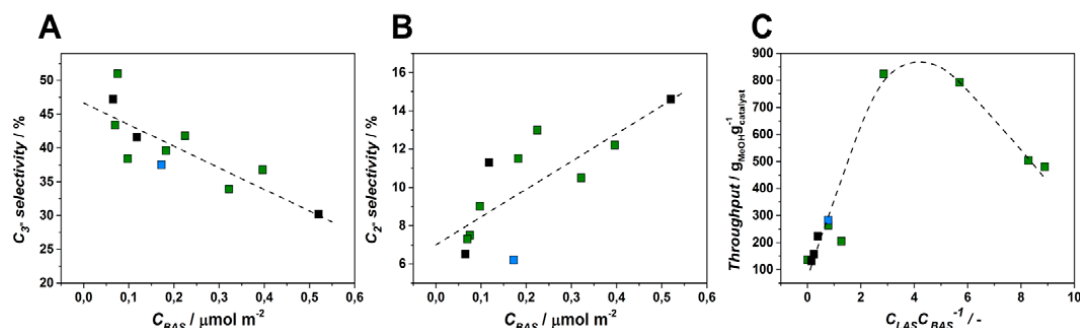


Figure 8. Descriptors of ZSM-5 acidity in MTO. **Z** (black) – pre-synthetically modified ZSM-5 with different Si/Al ratio; **M** (blue) – post-synthetically demetalated ZSM-5; **AE** (green) – zeolites modified by post-synthetic incorporation of alkaline-earth metals. Acidity-performance relationship clearly shows that the density of Brønsted acid (C_{BAS}) sites determines (A) propylene and (B) ethylene selectivity, while the ratio of Lewis and Brønsted acid sites (C_{BAS}/C_{LAS}^{-1}) governs catalyst lifetime (C).

density (C_{BAS}). Figure 8A demonstrates a clear linear correlation between BAS and selectivity to propylene and ethylene for all samples under study, independently on the method in which they were produced. At high BAS densities, strong sites are in closer proximity. As a consequence, more successive reactions can occur at these sites along the diffusion pathway.^[30] This increases the probability of a carbon atom ending up in an aromatic or coke species and, according to the dual-cycle concept, will result in an increased ethylene production. Low Brønsted acid site density, on the other hand, suppresses consecutive reactions leading to aromatization and coking, thus favouring methylation and cracking reactions. Altogether, these results suggest that Brønsted acid site isolation is the key factor to obtain a high propylene selectivity. We attribute the higher scattering found in figure 8B (ethylene selectivity) to the effect of secondary reactions taking place downstream of the “active catalyst zone”.^[33] Opposite trends obtained for ethylene and propylene also confirm that these two products are formed *via* two different competitive routes. Bjørgen *et al.*^[12] demonstrated that ethylene is mechanistically separated from other olefins being mostly formed *via* xylenes and/or trimethylbenzenes rather than by cracking reactions as other olefins. Although other authors have suggested that propylene can be also formed in the aromatic cycle,^[3] this reaction pathway is however much more selective to ethylene in the same manner as the olefin cycle can produce ethylene but is much more selective to other olefins.

Ethylene and propylene selectivities are not the only descriptors of catalytic performance. Catalyst lifetime, or methanol throughput expressed in $g_{MeOH}g_{cat}^{-1}$, is another crucial parameter for application. The relationship between BAS and methanol throughput is more complex in comparison to selectivity. Obviously, high Brønsted site densities will result in faster deactivation due to higher coking rates. Herein, not only the Brønsted acid site density but also their distribution plays an important role. Wang *et al.*^[8a] showed that the same concentration of Brønsted acid sites can still lead to different lifetime due to an uneven Al distribution and formation of Al pairs. The location of Al can be controlled during zeolite

synthesis by choosing an appropriate silica source. Lowering the amount of Al in the zeolite ensures the isolation of acid sites. Although this seems to decrease the coking rate, overall much less coke is required to fully deactivate this low Al containing catalyst. Therefore, the different resistance to deactivation of AE5 and Z3 with similar c_{BAS} is a strong argument to claim that BAS is not the only descriptor for catalyst lifetime. As the only obvious difference between these two catalysts is the presence of Lewis acid sites, we propose that this is another parameter affecting lifetime. Figure 8C shows methanol throughput plotted as a ratio of Lewis and Brønsted acid sites. The obtained “volcano” plot (Figure 8C) yields an optimum in the LAS/BAS ratio (between 2 and 6) for the highest methanol throughput. Interestingly, the two optima are AE3 and AE7, samples prepared by Ca and Mg incorporation, respectively, both with an AE to Al molar ratio of 2.

6.3.4 Effect of Lewis acidity.

The obtained interdependence of catalyst lifetime and concentration of Brønsted and Lewis acid sites is rather unexpected for MTO process. Indeed, the impact of Lewis acidity on MTO has been hardly discussed in the open literature, with only a few works dealing with this topic and often reporting a rather negative impact of Lewis acidity on performance. The majority of those works focus on Lewis acidity created by the presence of extraframework Al (EFAL) arising from steaming and reported catalyst performance at lower temperatures than the ones here used. Recently, Lercher *et al.*^[29] proposed that Lewis acidity is involved in hydrogen transfer reactions and represents a dominant pathway to paraffins and aromatics. Using ZSM-5 zeolites with different amount of BAS and LAS (LAS due to the presence of extra-framework Al), these authors showed that hydrogen transfer ability correlates well with LAS concentration. On the other hand, the role of extra-framework Al (EFAL) is often ascribed to strengthen the Brønsted acidity in its close proximity leading to the formation of so-called “super-acidic” BAS,^[34] the latter having the major impact on faster coking rates.

However, it is often reported that the presence of Lewis acidity in the form of EFAL^[35] or other species^[36] boosts activity in paraffin cracking reactions. The multiple explanations are not limited only by enhanced proton acidity due to electron density withdrawn by EFAL from BAS as described above. Another explanation also lies in enhanced enthalpies of alkane adsorption on EFAL. As the rate-determining step is the protonation of the alkane, an increase of surface coverage leads to significantly enhanced reaction rates.^[37]

Steaming of zeolites also leads to the prolonged lifetime in MTH process.^[38] The improved lifetime is however attributed to the decreased acidity and mesopores formation.

In contrast, it is reported that Lewis acidity in zeolites arising due to modification with alkaline-earth metals leads to the suppression of hydrogen transfer reactions in catalytic cracking of light alkanes.^[39] Besides, the presence of these elements enhance the surface basicity and decrease re-adsorption of light olefins, thus decreasing the chance of their participation in consecutive reactions.^[40]

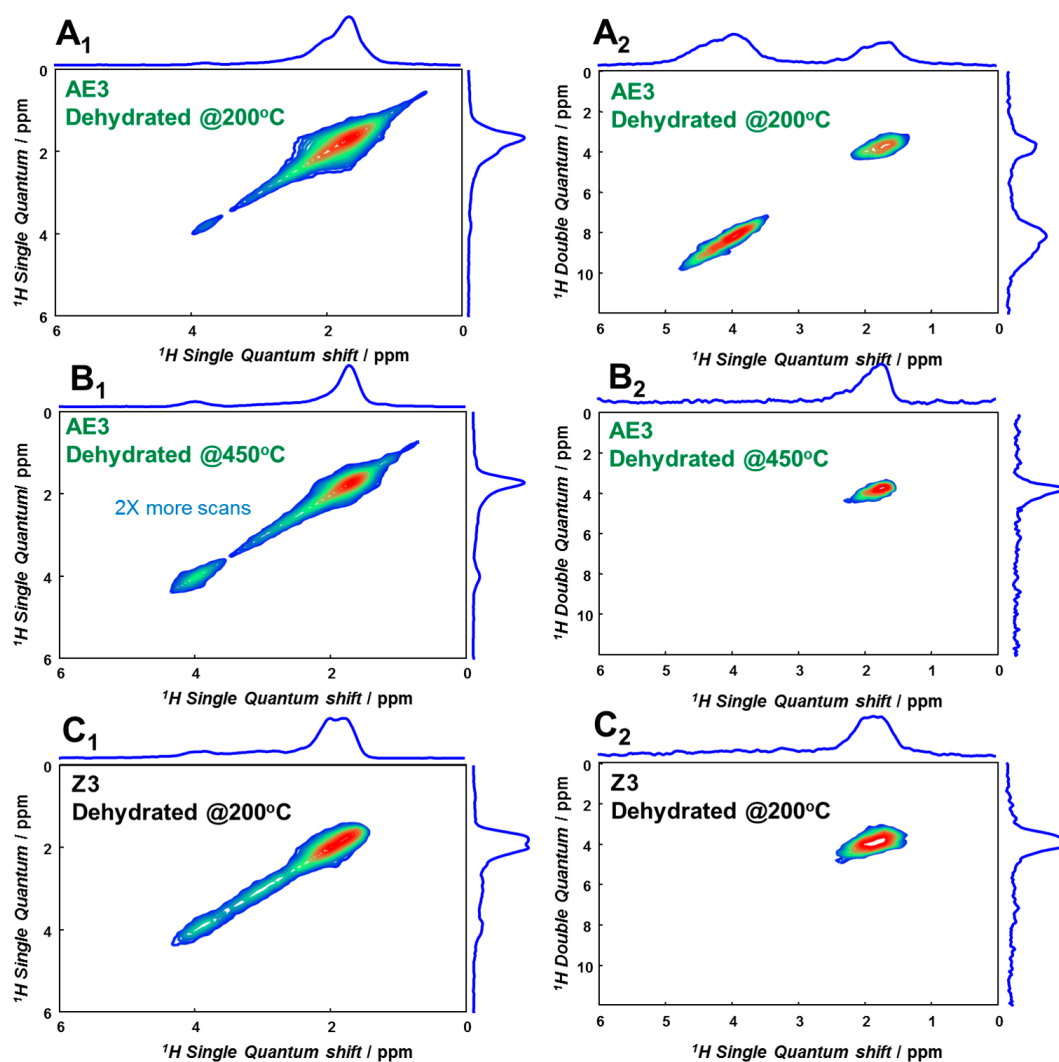


Figure 9. ^1H - ^1H RFDR (A_1 , B_1 , C_1) and ^1H - ^1H DQ (A_2 , B_2 , C_2) MAS NMR spectra of AE3 modified with Ca (A and B) dehydrated at 200°C (A), 450°C (B) and Z3 (C). Both samples are dehydrated at 200°C (1°C min^{-1}).

Based on the beneficial effect of the presence of EFAL and/or AE in catalytic cracking two possible explanations can be put forward, to relate the prolonged lifetime to the presence of AE in the zeolite. The reason behind the improved lifetimes lies either in the interaction of AE with BAS and/or with some of the MTO active species.

To gain insight in the nature of the Brønsted acid sites, two-dimensional ^1H - ^1H DQ (DQ=double-quantum) and ^1H - ^1H RFDR (RFDR=radiofrequency-driven recoupling) MAS NMR was carried out (Figure 9). These two methods are particularly powerful when combined;^[41] the double-quantum experiment does not give rise to auto-correlation cross-peaks for an isolated proton, whereas RFDR does.

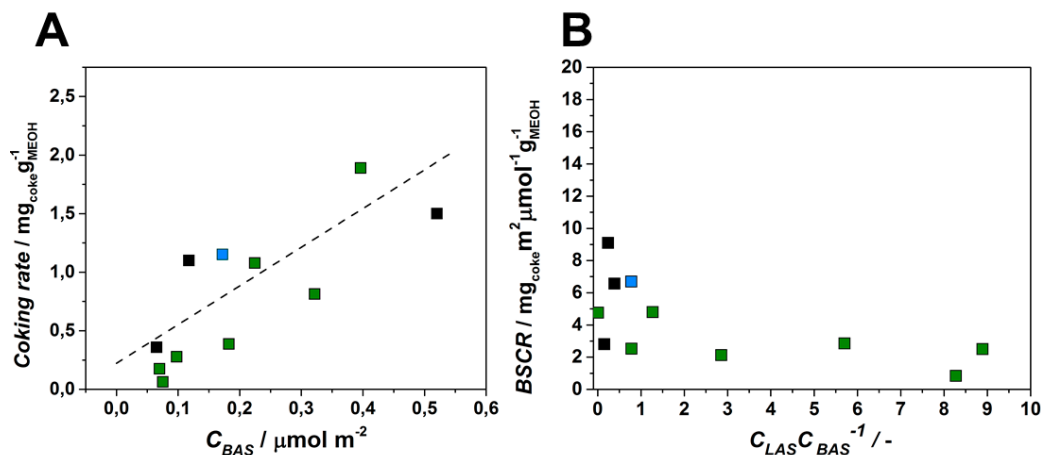
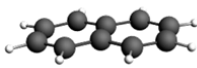
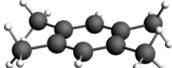


Figure 10. (A) Coking rate as a function of BAS concentration. (B) Brønsted specific coking rate as a function of LAS/BAS ratio. **Z** (black) – pre-synthetically modified ZSM-5 with different Si/Al ratio; **M** (blue) – post-synthetically demetallated ZSM-5; **AE** (green) – zeolites modified by post-synthetic incorporation of alkaline-earth metals.

Table 3. Interaction Energies between alkaline earth dimers and coke precursors. The contribution of dispersion to the total reaction energy is given between brackets behind the values.

		
$\text{Ca}_2(\text{OH})_2$	-85.9 kJ mol ⁻¹ (76.6% dispersion)	-95.8 kJ mol ⁻¹ (81.5% dispersion)
$\text{Mg}_2(\text{OH})_2$	-80.5 kJ mol ⁻¹ (73.8% dispersion)	-95.5 kJ mol ⁻¹ (77.3% dispersion)

The RFDR experiment tends to yield broader cross-peaks in comparison with the DQ experiment, but this is of no qualitative value to our analysis. The cross-peaks in the horizontal frequency span of 1-2 ppm belong to both terminal Si-OH protons and bridging Ca-OH protons.^[42] The fact that both the DQ and RFDR experiments produce correlations in the 2D dimension indeed indicates that these protons are not isolated from each other. Changes appear for the resonances around 4 ppm, arising from the acidic protons. When AE3 is fully dehydrated at 450°C (Figure C₂), something interesting is observed. The DQ correlation has vanished, but the RFDR correlation has not. This indicates that the acidic protons have become isolated entities. Note that we would obtain a similar scenario for C₁ and C₂, in the bottom row. This sample contains few Brønsted acid sites dispersed over the framework, which naturally, renders them isolated. As a consequence of this BAS isolation the high propylene selectivity is observed.

The effect of acidity of pre- and post-synthetically modified zeolites was further studied by analysing the coking rates of all the samples. Figure 10A shows a linear correlation between coking rate and BAS concentration (C_{BAS}), again independent on the sample and on the amount of Lewis acid sites. These

results further corroborate the effect of BAS isolation on the formation of coke species. More importantly, at similar coking rates, samples containing a higher amount of Lewis sites display a longer lifetime, in other words, although the same amount of coke per unit time is generated for those samples, more coke is necessary to fully deactivate the catalyst. Indeed, samples showing the longest lifetime (AE7 and AE3) are able to hold much more coke than the zeolite with similar acidity Z3 but lower amount of LAS (Table 2). In general, the resistance of Brønsted sites to deactivation, expressed as Brønsted specific coking rate (BSCR), tends to significantly increase for samples modified with alkaline-earth metals (Figure 10B). Considering that BAS and LAS are isolated from each other (*vide supra*), it is logical to assume that Lewis acid sites attach coke precursors, thus preventing the deactivation of BAS by coke deposition.

To support this hypothesis, we calculated interaction energies between the alkaline earth dimers and naphthalene and tetramethylbenzene. The latter two have been taken as two representative coke precursors (Table 3). Interactions between these fragments, computed at ZORA-BLYP-D3(BJ)/TZ2P, are considerable. A decomposition scheme to gauge the nature of this interaction showed that it is dispersion dominated, accounting for more than 70% in all investigated cases. The other part of the interaction matters a combined effort from the typical forces we associate with bonding – electrostatics, Pauli repulsion and orbital interaction. Bonding plays a minor role here. Hence, the alkaline earth dimers should be looked at as sites that are ‘sticky’ towards aromatic precursors. They attract them by dispersion interaction, and prevent them from participating further in methylation/cracking reactions that would eventually lead to coking.

6.4. Conclusions.

The current chapter is dedicated to the pre-synthetically and post-synthetically modified ZSM-5 zeolites with different concentrations and types of acid sites. Systematic analysis of the effect of Lewis and Brønsted acid sites on selectivity to ethylene and propylene and lifetime established them as two main performance descriptors. Both propylene and ethylene selectivity are linearly correlated with the density of Brønsted acid sites. Opposite trends observed for these two olefins indicated that they belong to the competing mechanistic cycles, isolation of BAS being the key strategy to enhance propylene selectivity.

Modification of zeolites with alkaline-earth metals results in the appearance of Lewis acidity significantly prolonging catalyst lifetime. The catalyst lifetime has a volcano-type dependency on the LAS and BAS densities ratio with an optimum for ratios between 3 and 6. The effect of Lewis acidity presence is tentatively attributed to the interaction with coke precursors confirmed by theoretical calculations. Alkaline earth sites act as sticky sites towards coke precursors, attracting them by dispersion forces, and therefore avoiding the rapid deactivation of Brønsted acid sites.

Current chapter provides readers with the design rules for the stable towards deactivation and selective to propylene MTO catalyst. They sound as simple as “isolate BAS and introduce coke collecting LAS”.

References

- [1] F. J. Keil, *Microporous Mesoporous Mater.* **1999**, *29*, 49-66.
- [2] F. L. Bleken, S. Chavan, U. Olsbye, M. Boltz, F. Ocampo, B. Louis, *Appl. Catal., A* **2012**, *447*, 178-185.
- [3] X. Y. Sun, S. Mueller, Y. Liu, H. Shi, G. L. Haller, M. Sanchez-Sanchez, A. C. van Veen, J. A. Lercher, *J. Catal.* **2014**, *317*, 185-197.
- [4] a) S. Teketel, W. Skistad, S. Benard, U. Olsbye, K. P. Lillerud, P. Beato, S. Svelle, *ACS Catal.* **2012**, *2*, 26-37; b) S. Teketel, L. F. Lundegaard, W. Skistad, S. M. Chavan, U. Olsbye, K. P. Lillerud, P. Beato, S. Svelle, *J. Catal.* **2015**, *327*, 22-32.
- [5] U. Olsbye, S. Svelle, M. Bjorgen, P. Beato, T. V. W. Janssens, F. Joensen, S. Bordiga, K. P. Lillerud, *Angew. Chem. Int. Ed.* **2012**, *51*, 5810-5831.
- [6] a) M. Milina, S. Mitchell, P. Crivelli, D. Cooke, J. Perez-Ramirez, *Nat. Commun.* **2014**, *5*; b) M. Milina, S. Mitchell, D. Cooke, P. Crivelli, J. Perez-Ramirez, *Angew. Chem. Int. Ed.* **2015**, *54*, 1591-1594.
- [7] F. Bleken, M. Bjorgen, L. Palumbo, S. Bordiga, S. Svelle, K.-P. Lillerud, U. Olsbye, *Top. Catal.* **2009**, *52*, 218-228.
- [8] a) T. Liang, J. Chen, Z. Qin, J. Li, P. Wang, S. Wang, G. Wang, M. Dong, W. Fan, J. Wang, *ACS Catal.* **2016**, *6*, 7311-7325; b) A. N. Mlinar, P. M. Zimmerman, F. E. Celik, M. Head-Gordon, A. T. Bell, *J. Catal.* **2012**, *288*, 65-73.
- [9] a) T. Armaroli, L. J. Simon, M. Digne, T. Montanari, M. Bevilacqua, V. Valtchev, J. Patarin, G. Busca, *Appl. Catal., A* **2006**, *306*, 78-84; b) I. Yarulina, J. Goetze, C. Gucuyener, L. van Thiel, A. Dikhtiarenko, J. Ruiz-Martinez, B. M. Weckhuysen, J. Gascon, F. Kapteijn, *Catal. Sci. Technol.* **2016**, *6*, 2663-2678.
- [10] a) M. A. Deimund, L. Harrison, J. D. Lunn, Y. Liu, A. Malek, R. Shayib, M. E. Davis, *ACS Catal.* **2016**, *6*, 542-550; b) Q. Qian, J. Ruiz-Martinez, M. Mokhtar, A. M. Asiri, S. A. Al-Thabaiti, S. N. Basahel, B. M. Weckhuysen, *Catal. Today* **2014**, *226*, 14-24.
- [11] A. Corma, *Chem. Rev.* **1995**, *95*, 559-614.
- [12] S. Svelle, F. Joensen, J. Nerlov, U. Olsbye, K. P. Lillerud, S. Kolboe, M. Bjorgen, *J. Am. Chem. Soc.* **2006**, *128*, 14770-14771.
- [13] J. F. Haw, W. G. Song, D. M. Marcus, J. B. Nicholas, *Acc. Chem. Res.* **2003**, *36*, 317-326.
- [14] a) K. Barbera, F. Bonino, S. Bordiga, T. V. W. Janssens, P. Beato, *J. Catal.* **2011**, *280*, 196-205; b) I. Yarulina, A. Dikhtiarenko, F. Kapteijn, J. Gascon, *Catal. Sci. Technol.* **2017**.
- [15] H. E. van der Bij, B. M. Weckhuysen, *Chem. Soc. Rev.* **2015**, *44*, 7406-7428.
- [16] F. Yaripour, Z. Shariatnia, S. Sahebdehfar, A. Irandoukht, *Microporous Mesoporous Mater.* **2015**, *203*, 41-53.
- [17] a) I. A. Bakare, O. Muraza, M. Yoshioka, Z. H. Yamani, T. Yokoi, *Catal. Sci. Technol.* **2016**; b) M. Stöcker, *Microporous Mesoporous Mater.* **1999**, *29*, 3-48; c) S. H. Zhang, B. L. Zhang, Z. X. Gao, Y. Z. Han, *Ind. Eng. Chem. Res.* **2010**, *49*, 2103-2106.
- [18] H. L. Janardhan, G. V. Shanbhag, A. B. Halgeri, *Appl. Catal., A* **2014**, *471*, 12-18.
- [19] Y. Hong, X. Yan, X. Liao, R. Li, S. Xu, L. Xiao, J. Fan, *Chem. Commun.* **2014**, *50*, 9679-9682.
- [20] a) X. Sun, S. Sartipi, F. Kapteijn, J. Gascon, *New J. Chem.* **2016**, *40*, 4167-4177; b) I. Yarulina, F. Kapteijn, J. Gascon, *Catal. Sci. Technol.* **2016**, *6*, 5320-5325.
- [21] I. Yarulina, S. Bailleul, A. Pustovarenko, J. R. Martinez, K. D. Wispelaere, J. Hajek, B. M. Weckhuysen, K. Houben, M. Baldus, V. Van Speybroeck, F. Kapteijn, J. Gascon, *ChemCatChem* **2016**, *8*, 3057-3063.
- [22] C. A. Emeis, *J. Catal.* **1993**, *141*, 347-354.
- [23] J. Rouquerol, P. Llewellyn, K. Sing, in *Adsorption by Powders and Porous Solids (Second Edition)*, Academic Press, Oxford, **2014**, pp. 467-527.
- [24] P. L. Llewellyn, J. P. Coulomb, Y. Grillet, J. Patarin, G. Andre, J. Rouquerol, *Langmuir* **1993**, *9*, 1852-1856.
- [25] J. Perez-Ramirez, C. H. Christensen, K. Egeblad, C. H. Christensen, J. C. Groen, *Chem. Soc. Rev.* **2008**, *37*, 2530-2542.
- [26] a) C. S. Mei, P. Y. Wen, Z. C. Liu, H. X. Liu, Y. D. Wang, W. M. Yang, Z. K. Xie, W. M. Hua, Z. Gao, *J. Catal.* **2008**, *258*, 243-249; b) M. Milina, S. Mitchell, N. L. Michels, J. Kenvin, J. Perez-Ramirez, *J. Catal.* **2013**, *308*, 398-407.
- [27] J. Brus, L. Kobera, W. Schoefberger, M. Urbanova, P. Klein, P. Sazama, E. Tabor, S. Sklenak, A. V. Fishchuk, J. Dedecek, *Angew. Chem. Int. Ed.* **2015**, *54*, 541-545.
- [28] D. Mores, J. Kornatowski, U. Olsbye, B. M. Weckhuysen, *Chem.-Eur. J.* **2011**, *17*, 2874-2884.
- [29] S. Müller, Y. Liu, F. M. Kirchberger, M. Tonigold, M. Sanchez-Sanchez, J. A. Lercher, *J. Am. Chem. Soc.* **2016**, *138*, 15994-16003.
- [30] M. Guisnet, L. Costa, F. R. Ribeiro, *J. Mol. Catal. A: Chem.* **2009**, *305*, 69-83.
- [31] S. Mitchell, A. B. Pinar, J. Kenvin, P. Crivelli, J. Kaerger, J. Perez-Ramirez, *Nat. Commun.* **2015**, *6*.

- [32] a) F. Schmidt, C. Hoffmann, F. Giordanino, S. Bordiga, P. Simon, W. Carrillo-Cabrera, S. Kaskel, *J. Catal.* **2013**, *307*, 238-245; b) F. L. Bleken, K. Barbera, F. Bonino, U. Olsbye, K. P. Lillerud, S. Bordiga, P. Beato, T. V. W. Janssens, S. Svelle, *J. Catal.* **2013**, *307*, 62-73.
- [33] H. Schulz, M. Wei, *Top. Catal.* **2014**, *57*, 683-692.
- [34] S. Li, A. Zheng, Y. Su, H. Zhang, L. Chen, J. Yang, C. Ye, F. Deng, *J. Am. Chem. Soc.* **2007**, *129*, 11161-11171.
- [35] a) S. Schallmoser, T. Ikuno, M. F. Wagenhofer, R. Kolvenbach, G. L. Haller, M. Sanchez-Sanchez, J. A. Lercher, *J. Catal.* **2014**, *316*, 93-102; b) M. Niwa, S. Sota, N. Katada, *Catal. Today* **2012**, *185*, 17-24; c) S. M. T. Almutairi, B. Mezari, G. A. Filonenko, P. C. M. M. Magusin, M. S. Rigutto, E. A. Pidko, E. J. M. Hensen, *ChemCatChem* **2013**, *5*, 452-466.
- [36] S.-W. Choi, W.-G. Kim, J.-S. So, J. S. Moore, Y. Liu, R. S. Dixit, J. G. Pendergast, C. Sievers, D. S. Sholl, S. Nair, C. W. Jones, *J. Catal.* **2017**, *345*, 113-123.
- [37] J. A. van Bokhoven, M. Tromp, D. C. Koningsberger, J. T. Miller, J. A. Z. Pieterse, J. A. Lercher, B. A. Williams, H. H. Kung, *J. Catal.* **2001**, *202*, 129-140.
- [38] a) L. R. Aramburo, S. Teketel, S. Svelle, S. R. Bare, B. Arstad, H. W. Zandbergen, U. Olsbye, F. M. F. de Groot, B. M. Weckhuysen, *J. Catal.* **2013**, *307*, 185-193; b) Z. B. Li, J. Martinez-Triguero, J. H. Yu, A. Corma, *J. Catal.* **2015**, *329*, 379-388.
- [39] a) N. Rahimi, R. Karimzadeh, *Appl. Catal., A* **2011**, *398*, 1-17; b) K. Wakui, K. Satoh, G. Sawada, K. Shiozawa, K. Matano, K. Suzuki, T. Hayakawa, Y. Yoshimura, K. Murata, F. Mizukami, *Catal. Lett.* **2002**, *84*, 259-264.
- [40] Y. Yoshimura, N. Kijima, T. Hayakawa, K. Murata, K. Suzuki, F. Mizukami, K. Matano, T. Konishi, T. Oikawa, M. Saito, T. Shiojima, K. Shiozawa, K. Wakui, G. Sawada, K. Sato, S. Matsuo, N. Yamaoka, *Catal. Surv. Jpn.* **2000**, *4*, 157-167.
- [41] C. Volkringer, M. Meddouri, T. Loiseau, N. Guillou, J. Marrot, G. Ferey, M. Haouas, F. Taulelle, N. Audebrand, M. Latroche, *Inorg. Chem.* **2008**, *47*, 11892-11901.
- [42] a) C. Ruspic, S. Nembenna, A. Hofmeister, J. Magull, S. Harder, H. W. Roesky, *J. Am. Chem. Soc.* **2006**, *128*, 15000-15004; b) E. Pustovgar, R. P. Sangodkar, A. S. Andreev, M. Palacios, B. F. Chmelka, R. J. Flatt, J. B. D. de Lacaillerie, *Nat. Commun.* **2016**, *7*; c) M. Hunger, D. Freude, H. Pfeifer, D. Prager, W. Reschetilowski, *Chem. Phys. Lett.* **1989**, *163*, 221-224.

Appendix

A

Methanol-to-Olefins Process over Zeolite Catalysts with DDR Topology: Effect of Composition and Structural Defects on Catalytic Performance

Table A1. Refinement data for Sigma1-315-M.

Crystal system	Trigonal
Space group	<i>R</i> -3 <i>m</i> (№ 166)
<i>a</i> / Å	13.8068(1)
<i>b</i> / Å	13.8068(1)
<i>c</i> / Å	40.8500(1)
$\alpha, \beta, \gamma / ^\circ$	90
<i>V</i> / Å ³	6715.86(1)
<i>Z</i>	12
Wavelength / Å	Co-K α / 1.78897
<i>T</i> / K	293
<i>D</i> _{calc} / g·cm ⁻³	1.783
2 θ range / °	5 – 50
<i>R</i> _p ⁱ	7.79
<i>R</i> _{wp} ⁱⁱ	11.22

$$^i R_p = \sum_i |y_{i,0} - y_{i,c}| / \sum_i |y_{i,0}|; \quad ^{ii} R_{wp} = \left[\sum_i w_i (y_{i,0} - y_{i,c})^2 / \sum_i w_i (y_{i,0})^2 \right]^{1/2}$$

Table A2. Carbon based selectivity of products from Methanol conversion over Sigma-1 zeolites at 450°C.

Sample	Light paraffins (%) ^a	Ethylene (%) ^a	Propylene (%) ^a	Butenes (%) ^a	Coke (%) ^b
Sigma1-120-M	3	25	37	9	26
Sigma1-315-L	2	24	35	10	26
Sigma1-315-M	2	36	35	9	18
Sigma1-315-S	4	39	35	8	14
Sigma1-315-S-m	3	42	41	6	8

^a Integral selectivities calculated for the active period of catalyst (*X* > 98%).

^b Calculated from TGA, assuming that all coke was formed during the active period (*X* > 98%).

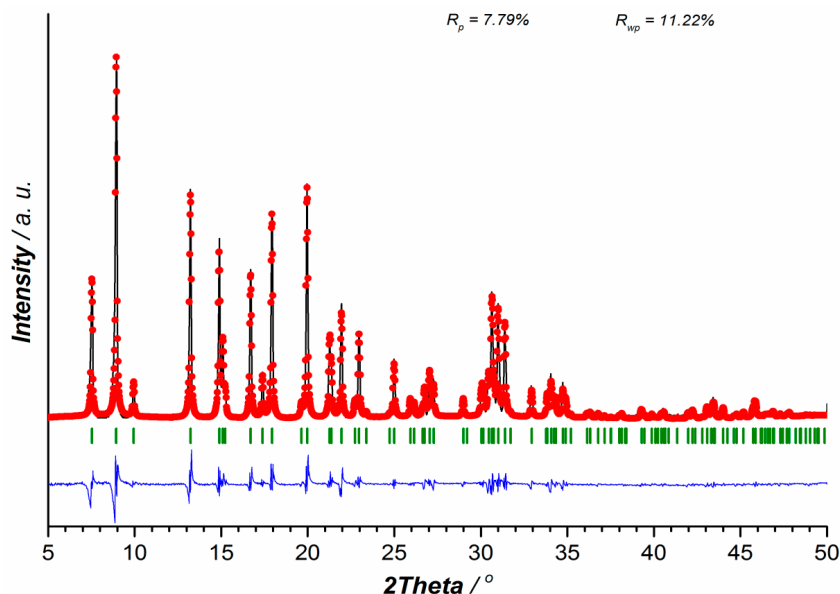


Figure A1. Pawley fitting plot of Sigma1-315-M. Pawley fit for Sigma1-315-M. The experimental data are presented as black solid line, calculated one by red dots and difference between them as blue solid line. The Bragg positions of the peaks are represented as green sticks. The blue line represents the difference between experimental data and fitting.

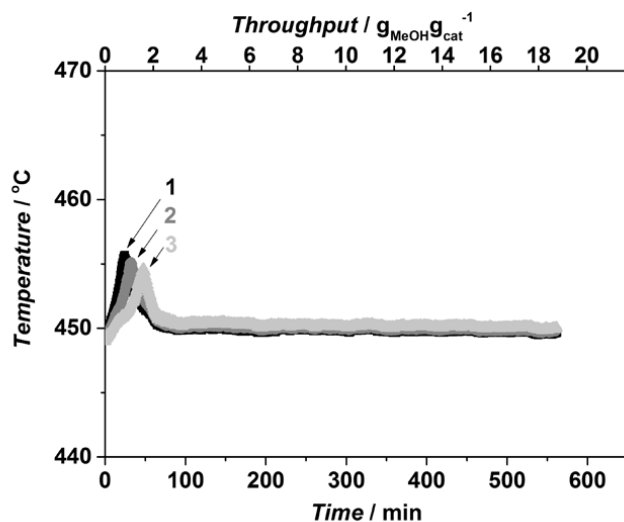


Figure A2. Temperature profiles in (1) top (2) middle and (3) bottom part of the catalytic bed as a function of time-on-stream for undiluted Sigma1-315-M at standard operating conditions.

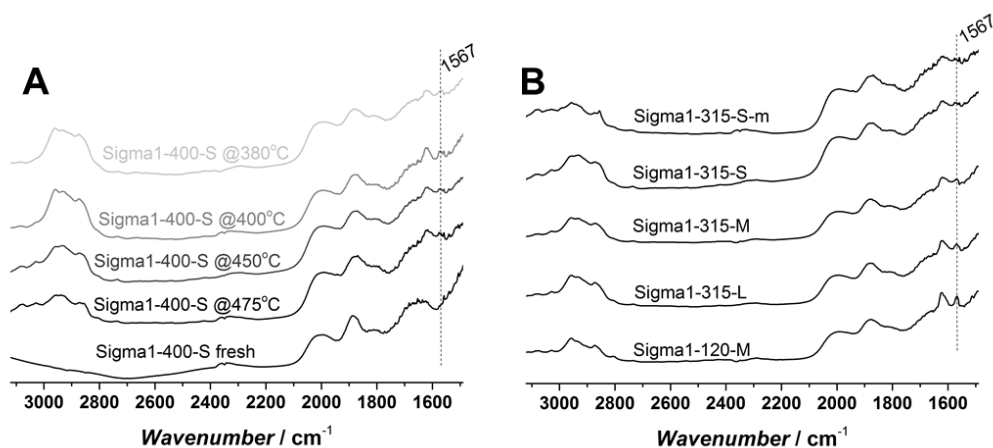


Figure A3. DRIFT spectra of (A) Sigma1-315-S spent at different temperatures; (B) Sigma-1 zeolites with different acidity and crystal size spent at 450 °C. Band at 1567 cm^{-1} is characteristic for C =C vibration of aromatic compounds.

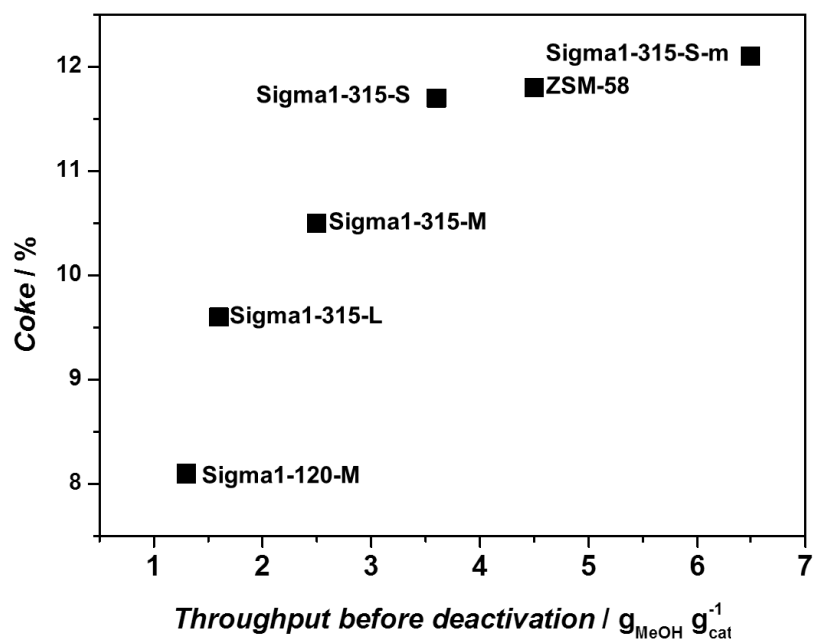


Figure A4. Amount of coke formed in catalysts deactivated at 450 °C as a function of MeOH throughput before deactivation.

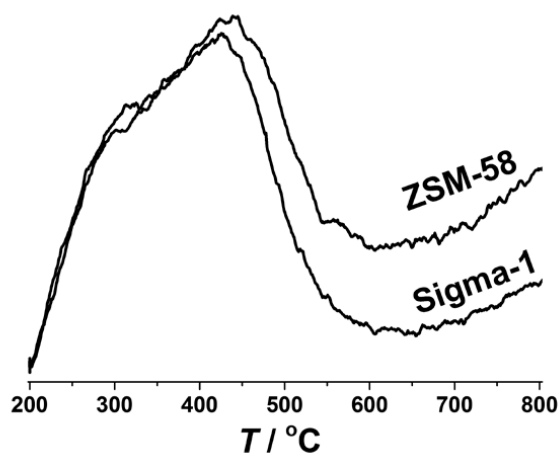


Figure A5. NH_3 TPD profiles of zeolites Sigma1-120-M ($\text{SiO}_2/\text{Al}_2\text{O}_3 = 120$) and ZSM-58 ($\text{SiO}_2/\text{Al}_2\text{O}_3 = 110$).

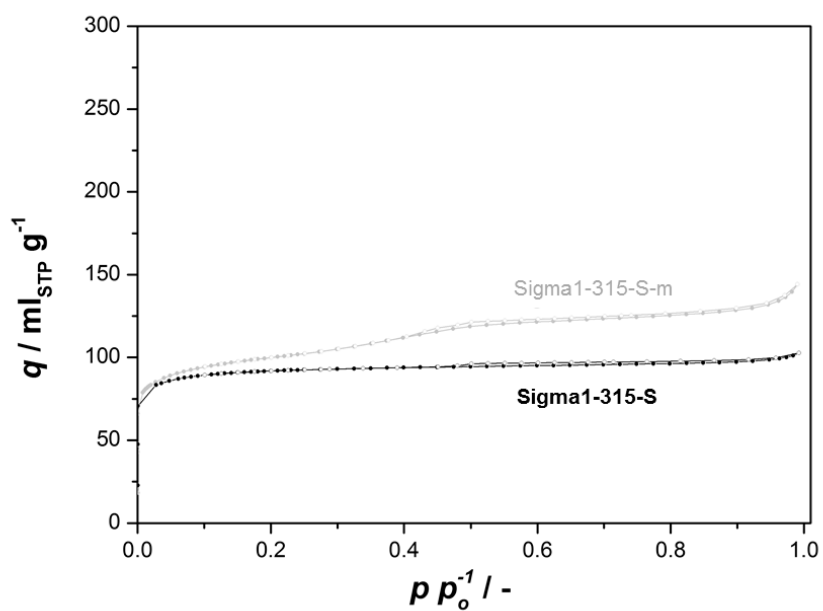


Figure A6. N_2 adsorption-desorption isotherm @ -196°C of Sigma1-315-S and Sigma1-315-S-m catalysts.

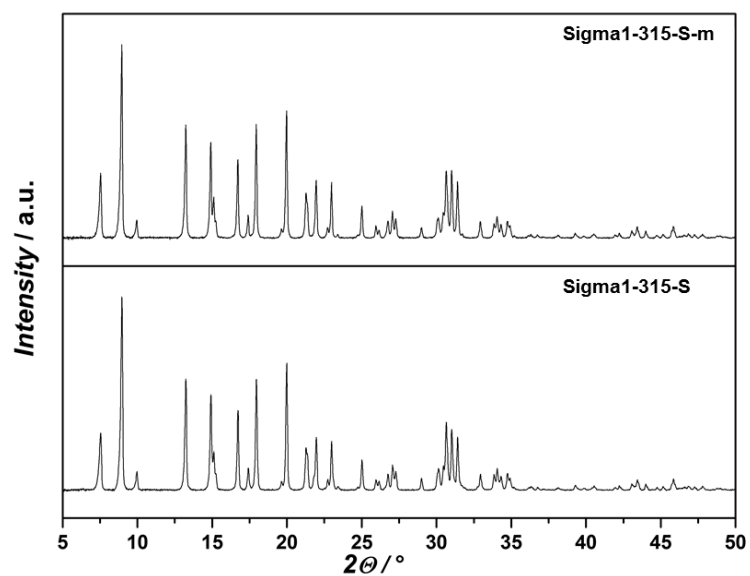


Figure A7. XRD patterns of calcined Sigma1-315-S and Sigma1-315-S-m zeolites.

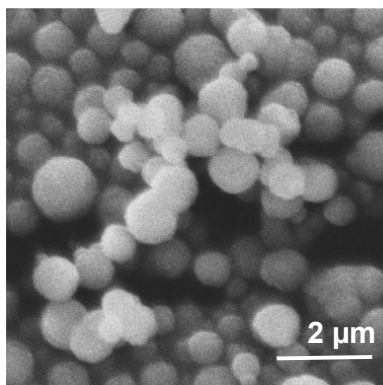


Figure A8. SEM micrograph of ZSM-58 with $\text{SiO}_2/\text{Al}_2\text{O}_3 = 110$.

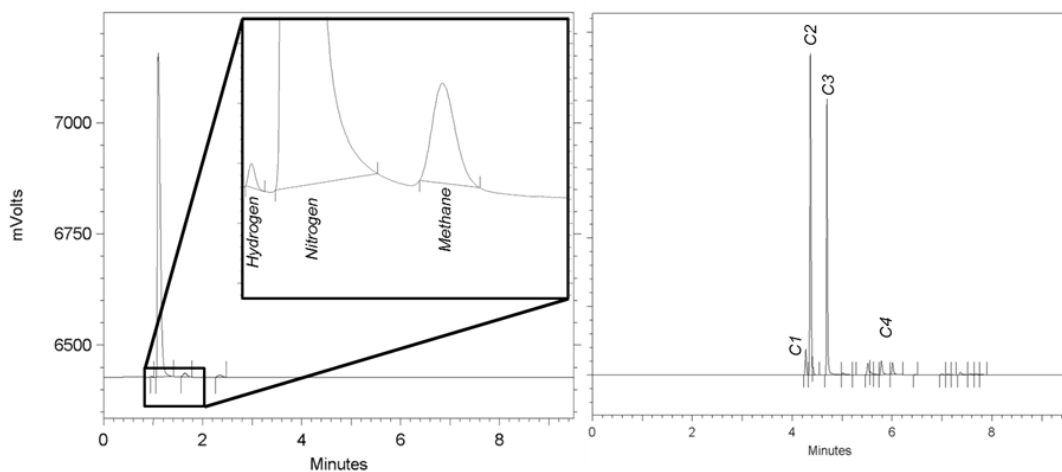


Figure A9. TCD (*left*) and FID (*right*) chromatograms showing typical product distribution of MTO process performed over zeolites with DDR topology.

Appendix

B

***Faster is not Always Better: Consequences
of Secondary Zeolite Growth on Catalytic
Performance in DMTO***

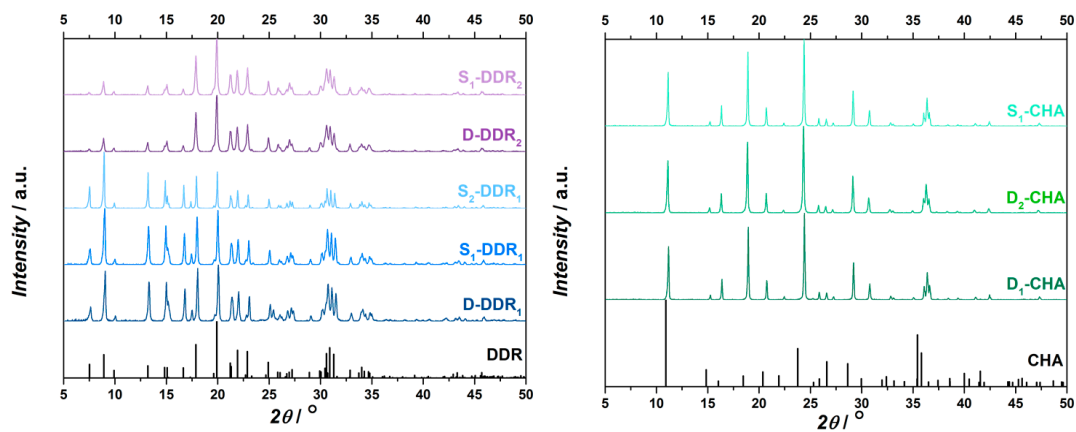


Figure B1. XRD patterns of zeolites with (left) DDR and (right) CHA topology together with reference patterns from database of zeolite structures.

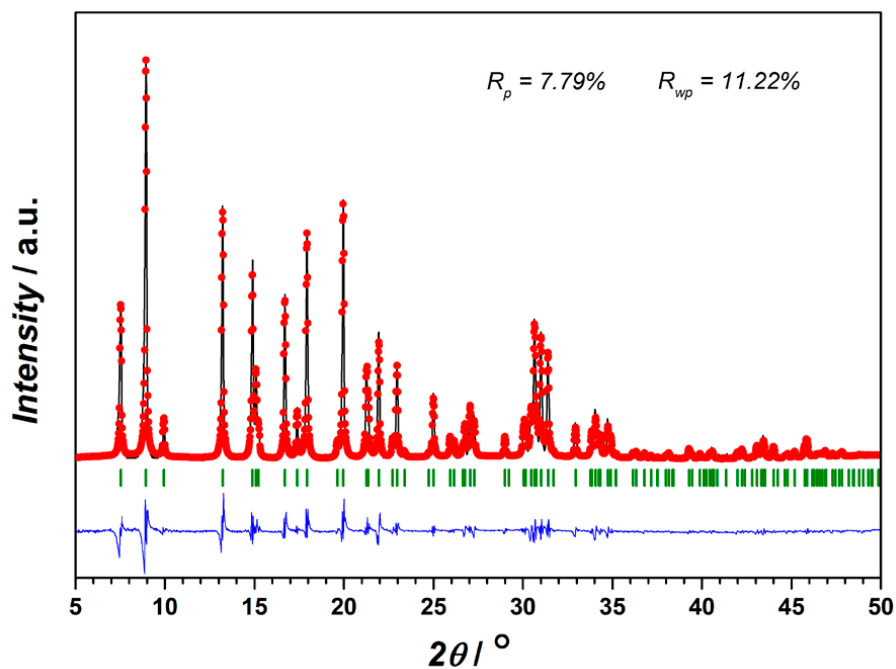


Figure B2. Pawley fitting plot of Sigma-1 zeolite. Experimental data are presented as a black solid line, calculated one by red dots and difference between them as blue solid line. The Bragg positions of the peaks are represented as green sticks. The blue line represents the difference between experimental data and fitting.

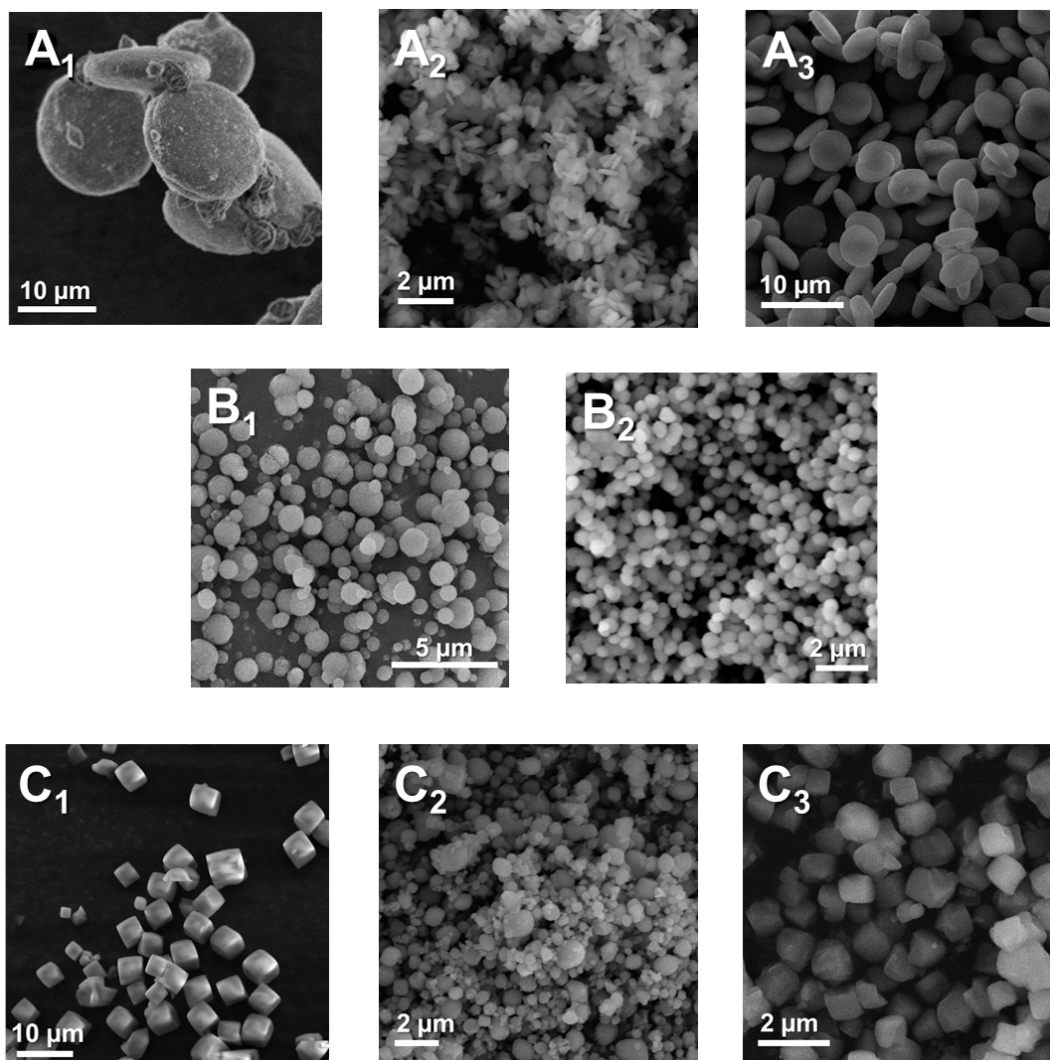


Figure B3. SEM images of (A) Sigma-1, (B) ZSM-58 and (C) SSZ-13 zeolites prepared by direct hydrothermal and seeded synthesis.

(A₁) – D-DDR₁

(A₂) – S₁-DDR₁

(A₃) – S₂-DDR₁

(B₁) – D-DDR₂

(B₂) – S₁-DDR₂

(C₁) – D₁-CHA

(C₂) – D₂-CHA

(C₃) – S₁-CHA

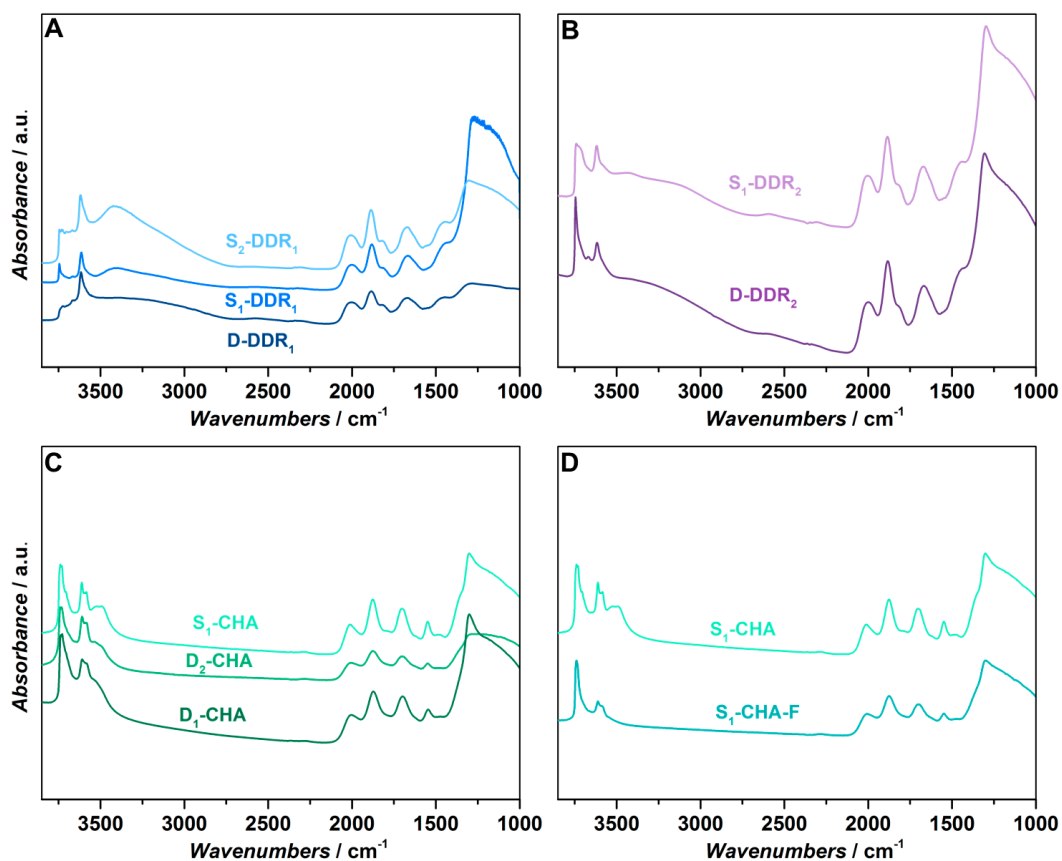


Figure B4. FTIR spectra of activated Sigma-1 (A), ZSM-58 (B), SSZ-13(C) and fluoride-modified SSZ-13 (D) zeolites.

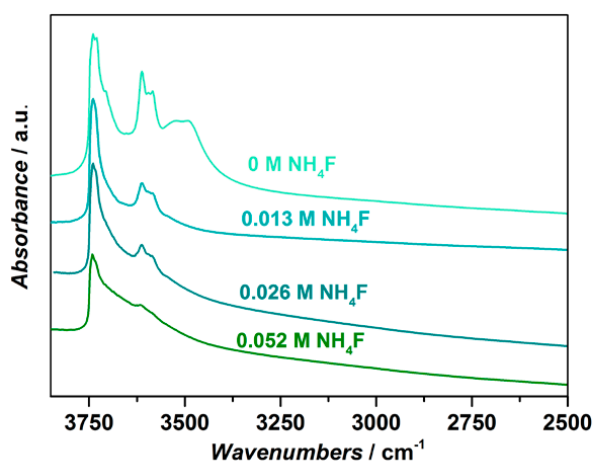


Figure B5. FTIR spectra of S1-CHA treated with different concentrations of NH₄F.

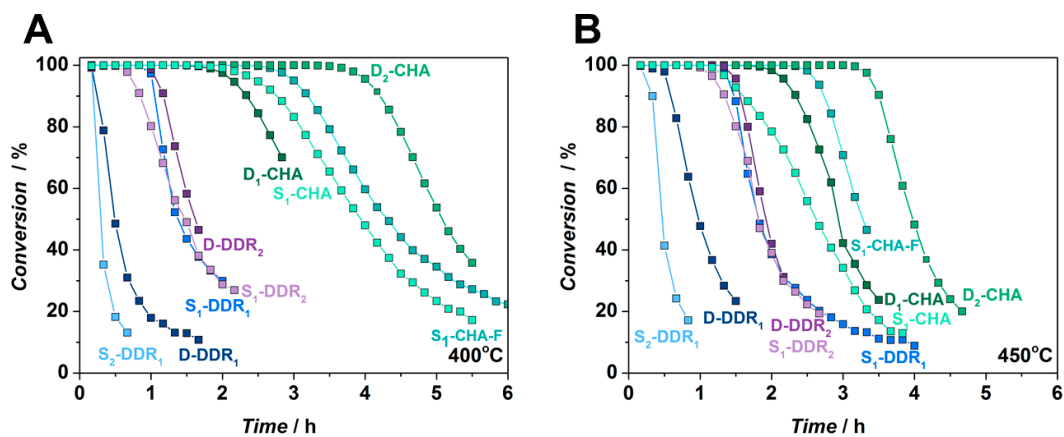


Figure B6. Dimethyl ether conversion as a function of time on stream at (A) 400°C and (B) 450°C for the zeolites under study. $M_{cat} = 0.5$ g, $WHSV = 1.23$ g_{DME} g_{cat}⁻¹h⁻¹.

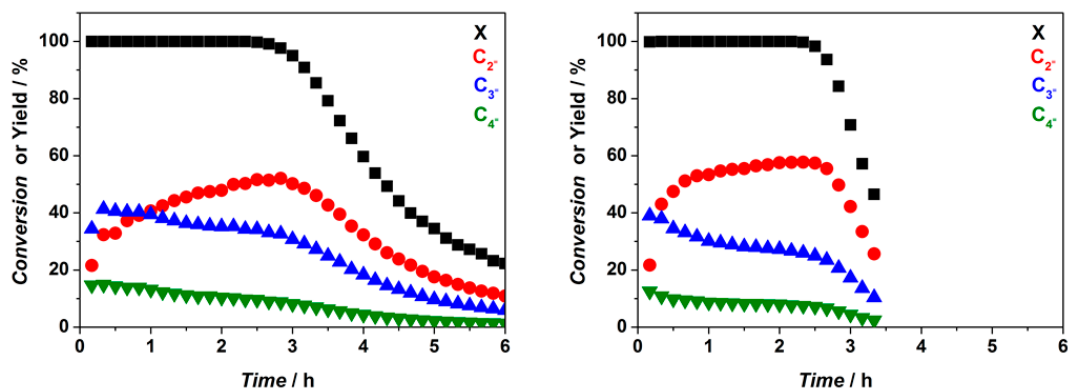


Figure B7. Dimethyl ether conversion and yields of ethylene, propylene and butenes as a function of time obtained over S₁-CHA-F (left) at 400°C and (right) at 450°C. $M_{cat} = 0.5$ g, $WHSV = 1.23$ g_{DME} g_{cat}⁻¹h⁻¹.

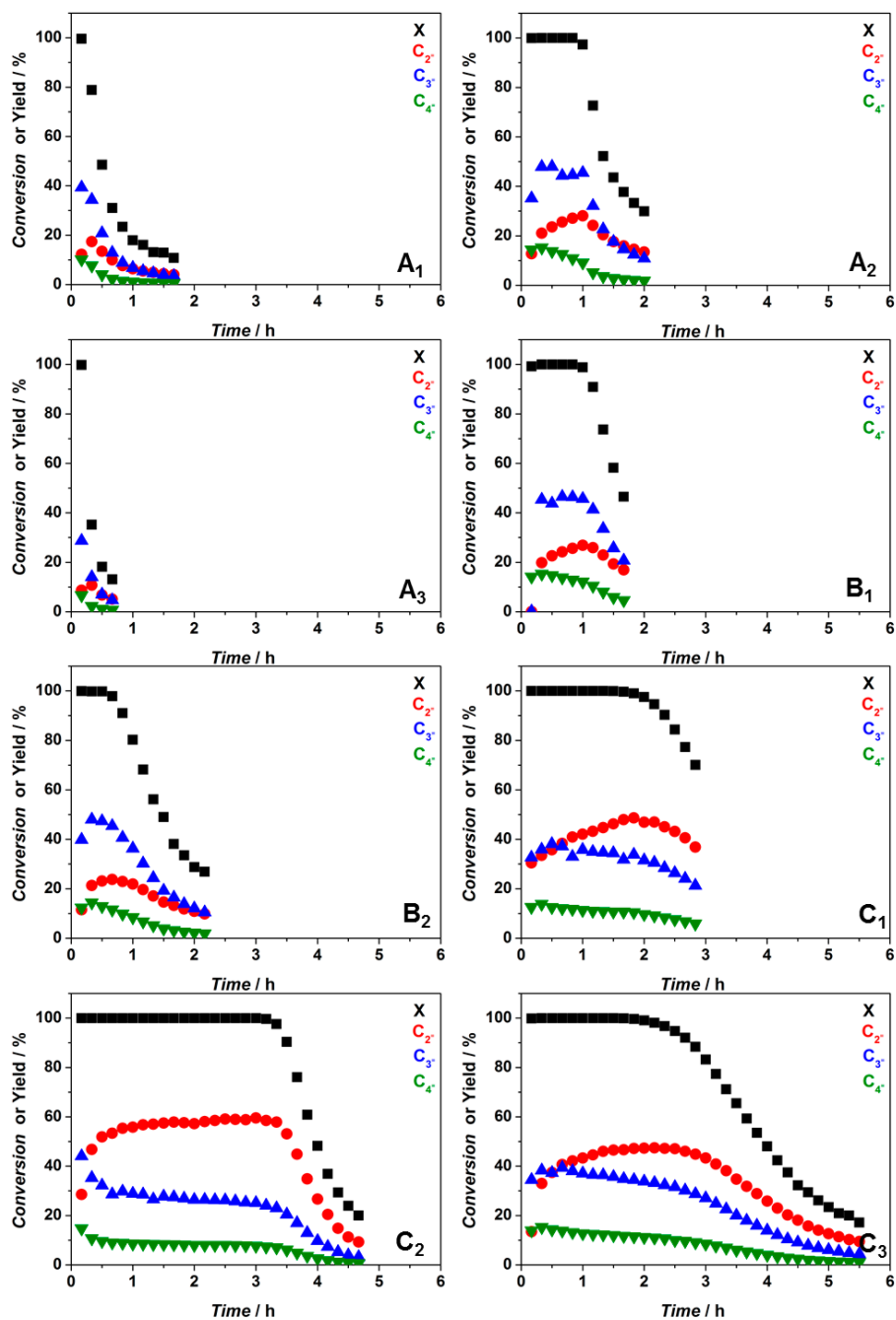


Figure B8. Dimethyl ether conversion and yields of ethylene, propylene and butenes as a function of time at 400°C for the zeolites under study. $M_{cat} = 0.5$ g, $WHSV = 1.23$ g_{DME} g_{cat}⁻¹h⁻¹. (A₁) – D-DDR₁; (A₂) – S₁-DDR₁; (A₃) – S₂-DDR₁; (B₁) – D-DDR₂; (B₂) – S₁-DDR₂; (C₁) – D₁-CHA; (C₂) – D₂-CHA; (C₃) – S₁-CHA.

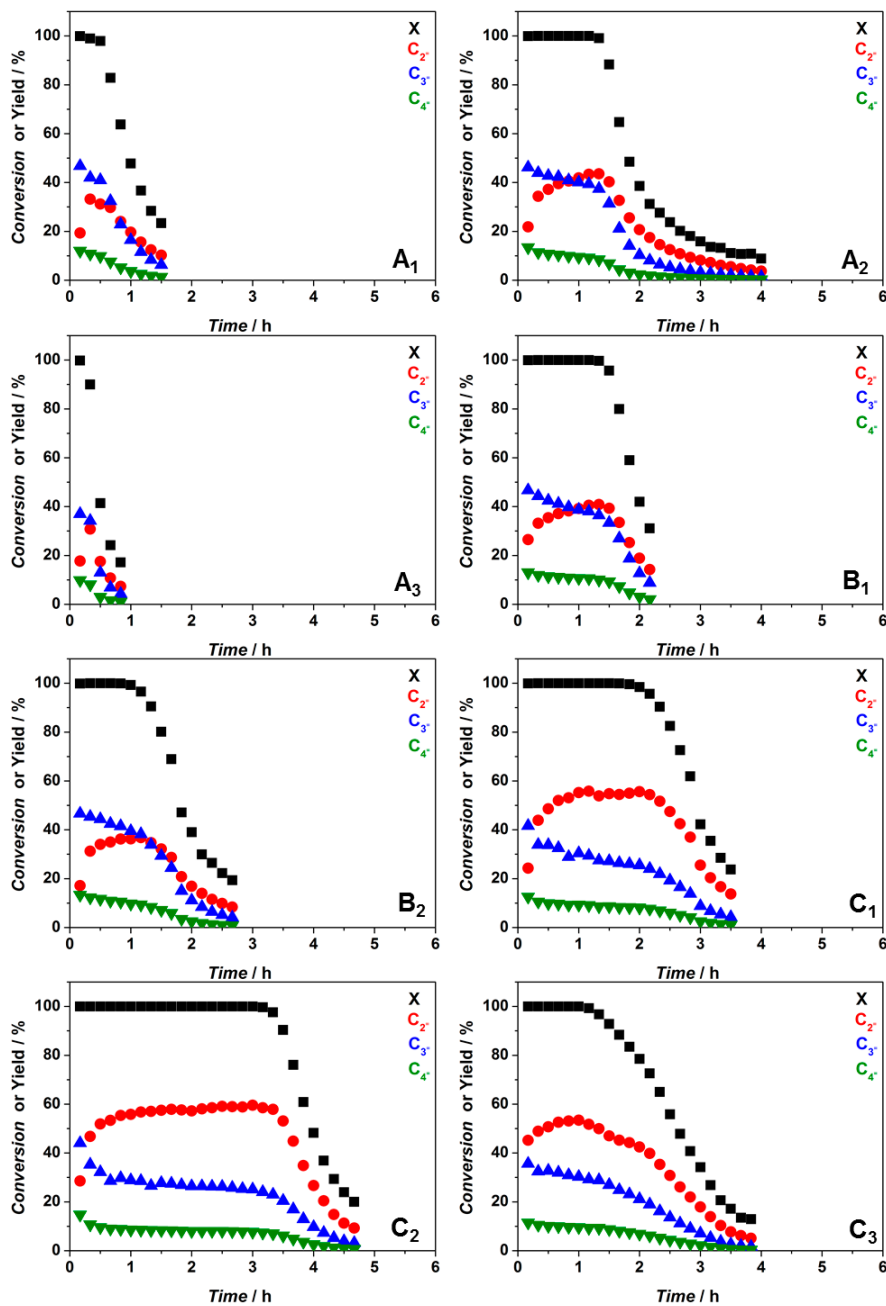


Figure B9. Dimethyl ether conversion and yields of ethylene, propylene and butenes as a function of time at 450°C for the zeolites under study. $M_{cat} = 0.5$ g, $WHSV = 1.23$ g_{DME} g_{cat}⁻¹h⁻¹. A₁) – D-DDR₁; (A₂) – S₁-DDR₁; (A₃) – S₂-DDR₁; (B₁) – D-DDR₂; (B₂) – S₁-DDR₂; (C₁) – D₁-CHA; (C₂) – D₂-CHA; (C₃) – S₁-CHA.

APPENDIX B

Appendix

C

***The Importance of Heat Effects in the
Methanol-to-Hydrocarbons Process over
ZSM-5: on the Role of Mesoporosity on
Catalyst Performance***

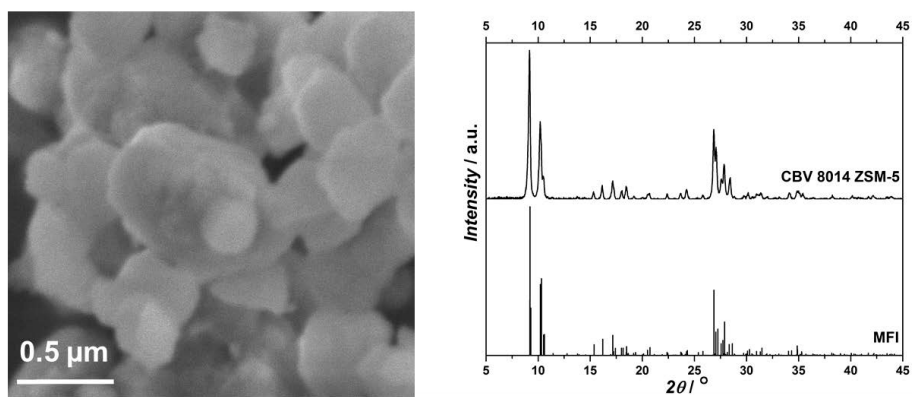


Figure C1. (Left) SEM micrograph of the parent ZSM-5 material. (Right) XRD patterns of parent ZSM-5 and reference MFI structure.

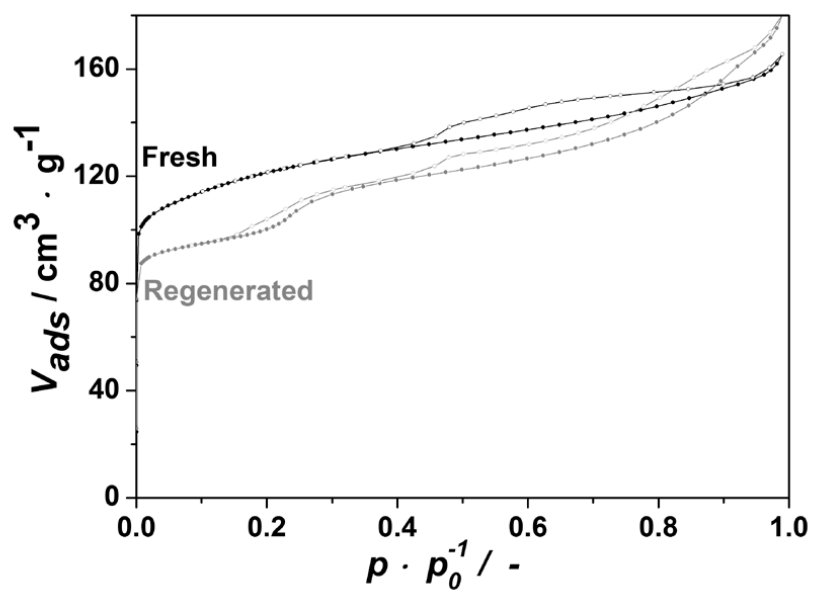


Figure C2. N₂ physisorption isotherms at -196°C of fresh ZSM-5 and regenerated sample after three catalytic runs.

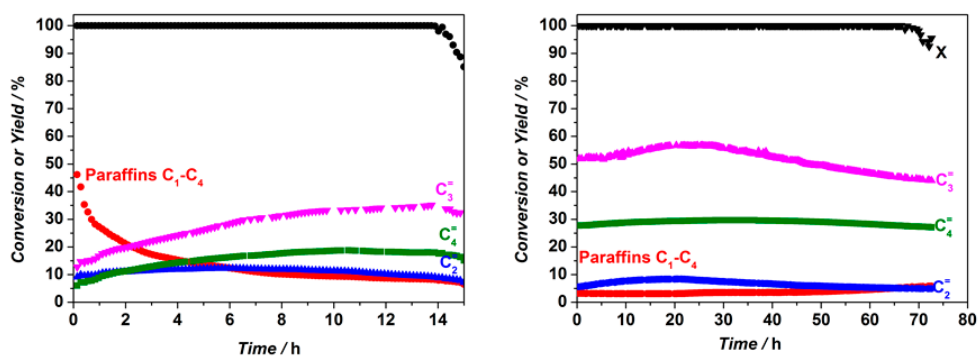
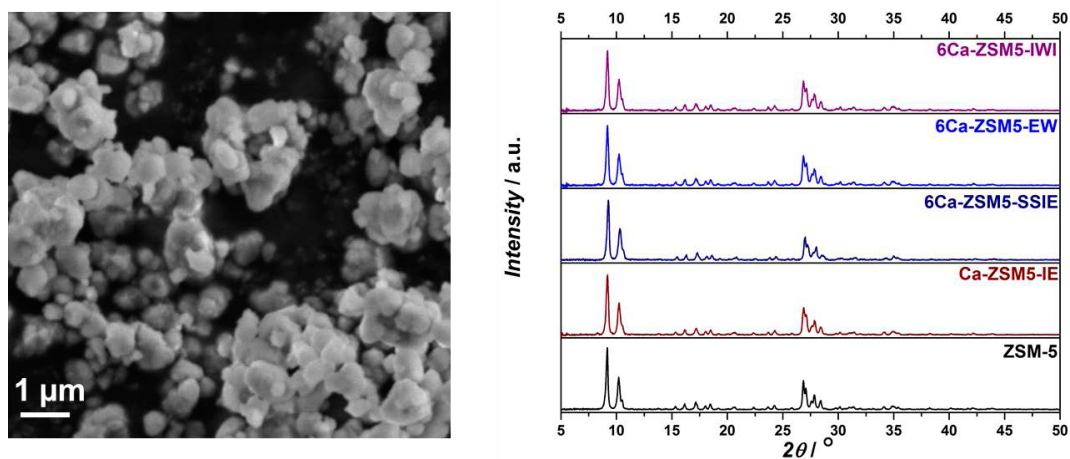
Appendix

D

Suppression of Aromatic Cycle in Methanol-to-Olefins Process over ZSM-5 by Post-synthetic Modification using Calcium

Table D1. Elemental composition of Ca-modified ZSM-5 derived from ICP-OES.

Catalyst	Si (wt. %)	Al (wt. %)	Ca (wt. %)	Si/Al (mol mol ⁻¹)	Ca/Al (mol mol ⁻¹)
ZSM-5	44	0.9	0	47	0
6Ca-ZSM5-IWI	43	0.8	6.4	52	5
2Ca-ZSM5-IWI	43	0.8	2.3	51	2

**Figure D1.** Methanol conversion (*black*) and yield of C₁-C₄ paraffins (*red*), ethylene (*blue*), propylene (*pink*) and butenes (*green*) as a function of time-on-stream for (*Left*) ZSM-5 and (*Right*) 6Ca-ZSM5-IWI.**Figure D2.** (*Left*) SEM picture of parent ZSM-5 material. (*Right*) XRD patterns of parent ZSM-5 and Ca-modified ZSM-5 samples prepared by different methods.

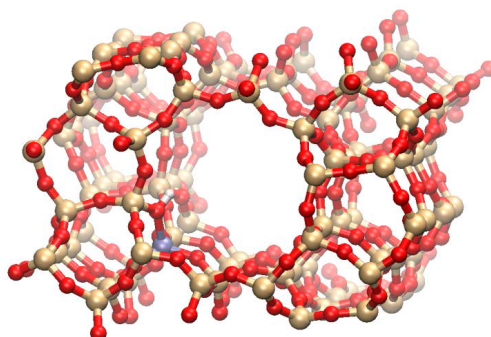


Figure D3. H-ZSM-5 unit cell used during the VASP simulations. In this figure, H is depicted in white, O in red, silicon in gold and Al in purple.

Computational Section.

Methodology.

To elucidate the nature of the active site in Ca-ZSM-5, periodic Density Functional Theory (DFT) calculations were performed using the Vienna Ab Initio Simulation Package (VASP 5.3) with the PBE functional and using Grimme D3 dispersion corrections.^[4] During the calculations, the projector augmented wave (PAW) method is used.^{[5],[6]} Furthermore, a plane-wave cutoff of 600 eV is used during the calculations and the self-consistent field (SCF) convergence criterion is set to 10^{-5} eV.

During the periodic VASP simulations, all proposed structures for the active site in Ca-ZSM-5 are built starting from an H-ZSM-5 unit cell, which consists of 96 T atoms, as represented in Figure D3. As can be seen, one Si is substituted by an Al per unit cell, corresponding to a Si/Al ratio of 95 and leading to one Brønsted acid site per unit cell. We consider only one acid site per unit cell, although the experimental Si/Al ratio is 40. However, given the size of the MFI unit cell, it is reasonable to assume that with such high Si/Al ratios, all Brønsted acid sites are isolated. Moreover, it has previously been reported that the rate per acid site of propene oligomerisation over H-MFI was affected by the Si/Al ratio for values between 12 and 40, but that a further increase from Si/Al 40 to 140 did not affect the rate.^[7] The Al substitution is located at the T12 position, similar to earlier work,^[8] which is at the intersection of the straight and zigzag channel offering maximum available space and creating the most accessible active site. During all simulations, the unit cell parameters are kept constant. However, the optimal volume of the unit cell of H-ZSM-5 is calculated by a least square fit to the Birch Murnaghan equation of state curve of the data points depicted in Figure D4. This led to an optimal unit cell volume of 5467.56 Å³. Subsequently, the unit cell parameters obtained from this structure are used to optimize all configurations with fixed cell parameters, which are given in Table D2.

For the normal mode analysis (NMA), a partial Hessian vibrational analysis (PHVA)^[9] is performed using VASP and TAMkin.^[10] This means that next to the Ca species an 8T cluster of the framework was

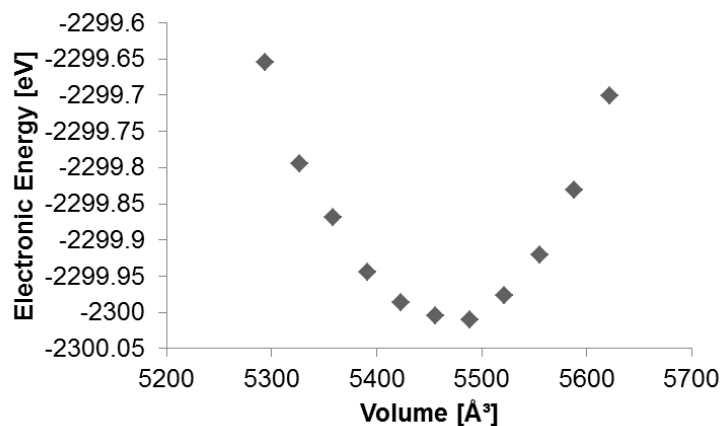


Figure D4. Data points used for the least-squares fit to the Birch Murnaghan equation of state curve.

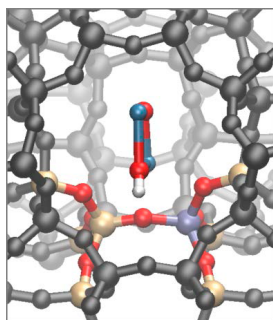


Figure D5. View along the zigzag channel of Ca-ZSM-5 in which the colored atoms represent the Ca species and 8T cluster which are taken into account during the NMA. In this figure, the following color code is used: the part of the ZSM-5 framework that is not used during the PHVA is set to black, Al is purple, Si is golden, H is white, O is red and Ca is depicted in light blue.

taken into account during the NMA, as indicated in Figure D5 for one of the optimized CaOCaOH^+ structures.

Determination of stable configurations.

The different configurations of the active site of Ca-ZSM-5, proposed based on literature^[11] combined with the assumption of isolated active sites due to the high Si/Al ratio, are depicted in Figure D7 and Figure D8 for CaOH^+ and CaOCaOH^+ , respectively. The corresponding electronic and relative energies are given in Table D2. For CaOH^+ , three configurations are taken into account, since the short chain can be oriented straight up, along the zigzag channel or to the intersection. For CaOCaOH^+ , a larger number of configurations were considered as more orientations are possible due to the length of the chain. For the dimer complexes of with Calcium also a second type of structures was found corresponding to a curled configuration. Due to the experimentally defined optimal Ca:Al ratio of 2, the analysis in this work is focused upon the CaOCaOH^+ structures rather than CaOH^+ .

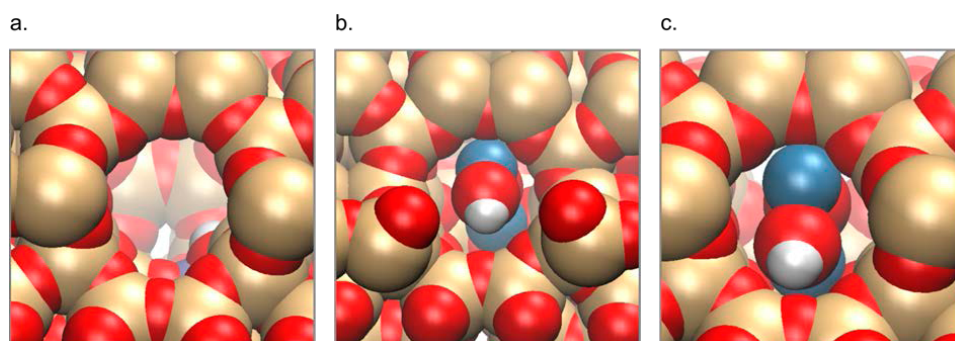


Figure D6. Snapshot of the view along the zigzag channel within the pristine ZSM-5 catalyst (a), the most stable straight configuration of CaOCaOH^+ (b) and the most stable curled configuration of CaOCaOH^+ (c) in a Van der Waals representation. The induced space restrictions by the Ca incorporated structures are clearly visible from the figures.

Table D2. Unit cell parameters used during the VASP simulations.

a [Å]	b [Å]	c [Å]	α [°]	β [°]	γ [°]
20.02	20.25	13.49	89.87	89.69	90.10

Table D3. Electronic energies and relative energies of all considered configurations of the active site in Ca-ZSM-5. Relative energies are referred to configurations a within each subclass.

Name	Electronic Energy [eV]	Relative energy [kJ/mol]
CaOH⁺		
Configuration a	-2311.1189	0.00
Configuration b	-2311.2253	-10.27
Configuration c	-2310.9842	13.00
CaOCaOH⁺		
Straight tail		
Configuration a	-2321.9594	0.00
Configuration b	-2322.0603	-9.74
Configuration c	-2322.3535	-38.02
Configuration d	-2322.1875	-22.53
Configuration e	-2322.3981	-42.33
Configuration f	-2321.8744	7.53
Curled tail		
Configuration a	-2323.0502	-105.24
Configuration b	-2322.5069	-52.82
Configuration c	-2322.8556	-86.47

Furthermore, a snapshot of the view along the zigzag channel of the most stable straight and curled configuration using a van der Waals representation is given in Figure D6. From this figure it is clearly visible that the embedded Ca dimer structures induce serious space restrictions in the catalyst pores.

All simulations were performed with fixed unit cell parameters as tabulated in Table D2.

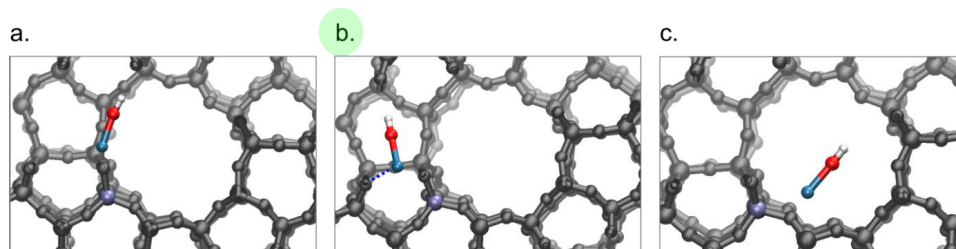


Figure D7. View along the zigzag channel of Ca-ZSM-5 in which the colored atoms represent the Ca species and 8T clusters which are taken into account during the NMA. In this figure, the following color code is used: the part of the ZSM-5 framework that is not used during the PHVA is set to black, Al is purple, Si is golden, H is white, O is red and Ca is depicted in light blue.

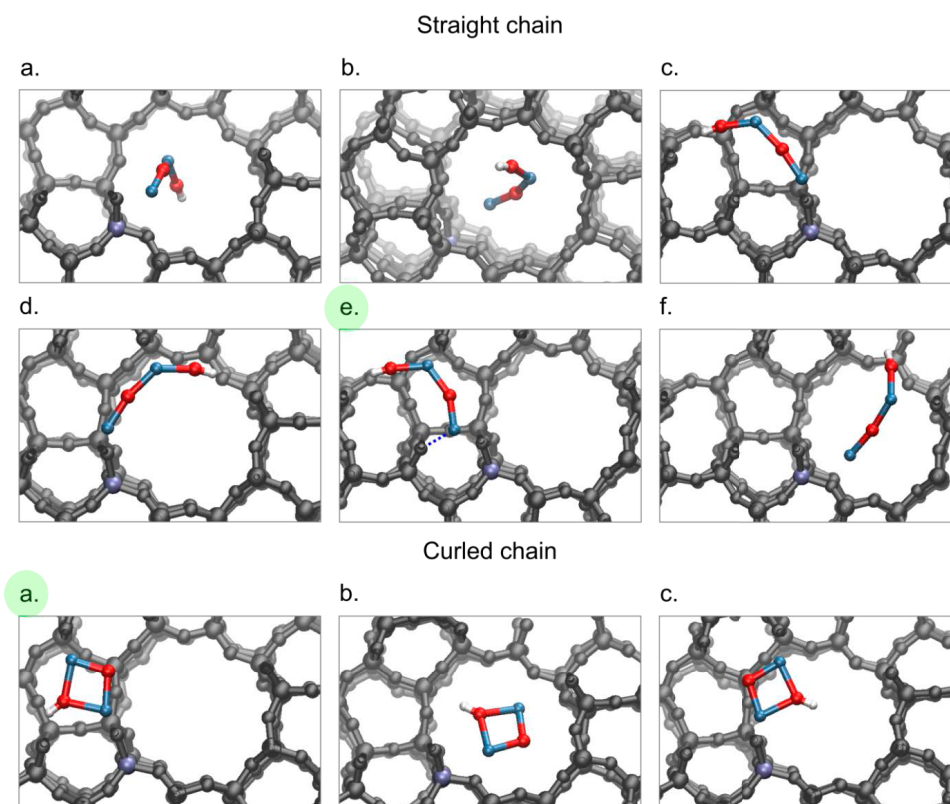


Figure D8. Optimized geometries for CaO-CaOH^+ for the nine considered configurations with the most stable configuration marked in green. In this figure, the same color code is used as for Figure D7.

Summary and Outlook

Summary.

The Methanol-to-olefins (MTO) process is an alternative route to obtain short chain olefins without relying on the use of oil as feedstock. One of the most important challenges in this process is the development of stable and selective catalysts, with propylene being currently the most desired product. Facing today's fast-changing world and its demands, the strategy of this thesis was to investigate different means allowing to control selectivity to short chain olefins and to tune the ethylene/propylene ratio in MTO. The entire thesis is dedicated to unravel "which strings need to be pulled for the desired product distribution in MTO." Though the thesis is focused on selectivity, the work is not limited to it, as special attention is also put to the development of catalysts stable to deactivation. The control over both factors was achieved by identifying the most important structure-activity relationships that favour or suppress one of the routes of the dual-cycle mechanism (thoroughly described in **Chapter 1**). These parameters – topology and acidity – are two main strings, which were pulled to manipulate the reaction mechanism in the desired direction.

Two main schemes were adapted as the tools to control selectivity (*i*) *via* stabilizing the aromatic cycle as described in **Part I** using 8-ring DDR and CHA zeolites and (*ii*) *via* modification of Brønsted acidity focusing on the 10-ring ZSM-5 zeolite in **Part II**.

Part I includes Chapters 2 and 3. **Chapter 2** focuses on the investigation of zeolites with DDR topology (ZSM-58 and Sigma-1) as potential catalysts for MTO application. Due to the particular combination of cage and window dimensions, DDR exhibited selectivity up to 90% towards ethylene and propylene, and a negligible amount of paraffins – an undisputed advantage allowing to reduce energy intensive separation steps. Systematic analysis of the effect of physicochemical properties on catalyst lifetime revealed that both a decrease in crystal size and concentration of acid sites prolonged catalyst lifetime, expressed in 'throughput' or productivity, from 1.3 g_{MEOH} g_{cat}⁻¹ up to 3.6 g_{MEOH} g_{cat}⁻¹. On the other hand, it was found that the ethylene/propylene ratio could be tuned by adjusting the reaction temperature and concentration of acid sites. In general, factors that led to the highest selectivity to propylene also resulted in the lowest selectivity to ethylene, indicating that these olefins are formed through competing reaction pathways. Another important parameter affecting catalyst lifetime – generally less discussed for MTO – was the presence of internal defects. The presence of structural defects led to a much faster deactivation of Sigma-1 in comparison to defect-free ZSM-58, both zeolites having the same DDR topology.

The latter observation triggered further research on the origin of defects and their influence on MTO performance, reported in **Chapter 3**. The initial surmise was that seeded growth might have an impact on the increased concentration of internal defects due to faster crystal growth kinetics. Therefore zeolites with DDR (Sigma-1 and ZSM-58) and CHA (SSZ-13) structure were synthesized *via* direct and secondary growth approach but having the same concentration of Brønsted acid sites and the same crystal size. Analysis of the surface properties, performed by Infrared spectroscopy, revealed the

presence of multiple internal defects (band at 3729 cm^{-1}) and silanol nests (at 3400 cm^{-1}) only for zeolites synthesized *via* seeded growth approach, independent of topology. These defects led to higher coking rates and, as a consequence, to faster deactivation. Higher coking rates are explained on the basis of interaction of coke precursors with slightly acidic silanol groups, causing their retention inside the zeolite cages and to enhanced hydrogen transfer reactions, facilitating coke formation. This chapter concludes that crystal quality is a more important parameter than crystal size. On the other hand, these defects can be healed *via* post-synthetic treatment with NH_4F . Besides, comparison of zeolites with DDR and CHA topology in the dimethyl ether conversion to olefins (DMTO) revealed the strong influence of cage and window dimensions on product distribution. The larger cage dimensions of CHA promoted a higher selectivity to ethylene and longer lifetimes, the latter being the result of ability to hold more aromatics due not only to the larger cages but also to the 3D-connected porosity of this zeolite.

Though both DDR and CHA zeolites showed high selectivity to short chain olefins, the relatively fast deactivation of these zeolites (something common for all 8-membered ring zeolites) due to coke deposition renders them as non-ideal MTO catalysts, especially when fixed bed operation is envisaged. In view of these results, ZSM-5 (10-membered ring zeolite), was studied in **Part II** of the thesis. In **Chapter 4**, the inconsistency of catalyst lifetimes reported in literature for ZSM-5 with similar acidic and morphological properties was analyzed. By monitoring temperature profiles inside the catalytic bed during MTO process under industrially relevant conditions, a temperature rise of 80°C in small-scale reactors was observed. Even when using a significant degree of dilution with inert SiC , it was still impossible to reach fully isothermal behavior ($\Delta T_{ad} = 10^\circ\text{C}$). Application of mesoporous zeolites resulted in a lower heat generation per unit volume zeolite, explaining the improved performance not only by an improved mass transfer but also because of a moderated heat generation. Moreover, under industrially relevant conditions, the parent ZSM-5 catalyst was subjected to extensive dealumination due to *in-situ* steaming, accelerated by the observed temperature rise increasing the degree of dealumination. As a result of this dealumination, the concentration of acid sites was significantly reduced and mesopores were formed. Both factors resulted in lifetime improvements by a factor of three for ZSM-5 after two catalytic runs.

Chapter 5 is dedicated to modification of Brønsted acidity with the main aim to improve the selectivity to short chain olefins. Incorporation of calcium into ZSM-5 achieved by post-synthetic modification resulted in an almost complete disappearance of Brønsted acid sites. Acidity characterization using a combination of techniques (NH_3 TPD, FT-IR using pyridine and CO as probe molecules, ^1H - ^{31}P CP MAS NMR with TMPO as a probe molecule) suggested transformation of Brønsted acid sites into Lewis ones. This modification led to significant changes in catalytic behavior, namely: selectivity to propylene and butenes increased at the expense of selectivity to ethylene, paraffins and aromatics, the latter two being negligibly low. Analysis of the product distribution pointed to the almost complete suppression of the aromatic cycle and to a decrease of hydrogen transfer reactions upon post-synthetic modification with Ca. A decreased formation of the aromatic species acting also as coke precursors resulted in an up to a

9-times prolonged catalyst lifetime with the highest throughput $792 \text{ g}_{\text{MeOH}} \text{ g}_{\text{cat}}^{-1}$. Among the different methods of Ca incorporation, incipient wetness impregnation turned out to be the best one, leading to the lowest concentration of acid sites left. On the other hand, variation of Ca loading, revealed that the optimal molar ratio to give the highest propylene selectivity (53%) was Ca : Al = 5:1, while the highest throughput was achieved with Ca : Al = 2:1. Periodic DFT calculations suggested that Ca-species are present in the form of CaOCaOH^+ moieties located in the channel intersections.

Chapter 6 continues with the investigation of the effect of post-synthetic ZSM-5 modification in MTO. The disappearance of Brønsted acidity and simultaneous appearance of Lewis acidity made it difficult to identify the most important factor resulting in such improved catalytic performance. To answer this question, three series of post- and pre-synthetically modified ZSM-5 samples were prepared having different amounts of Brønsted and Lewis acid sites. A systematic analysis of catalyst lifetime and selectivity to propylene and ethylene as a function of Brønsted and Lewis acid site density was performed. Linear correlations with opposite trends were found for propylene and ethylene selectivity as a function of Brønsted acid site density, indicating that product distribution depends mainly on this parameter and that isolation of Brønsted acid sites is key to enhance the selectivity to propylene. On the other hand, a clear interdependence between methanol throughput and the ratio of Lewis and Brønsted acid sites was found. In the observed volcano plot, an optimal ratio of Lewis to Brønsted acid sites between two to four results in the lowest deactivation rates, independent of the method used to achieve such ratio. Further calculations suggest that Lewis acid sites act as “cleaning sites”, strongly interacting with coke precursors and preventing deactivation of Brønsted acid sites.

Evaluative Remarks.

This PhD thesis opened a tiny little door to the gigantic MTO world with rooms of topologies and mechanistic halls. During the journey through this world, another secret room – known but forgotten – was found. It contains Lewis acidity originating from different modifications by metals and non-metals. The current thesis is mainly focused on Lewis acidity originating from modification with alkaline-earth metals, showing the clear impact on MTO performance in terms of both selectivity and lifetime. This impact was understood with the help of multiple characterization techniques and theoretical calculations; however, the knowledge should be unified and extended to other types of modifications.

The understanding of the effect of Lewis acidity is of paramount importance as it is very often present in the zeolite in the form of extra-framework Al. Besides, Lewis acidity can be easily generated in the zeolite by *in-situ* steaming during the MTO conversion, even if it is not present in the fresh zeolite. The multiple controversial data should be clarified further. Herein, it is important to understand whether the presence of Lewis acidity changes the nature of coke species and, if yes, what they look like.

While trying to understand how to improve selectivity through topology selection and Brønsted acidity modification, it was found that other parameters such as internal defects, crystal size, and nature of acidity sometimes have an even greater influence on selectivity and lifetime than these, at first thought,

primary parameters. Therefore, the MTO catalyst should not be interpreted as a zeolite of certain topology having certain Si/Al ratio. Instead, it should be treated as a complex system where every single parameter, including defects, density and location of acid sites, their nature and strength and many other factors are of importance and should be addressed systematically. A further complicating factor is the nearly unavoidable integral reactor operation. At MTO process conditions full conversion is usually obtained, implying that the catalyst along the bed length is exposed to different gas compositions that give rise to temporal local developments of carbon pool deposits of different kinds, water production, steaming of catalyst and possible temperature changes. Several of these elements have been described in this thesis and outlined in literature.^[1] This clearly illustrates the complexity of the study of this conversion process.

Outlook

Conversion of methanol to olefins has already been realized into an industrial process using both 8-ring (SAPO-34) and 10-ring zeolites (ZSM-5) pointing at its importance and relevance.^[2] In view of such industrial success, one could have the impression that MTO is already a sufficiently elaborated process with both clarified mechanism and well-engineered catalyst. As demonstrated in this PhD thesis, this is not the case.

From the mechanistic point of view, a number of milestones are important to gain a deeper understanding. Since the dual-cycle mechanism and the active species of the hydrocarbon pool are mostly clarified; in our opinion, focus will be shifted towards understanding of the formation of the first C-C bond from methanol. Although several theories have been postulated about the nature of this first bond formation, to date no experimental confirmation provided evidence to the theoretically determined intermediates. Very recently, Weckhuysen *et al.*^[3] made an important step in this direction by demonstrating the formation of methyl acetate as a key intermediate in the formation of the first C-C bond *via* a combination of UV/Vis, MS and solid state NMR. In the future, we anticipate many more works in this direction.

When it comes to catalyst engineering, this PhD thesis clearly demonstrates that there is still quite some room for improvement both in terms of selectivity to short chain olefins and of lifetime. Authors certainly believe that the current tendency in MTO to apply mesoporous zeolites in prolonging lifetime will be displaced. Instead of improving methanol throughput by increasing the coke accumulation capacity (due to mesopore formation), further research will be rather dedicated to engineering of an active site able to decrease coking rate or even to avoid coke formation. This will be done by thorough understanding of hydrogen-transfer pathways leading to coke formation in order to further mitigate catalyst coking. This topic was hardly addressed till now, and so far there is only one publication dedicated solely to hydride transfer reactions in methanol conversion reactions.^[4]

Further synthetic tools to allow the isolation of acid sites and the understanding of multifunctional catalysis within the framework of MTO will certainly pave the way for future developments. From this

perspective, utilization of the alkaline-earth modified zeolites as MTO catalysts elaborated in this thesis can be considered as a starting point in this direction. Application of this type of catalysts is not something new and there are numerous studies from the early 90's dealing with this topic. In contrast to these old studies, we are currently able to rationalize the observed improved catalytic performance by combining advanced characterization tools, rigorous catalyst testing and theory. Further studies on this topic will be dedicated to the analysis of the coke species still deactivating the catalyst. With the help of *in-situ* UV/Vis, confocal fluorescence microscopy and X-ray microtomography, it will be possible to further compare the main differences in the nature and location of coke precursors appearing in modified and non-modified zeolites. On the other hand, the field of 12-ring zeolites that promptly deactivate under MTO conditions represents an inviting avenue for active site engineering and will be explored further. The same modification tools applied to ZSM-5 must be tried for BEA and MOR topologies. This will help to understand further the role of topology on formation of coke species, catalyst lifetime and selectivity and will verify if the role of topology is indeed decisive in MTO. Besides, it is of scientific curiosity to find out whether the aromatic cycle can be suppressed in topologies that normally promote it. Altogether, these efforts should eventually allow the rational design of superior catalysts that may yield much more intensified MTO processes and also assist in better understanding of other important zeolite catalysed reactions, from catalytic cracking to alkylations.

Summarizing, there are still multiple mechanistic questions to be answered, multiple tools to be developed for the engineering of an active site and multiple new characterization techniques to be applied to MTO to elaborate on active species and coke precursors. These are three main directions which one will never get tired and bored to explore especially applied to MTP, MTO, MTG, MTH and MTA processes.

References

- [1] H. Schulz, M. Wei, *Top. Catal.* **2014**, *57*, 683-692.
- [2] U. Olsbye, S. Svelle, M. Bjorgen, P. Beato, T. V. W. Janssens, F. Joensen, S. Bordiga, K. P. Lillerud, *Angew. Chem. Int. Ed.* **2012**, *51*, 5810-5831.
- [3] A. D. Chowdhury, K. Houben, G. T. Whiting, M. Mokhtar, A. M. Asiri, S. A. Al-Thabaiti, S. N. Basahel, M. Baldus, B. M. Weckhuysen, *Angew. Chem. Int. Ed. Engl.* **2016**, *55*, 15840-15845.
- [4] S. Müller, Y. Liu, F. M. Kirchberger, M. Tonigold, M. Sanchez-Sanchez, J. A. Lercher, *J. Am. Chem. Soc.* **2016**, *138*, 15994-16003.

Samenvatting en Vooruitblik

Samenvatting.

Het Methanol-to-Olefines (MTO) proces is een alternatieve route om korte olefines te verkrijgen zonder het gebruik van aardolie als grondstof. Een van de grootste uitdagingen in dit proces is de ontwikkeling van stabiele en selectieve katalysatoren, waar propyleen het meest gewenste product is. Om de huidige trend van de wereldeconomie bij te kunnen benen, was de gevolgde strategie in het onderzoek, beschreven in dit proefschrift, de verschillende manieren te onderzoeken om de selectiviteit naar korte olefines te kunnen sturen en om de manier te vinden om de ethyleen/propyleen productverhouding te kunnen sturen. Het proefschrift staat geheel in het teken van het ontrafelen van de relaties die de gewenste productverdeling bepalen. Hoewel het optimaliseren van de selectiviteit centraal staat, is het niet gelimiteerd tot dit onderwerp. In tegendeel, speciale aandacht is besteed aan de ontwikkeling van stabiele katalysatoren die minder last hebben van deactivering. De controle over beide factoren is bereikt door het identificeren van de belangrijkste structuur-activiteit relaties die leiden tot het onderdrukken van één van de twee routes in het dual-cycle mechanisme (de olefine- en aromaatcyclus, uitgebreid beschreven in **Hoofdstuk 1**). Topologie en zuurheid (acidity) zijn de twee belangrijkste parameters die het reactienetwerk (in de gewenste richting) sturen.

Dit proefschrift omvat twee delen waarin manieren worden onderzocht om de selectiviteit te veranderen. In **deel I** wordt dit gedaan via het stabiliseren van de aromaatcyclus, gebruik makend van 8-ring DDR en CHA zeolieten, terwijl in **deel II** de Brønsted acidity van de ZSM-5 zeoliet wordt aangepast.

Deel I omvat Hoofdstuk 2 en 3. **Hoofdstuk 2** richt zich op het onderzoek naar zeolieten met DDR topologie (ZSM-58 en Sigma-1) als potentiële katalysatoren voor toepassing in MTO. Door de specifieke combinatie van de cage en window afmetingen vertonen DDR zeolieten tot 90% selectiviteit naar ethyleen en propyleen, en een verwaarloosbare hoeveelheid paraffines. Deze prestatie is een onbetwist voordeel dat kan leiden tot het reduceren van energie-intensieve scheidingsstappen. De systematische analyse van het effect van de fysico-chemische eigenschappen op de levensduur van de katalysator leidde tot het inzicht dat een verlaging van zowel de kristallietgrootte als de concentratie van zure sites de levensduur sterk kan vergroten, uitgedrukt in omzettingcapaciteit, van $1.3 \text{ g}_{\text{MEOH}} \text{ g}_{\text{cat}}^{-1}$ tot $3.6 \text{ g}_{\text{MEOH}} \text{ g}_{\text{cat}}^{-1}$. Daarentegen bleek dat de concentratie van zure sites en reactietemperatuur van grote invloed was op de ethyleen/propyleen verhouding. Over het algemeen werd gevonden dat de factoren die leidden tot de hoogste selectiviteit naar propyleen zorgden voor de laagste selectiviteit naar ethyleen, wat aangeeft dat deze olefines worden gevormd door concurrerende reactiepaden. Een andere belangrijke parameter die de levensduur van de katalysator beïnvloedt – een onderwerp dat weinig bediscussieerd wordt in MTO onderzoek – is de aanwezigheid van interne defecten in de zeolietstructuur. De aanwezigheid van structuurdefecten leidde tot sterk versnelde deactivering van Sigma-1 in tegenstelling tot het defectarme ZSM-58, beide zeolieten met dezelfde DDR topologie.

De laatstgenoemde observatie was de aanleiding tot dieper onderzoek naar de herkomst van defecten en de invloed daarvan op de MTO prestaties, gerapporteerd in **Hoofdstuk 3**. Het initiële vermoeden bestond dat 'seeded growth' een invloed zou hebben op de concentratie interne defecten door snellere kristalgroei kinetiek. Om die reden werden zeolieten met DDR (Sigma-1 en ZSM-58) en CHA (SSZ-13) topologie gesynthetiseerd via directe en 'secondary growth' methodes, doch met dezelfde concentratie Brønsted zure sites en identieke kristallietgrootte. De analyse van de oppervlakte-eigenschappen met infrarood spectroscopie, onthulde de aanwezigheid van meervoudige interne defecten (band rond 3729 cm^{-1}) en silanolgroepen (op 3400 cm^{-1}) alleen bij de zeolieten welke via seeded growth waren geproduceerd, onafhankelijk van de topologie. Deze defecten leidden tot snellere koolstofafzetting (coking rates) en als consequentie een snellere deactivering. Hogere coking rates kunnen worden verklaard op basis van de interactie van coke precursors met lichtzure silanol groepen, wat leidt tot retentie in the zeolite cages en verhoogde waterstof-overdracht reacties en wat uiteindelijk de vorming van coke faciliteert. In dit hoofdstuk wordt geconcludeerd dat de kristallietkwaliteit een belangrijker parameter is dan kristallietgrootte. Daarentegen kunnen voornoemde defecten worden gerepareerd via post-synthetische behandeling met NH_4F . Bovendien werd de sterke invloed van de cage en window afmetingen op de productverdelingen blootgelegd door vergelijking van zeolieten met DDR en CHA topologie in de omzetting van dimethyl ether naar olefines (DMTO). Grotere cage afmetingen van CHA zeolieten bevorderde de selectiviteit naar ethyleen en zorgde voor een langere levensduur, wat in dit geval het resultaat was van het vermogen om meer aromaten vast te houden door een combinatie van grotere cages en de drie-dimensionale poriestructuur van dit zeoliet.

Hoewel zowel DDR als CHA zeolieten een hoge selectiviteit naar korte olefines vertoonden, zorgt de relatief snelle deactivering (een kenmerkende eigenschap van 8-ring zeolieten) door coke afzetting ervoor dat dit geen ideale MTO katalysatoren zijn, zeker niet wanneer men een vast-bed operatie voor ogen heeft. Deze resultaten leidden tot het onderzoek aan ZSM-5 in **deel II** van dit proefschrift.

In **Hoofdstuk 4** is de inconsistentie in levensduur van ZSM-5 katalysatoren, zoals gerapporteerd in de literatuur, geanalyseerd. Door het volgen van de temperatuurprofielen in het katalytische bed gedurende het MTO proces onder industrieel relevante condities werden temperatuursexkursies tot $80\text{ }^\circ\text{C}$ waargenomen in kleinschalige reactoren. Zelfs wanneer er een aanzienlijke verdunning van de katalysator met inert SiC werd gebruikt was het onmogelijk om volledig isotherm te opereren ($\Delta T_{ad} = 10\text{ }^\circ\text{C}$). De toepassing van mesoporeuze zeolieten leidde tot een lagere warmtegeneratie per volume-eenheid zeoliet en een verbeterde activiteit, bewerkstelligd door zowel een verbeterde massaoverdracht als verminderde warmtegeneratie. Daarnaast werd de originele ZSM-5 katalysator onder industrieel relevante condities blootgesteld aan extensieve de-aluminering door 'in situ steaming' (water is ook een product), wat werd versneld door de temperatuursverhoging en tot een hogere de-alumineringsgraad leidde. Het resultaat van de de-aluminering was een significant lagere concentratie zure sites en de

introductie van mesoporiën. Beide factoren resulteerden in een drievoudige verlenging van de ZSM-5 levensduur na twee katalytische tests.

Hoofdstuk 5 is gewijd aan het veranderen van de Brønsted acidity met als belangrijkste doel de selectiviteit naar korte olefines te verbeteren. Het introduceren van calcium in het ZSM-5 kristal door post-synthetische modificatie resulteerde in het vrijwel geheel verdwijnen van de Brønsted zure sites. Karakterisering van de acidity met een combinatie van technieken zoals NH_3 TPD, FT-IR met pyridine en CO als probe molecules, ^1H - ^{31}P CP MAS NMR met TMPO als probe molecule suggereerde dat Brønsted zure sites werden omgezet naar Lewis zure sites. De post-synthetische modificatie met calcium zorgde voor grote veranderingen in het katalytisch gedrag; de selectiviteit naar propyleen en butyleen werd verhoogd ten koste van de selectiviteit naar ethyleen, paraffines en aromaten, waarbij de fractie van de twee laatstgenoemde verwaarloosbaar klein was. Verdere analyse van de productdistributie wees uit dat de aromaatcyclus bijna compleet werd onderdrukt en dat de waterstof-overdrachtsreacties sterk werden onderdrukt door de modificatie met calcium. De onderdrukking van de vorming van aromatische verbindingen en daarmee coke precursors resulteerde bovendien tot een negenvoudige verlenging van de katalytische levensduur met de hoogste doorzet van $792 \text{ g}_{\text{MeOH}} \text{ g}_{\text{cat}}^{-1}$. Poriëvolume impregnatie met een calcium precursor oplossing gaf de beste resultaten en leidde tot de laagste concentratie van zure sites. Door variatie van de calciumbelading werd gevonden dat de optimale molaire Ca/Al verhouding voor de hoogste propyleenselectiviteit van 53% de waarde 5:1 heeft, terwijl de hoogste doorzet werd gehaald met een Ca/Al verhouding van 2:1. 'Periodic DFT' berekeningen geven aanwijzingen dat calciumverbindingen aanwezig zijn in de vorm van CaOCaOH^+ deeltjes gelocaliseerd op de kruispunten in de zeolietkanalen.

In **Hoofdstuk 6** wordt de invloed van Ca op de post-synthetisch gemodificeerde ZSM-5 in het MTO proces nader onderzocht. Het verdwijnen van de Brønsted acidity en het tegelijkertijd verschijnen van de Lewis acidity maakte het lastig om eenduidig aan te geven wat nu leidt tot het verbeterde katalytische gedrag. Om deze vraag te beantwoorden werden drie series post- en pre-synthetisch gemodificeerde ZSM-5 monsters bereid met verschillende concentraties Brønsted en Lewis zure sites. Er is een systematische analyse gemaakt van de levensduur van de katalysator en de selectiviteit naar propyleen en ethyleen als functie van Brønsted en Lewis zure sites dichtheid. Lineaire correlaties met tegengestelde trends werden gevonden voor de propyleen en ethyleen selectiviteit als functie van Brønsted zure sites dichtheid, indicatief voor een productdistributie die voornamelijk afhangt van deze parameter. Verder ook dat de verdunning van de Brønsted zure sites de sleutel is tot het verbeteren van de propyleen selectiviteit. Er werd een duidelijke afhankelijkheid gevonden tussen de methanol doorzet en de verhouding van de concentratie Lewis en Brønsted zure sites. In de verkregen volcano-plot werd een optimale verhouding van Lewis en Brønsted zure sites van 2 tot 4 gevonden voor de laagste deactiveringssnelheid, onafhankelijk van de bereidingswijze van de katalysator om deze verhouding te verkrijgen. Verdere DFT berekeningen wekken de suggestie dat Lewis zure sites dienen als "cleaning

sites"; deze hebben een sterke interactie met coke precursors en verlagen daarmee de deactiveringssnelheid van Brønsted zure sites.

Evaluatie

Dit proefschrift heeft een kleine deur geopend naar de gigantische MTO wereld met kamers vol topologieën en mechanistische hallen. Gedurende de reis door deze wereld werd een geheime kamer gevonden, weliswaar bekend maar vergeten. Deze kamer bevat Lewis acidity ontstaan door verschillende vormen van modificaties met metalen en niet-metalen. Het alhier gepresenteerde proefschrift focust hoofdzakelijk op Lewis acidity verkregen vanuit modificatie met aardalkalimetalen, wat een duidelijke stempel drukt op de MTO resultaten met betrekking tot zowel selectiviteit als levensduur. De eigenlijke impact kon pas goed begrepen worden door het toepassen van meerdere karakteriseringstechnieken en theoretische berekeningen. Deze kennis zou moeten worden uitgebreid met andere soorten modificaties.

Het begrijpen van het Lewis acidity effect is van groot belang omdat het vaak in de vorm van 'extra-framework' Al in de zeoliet aanwezig is. Daarnaast kan Lewis acidity gemakkelijk worden verkregen in het zeoliet door de *in situ* steaming gedurende het MTO proces, zelfs als het niet aanwezig was vanaf de beginsituatie. De vele controversiële data moet daarom nader worden verklaard. Het is hier van belang om te begrijpen of de aanwezigheid van Lewis acidity de aard van de coke veranderd, en zo ja, hoe deze moleculen eruitzien.

Gedurende de pogingen om de selectiviteit te verbeteren door de selectie van zeoliettopologie en Brønsted acidity modificatie, werd gevonden dat andere parameters zoals interne defecten, kristallietgrootte en de oorsprong van de zuurgraad in sommige gevallen een grotere invloed hebben op selectiviteit en levensduur dan de initiële parameters. Om deze reden kan een MTO katalysator niet simpel worden beschouwd als een zeoliet met een bepaalde topologie en Si/Al ratio, maar juist als een complex systeem waar iedere afzonderlijke parameter, inclusief defecten en dichtheid, locatie, aard en sterkte van de zure sites, van invloed is en systematisch behandeld moet worden. Een andere factor die de zaak verder compliceert is de nagenoeg onvermijdelijke integrale reactor operatie. Normaliter wordt tijdens de MTO procescondities een volledige conversiegraad behaald, wat betekent dat de katalysator in de lengterichting van het bed wordt blootgesteld aan verschillende gassamenstellingen die ervoor zorgen dat er lokaal tijdelijke veranderingen plaatsvinden in de 'carbon pool' afzettingen, de water productie, steaming van de katalysator en niet te vergeten temperatuurvariaties. Een aantal van deze elementen is beschreven in het hier voorliggende proefschrift alswel in de open literatuur. Dit illustreert duidelijk de complexiteit van het onderzoek in dit conversieproces.

Vooruitblik

De conversie van methanol naar olefines is reeds industrieel gerealiseerd in processen die gebruik maken van zowel de 8-ring SAPO-34 en 10-ring ZSM-5 zeolieten, om maar aan te geven dat het onderzoek belangrijk en relevant is. Gezien de behaalde industriële successen, zou men de indruk kunnen hebben dat MTO een proces is met een reeds zeer toereikende beschrijving van het reactiemechanisme en katalysatorformule. Zoals gedemonstreerd in dit proefschrift, is dit zeker niet het geval.

Vanuit de mechanistische kant van het verhaal zijn er een aantal mijlpalen te bereiken om tot een beter begrip te komen. Omdat het dual-cycle mechanisme en de actieve deeltjes in de hydrocarbon pool overwegend inzichtelijk zijn gemaakt, is naar onze mening een verschuiving nodig naar het begrip van de vorming van de eerste C-C binding vanuit methanol. Hoewel er meerdere theorieën zijn gepostuleerd over de aard van de vorming van de eerste binding, is er tot op de dag van vandaag geen experimenteel bewijs geleverd voor de theoretisch voorgestelde intermediairen. Zeer recentelijk is er een belangrijke stap gezet in de groep van Weckhuysen waarin men door middel van gecombineerde UV/Vis, MS en vaste stof NMR demonstreerden dat methylacetaat de voornaamste tussenverbinding is in de vorming van de eerste C-C binding. We verwachten in de toekomst nog vele andere studies in deze richting.

Wanneer het op katalysator techniek aankomt, laat dit proefschrift duidelijk zien dat er nog een lange weg aan verbetering te gaan is zowel met betrekking tot selectiviteit naar korte olefines als levensduur. Onderzoekers geven aan dat de huidige tendens in MTO waarin mesoporeuze zeolieten worden gebruikt om de levensduur te verlengen zal verschuiven. In plaats van het verbeteren van de methanol doorzet door het verhogen van de coke-opslagcapaciteit door mesoporiën, zal verder onderzoek moeten worden gewijd aan het ontwerpen van een actieve site die de coking rate kan verminderen of juist de vorming van coke van verhinderen. Dit is alleen mogelijk wanneer we de waterstof-overdracht routes die coke produceren volledig begrijpen. Bovengenoemd onderwerp is tot nu toe amper behandeld, en er is tot dusver slechts een enkele publicatie verschenen die uitsluitend is gewijd aan waterstof-overdrachtsreacties in methanol conversie reacties.

Toekomstige ontwikkelingen zullen kunnen worden gedaan met de introductie van vernieuwde of verbeterde katalysator-synthese methodes, om zo de zure sites te isoleren, de locatie te bepalen en te begrijpen hoe de multifunctionele katalyse plaatsvindt in het zeoliet. Vanuit dit perspectief zijn de aardalkali-gemodificeerde zeolieten zoals beschreven in dit proefschrift een uitstekend startpunt. De toepassing van dit type katalysatoren is niet iets compleet nieuws; er zijn meerdere studies uit de jaren '90 over dit onderwerp. In tegenstelling tot deze studies zijn we tegenwoordig in staat om de verbeterde katalytische activiteit te verklaren met het behulp van geavanceerde karakteriseringsmethodes, uitvoerige katalytische tests en theoretische berekeningen. Wat rest is de analyse van de coke deeltjes die vandaag de dag nog steeds zorgen voor katalysatordeactivering. Met behulp van *in-situ* UV/Vis, confocal fluorescence microscopy en X-ray microtomography is het mogelijk om de belangrijkste

verschillen te vergelijken van de coke precursors in zowel gemodificeerde als oorspronkelijke zeolieten. Daarentegen zijn de 12-ring zeolieten met hun instantane deactivering onder MTO condities een interessant onderzoeksveld met betrekking tot het ontwerp van de actieve site. Ook zijn de modificatiemethoden toegepast op ZSM-5 wellicht toe te passen op BEA en MOR zeolieten. Het laatstgenoemde voorstel is de manier om uit te zoeken of topologie een beslissende rol speelt met betrekking tot coke-vorming, katalysatorlevensduur en selectiviteit. Daarnaast is er een zekere wetenschappelijke nieuwsgierigheid ten aanzien van de onderdrukking van de aromatische cyclus in topologieën die deze normaliter bevorderen. Alles samengenomen zouden deze inspanningen uiteindelijk kunnen leiden tot het ontwerp van superieure katalysatoren die intensievere MTO processen kunnen voortbrengen en een betere uitleg geven aan andere belangrijke zeoliet-gekatalyseerde reacties zoals katalytisch kraken en alkyleringsreacties.

Samenvattend, er zijn nog meerdere mechanistische vragen te beantwoorden, meer gereedschap te ontwikkelen voor actieve site ontwerp en meerdere karakteriseringstechnieken toe te passen op het MTO proces om het begrip omtrent de actieve sites en coke precursors verder uit te werken en door te ontwikkelen. De drie voornaamste onderzoeksrichtingen hierboven beschreven staan garant dat het nooit saai wordt om verdere stappen te zetten in methanol conversie processen.

Acknowledgements

According to the non-published statistics, what a potential reader of this thesis will do is pick up my book, flip to the publication list critically evaluating it, then to the conferences list to examine the quality of my scientific tourism and finally to the acknowledgements to look for his/her own name. Dear reader, I hope you will be satisfied with my 'thank you' word.

But people whom I would like to acknowledge first are interested in the content of this thesis rather than the current chapter. My endless gratitude goes for my professors: Jorge and Freek. Jorge, I am extremely thankful to you that I could break into your office with every question (important and urgent in my opinion) or just to proudly show my first ever synthesized zeolites whenever I wanted and I would be always very welcomed. Thank you for your wisdom, advice and support, for being a lighthouse of my research lost in the storm of my own doubts. Freek, thank you so much for the Catalysis Engineering Group the way we have it, for our discussions and conference trips, and for the owl muffins. I would not choose a better place to be shaped both scientifically and personally.

My special thanks go to the committee members, who agreed to evaluate my thesis and who will probably ask me tons of tricky questions during the defence. I am actually thrilled that all my personal MTO heroes are going to be there.

I am also very thankful to the TASC-Syngas members for the inspiring discussions during the project meetings and tons of ideas we generated: Joris, Javier and Bert (UU); Robert, Lukasz, Kirsten, Christiane and Ekkehard (BASF), Jurjen and Sven (DSM Resolve).

Michiel, special thanks to you for your sobering questions, which made me re-think many points of my research.

There are people who make our everyday life much easier, to whom we come like 4-year old children with our broken scientific toys begging for help. Bart, you are our personal Korben Dallas from 'The Fifth Element', as your mission is to quietly save our Catalysis Engineering galaxy from the catastrophe. I still wonder how you manage to do it on a daily bases. Harrie, thank you for being so eager to help with every single piece of equipment. Willy, thank you for keeping tidiness everywhere, the lab would be ruined without you. Kevin, thank you for the entertainments like "let's make the 35 m GC column out of this 100 m". Els, thank you for arranging our PhD lives and making them so comfortable within the group. Thanks to Caroline, Bart and Duco, Ben and Ruben for your help.

Thanks to my students for letting me develop my teaching skills and volunteering to realize my scientific ideas. Romke, Leonard, Rommy, Sara, Sara, Eva, Mike, I was very lucky with you.

I was also very lucky with my cosy office and my officemates certainly contributed to this cosiness. Vera, thanks a lot for helping me during my first months in CE to find the location of my office and for rescuing me from the basement when I was lost. Alma, thanks a lot for always having an opinion and

also for sharing my “nesting syndrome” which resulted in our office looking like an art gallery. Alla, my dear Alla, thanks to you for being you.

I acknowledge my Post-Soviet Catalysis community without whom I cannot imagine my PhD life. Nastya, thanks for sharing my passion to science and on-line shopping, for fruitful discussions about the science and again on-line shopping...and empathizing the grief of my not-stabilized flows. Alyona, thanks a lot for keeping an eye on the weather forecast and for being such a lovely person. Alla, thank you again, you deserve to be acknowledged one million times for your kindness, knockout covers and intimate talks. Dima, thanks for not letting me starve and sharing all your chocolates, my dentist is very eager to meet you. Lesha, you are for me the humanized version of Avanta+ encyclopedia with strong affinity to 90's culture, thanks for always having an answer.

Thanks to Ági for founding and chairing the Catalysis Crochet Club (CCC), where one could sink her grief of non-stabilized flows; and to Máté, who had to escape somewhere to let CCC take place; and to Ina for levelling up the topics of CCC. Thanks a lot to my dear Canan for all these zeolite recipes, movies and pizzas, flower carpets, and “you can do it”. Hiç korkma, Canan, and I miss you so much. Thanks to Lide for conference in Cape Town (Nastya, don't be jealous) and penguins, this was certainly the highlight of 2017. Thanks a lot to Eduardo for being the spirit and energizer of the group; I guess this is the consequence of unlimited pasta consumption. Thanks to Xiaohui for patrolling the corridors of CE every night and protecting CE from the low impact factor evil with the magic of purple powder. Thanks to Robert for tolerating Nastya's jokes - such strong nerves! Thanks to Tim for calming down my panic and translating my awkward propositions so fast. Thanks to Maarten for the calculation hobby, from which I certainly benefited, devotion to science and patience in answering my e-mails.

Thanks to Sina, Pablo, Abrar, Filipe, Tania, Elena, Maxim, Damla, Sumit, Beba, Jara, Maria Jose, Yixiao, Rupali, Adrian, Anahid, Eli, Meixia, Riming, Xinlei for contributing to the CE team.

I feel an urge to acknowledge people who might never open this book, though I will make sure that my ‘thank you’ word will reach them. Thanks a lot to my chemistry teacher, G.A. Ceban, who spent so many hours training me for Chemistry Competitions and who inspired me in so many senses. Thanks a lot to Fernando, who taught me how to present and how to write papers and who also makes wonderful cocktails.

Thanks a lot to my dearest friends. To Natasha, who honestly thinks that my job is to wash glassware in the lab but still loves me. To Masha, who changed from a punk to “ideal mummy”. To Sasha, who keep chasing me and Artur all around the world. I wonder if we can escape from you.

A big piece of this thesis belongs to my family. Mama, papa, thanks for letting me follow my heart and for supporting my weird and irrational decisions to become a chemist. I owe you so much. Even more I owe to my granny, who wouldn't sleep well till my paper is accepted, and who certainly knows that everything will be fine.

Finally, I am very thankful to Artur who let me in his life and let me change it. I am so happy that I can share my macarons with you.

List of Publications and presentations

Publications related to this thesis:

- Yarulina, I., Dikhtiarenko, A., Kapteijn, F., Gascon, J. Consequences of secondary zeolite growth on catalytic performance in DMTO studied over DDR and CHA. *Catalysis Science & Technology*, **2017**, 7, 300-309.
- Yarulina, I., Bailleul, S., Pustovarenko, A., Ruiz-Martinez, J., De Wispelaere, K., Hajek, J., Weckhuysen, B. M., Houben, K., Baldus, M., Van Speybroeck, V., Kapteijn, F., Gascon, J. Suppression of the aromatic cycle in methanol-to-olefins reaction over ZSM-5 by post-synthetic modification using calcium. *ChemCatChem*, **2016**, 8, 3057-3063. (Front Cover)
- Yarulina, I., Kapteijn, F., Gascon, J. The importance of heat effects in the methanol to hydrocarbons reaction over ZSM-5: on the role of mesoporosity on catalyst performance. *Catalysis Science & Technology*, **2016**, 6, 5320-5325.
- Yarulina, I., Goetze, J., Gücüyener, C., van Thiel, L., Dikhtiarenko, A., Ruiz-Martinez, J., Weckhuysen, B., Gascon, J., Kapteijn, F. Methanol-to-olefins process over zeolite catalysts with DDR topology: effect of composition and structural defects on catalytic performance. *Catalysis Science & Technology*, **2016**, 6, 2663-2678. (Front Cover)
- Yarulina, I., Goesten, M., Bailleul, S., de Wispelaere, K., Espin, J., Mezari, B., Hensen, E., van Speybroeck, V., Olsbye, U., Pérez-Ramírez, J., Kapteijn, F., Gascon, J. The importance of Lewis and Brønsted acid sites for methanol-to-propylene process. (In Preparation)

Other publications:

- Goetze, J., Meirer, F., Yarulina, I., Gascon, J., Kapteijn, F., Ruiz-Martínez, J., Weckhuysen, B. New insights in the activity and deactivation of the methanol-to-olefins reaction over different small-pore zeolites as studied with operando UV/Vis spectroscopy. *ACS Catalysis*. **2017**. (Under Revision)
- Yarulin, A., Berguerand, C., Yuranov, I., Cárdenas-Lizana, F., Prokopyeva, I., Kiwi-Minsker, L. Pt-Zn nanoparticles supported on porous polymeric matrix for selective 3-nitrostyrene hydrogenation. *Journal of Catalysis*, **2015**, 321, 7-12.
- Lamey, D., Prokopyeva, I., Cárdenas-Lizana, F., Kiwi-Minsker, L. Impact of organic-ligand shell on catalytic performance of colloidal Pd nanoparticles for alkyne gas-phase hydrogenation. *Catalysis Today*, **2014**, 235, 79-89.
- Vollmer, I., Kosinov, N., Yarulina, I., Hensen, E., Gascon, J., Kapteijn, F. Is the local molybdenum geometry in HZSM-5 relevant for its performance in the aromatization of methane? (In Preparation)

- *Vollmer, I., Yarulina, I., Gascon, J., Kapteijn, F.* Isolating the active Mo species from coke formation in methane dehydroaromatization. (In Preparation)

Presentations:

- *Yarulina, I., Radersma, M., Kapteijn, F., Gascon, J.* The interplay of Lewis and Brønsted acid sites in the catalytic performance of ZSM-5 in MTO. *NCCC (Netherlands' Catalysis and Chemistry Conference) XVIII*, Noordwijkerhout, the Netherlands, March **2017 (oral)**.
- *Yarulina, I., Radersma, M., Kapteijn, F., Gascon, J.* The interplay of Lewis and Brønsted acid sites in the catalytic performance of ZSM-5 in MTO. *Faraday Discussion. Catalysis for Fuels*, Cape Town, South Africa, January **2017 (poster)**.
- *Yarulina, I., Radersma, M., Kapteijn, F., Gascon, J.* Synergetic effect of Lewis and Brønsted acidity in methanol to olefins reaction. *Invited Lecture*, Ludwigshafen, Germany, December **2016 (oral)**.
- *Yarulina, I., Radersma, M., Kapteijn, F., Gascon, J.* Synergetic effect of Lewis and Brønsted acidity in methanol to olefins reaction. *CHAINS (Chemistry as Innovating Science)*, Veldhoven, the Netherlands, December **2016 (oral)**.
- *Prokopyeva, I., Pustovarenko, A., Ruiz-Martinez, J., Weckhuysen, B., Houben, K., Baldus, M., Kapteijn, F., Gascon, J.* Suppression of aromatic cycle in methanol to olefins reaction. *NCCC (Netherlands' Catalysis and Chemistry Conference) XVII*, Noordwijkerhout, the Netherlands, March **2016 (oral)**.
- *Prokopyeva, I., Pereira, S., Lopes, F., Gascon, J., Kapteijn, F.* Heat effects determine catalyst lifetime in methanol-to-hydrocarbons reaction. *AIChE (American Institute of Chemical Engineers) Annual Meeting 15*, Salt Lake City, USA. November **2015 (oral)**.
- *Prokopyeva, I., Pereira, S., Gascon, J., Kapteijn, F.* Heat effects determine catalyst lifetime in methanol-to-hydrocarbons reaction. *3rd ALP (Ambitious Leader's Program) International Symposium*, Sapporo Japan, November **2015 (poster)**.
- *Prokopyeva, I., Gücüyener, C., Gascon, J., Kapteijn, F.* Conversion of methanol to olefins over zeolites with DDR topology: the role of template on catalytic performance. *NCCC (Netherlands' Catalysis and Chemistry Conference) XVI*, Noordwijkerhout, the Netherlands, March **2015 (poster)**.
- *Prokopyeva, I., Gücüyener, C., Dikhtiarenko, A., Gascon, J., Kapteijn, F.* Conversion of methanol to olefins over zeolites with DDR topology: the role of template on catalytic performance. *2nd DPTI (Delft Process Technology Institute) Annual Event*, Rotterdam, the Netherlands, November **2014 (poster)**.
- *Prokopyeva, I., Gücüyener, C., Dikhtiarenko, A., Gascon, J., Kapteijn, F.* Conversion of methanol to olefins over zeolites with DDR topology: the role of template on catalytic

performance. *NPS (Netherlands Process Technology Symposium) 14*, Utrecht, the Netherlands, November **2014 (oral)**.

- Prokopyeva, I., Gascon, J., Kapteijn, Towards selective and stable methanol conversion: alternative route to C2-C4 olefins with zeolite materials. *1st DPTI (Delft Process Technology Institute) Annual Event*, Kijkduin, the Netherlands, November **2013 (poster)**.

About the Author



Irina Yarulina (Prokopyeva) was born on the 7th of January 1988 in Comrat, USSR. She graduated from the Theoretical Lyceum with the specialization in Formal and Physical Sciences in 2006 and finished the School of Fine Arts in the same year. After her graduation, she entered the Lomonosov Moscow State University of Fine Chemical Technology where she obtained her BSc and MSc degrees, both *cum laude*. Irina did her BSc project in 2010 under the supervision of Dr. Egorova in the Department of Petrochemical Synthesis and Artificial Liquid Fuel studying the mechanism of isopropyl alcohol dehydrogenation over Cu supported on structured carbon materials. Her MSc thesis research entitled “Study of acetylene hydrogenation over monodispersed Pd: synthesis and kinetics” was carried out in the Group of Chemical Reaction Engineering of Prof. Kiwi in the Swiss Federal Institute of Technology (EPFL, Switzerland).

After graduating from the university, Irina moved to the Netherlands in 2013 to start her PhD in the Catalysis Engineering Group of Delft University of Technology, under the supervision of Prof. Kapteijn and Prof. Gascon. Her PhD project was dedicated to the engineering of stable and selective catalysts for methanol-to-olefins process and is elucidated in detail in the current book.

